Wave Mechanics and Wave Loads on Marine Structures

Paolo Boccotti

ELSEVIER

AMSTERDAM • BOSTON • HEIDELBERG • LONDON
NEW YORK • OXFORD • PARIS • SAN DIEGO
SAN FRANCISCO • SINGAPORE • SYDNEY • TOKYO

Butterworth-Heinemann is an imprint of Elsevier

Butterworth-Heinemann is an imprint of Elsevier
The Boulevard, Langford Lane, Kidlington, Oxford OX5 1GB, UK
225 Wyman Street, Waltham, MA 02451, USA

Notices

Knowledge and best practice in this field are constantly changing. As new research and experience broaden our understanding, changes in research methods, professional practices, or medical treatment may become necessary.

Practitioners and researchers must always rely on their own experience and knowledge in evaluating and using any information, methods, compounds, or experiments described herein. In using such information or methods they should be mindful of their own safety and the safety of others, including parties for whom they have a professional responsibility.

To the fullest extent of the law, neither the Publisher nor the authors, contributors, or editors, assume any liability for any injury and/or damage to persons or property as a matter of products liability, negligence or otherwise, or from any use or operation of any methods, products, instructions, or ideas contained in the material herein.

British Library Cataloguing in Publication Data
A catalogue record for this book is available from the British Library

Library of Congress Cataloging-in-Publication Data
A catalog record for this book is available from the Library of Congress

ISBN: 978-0-12-800343-5

Printed and bound in USA

To B.V. Maria

Preface

A science calls for a unifying idea capable of yielding a powerful synthesis. In particular, ocean engineering science calls for unification of

1. the deterministic and the stochastic approach to wave theory;
2. the approach of field measurements, and the approach of experiments in wave tanks.

This unification is obtained through quasi-determinism (QD) theory and small-scale field experiments (SSFEs).

With the QD theory, a deterministic wave mechanics is born by the theory of probability. The SSFEs are experiments performed, like in a big wave tank, in sea areas or lakes where wind seas have some small size.

An ocean engineering science may be founded on QD theory and SSFEs. This is an important novelty, because in all the books I have consulted the deterministic approach and the stochastic approach to wave theory are conceptually separated; and, similarly, there are two distinct experimental activities: field measurements and wave tank experiments.

In 15 papers published in Ocean Engineering, J. Waterway, Port, Coastal, and Ocean Engineering, J. Fluid Mechanics, Probabilistic Engineering Mechanics, and J. Offshore Mechanics and Artic Engineering, and in a previous book published by Elsevier (2000), I presented the QD theory and many results of SSFEs. However, I did not point out openly that an ocean engineering science may be founded on these two pillars. Here, I intend to do this; and for this aim I shall present the QD theory in a simpler form, and devote a larger room to calculation of wave loads.

This book covers a wide area of potential interest: civil engineering, naval architecture, and mechanical engineering (because of the large room reserved to the problem of wave energy conversion). The area of greatest potential interest is civil engineering, and more specifically: ocean engineering, offshore engineering, port engineering, and coastal engineering. The book has been conceived to be read by students, researchers, and engineers.

The software illustrated in this book and given in the companion website is original and has only the didactic scope to make the new concepts clearer.

Wave Mechanics and Wave Loads on Marine Structures is a prerequisite to books like *Handbook of Offshore Engineering by Chakrabarti* (Elsevier, 2005), roughly, as a book on solid mechanics is a prerequisite to books on steel design or concrete design.

Paolo Boccotti
Reggio Calabria, Italy
March 2014

Acknowledgments

I express my gratitude to Dr. Vincenzo Fiamma and Dr. Alessandra Romolo for their assistance in the final refinement of the book.

Paolo Boccotti

Symbols

(Some symbols used in only one section are not included in the list.)

a	Wave amplitude
a	Triangle (ETS) height
A	Absorption coefficient
a_x, a_y, a_z	Particle acceleration
b	Width
b	Threshold or given value of the surface elevation
b	Threshold or given value of a wave crest height
b	Triangle (ETS) base
c	Wave propagation speed
C	Height of a wave crest
C	Energy-flux/energy factor
C_d	Diffraction coefficient
C_r	Refraction coefficient
C_s	Shoaling coefficient
C_{dg}	Drag coefficient
C_{in}	Inertia coefficient
c_G	Group velocity
c_R	Propagation speed of the reflected wave energy
d	Water depth
D	Diameter
D	Directional distribution
D	Persistence above a fixed threshold
$\mathscr{E}$	Mean wave energy per unit surface
$\mathscr{E}$	Dimensionless frequency spectrum
E	Frequency spectrum (omnidirectional spectrum)
EP	Electrical power
f	Frequency
f	General function
F	General function
F	Function in the diffraction theory
f_x, f_y, f_z	Force per unit length
F_x, F_y, F_z	Force, or force per unit length
$\mathscr{F}_{\mathscr{R}}$	Phase-speed reduction factor
g	Acceleration due to gravity
G	Function in the diffraction theory
h	Threshold or given value of the significant wave height
h	Energy per unit weight at various locations of a converter
H	Wave height
H_s	Significant wave height
H_{s0}	Significant wave height on deep water

k	Wave number
k	Exponent in the gas law
K	Constant
K	Head loss factor
K', K''	Parameters regression base height of ETS
K_1, K_2	Parameters distribution wave heights in a sea state
K_0	Parameter relationship between T_p and H_s for wind seas
K_E	Keleugan−Carpenter number
$K(n)$	Normalizing factor directional distribution
L	Lifetime of a structure
L	Wavelength
L_0	Wavelength on deep water
L_p	Wavelength relevant to wave period T_p
L_{p0}	Wavelength, on deep water, relevant to wave period T_p
m_j	jth spectral moment (with angular frequencies)
m_0	Variance of the surface elevation of a sea state
M	Determinant of a covariance matrix
M	Moment of a force
M_a	Air mass
M_{ij}	i,j cofactor of a covariance matrix
n_p	Width parameter of the directional distribution at the peak frequency
p	Pressure
p	Probability density function
P	Probability of exceedance
$\mathscr{P}$	Probability
p_a	Absolute pressure air
Q	Flow rate per unit length
r	Polar coordinate
R	Radius
R	Return period
R	Resonance coefficient
s	Local propagation axis
S	Directional spectrum
t	Time
t_o	Special time instant
T	Wave period
T	Time lag
T^*	Lag of the absolute minimum of the autocovariance
T_p	Peak period
T_h	Period of a very large wave
T_m	Mean wave period
u	Dummy variable
u	Current velocity
u	Wind speed at an elevation of 10 m above the mean sea surface
u	Velocity in the vertical duct of a U-OWC

u	Parameter of the Weibull 2-parameter distribution
v_x, v_y, v_z	Particle velocity
w	Dummy variable
w	Dimensionless frequency ($=\omega/\omega_p$)
w	Parameter of the Weibull 2-parameter distribution
x	Dummy variable
x	Horizontal coordinate axis
x_o	Fixed value of x
X	Space lag
y	Horizontal coordinate axis
y_o	Fixed value of y
Y	Space lag
$\mathscr{Y}$	Fetch
z	Vertical coordinate axis with origin at the still water level
α	Angle between x-axis and direction of wave advance
α	Quotient between wave height and RMS surface elevation of a sea state
A	Energy scale parameter JONSWAP spectrum (α in the original paper)
β	Dimensionless wave height with a universal distribution
β	Polar coordinate
β	Ratio between the wave height at a U-OWC and the wave height at a vertical breakwater
γ	Specific weight of water
Δp	Wave pressure
$\Delta\omega$	Angular frequency resolution
ε	Phase angle
ζ	Vertical coordinate axis with origin at the seabed
η	Surface elevation (assumed to have a zero mean)
θ	Angle between the y-axis and the direction of wave advance
θ_d	Angle of the dominant direction
λ	Sea bottom slope
ν	Chinematic viscosity
ξ	Dummy variable whose domain is (0,1)
ξ	Ratio between crest height and wave height
ξ	Height of the air pocket of a U-OWC
ρ	Water density
σ	RMS surface elevation of a sea state
τ	Time lag between crest and trough
τ	Ratio between a time lag T and peak period T_p
τ	Time lag covariance pressure-discharge in a converter
ϕ	Velocity potential
Φ	Cross-covariance of surface elevation and velocity potential
Φ	Mean energy flux per unit length
χ	Ratio between c_R and c_G
χ_1	Shape parameter JONSWAP spectrum (γ in the original paper)

χ_2	Shape parameter JONSWAP spectrum (σ in the original paper)
ψ	Autocovariance function
ψ^*	Narrow bandedness parameter (= absolute value of the ratio between the minimum and the maximum of the autocovariance function)
Ψ	Cross-covariance of surface elevation
$\widehat{\Psi}$	Cross-correlation of surface elevation
ω	Angular frequency
ω_p	Dominant angular frequency of the spectrum

Mathematical Symbols

$\langle f(t) \rangle$	Time average of function $f(t)$
$f(t)$	Time derivative of function $f(t)$

Symbols Used in All the FORTRAN Programs

PG $= \pi$
DPG $= 2\pi$

Abbreviations and Acronyms

CV	Control volume
DSSP	Design sea state pattern
DWR	Duration of a wave record
ETS	Equivalent triangular storm
GA	Gauge array
GM	Goda's model
LHS	Left-hand side
MWL	Mean water level
NDBC	National Data Buoy Center of NOAA
NOAA	National Oceanic and Atmospheric Administration, USA
NOEL	Natural Ocean Engineering Laboratory, Italy
OWC	Oscillating water column
pdf	Probability density function
POT	Peaks over threshold
QD	Quasi-determinism
RHS	Right-hand side
RMS	Root mean square
RPP	Random point process
SSFE	Small-scale field experiment
U-OWC	U-shaped OWC
VHM	Virtual-height model

Chapter 1

Wave Mechanics: Basic Concepts

CHAPTER OUTLINE

1.1 THE SYSTEM OF EQUATIONS

In an irrotational two-dimensional flow (y,z), a velocity potential exists such that

$$v_y = \frac{\partial \phi}{\partial y} \tag{1.1}$$

$$v_z = \frac{\partial \phi}{\partial z} \tag{1.2}$$

where v_y, v_z are the y, z components of the particle velocity.

The Euler equation gives the particle acceleration

$$a_y = \frac{\partial v_y}{\partial t} + v_y \frac{\partial v_y}{\partial y} + v_z \frac{\partial v_y}{\partial z} \tag{1.3}$$

Wave Mechanics and Wave Loads on Marine Structures. http://dx.doi.org/10.1016/B978-0-12-800343-5.00001-9

$$a_z = \frac{\partial v_z}{\partial t} + v_y \frac{\partial v_z}{\partial y} + v_z \frac{\partial v_z}{\partial z} \tag{1.4}$$

The Bernoulli equation states that

$$p + \rho g z + \rho \frac{\partial \phi}{\partial t} + \frac{1}{2}\rho \left[\left(\frac{\partial \phi}{\partial y} \right)^2 + \left(\frac{\partial \phi}{\partial z} \right)^2 \right] = f(t) \tag{1.5}$$

where p is the pressure and $f(t)$ is an arbitrary function of time. The general equations of a wave motion are

$$g\eta + \left(\frac{\partial \phi}{\partial t} \right)_{z=\eta} + \frac{1}{2} \left[\left(\frac{\partial \phi}{\partial y} \right)^2 + \left(\frac{\partial \phi}{\partial z} \right)^2 \right]_{z=\eta} = \frac{1}{\rho} f(t) \tag{1.6}$$

$$\left(\frac{\partial \phi}{\partial z} \right)_{z=\eta} = \left(\frac{\partial \phi}{\partial y} \right)_{z=\eta} \frac{\partial \eta}{\partial y} + \frac{\partial \eta}{\partial t} \tag{1.7}$$

$$\frac{\partial^2 \phi}{\partial y^2} + \frac{\partial^2 \phi}{\partial z^2} = 0 \tag{1.8}$$

$$\left(\frac{\partial \phi}{\partial z} \right)_{z=-d} = 0 \tag{1.9}$$

The first one exploits the Bernoulli equation to say that the pressure at the elevation $z = \eta(y,t)$ is zero. The second one says that $\eta(y,t)$ is the elevation of the free surface. The third one is the continuity equation. The fourth one is the boundary condition at the bottom depth. The second equation is proven as follows. The LHS of the following equation represents the difference between the water mass entering the control volume (CV) of Fig. 1.1 and the water mass exiting from the CV in a small time interval dt, and the RHS represents the variation of the water mass in the small interval dt in the CV:

$$-\rho \int_{-d}^{\eta} \frac{\partial^2 \phi}{\partial y^2} \mathrm{d}y\mathrm{d}z\mathrm{d}t - \rho \left(\frac{\partial \phi}{\partial y} \right)_{z=\eta} \left(\frac{\partial \eta}{\partial y} \right) \mathrm{d}y\mathrm{d}t = \rho \frac{\partial \eta}{\partial t} \mathrm{d}t\mathrm{d}y \tag{1.10}$$

Using the continuity Eqn (1.8) and the boundary condition Eqn (1.9), we get

$$\int_{-d}^{\eta} \frac{\partial^2 \phi}{\partial y^2} \mathrm{d}z = -\left(\frac{\partial \phi}{\partial z} \right)_{z=\eta} \tag{1.11}$$

which, together with Eqn (1.10), yields Eqn (1.7).

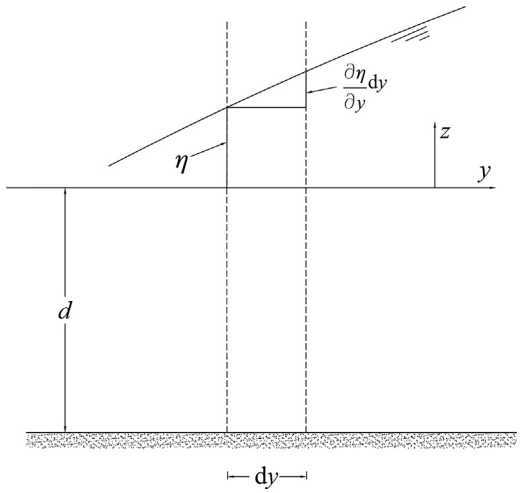

■ **FIGURE 1.1 The small volume used for obtaining Eqn (1.7).**

1.2 INTRODUCTION TO WAVE MECHANICS

A vertical plate swinging periodically at one end of a channel generates waves on the free surface. If we take a photo of the water surface, we get a picture of the surface elevation η as a function of abscissa y along the propagation axis (the channel's axis). Function $\eta(y)$ at a fixed instant represents the waves on the space domain (see Fig. 1.2(a)). If we record the surface elevation at a fixed point as a function of time t, we get the waves on the time domain (see Fig. 1.2(b)).

From Fig. 1.2(a) and (b) of the waves on the space domain and on the time domain, we get the definitions of the basic parameters: wave height H, which

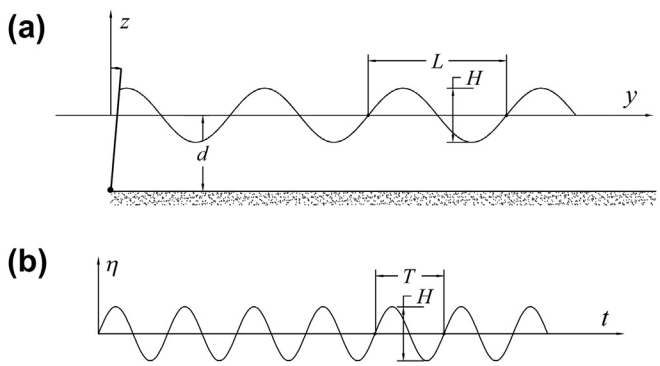

■ **FIGURE 1.2** (a) Waves on the space domain. (b) Waves on the time domain.

is the vertical distance between the highest and the lowest surface elevation in a wave; wavelength L, which is the interval between one zero up-crossing and the next of the wave on the space domain; and wave period T, which is the interval between one zero up-crossing and the next one of the wave on the time domain. Besides these three parameters, it is convenient to define the wave steepness, which is the ratio H/L, and moreover

1. the wave amplitude

$$a \equiv H/2 \tag{1.12}$$

2. the angular frequency

$$\omega \equiv 2\pi/T \tag{1.13}$$

3. the wave number

$$k \equiv 2\pi/L \tag{1.14}$$

The scheme of Fig. 1.3 should be useful to understand the wave motion. Each point in the figure moves along a circular orbit, with constant speed. The time taken to cover the orbit (circumference) is T, and the figure shows two instant pictures taken at a time interval of $T/4$ from each other. The line connecting the points represents a wave. We see the wave advance of $L/4$ in a time interval of $T/4$, and this means that the phase speed of the wave is

$$c = L/T \tag{1.15}$$

The speed v of each point is generally different from c; indeed,

$$v = 2\pi R/T \tag{1.16}$$

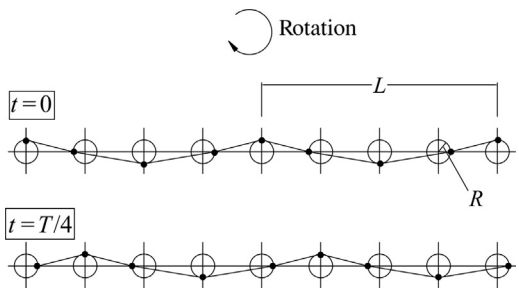

■ **FIGURE 1.3** **Each point covers a circular orbit of radius R in a time T; the line connecting the points is a wave whose propagation speed is L/T.**

1.3 STOKES' THEORY TO THE FIRST ORDER

Let us fix period and swinging amplitude, and let us set the wavemaker in motion. Waves with a height H_1 will form.

Let us stop the wavemaker, and let us set the engine in a different manner: the same period, a smaller swinging amplitude. Then let us start again. Waves with a height H_2 smaller than H_1 will form. The wave period will be the same as before. Indeed, the wave period proves to be the same as the period of the wavemaker.

Let us repeat the process many times—each time with the same period T and with wave heights smaller and smaller. Doing so, in the first wave generations, which are the ones with the greater heights, we shall note asymmetry between the wave crest and trough: the crest will be steeper than the trough. Then, we shall find that a gradual lowering of the wave height, under the same period, leads to waves with a smaller asymmetry; the wave approaches a sinusoidal wave with a wavelength that depends on d and T.

Summarizing:

$$\text{as } H \to 0 \ (d \text{ and } T \text{ fixed}): \quad \eta(y,t) = \frac{H}{2}\cos\left(\frac{2\pi}{L}y - \frac{2\pi}{T}t\right) \tag{1.17}$$

where, for the moment, wavelength L is unknown. Function (1.17) represents a periodic wave of length L on the space domain and it represents a periodic wave of period T on the time domain. The negative sign in the cosine implies that the wave travels along the y-axis (with a positive sign the wave would travel in the opposite direction).

Generating waves with smaller and smaller heights (and a fixed period), we shall also note that the velocity components, at any fixed depth, will tend to fluctuate in space−time like $\eta(y,t)$: v_y in phase with η and v_z with some phase angle. Moreover, the particle velocity will prove to be proportional to the wave height.

From these observations on particle velocity, we can draw the following identikit of the velocity potential:

$$\text{as } H \to 0 \ (d \text{ and } T \text{ fixed}): \quad \phi(y,z,t) = Hf_1(z;d,T,L) \times \cos\left(\frac{2\pi}{L}y - \frac{2\pi}{T}t + \varepsilon\right) + f_2(t) \tag{1.18}$$

where $f_1(z; d, T, L)$ denotes a function of z, wherein parameters d, T, and L may generally be present. For the moment, functions f_1 and f_2 and phase angle ε are unknown.

The Eqns (1.17) and (1.18) show that both η and ϕ are infinitesimal of order H. In particular, the fact that η is infinitesimal enables us to rewrite Eqns (1.6) and (1.7) in the form

$$g\eta + \left(\frac{\partial\phi}{\partial t}\right)_{z=0} + \left(\frac{\partial^2\phi}{\partial z\partial t}\right)_{z=0}\eta + \frac{1}{2}\left[\left(\frac{\partial\phi}{\partial y}\right)^2 + \left(\frac{\partial\phi}{\partial z}\right)^2\right]_{z=0} + \frac{1}{2}\left\{\frac{\partial}{\partial z}\left[\left(\frac{\partial\phi}{\partial y}\right)^2 + \left(\frac{\partial\phi}{\partial z}\right)^2\right]\right\}_{z=0}\eta = \frac{1}{\rho}f(t) \tag{1.19}$$

$$\left(\frac{\partial\phi}{\partial z}\right)_{z=0} + \left(\frac{\partial^2\phi}{\partial z^2}\right)_{z=0}\eta = \left[\left(\frac{\partial\phi}{\partial y}\right)_{z=0} + \left(\frac{\partial^2\phi}{\partial z\partial y}\right)_{z=0}\eta\right]\frac{\partial\eta}{\partial y} + \frac{\partial\eta}{\partial t} \tag{1.20}$$

where the value of a function at $z = \eta$ has been expressed as: (value of the function at $z = 0$) + (value of the derivative with respect to z, at $z = 0$) $\times$ η. Neglecting the terms of orders smaller than or equal to H^2, Eqns (1.19) and (1.20) may be reduced to

$$\left(\frac{\partial\phi}{\partial t}\right)_{z=0} = -g\eta + \frac{1}{\rho}f(t) \tag{1.21}$$

$$\left(\frac{\partial\phi}{\partial z}\right)_{z=0} = \frac{\partial\eta}{\partial t} \tag{1.22}$$

There is only one form of $\phi\,(y, z, t)$—Eqn (1.18)—that satisfies Eqns (1.8), (1.9) and (1.21). This is

$$\phi(y,z,t) = g\frac{H}{2}\omega^{-1}\frac{\cosh\left[k(d+z)\right]}{\cosh\left(kd\right)}\sin\left(ky-\omega t\right) + \frac{1}{\rho}\int_0^t f(t')\mathrm{d}t' \tag{1.23}$$

There remains Eqn (1.22) to be satisfied, and this implies the existence of the following relationship among wavelength, water depth, and wave period:

$$L = \frac{gT^2}{2\pi}\tanh\left(\frac{2\pi d}{L}\right) \tag{1.24}$$

This is the dispersion relationship. For calculating L by means of this relationship, it is convenient to define the sequence

$$L_i = L_0\tanh\left(\frac{2\pi d}{L_{i-1}}\right) \tag{1.25}$$

with

$$L_0 \equiv \frac{gT^2}{2\pi} \tag{1.26}$$

The sequence converges, and it can be easily verified that

$$L_i < L \quad \text{if } i \text{ is an odd number} \tag{1.27}$$

$$L_i > L \quad \text{if } i \text{ is an even number} \tag{1.28}$$

Hence, L is the limit of the sequence.

Since $f(t)$ is an arbitrary function of time, the velocity potential Eqn (1.23) is indeterminate. However, the functions that are of interest, that is to say $\mathbf{v}(y, z, t)$ and $p(y, z, t)$, prove to be independent of $f(t)$, and thus they are definite. In particular, the components of vector $\mathbf{v}$ proceed through Eqns (1.1) and (1.2) and prove to be

$$v_y(y,z,t) = g\frac{H}{2}\omega^{-1}k\frac{\cosh\left[k(d+z)\right]}{\cosh\left(kd\right)}\cos\left(ky-\omega t\right) \tag{1.29}$$

$$v_z(y,z,t) = g\frac{H}{2}\omega^{-1}k\frac{\sinh\left[k(d+z)\right]}{\cosh\left(kd\right)}\sin\left(ky-\omega t\right) \tag{1.30}$$

As to the pressure, it is obtained by means of the Bernoulli Eqn (1.5). The result is

$$p(y,z,t) = -\rho g z + \rho g\frac{H}{2}\frac{\cosh\left[k(d+z)\right]}{\cosh\left(kd\right)}\cos\left(ky-\omega t\right) \tag{1.31}$$

(where the terms of order smaller than or equal to H^2 have been neglected).

1.4 STOKES' THEORY TO THE SECOND ORDER

Surface elevation and velocity potential can be expressed in the form

$$\eta \equiv \eta' + \eta'' + o\left(H^2\right), \quad \phi \equiv \phi' + \phi'' + o\left(H^2\right) \tag{1.32}$$

where η' and ϕ' are the terms of order H, the formulas of which are, respectively, Eqns (1.17) and (1.23), η'' and ϕ'' are the terms of order H^2 that we shall obtain in what follows, and $o(H^2)$ is for *terms of order smaller than* H^2, that is, terms of order H^3, H^4, and so on.

From definition Eqn (1.32), we have

$$\left(\frac{\partial\phi}{\partial t}\right)_{z=\eta} = \left(\frac{\partial\phi'}{\partial t}\right)_{z=0} + \left(\frac{\partial\phi''}{\partial t}\right)_{z=0} + \left(\frac{\partial^2\phi'}{\partial z\partial t}\right)_{z=0}\eta' + o\left(H^2\right) \tag{1.33}$$

This is the form exact to the order H^2 of one term of the system of Eqns (1.6)–(1.9). Similarly, we can also write the form exact to the order H^2 of the other terms of the aforesaid system of equations. The result is

$$\boxed{g\eta'} + g\eta'' + \boxed{\left(\frac{\partial\phi'}{\partial t}\right)_{z=0}} + \left(\frac{\partial\phi''}{\partial t}\right)_{z=0} + \left(\frac{\partial^2\phi'}{\partial z\partial t}\right)_{z=0}\eta'$$

$$+\frac{1}{2}\left(\frac{\partial\phi'}{\partial y}\right)^2_{z=0} + \frac{1}{2}\left(\frac{\partial\phi'}{\partial z}\right)^2_{z=0} = \boxed{\frac{1}{\rho}f(t)} \tag{1.34}$$

$$\boxed{\left(\frac{\partial\phi'}{\partial z}\right)_{z=0}} + \left(\frac{\partial\phi''}{\partial z}\right)_{z=0} + \left(\frac{\partial^2\phi'}{\partial z^2}\right)_{z=0}\eta' = \left(\frac{\partial\phi'}{\partial y}\right)_{z=0}\frac{\partial\eta'}{\partial y} + \boxed{\frac{\partial\eta'}{\partial t}} + \frac{\partial\eta''}{\partial t} \tag{1.35}$$

$$\boxed{\frac{\partial^2\phi'}{\partial y^2}} + \frac{\partial^2\phi''}{\partial y^2} + \boxed{\frac{\partial^2\phi'}{\partial z^2}} + \frac{\partial^2\phi''}{\partial z^2} = 0 \tag{1.36}$$

$$\boxed{\left(\frac{\partial\phi'}{\partial z}\right)_{z=-d}} + \left(\frac{\partial\phi''}{\partial z}\right)_{z=-d} = 0 \tag{1.37}$$

where the framed terms form the linear equations that are satisfied if η' and ϕ' are given by Eqns (1.17) and (1.23). Therefore, the framed terms can be canceled.

In order to solve the system Eqns (1.34)–(1.37) of the two unknown functions η'' and ϕ'', we may differentiate with respect to time all the terms of Eqn (1.34), multiply by g all the terms of Eqn (1.35), and finally add Eqn (1.35) to Eqn (1.34); in doing so we eliminate η''; that is, we obtain an equation with only the unknown function ϕ'', and the known functions η' and ϕ'. Then, substituting η' and ϕ' by their expressions Eqns (1.17) and (1.23), we get

$$\left(\frac{\partial^2\phi''}{\partial t^2}\right)_{z=0} + g\left(\frac{\partial\phi''}{\partial z}\right)_{z=0} = \frac{3}{8}H^2\omega^3\left[1 - \frac{1}{\tanh^2(kd)}\right]\sin\left[2(ky - \omega t)\right] \tag{1.38}$$

Therefore, function ϕ'' must satisfy this equation proceeding from Eqns (1.34) and (1.35), as well as the Eqns (1.36) and (1.37). The solution is a function of the kind

$$\phi''(y, z, t) = A\cosh\left[2k(d + z)\right]\sin\left[2(ky - \omega t)\right] + Bt + Cy \tag{1.39}$$

where A, B, and C are *unknown constants*. Substituting this expression of ϕ'' in Eqn (1.38), we get

$$A = \frac{3}{32}H^2\omega\frac{1}{\sinh^4(kd)} \tag{1.40}$$

At this stage, having obtained the expression of ϕ'' (apart from constants B and C), we can obtain the expression of η'' by means of Eqn (1.34). The result is

$$\eta''(y,t) = \frac{H^2}{16}\frac{\omega^2}{g}\left\{-\frac{1}{\sinh^2(kd)} + F_1(kd)\cos\left[2(ky-\omega t)\right]\right\} - \frac{B}{g} \tag{1.41}$$

where

$$F_1(kd) \equiv 3 - \frac{1}{\tanh^2(kd)} + 3\frac{\cosh(2kd)}{\sinh^4(kd)} \tag{1.42}$$

Constant B can then be obtained given that the mean surface elevation is zero, so that the water mass in the tank is the same under the wave motion and when it is calm.

The conclusion is

$$\eta''(y,t) = \frac{H^2}{16}\frac{\omega^2}{g}F_1(kd)\cos\left[2(ky-\omega t)\right] \tag{1.43}$$

$$\begin{aligned}\phi''(y,z,t) = {} & \frac{3}{32}H^2\omega\frac{1}{\sinh^4(kd)}\cosh\left[2k(d+z)\right]\sin\left[2(ky-\omega t)\right] \\ & -\frac{H^2}{16}\omega^2\frac{1}{\sinh^2(kd)}t + Cy\end{aligned} \tag{1.44}$$

where constant C is obtained from the condition that the average flow in the waveflume is zero.

$F_1(kd)$ (function (1.42)) is positive all over its domain, and, as a consequence, the sum of η'' and η' leads to a wave profile like that of Fig. 1.4: the crest sharpens and the trough flattens. Thus, the nonlinear theory

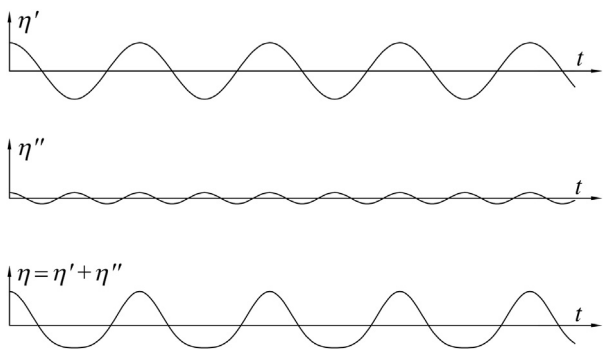

■ **FIGURE 1.4 The second-order term η'' makes the wave crest steeper and flattens the wave trough.**

succeeds in predicting the characteristic asymmetry between crest and trough (see Section 1.3).

The second-order term of the fluctuating pressure head is

$$\frac{\Delta p''}{\gamma} = -\frac{1}{g}\frac{\partial \phi''}{\partial t} - \frac{1}{2g}\left[\left(\frac{\partial \phi'}{\partial y}\right)^2 + \left(\frac{\partial \phi'}{\partial z}\right)^2\right] \tag{1.45}$$

Here, note that the kinetic term (that is, the second addendum on the RHS of this equation) is always negative. Hence, because of the kinetic term, the fluctuating pressure head at some depth (especially on deep water) may have an asymmetry trough/crest opposite to that of the surface waves.

1.5 WAVE–CURRENT INTERACTION

Let us consider a periodic wave traveling on a current of speed u, in the limit $H \to 0$ for fixed d, T, and u. Let us assume the current velocity to be parallel to the wave propagation. The current direction can be the same or opposite to the direction of wave advance; that is, u may be positive or negative.

The surface elevation will have the same form Eqn (1.17) valid in absence of current, except for a different relation between wave number and water depth and wave period; that is,

$$\eta(y,t) = \frac{H}{2}\cos\left(k_c y - \omega t\right) \tag{1.46}$$

where k_c is the wave number generally different from k, which must be determined. This new wave number will depend not only on d and T, but also on u. As to the velocity potential, it will be the sum of two terms: one of the uniform current and one like Eqn (1.23) (the velocity potential of a wave without current). Accordingly, we write

$$\phi(y,z,t) = uy + A\frac{\cosh\left[k_c(d+z)\right]}{\cosh\left(k_c d\right)}\sin\left(k_c y - \omega t\right) + F(t) \tag{1.47}$$

where A is a dimensional constant and $F(t)$ a function of time, both of which need to be determined. Without the current ($u = 0$), A is equal to $g\frac{H}{2}\omega^{-1}$. Naturally, with the current, A will depend on u.

Let us seek k_c, A, and $F(t)$ such that η and ϕ satisfy the differential Eqns (1.6)–(1.9) of general validity. As to Eqns (1.8) and (1.9), it is easy to verify that they are satisfied whatever the k_c, A, and $F(t)$. Let us now

pass to Eqns (1.6) and (1.7). This time $\partial\phi/\partial y$ is the sum of a finite term u and of a term of order H due to the wave. Therefore, the terms

$$\left(\frac{\partial\phi}{\partial y}\right)^2_{z=\eta} \quad \text{and} \quad \left(\frac{\partial\phi}{\partial y}\right)_{z=\eta}\frac{\partial\eta}{\partial y}$$

respectively, of Eqn (1.6) and of Eqn (1.7), are no longer negligible to Stokes' first order, and these equations yield

$$\begin{aligned} g\frac{H}{2}\cos\left(k_c y-\omega t\right)-A\omega\cos\left(k_c y-\omega t\right)+\dot{F}(t)+\frac{1}{2}u^2 \\ +uAk_c\cos\left(k_c y-\omega t\right)=\frac{1}{\rho}f(t) \end{aligned} \tag{1.48}$$

$$Ak_c\tanh\left(k_c d\right)\sin\left(k_c y-\omega t\right)=-u\frac{H}{2}k_c\sin\left(k_c y-\omega t\right)+\frac{H}{2}\omega\sin\left(k_c y-\omega t\right) \tag{1.49}$$

where $\dot{F}(t)$ denotes the derivative of $F(t)$. Equation (1.48) is satisfied if and only if

$$A=g\frac{H}{2}(\omega-uk_c)^{-1} \tag{1.50}$$

$$F(t)=-\frac{1}{2}u^2t+\frac{1}{\rho}\int_0^t f(t')\mathrm{d}t' \tag{1.51}$$

and therefore,

$$\begin{aligned} \phi(y,z,t)=uy+g\frac{H}{2}(\omega-uk_c)^{-1}\frac{\cosh\left[k_c(d+z)\right]}{\cosh\left(k_c d\right)}\sin\left(k_c y-\omega t\right) \\ -\frac{1}{2}u^2t+\frac{1}{\rho}\int_0^t f(t')\mathrm{d}t' \end{aligned} \tag{1.52}$$

Finally, Eqn (1.49) is satisfied if and only if

$$k_c\tanh\left(k_c d\right)=\frac{\left(\omega-uk_c\right)^2}{g} \tag{1.53}$$

From Eqn (1.52) of the velocity potential, and Eqns (1.3) and (1.4) relating particle acceleration to particle velocity, it follows that

$$a_y(y,z,t)=g\frac{H}{2}k_c\frac{\cosh\left(k_c\zeta\right)}{\cosh\left(k_c d\right)}\sin\left(k_c y-\omega t\right)+o(H) \tag{1.54}$$

$$a_z(y,z,t)=-g\frac{H}{2}k_c\frac{\sinh\left(k_c\zeta\right)}{\cosh\left(k_c d\right)}\cos\left(k_c y-\omega t\right)+o(H) \tag{1.55}$$

1.6 PRELIMINARY REMARKS ON THREE-DIMENSIONAL WAVES

The surface elevation of a wave whose propagation direction makes an arbitrary angle θ with y-axis is given by

$$\eta(x, y, t) = \frac{H}{2}\cos\left(kx\sin\theta + ky\cos\theta - \omega t\right) \tag{1.56}$$

To prove this, let us imagine a point moving with a uniform speed L/T along a straight line making an angle θ with the y-axis. If the point starts from $x = 0$, $y = 0$ at time $t = 0$, its position is given by

$$x_P = \frac{L}{T}t\sin\theta, \quad y_P = \frac{L}{T}t\cos\theta \tag{1.57}$$

so that the surface elevation at this point proves to be

$$\eta(x_P, y_P, t) = \frac{H}{2}\cos\left(\frac{2\pi}{T}t\sin^2\theta + \frac{2\pi}{T}t\cos^2\theta - \frac{2\pi}{T}t\right) = \frac{H}{2} \tag{1.58}$$

and hence, it keeps constant in time, which confirms that the trajectory and speed of the wave is coincident with the trajectory and speed of the point.

The velocity potential attacked to surface elevation Eqn (1.56) is

$$\phi(x, y, z, t) = g\frac{H}{2}\omega^{-1}\frac{\cosh\left[k(d+z)\right]}{\cosh\left(kd\right)}\sin\left(kx\sin\theta + ky\cos\theta - \omega t\right) \tag{1.59}$$

Here, we can readily verify that the two functions (1.56) and (1.59) satisfy Eqns (1.21) and (1.22), provided that $f(t) = 0$ in Eqn (1.21), as well as the boundary condition at the bottom; see Eqn (1.9). Note: These equations, having been obtained for the two-dimensional flow y-z, retain their validity even for the three-dimensional flow x-y-z. As to $f(t) = 0$, we have already seen that $\mathbf{v}$ and p do not change whatever the $f(t)$, and therefore it is justified and advisable to put directly $f(t) = 0$ in Eqn (1.21).

Of the whole system of linear flow equations, that is, the system consisting of Eqns (1.8) and (1.9) and Eqns (1.21) and (1.22), the only equation that needs to be adjusted from the two-dimensional to the three-dimensional flow is Eqn (1.8). For the three-dimensional flow, it becomes

$$\frac{\partial^2\phi}{\partial x^2} + \frac{\partial^2\phi}{\partial y^2} + \frac{\partial^2\phi}{\partial z^2} = 0 \tag{1.60}$$

which is satisfied by function (1.59).

1.7 WAVE REFLECTION

1.7.1 General Solution for η and ϕ

Let us consider the flow field if a wave train attacks a long vertical breakwater. Let us assume that the breakwater is along line $y = 0$, and the direction of the incident waves makes an angle θ with the y-axis (see Fig. 1.5).

On the ground of some intuitive considerations, we could at once say that specular reflection will occur and that the height and period of the reflected waves will be equal to the height and period of the incident waves; but we believe it to be useful to prove such intuitive knowledge. Therefore, we assume that the direction of the reflected waves makes an unknown angle $\tilde{\theta}$ with the y-axis, and in addition, we allow the possibility that the reflected waves may have a height $\tilde{H}$ and a period $\tilde{T}$ different from height H and period T of the incident waves.

The η and ϕ of the incident waves are given by Eqns (1.56) and (1.59), and the η and ϕ of the reflected waves are given by the same equations with $\tilde{H}$, $\tilde{\omega}$, $\tilde{k}$, and $\tilde{\theta}$ in place of H, ω, k, and θ:

$$\text{reflected waves} \begin{cases} \eta(x,y,t) = \dfrac{\tilde{H}}{2}\cos\left(\tilde{k}x\sin\tilde{\theta} + \tilde{k}y\cos\tilde{\theta} - \tilde{\omega}t + \varepsilon\right) & (1.61) \\ \phi(x,y,z,t) = g\dfrac{\tilde{H}}{2}\tilde{\omega}^{-1}\dfrac{\cosh\left[\tilde{k}(d+z)\right]}{\cosh\left(\tilde{k}d\right)} \\ \qquad \times \sin\left(\tilde{k}x\sin\tilde{\theta} + \tilde{k}y\cos\tilde{\theta} - \tilde{\omega}t + \varepsilon\right) & (1.62) \end{cases}$$

We cannot exclude some phase angle between the reflected and the incident waves, and this is why in the expressions of the reflected waves we have put a phase angle ε that must be determined.

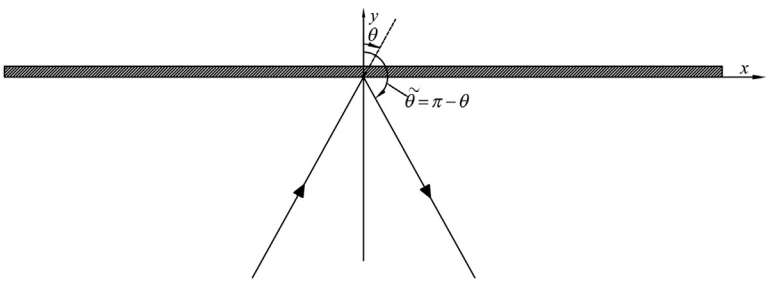

■ FIGURE 1.5 Reflection: reference scheme.

The flow field before the wall is given by the sum of the incident waves (Eqns (1.56) and (1.59) of η and ϕ) and of the reflected waves (Eqns (1.61) and (1.62)):

$$\begin{aligned}\eta(x,y,t) &= \frac{H}{2}\cos\left(kx\sin\theta + ky\cos\theta - \omega t\right) \\ &\quad + \frac{\tilde{H}}{2}\cos\left(\tilde{k}x\sin\tilde{\theta} + \tilde{k}y\cos\tilde{\theta} - \tilde{\omega}t + \varepsilon\right)\end{aligned} \tag{1.63}$$

$$\begin{aligned}\phi(x,y,z,t) &= g\frac{H}{2}\omega^{-1}\frac{\cosh\left[k(d+z)\right]}{\cosh\left(kd\right)}\sin\left(kx\sin\theta + ky\cos\theta - \omega t\right) \\ &\quad + g\frac{\tilde{H}}{2}\tilde{\omega}^{-1}\frac{\cosh\left[\tilde{k}(d+z)\right]}{\cosh\left(\tilde{k}d\right)}\sin\left(\tilde{k}x\sin\tilde{\theta} + \tilde{k}y\cos\tilde{\theta} - \tilde{\omega}t + \varepsilon\right)\end{aligned} \tag{1.64}$$

The boundary condition is

$$\left(\frac{\partial\phi}{\partial y}\right)_{y=0} = 0 \tag{1.65}$$

that is,

$$\begin{aligned}&H\omega^{-1}k\cos\theta\,\frac{\cosh\left[k(d+z)\right]}{\cosh\left(kd\right)}\cos(kx\sin\theta - \omega t) \\ &= -\tilde{H}\tilde{\omega}^{-1}\tilde{k}\cos\tilde{\theta}\,\frac{\cosh\left[\tilde{k}(d+z)\right]}{\cosh\left(\tilde{k}d\right)}\cos\left(\tilde{k}x\sin\tilde{\theta} - \tilde{\omega}t + \varepsilon\right)\end{aligned} \tag{1.66}$$

and it is satisfied whichever the x, z, and t, if and only if

$$\tilde{\omega} = \omega \Rightarrow \tilde{k} = k,\ \ \tilde{H} = H,\ \ \tilde{\theta} = \pi - \theta,\ \ \varepsilon = n2\pi \text{ with } n = 0, 1, 2\ldots\ldots \tag{1.67}$$

Because of the equalities in Eqn (1.67), the two functions (1.63 and 1.64) can be rewritten in the form

$$\eta(x,y,t) = H\cos\left(kx\sin\theta - \omega t\right)\cos\left(ky\cos\theta\right) \tag{1.68}$$

$$\phi(x,y,z,t) = gH\omega^{-1}\frac{\cosh\left[k(d+z)\right]}{\cosh\left(kd\right)}\sin\left(kx\sin\theta - \omega t\right)\cos\left(ky\cos\theta\right) \tag{1.69}$$

1.7.2 The Orthogonal Attack

In the basic case of $\theta = 0$, in which the wave attacks the breakwater orthogonally, the flow becomes two-dimensional y-z and the formulas of η and ϕ reduce themselves to

$$\eta(y,t) = H\cos\left(\omega t\right)\cos\left(ky\right) \tag{1.70}$$

$$\phi(y,z,t) = -gH\omega^{-1}\frac{\cosh[k(d+z)]}{\cosh(kd)}\sin(\omega t)\cos(ky) \tag{1.71}$$

and hence the velocity components are

$$v_y(y,z,t) = gH\omega^{-1}k\frac{\cosh[k(d+z)]}{\cosh(kd)}\sin(\omega t)\sin(ky) \tag{1.72}$$

$$v_z(y,z,t) = -gH\omega^{-1}k\frac{\sinh[k(d+z)]}{\cosh(kd)}\sin(\omega t)\cos(ky) \tag{1.73}$$

Three instant pictures of this basic case are given in Fig. 1.6.

At time $t = 0$, both v_y and v_z are zero everywhere, given that both v_y and v_z are proportional to $\sin(\omega t)$. At that time ($t = 0$), the surface elevation gets to

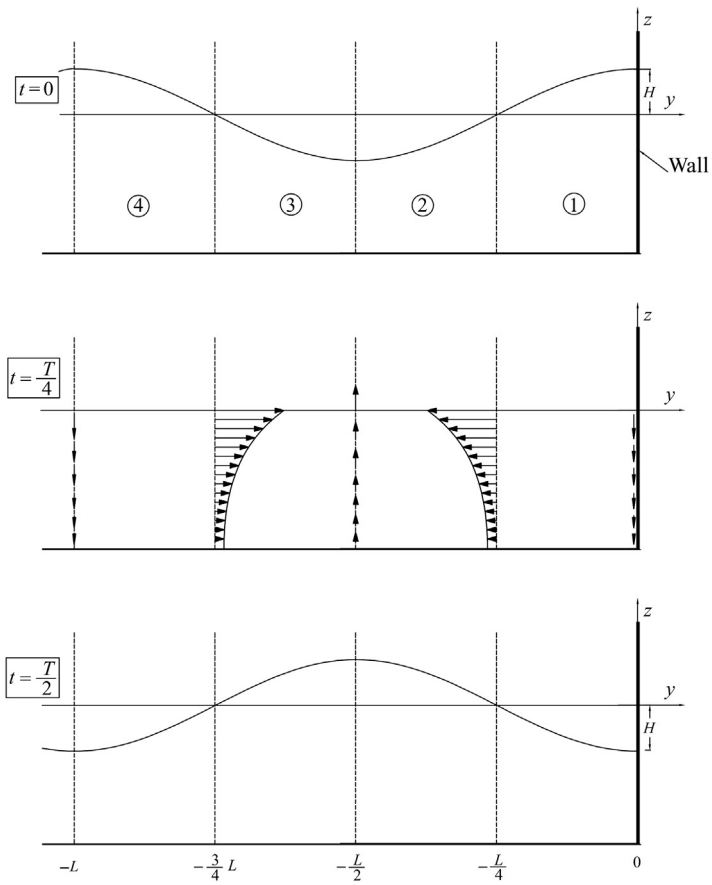

■ **FIGURE 1.6 Three snapshots of the wave field before a vertical breakwater.**

its maximum (positive or negative) at each location. In particular, at the wall, the surface elevation at $t = 0$ is equal to the crest-to-trough height of the incident wave.

At time $t = T/4$, the surface elevation is zero everywhere, given that η is proportional to $\cos(\omega t)$. The horizontal velocity has its negative maximum at $y = -L/4$, and it has its positive maximum at $y = -\frac{3}{4}L$. The vertical velocity has its negative maximum at the wall ($y = 0$) and at $y = -L$, and it has its positive maximum at $y = -L/2$.

At time $t = T/2$, the surface elevation is opposite with respect to the surface elevation at $t = 0$. Thus, a consistent picture emerges, where:

1. at time $t = 0$, the water surface is higher than the MWL in sections ① and ④, and is lower than the mean water level (MWL) in sections ② and ③ (Fig. 1.6);
2. vice-versa, at time $t = T/2$ the water surface is lower than the MWL in sections ① and ④, and is higher than the MWL in sections ② and ③;
3. consistently, at the intermediate time instant $t = T/4$, the water flows from sections ① and ④ toward sections ② and ③.

There are some points (nodes) where the surface elevation is always zero, and where the horizontal velocity attains its absolute maximum. These points are at $\frac{1}{4}, \frac{3}{4}, \frac{5}{4}, \ldots$ wavelengths from the wall. Then there are the antinodes, at $0, \frac{1}{2}, 1, \frac{3}{2}, \ldots$ wavelengths from the wall, where the wave height (on the time domain) and the vertical velocity attain their absolute maximum.

The wave height in the time domain at the antinodes is $2H$, which is twice the wave height that would be there without the wall. The velocity maxima are also twice the maxima in the absence of the wall.

1.7.3 The Pressure Distribution on the Breakwater

Whichever the angle θ of the waves, the maximum pressure at any fixed section of the breakwater, according to Stokes' first order, is given by

$$p(z) = -\rho g z + \rho g H \frac{\cosh\left[k(d+z)\right]}{\cosh\left(kd\right)} \tag{1.74}$$

which proceeds from Eqn (1.69) of ϕ, and can be rewritten in the equivalent form (apart from a term of order H^2):

$$p(z)\begin{cases} = -\rho g z + \rho g H \dfrac{\cosh\left[k(d+z)\right]}{\cosh\left(kd\right)} & \text{if} \quad z \le 0 \qquad (1.75) \\ = \rho g (H - z) & \text{if} \quad 0 \le z \le H \qquad (1.76) \end{cases}$$

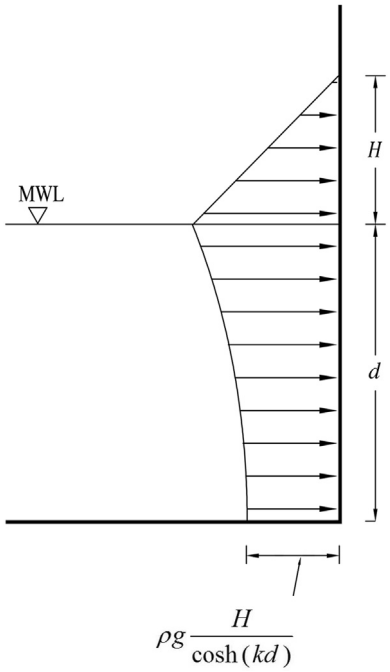

■ **FIGURE 1.7 The pressure exerted on a vertical breakwater by a wave crest.**

The wave pressure, that is, the difference between the actual pressure and the static pressure, is shown in Fig. 1.7.

For the formal step from Eqns (1.74)–(1.76), note that

$$H\frac{\cosh[k(d+z)]}{\cosh(kd)} = H + o(H) \text{ if } 0 < z < H \tag{1.77}$$

1.8 WAVE DIFFRACTION

1.8.1 Interaction with a Semi-infinite Breakwater

Let us consider a vertical breakwater along the line $y = 0$, with the origin at $x = 0$ and negligible thickness. The flow field that would be there without the breakwater is the one given by formulas (1.56) and (1.59) of η and ϕ.

From the solution of Penney and Price (1952), the surface elevation and the velocity potential to Stokes' first order, in polar coordinates, are given by

$$\eta(r,\beta,t) = \frac{H}{2}[F(r,\beta;\omega,\theta)\cos(\omega t) + G(r,\beta;\omega,\theta)\sin(\omega t)] \tag{1.78}$$

$$\phi(r,\beta,z,t) = g\frac{H}{2}\omega^{-1}\frac{\cosh[k(d+z)]}{\cosh(kd)}[G(r,\beta;\omega,\theta)\cos(\omega t) - F(r,\beta;\omega,\theta)\sin(\omega t)] \tag{1.79}$$

where

$$F(r,\beta;\omega,\theta) \equiv A(u_1)\cos q_1 + A(u_2)\cos q_2 - B(u_1)\sin q_1 - B(u_2)\sin q_2 \tag{1.80}$$

$$G(r,\beta;\omega,\theta) \equiv A(u_1)\sin q_1 + A(u_2)\sin q_2 + B(u_1)\cos q_1 + B(u_2)\cos q_2 \tag{1.81}$$

$$A(u) \equiv \frac{1}{2}[1 + S_{FR}(u) + C_{FR}(u)], \quad B(u) \equiv \frac{1}{2}[S_{FR}(u) - C_{FR}(u)] \tag{1.82}$$

$$S_{FR}(u) \equiv \int_0^u \sin\left(\frac{\pi}{2}x^2\right)dx, \quad C_{FR}(u) \equiv \int_0^u \cos\left(\frac{\pi}{2}x^2\right)dx \tag{1.83}$$

$$u_1 \equiv 2\sqrt{kr/\pi}\sin\left[\frac{1}{2}\left(\beta+\theta-\frac{\pi}{2}\right)\right], \quad u_2 \equiv -2\sqrt{kr/\pi}\sin\left[\frac{1}{2}\left(\beta-\theta+\frac{\pi}{2}\right)\right] \tag{1.84}$$

$$q_1 \equiv kr\sin(\beta+\theta), \quad q_2 \equiv -kr\sin(\beta-\theta) \tag{1.85}$$

cf. Fig. 1.8 for the symbols.

Let us arbitrarily fix a point r, β and let us write F and G in place of $F(r, \beta, \omega, \theta)$ and $G(r, \beta; \omega, \theta)$. The surface elevation on the time domain, at the fixed point, has its maxima and minima at times t_m such that

$$\omega t_m = \arctan\left(\frac{G}{F}\right) \tag{1.86}$$

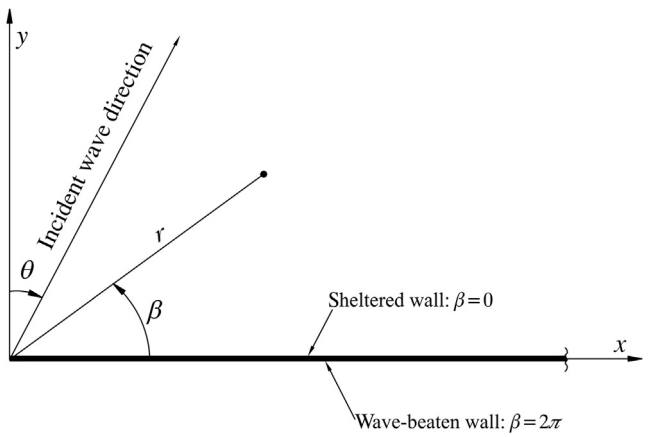

■ **FIGURE 1.8 Reference scheme for the interaction between waves and a semi-infinite breakwater.**

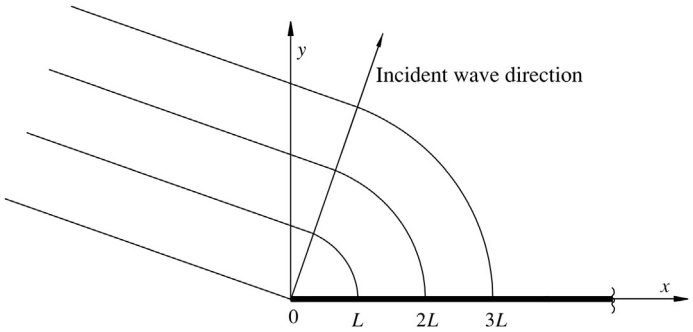

■ **FIGURE 1.9 Wavefronts behind a semi-infinite breakwater.**

Equation (1.86) admits two solutions:

$$\sin(\omega t_{m1}) = \frac{G}{\sqrt{F^2+G^2}}, \quad \cos(\omega t_{m1}) = \frac{F}{\sqrt{F^2+G^2}} \tag{1.87}$$

and

$$\sin(\omega t_{m2}) = -\sin(\omega t_{m1}), \quad \cos(\omega t_{m2}) = -\cos(\omega t_{m1}) \tag{1.88}$$

which, once substituted in Eqn (1.78), give

$$\eta(t_{m1}) = \frac{H}{2}\sqrt{F^2+G^2}, \quad \eta(t_{m2}) = -\frac{H}{2}\sqrt{F^2+G^2} \tag{1.89}$$

Therefore, t_{m1} is the time instant of the crest and t_{m2} is the time instant of the trough at the fixed point. Clearly, instants t_{m1} and t_{m2} generally change from one point to another since they depend on functions F and G. The wavefronts (see Fig. 1.9) are the lines connecting points with the same value of t_{m1} (or t_{m2}).

1.8.2 The Diffraction Coefficient

From Eqn (1.89), it follows that the wave height (that is, the height of the wave on the time domain) is

$$H(r,\beta) = H\sqrt{F^2+G^2} \tag{1.90}$$

As a consequence, the diffraction coefficient, which is defined as the quotient between the wave height at a given point and the height of the incident waves, is given by

$$C_d(r,\beta) = \sqrt{F^2+G^2} \tag{1.91}$$

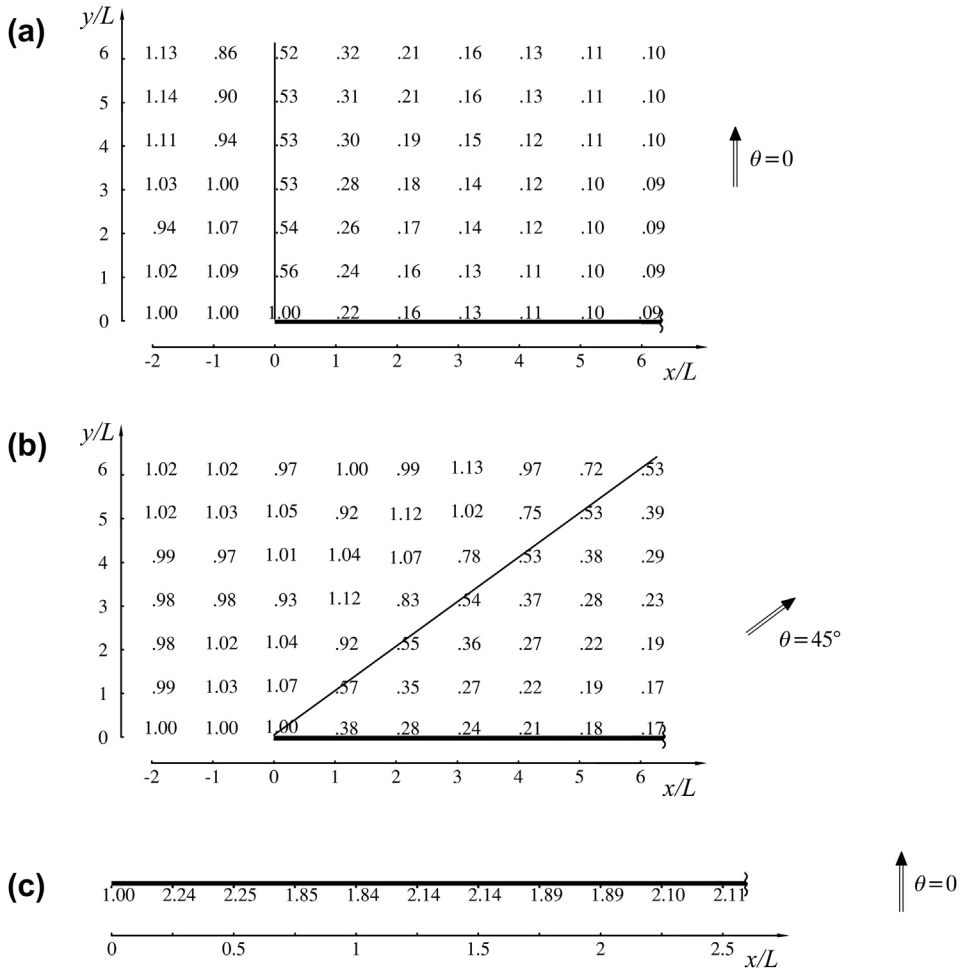

■ **FIGURE 1.10 Diffraction coefficient.** (a) Behind the breakwater (orthogonal wave attack), (b) behind the breakwater (inclined attack), and (c) along the wave-beaten wall (orthogonal attack).

The C_d for two different angles of the wave direction are given in Fig. 1.10(a) and (b). Of course, the diffraction coefficient at the sheltered side of the breakwater gets smaller and smaller with the distance from the tip of the breakwater. At the wave-beaten side of the breakwater ($\beta = 2\pi$), C_d takes on a maximum somewhat greater than 2.0, close to the tip of the breakwater (Fig. 1.10(c)).

1.9 ENERGY FLUX AND WAVE ENERGY

Let us consider a y-z flow, with y being the wave direction. The mean energy flux per unit length is given by

$$\Phi = \left\langle \int_{-d}^{\eta} \left[p + \rho g z + \frac{1}{2}\rho\left(v_y^2 + v_z^2\right)\right] v_y \mathrm{d}z \right\rangle \tag{1.92}$$

where the angle brackets denote an average with respect to time t. With Eqn (1.31) of p and Eqn (1.29) of v_y, and neglecting the terms of an order smaller than H^2, we get

$$\begin{aligned}\Phi = \Bigg\langle \int_{-d}^{0} \rho g \frac{H}{2} \frac{\cosh\left[k(d+z)\right]}{\cosh\left(kd\right)} \cos\left(ky - \omega t\right) \\ \times g \frac{H}{2} \omega^{-1} k \frac{\cosh\left[k(d+z)\right]}{\cosh\left(kd\right)} \cos\left(ky - \omega t\right) \mathrm{d}z \Bigg\rangle\end{aligned} \tag{1.93}$$

On inverting the order average with respect to t-integral with respect to z, we arrive at

$$\Phi = \rho g^2 \frac{H^2}{8} \omega^{-1} k \int_{-d}^{0} \frac{\cosh^2\left[k(d+z)\right]}{\cosh^2\left(kd\right)} \mathrm{d}z \tag{1.94}$$

Since

$$k \int_{-d}^{0} \cosh^2[k(d+z)]\mathrm{d}z = \frac{1}{4}[\sinh(2kd) + 2kd] \tag{1.95}$$

Equation (1.94) becomes

$$\Phi = \rho g^2 \frac{H^2}{8} \omega^{-1} \frac{1}{4} \frac{[\sinh\left(2kd\right) + 2kd]}{\cosh^2\left(kd\right)} \tag{1.96}$$

Finally, multiplying and dividing the RHS by $\sinh(kd)$, it follows that

$$\Phi = \rho g \frac{H^2}{8} \frac{c}{2} \left[1 + \frac{2kd}{\sinh\left(2kd\right)}\right] \tag{1.97}$$

where use has been made of the equation of the phase speed

$$c = \frac{L}{T} = \frac{gT}{2\pi} \tanh\left(kd\right) \tag{1.98}$$

Let us pass to the equation of the mean wave energy per unit surface. This is

$$\mathscr{E} = \left\langle \int_0^{\eta} \rho g z \right\rangle + \left\langle \int_{-d}^{\eta} \frac{1}{2}\rho\left(v_y^2 + v_z^2\right) \mathrm{d}z \right\rangle \tag{1.99}$$

where, neglecting the terms of order smaller than H^2, and performing a few steps like those we have done for obtaining the compact form of Φ, we arrive at

$$\mathscr{E} = \frac{1}{8}\rho g H^2 \tag{1.100}$$

1.10 THE GROUP VELOCITY

Let us assume that the wavemaker of a waveflume is switched. Initially, we would see some waves close to the wavemaker with the rest of the waveflume still being calm. Then, we would see the wave zone widen gradually. We have

1. average energy entering the CV of Fig. 1.11(a) in the unit time $= \Phi b$,
2. average increment of the wave energy in the CV in the unit time $= \mathscr{E} b c_G$,

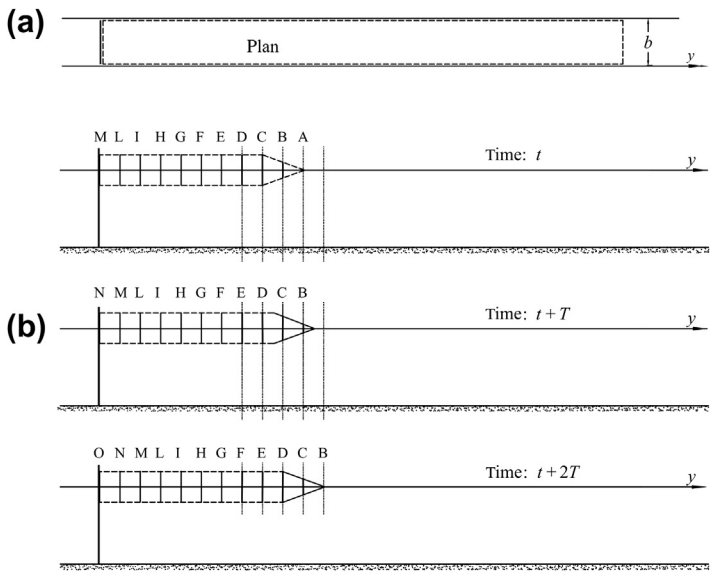

■ **FIGURE 1.11** (a) Plan view of a waveflume and control volume for the deduction of Eqn (1.102) of c_G. (b) Three pictures taken a wave period from each other, while the wave motion advances on an initially still basin (the waves are sketched as vertical segments).

where c_G is the propagation speed of the wave motion on the waveflume. Hence,

$$\Phi b = \mathscr{E} b c_G \tag{1.101}$$

and, with Eqns (1.97) and (1.100) of Φ and $\mathscr{E}$:

$$c_G = \frac{c}{2}\left[1 + \frac{2kd}{\sinh(2kd)}\right] \tag{1.102}$$

Here, it can be readily verified that c_G is generally smaller than c, and on deep water, c_G is half the c. Let us see the reason for this.

Figure 1.11(b) shows three instant pictures of the waveflume taken an interval T from each other. The waves are sketched as vertical segments; the height of the segment is equal to the wave height and the interval between two consecutive segments is equal to the wavelength. Each single wave advances a wavelength L in a wave period T, so that its propagation speed (phase speed) is L/T. It is not so for the wave group that advances by a wavelength in two wave periods, so that its propagation speed is $c/2$. The propagation speed of the group is smaller than the propagation speed of each single wave, simply because each single wave goes to die at the group head. In particular, in the first picture, wave A is going to die; then in the third picture, two periods later, wave B is going to die; then it will be the turn of C, D, and so on. (Of course, the envelope front in Fig. 1.11(b) has been somewhat simplified.)

1.11 CONCLUSION

The basic concepts of this chapter are founded on the work of Airy (1845) and Stokes (1847).

REFERENCES

Airy, G.B., 1845. Tides and Waves. Encyclopaedia Metropolitana. Scientific Department, London, pp. 241–396.

Penney, W.G., Price, A.T., 1952. The diffraction theory of sea waves and the shelter afforded by breakwaters. Philos. Trans. R. Soc. Lond. A 244, 236–253.

Stokes, G.G., 1847. On the theory of oscillatory waves. Trans. Cambridge Philos. Soc. 8, 441–455.

Chapter 2

Wave Transformation near Coasts

CHAPTER OUTLINE

2.1 REFRACTION WITH STRAIGHT CONTOUR LINES

With reference to Fig. 2.1, s is the local direction of wave advance at a point P on water depth, d, and α is the angle between the wave direction and x-axis. We assume that the seabed is gently sloped so that in a neighborhood of point P, the horizontal particle velocity is

$$v_s(s,z,t) = g\frac{H}{2}\omega^{-1}k\frac{\cosh\left[k(d+z)\right]}{\cosh\left(kd\right)}\cos\left(ks-\omega t\right) \tag{2.1}$$

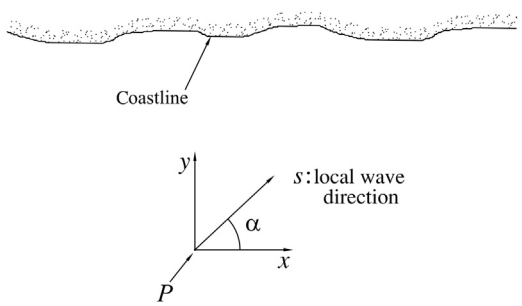

■ **FIGURE 2.1 Reference scheme: waves approaching a coast.**

Wave Mechanics and Wave Loads on Marine Structures. http://dx.doi.org/10.1016/B978-0-12-800343-5.00002-0

The x,y component of the radiation stress tensor, that is, the x-component of the mean flux of linear momentum, per unit length, through a y-orthogonal plane is

$$R_{yx} = \left\langle \int_{-d}^{\eta} \rho v_s^2 \sin\alpha \cos\alpha \, dz \right\rangle \tag{2.2}$$

Here we may proceed like we have done for Φ in Section 1.9. That is, we neglect the terms of order smaller than H^2, which enables us to pass

$$\text{from} \int_{-d}^{\eta} \text{ to } \int_{-d}^{0}$$

then we invert the order average with respect to time t—integral with respect to z, and we can arrive at

$$R_{xy} = R_{yx} = \frac{1}{16}\rho g H^2 \left[1 + \frac{2kd}{\sinh(2kd)}\right] \sin\alpha \cos\alpha \tag{2.3}$$

Let us consider the control volume (CV) of Fig. 2.2 before a coast. Because of the x-parallel contour lines, the mean characteristics of the wave motion do not change with x and change only with y. Therefore, the energy equation and the x-component of the linear momentum equation when applied to the CV of Fig. 2.2 give

$$\Phi(y_2)\sin\alpha_2 = \Phi(y_1)\sin\alpha_1 \tag{2.4}$$

$$R_{yx}(y_2) = R_{yx}(y_1) \tag{2.5}$$

If y_1 is on deep water and y_2 is on water depth, d, these two equations yield

$$H^2 \tanh(kd)\left[1 + \frac{2kd}{\sinh(2kd)}\right] \sin\alpha = H_0^2 \sin\alpha_0 \tag{2.6}$$

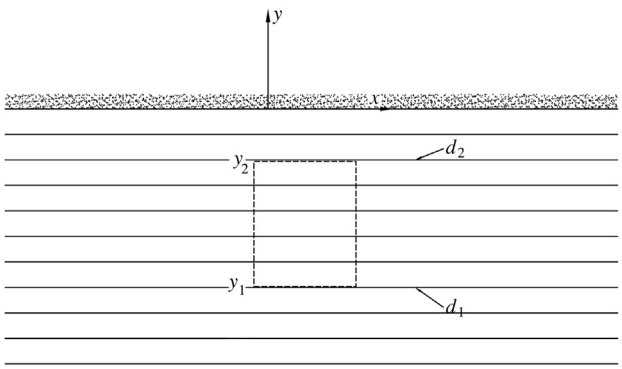

■ **FIGURE 2.2 The control volume extending from water depth d_1 to water depth d_2, with straight contour lines.**

$$H^2\left[1+\frac{2kd}{\sinh(2kd)}\right]\sin\alpha\cos\alpha = H_0^2\sin\alpha_0\cos\alpha_0 \tag{2.7}$$

where use has been made of Eqn (1.97) of Φ and Eqn (2.3) of R_{yx}.

From (Eqns (2.6) and (2.7)) we obtain

$$\cos\alpha = \cos\alpha_0\tanh(kd) = \cos\alpha_0 c/c_0 \tag{2.8}$$

which enables us to obtain angle α on water depth, d, once angle α_0 on deep water is known.

Referring to the basic case in which the wave travels landward, angles α_0 and α range between 0 and π, and thus

$$\sin\alpha_0 = \sqrt{1-\cos^2\alpha_0} \tag{2.9}$$

$$\sin\alpha = \sqrt{1-\tanh^2(kd)\cos^2\alpha_0} \tag{2.10}$$

At this stage, with $\cos\alpha$ and $\sin\alpha$ being known, we can operate on either (Eqn (2.6)) or (Eqn (2.7)) to obtain also H. The result is

$$H = H_0\sqrt{\frac{\sinh(2kd)}{\tanh(kd)[\sinh(2kd)+2kd]}}\sqrt[4]{\frac{1-\cos^2\alpha_0}{1-\tanh^2(kd)\cos^2\alpha_0}} \tag{2.11}$$

This equation enables us to get wave height H on water depth d, once height H_0 and angle α_0 on deep water are known. The ratio H/H_0 for $\alpha_0 = 90^\circ$ is the shoaling coefficient (C_s).

Figure 2.3 shows the ratio H/H_0 as a function of d/L_0 for some given value of α_0. (Note Eqn (2.11) gives H/H_0 as a function of kd, whereas Fig. 2.3 shows H/H_0 as a function of d/L_0. This is possible because kd is a function of d/L_0. Indeed from (Eqn (1.24)), it follows that

$$\frac{d}{L_0} = \frac{d}{L}\tanh\left(2\pi\frac{d}{L}\right) \tag{2.12}$$

which implies that a unique value of $kd = 2\pi d/L$ exists for any given value of d/L_0.) As d/L_0 approaches zero, H/H_0 tends to infinity. Of course, this growth of wave height is interrupted by wave breaking.

2.2 REFRACTION WITH ARBITRARY CONTOUR LINES

2.2.1 Wave Orthogonals

In the previous section, we solved the problem of the control volume extending from deep to shallow water for the basic case of straight contour lines. Here, we deal with the same problem for the case of arbitrary contour

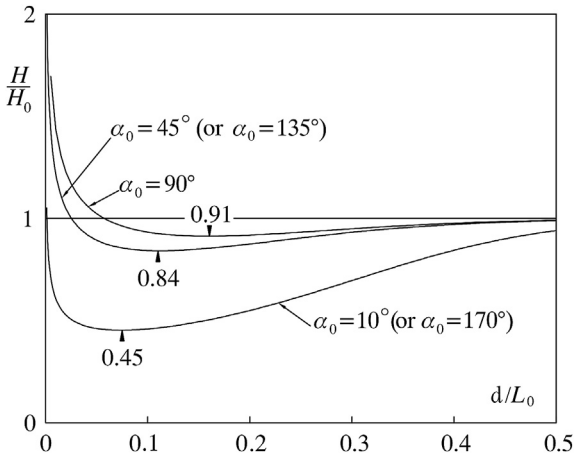

■ **FIGURE 2.3 Variation of the wave height with the water depth for given wave direction on deep water. (Obtained by means of Eqn (2.11).)**

lines. To this end, it is convenient to preliminarily solve the refraction problem.

Let us fix a point P in the horizontal plane, and let us define the natural coordinates: s with the local wave direction and q orthogonal to s. The inclination of a small stretch $\mathrm{d}q$ of wave front varies in a small time interval $\mathrm{d}t$ of

$$\mathrm{d}\alpha = \frac{c\mathrm{d}t - \left(c + \frac{\partial c}{\partial q}\mathrm{d}q\right)\mathrm{d}t}{\mathrm{d}q} = -\frac{\partial c}{\partial q}\mathrm{d}t \tag{2.13}$$

where α and c denote, respectively, the angle of the wave front and the propagation speed at point P (see Fig. 2.4). Since

$$\mathrm{d}s = c\mathrm{d}t \tag{2.14}$$

(Eqn (2.13)) may by rewritten as

$$\frac{\mathrm{d}\alpha}{\mathrm{d}s} = -\frac{1}{c}\frac{\partial c}{\partial q} \tag{2.15}$$

Here, it is convenient to express $\partial c/\partial q$ in terms of the derivatives $\partial c/\partial x$ and $\partial c/\partial y$ (x and y being as usual the fixed axes). Since

$$\frac{\partial c}{\partial q}\mathrm{d}q = \frac{\partial c}{\partial x}(-\mathrm{d}q\sin\alpha) + \frac{\partial c}{\partial y}\mathrm{d}q\cos\alpha \tag{2.16}$$

it follows that

$$\frac{\mathrm{d}\alpha}{\mathrm{d}s} = \frac{1}{c}\left(\frac{\partial c}{\partial x}\sin\alpha - \frac{\partial c}{\partial y}\cos\alpha\right) \tag{2.17}$$

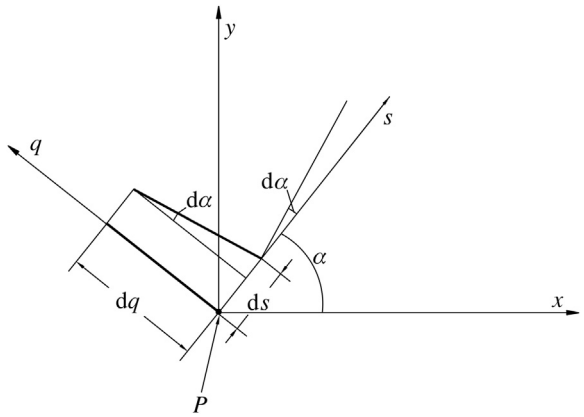

■ **FIGURE 2.4 Refraction: the short stretch dq of wave front, covering the distance ds, rotates through dα.**

Applying the chain rule, Eqn (2.17) may be rewritten in the form

$$\frac{\mathrm{d}\alpha}{\mathrm{d}s} = \frac{1}{c}\left(\frac{\mathrm{d}c}{\mathrm{d}d}\,\frac{\partial d}{\partial x}\sin\alpha - \frac{\mathrm{d}c}{\mathrm{d}d}\,\frac{\partial d}{\partial y}\cos\alpha\right) \tag{2.18}$$

Hence, obtaining the formula of dc/dd from (Eqn (1.24)) of L, we arrive at

$$\frac{\mathrm{d}\alpha}{\mathrm{d}s} = \frac{2k}{\sinh(2kd) + 2kd}\left(\frac{\partial d}{\partial x}\sin\alpha - \frac{\partial d}{\partial y}\cos\alpha\right) \tag{2.19}$$

This form of dα/ds is convenient for obtaining a wave orthogonal; that is, a curve whose tangent vector gives the local wave direction. Given angle α_0 and a point x_0,y_0 of the orthogonal on deep water, this orthogonal is calculated with finite increments Δs through

$$\alpha(s + \Delta s) = \alpha(s) + \frac{\mathrm{d}\alpha}{\mathrm{d}s}\Delta s \tag{2.20}$$

$$x(s + \Delta s) = x(s) + \cos\alpha\,\Delta s - \frac{1}{2}\sin\alpha\,\frac{\mathrm{d}\alpha}{\mathrm{d}s}\Delta s^2 \tag{2.21}$$

$$y(s + \Delta s) = y(s) + \sin\alpha\,\Delta s + \frac{1}{2}\cos\alpha\,\frac{\mathrm{d}\alpha}{\mathrm{d}s}\Delta s^2 \tag{2.22}$$

Of course, the wave orthogonal depends on the wave period. As an example, Fig. 2.5 shows some wave orthogonals before a promontory, for two distinct values of angle α_0, and the same wave period.

2.2.2 Effects on the Wave Height

Let us consider a CV whose horizontal section is bounded by two adjacent wave orthogonals (2 and 3 in Fig. 2.6) and two short stretches of wave front

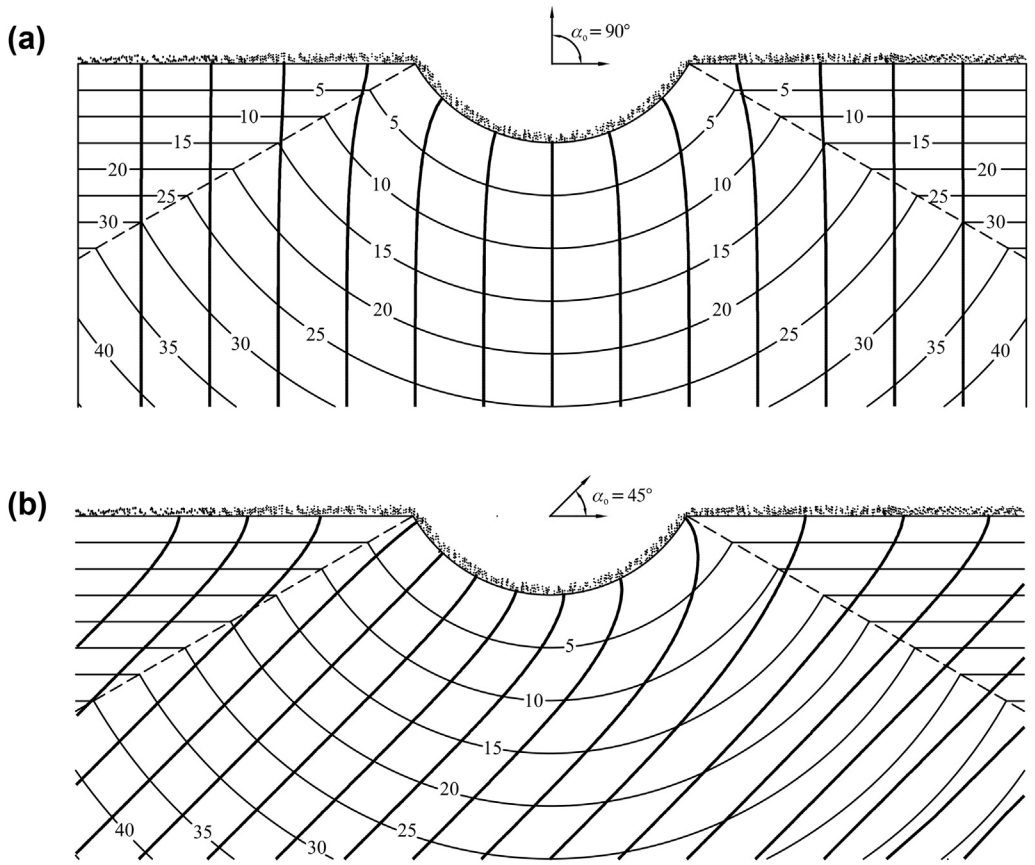

■ **FIGURE 2.5** Two sets of wave orthogonals ((a) and (b)) for two distinct wave directions on deep water, and the same wave period ($T = 10$ s). (Obtained by means of Eqns (2.19)—(2.22).)

(0 and 1 in Fig. 2.6). There is no energy flux through the two orthogonals. Hence, the mean energy flux through the stretch of wave front 0 on deep water must equal the mean energy flux through the stretch of wave front 1 on given water depth d. With Eqn (1.97) of the mean energy flux per unit length, we obtain

$$\frac{1}{8}\rho g H_0^2 c_0 \frac{1}{2} b_0 = \frac{1}{8}\rho g H^2 c \frac{1}{2}\left[1 + \frac{2kd}{\sinh(2kd)}\right] b_1 \tag{2.23}$$

which is reduced to

$$H = H_0 \sqrt{\frac{\sinh(2kd)}{\tanh(kd)[\sinh(2kd) + 2kd]}} \sqrt{\frac{b_0}{b_1}} \tag{2.24}$$

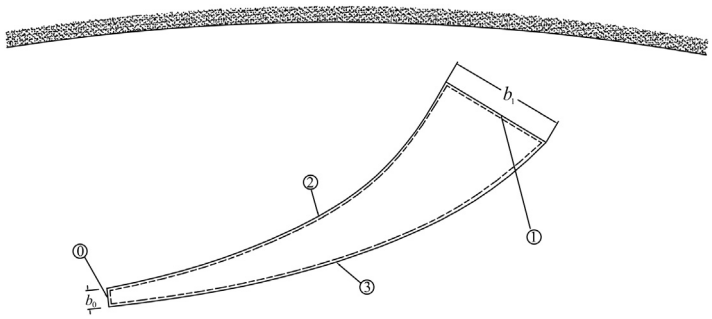

■ **FIGURE 2.6 A control volume from deep to shallow water bounded by two wave orthogonals and two short stretches of wave front.**

where d, H, and k are water depth, wave height, and wave number at section ①, and H_0 is the wave height at section ⓪ on deep water. Clearly, this result requires b_1 to be small enough and for the wave height to be nearly constant on the stretch of wave front.

2.3 WAVE—CURRENT INTERACTION IN SOME STRAITS

2.3.1 Current Only

Let us consider a marine strait. To fix our ideas, we may think of the Straits of Messina. Along the longitudinal axis, the water depth reduces to a minimum. In particular, in the Straits of Messina, the water depth is at a minimum (nearly 100 m) somewhat northerly of Messina. Often, some currents take place where the strait has its lowest depth. These currents in the Straits of Messina are due to the flow from the Ionian Sea to the Tyrrhenian Sea and vice versa.

Let us think of a strait as a straight channel of constant width, with a minimum water depth at $y = 0$ and with water depth tending to infinity as $y \to \pm\infty$. As in the problem of shoaling-refraction, let us assume the bottom slope to approach zero.

Let us analyze first the case of a current without waves, with a discharge Q per unit length. Referring to Fig. 2.7, we call

S	the difference between the still water level and the actual water level;
d	the depth of the still water;
$\tilde{d} \equiv d - S$	the water depth; and
$u = Q/\tilde{d}$	the velocity of the current.

Under ideal flow assumptions, the Bernoulli equation implies

$$S = \frac{u^2}{2g} \tag{2.25}$$

As a consequence, u, d, and Q are related to each other by

$$u = \frac{Q}{d - u^2/2g} \tag{2.26}$$

which may be rewritten in the form

$$\frac{ud}{Q} = 1 + \left(\frac{Q}{Q^*}\right)^2 \left(\frac{ud}{Q}\right)^3 \tag{2.27}$$

with

$$Q^* \equiv \sqrt{2gd}\, d \tag{2.28}$$

Equality (Eqn (2.27)) admits two positive solutions for ud/Q, provided that

$$|Q| \langle Q_{\max} = \frac{2}{3\sqrt{3}} Q^* \tag{2.29}$$

The lowest of these two solutions is the right one. The second solution yields $d - S \to 0$ as Q approaches zero, and hence must be discarded.

2.3.2 Current + Waves: The Wavelength

If we multiply by d both sides of (Eqn (1.53)) and use definition (Eqn (1.26)) of L_0, we may rewrite (Eqn (1.53)) in the form

$$\frac{d}{L_c} \tanh\left(2\pi \frac{d}{L_c}\right) = a\left(\frac{d}{L_c} - b\right)^2 \tag{2.30}$$

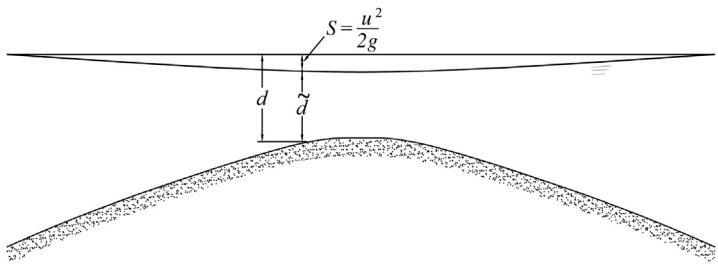

■ **FIGURE 2.7 Reference scheme for a steady current on a channel of varying depth.** The bottom slope is assumed to approach zero.

where L_c denotes wavelength on current:

$$L_c \equiv 2\pi/k_c \tag{2.31}$$

and where

$$a \equiv \frac{1}{d/L_0}\left(\frac{u}{c_0}\right)^2 \tag{2.32}$$

$$b \equiv \frac{d}{L_0}\Big/\left(\frac{u}{c_0}\right) \tag{2.33}$$

with $c_0 \equiv L_0/T$ and $u \neq 0$.

The d/L_c satisfying (Eqn (1.47)) is equal to the positive value of x (provided that it exists) such that function

$$f_1(x) \equiv x \tanh(2\pi x) \tag{2.34}$$

is equal to function

$$f_2(x) \equiv a(x-b)^2 \tag{2.35}$$

Therefore, in order to get the wavelength L_c on the current, we must seek the d/L_c such that

$$f_1\left(\frac{d}{L_c}\right) = f_2\left(\frac{d}{L_c}\right) \tag{2.36}$$

The two functions $f_1(x)$ and $f_2(x)$ are represented in Fig. 2.8 for $d/L_0 = 0.2$ and a few values of u/c_0.

Generally, there are two values of d/L_c that satisfy Eqn (2.36). However, the solution must be the smallest one of these two, if we admit that d/L_c is a continuous function of u/c_0 for given d/L_0. For any given d/L_0, a negative value $(u/c_0)_{crit}$ exists for which there is a unique d/L_c satisfying (Eqn (2.36)).

For negative (u/c_0), whose absolute value is greater than $\left|(u/c_0)_{crit}\right|$, there does not exist any d/L_c that satisfies (Eqn (2.36)) (Fig. 2.8(d)). In this case, the wave cannot travel against the stream.

2.3.3 Current + Waves: The Wave Height

A detailed derivation of the solution for the variation of the wave height along the strait is given by (Boccotti, 2000, Section 2.10). Here, we see how to apply this solution.

The input data are H_0, T, and Q. The target is the wave height H on a given water depth d (d being the depth of the still water level). Let us fix a sequence

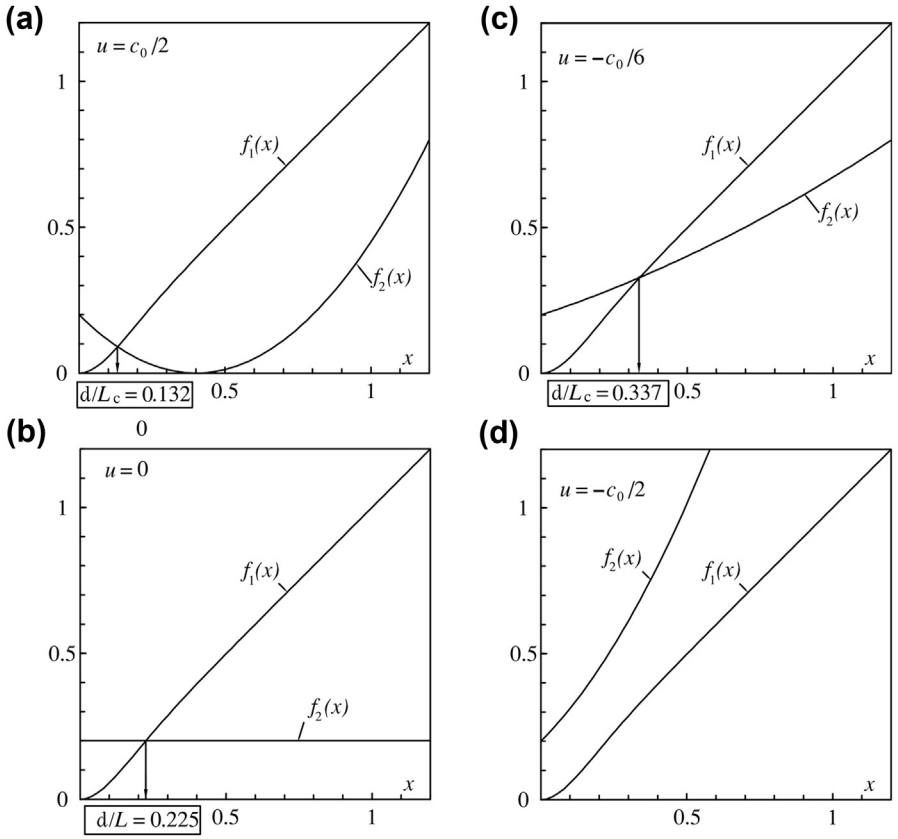

■ **FIGURE 2.8** The wavelength on water depth $d/L_0 = 0.2$ for: (a) a positive current; (b) no current; (c) a low negative current; and (d) a strong negative current, for which Eqn (2.30) does not admit any solution (the wave is not able to travel against the stream).

of growing depths d_i ($i = 1, \ldots, N$) with $d_1 = d$. For each depth d_i, we do the following:

Step (1) to find the smallest positive solution for the equation

$$x = 1 + \left(\frac{Q}{Q_i}\right)^2 x^3 \quad \text{with} \quad Q_i = \sqrt{2gd_i}\, d_i \tag{2.37}$$

and compute

$$u_i = \left(\frac{Q}{d_i}\right)x, \quad S_i = \frac{u_i^2}{2g}, \quad \widetilde{d}_i = d_i - S_i \tag{2.38}$$

Step (2) to find the smallest positive solution (x_i') of the equation

$$x \tanh(2\pi x) = a_i(x - b_i)^2 \quad \text{with} \quad a_i = \frac{L_0}{\widetilde{d}_i}\left(\frac{u_i}{c_0}\right)^2, \quad b_i = \frac{\widetilde{d}_i/L_0}{u_i/c_0} \tag{2.39}$$

and compute

$$L_{c_i} = \frac{\widetilde{d}_i}{x_i'}, k_{c_i} = \frac{2\pi}{L_{c_i}} \tag{2.40}$$

Step (3) to compute

$$O_i = (\omega - u_i k_{c_i})^{-1} \tag{2.41}$$

$$CH_i = \cosh^2\left(k_{c_i}\widetilde{d}_i\right) \tag{2.42}$$

$$SH_i = \sinh\left(2k_{c_i}\widetilde{d}_i\right) \tag{2.43}$$

$$K_i = \frac{1}{16} g O_i^2 u_i k_{c_i}^2 \frac{\widetilde{d}_i}{CH_i} + \frac{1}{32} g \left[\frac{2k_{c_i}\widetilde{d}_i + SH_i}{CH_i}\right] O_i(1 + u_i k_{c_i} O_i) + \frac{u_i}{8} \tag{2.44}$$

$$A_i = \left(g\frac{H_0^2}{16}\omega^{-1} - \frac{1}{2}\pi S_i \frac{H_0^2}{T}\right)\frac{1}{K_i} \tag{2.45}$$

$$B_i = \frac{2S_i u_i - Q}{K_i} \tag{2.46}$$

$$C_i = -\frac{H_0^2}{16} + \frac{1}{2}\pi \frac{u_i}{g}\frac{H_0^2}{T} \tag{2.47}$$

$$D_i = \frac{1}{16} + \frac{1}{8} g O_i^2 k_{c_i}^2 \frac{\widetilde{d}_i}{CH_i} \tag{2.48}$$

$$E_i = -3S_i \tag{2.49}$$

$$F_i = C_i + A_i D_i \tag{2.50}$$

$$G_i = B_i D_i + E_i \tag{2.51}$$

Step (4) to obtain the sequence Δ_i for i from $i = N - 1$ to 1 by means of

$$\Delta_i = \frac{0.5(d_i + d_{i+1})\Delta_{i+1} - F_i + F_{i+1} + G_{i+1}\Delta_{i+1}}{G_i + 0.5(d_i + d_{i+1})} \tag{2.52}$$

where Δ_i represents the wave set-down (or set-up) on water depth d_i (d_N is taken so large that Δ_N may be assumed to be zero);

Step (5) to obtain the wave height H on the given water depth d by means of

$$H = \sqrt{A_1 + B_1\Delta_1} \tag{2.53}$$

2.4 WORKED EXAMPLE

Let us imagine building a submerged tunnel across a strait—see Fig. 2.9. Let us compute the Froude–Krylov force, that is, the force on a ideal water

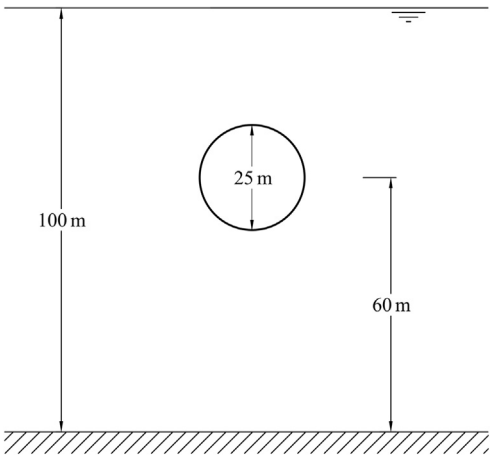

■ **FIGURE 2.9 Reference scheme for the worked example of Section 2.4: evaluation of the Froude–Krylov force on a submerged tunnel loaded by waves on an adverse current.**

cylinder having the same radius and being located at the same depth as the tunnel.

The components of the Froude–Krylov force per unit length may be estimated as

$$f_y = \rho\pi R^2 a_y \tag{2.54}$$

$$f_z = \rho\pi R^2 a_z \tag{2.55}$$

where the a_y and a_z are given by Eqns (1.54) and (1.55).

Let $H_0 = 15$ m, $T = 12$ s, $Q = -200$ m^3/s/m (negative Q means that the current is adverse to the wave propagation). The still water depth, d, and the elevation ζ of the cylinder center above the seabed are, respectively, 100 and 60 m as shown in Fig. 2.9. The diameter of the cylinder is of 25 m.

The calculation is done with the following FORTRAN program.

```
PROGRAM CURRENT
DIMENSION AV(1000),BV(1000),DV(1000),GV(1000),FV(1000)
DIMENSION DELTAV(1000),RKCIV(1000),DSTIV(1000)
PG=3.141592
DPG=2.*PG
DG=2.*9.8
RO=1030.

WRITE(6,*)'d,zitac,diam'
READ(5,*)D,ZITAC,DIAM
ZC=D-ZITAC
```

```
     .RAGG=DIAM/2.
      AREA=PG*RAGG*RAGG
      WRITE(6,*)'HO,T'
      READ(5,*)HO,T
      OM=DPG/T
      WRITE(6,*)'Q m3/s/m (positive or negative)'
      READ(5,*)Q
      TOLL=1.E-6
      IF(Q.EQ.0)Q=TOLL

c preliminary control
      QMAX=SQRT(2.*9.8*D)*D*2./SQRT(27.)
      IF(ABS(Q).GT.QMAX)STOP

      N=200
      DD=1
      DO 100 I=1,N

c loop 100: growing water depths
      DI=D+FLOAT(I-1)*DD
      DV(I)=DI

c step 1): ui
      QI=SQRT(2.*9.8*DI)*DI
      X=1
      DX=0.01
      QQ=(Q/QI)**2

c loop 90: smallest positive solution of Eqn (2.37)
90    X=X+DX
      F1=X
      F2=1.+QQ*X*X*X
      IF(F1.LT.F2)GO TO 90
      X=X-DX
      DX=DX/10.
      IF(DX.GT.2.E-5)GO TO 90
      UI=(Q/DI)*X
      SI=UI*UI/DG
      DSTI=DI-SI
      DSTIV(I)=DSTI

c step 2):Lci (RLCI)
      RLO=1.56*T*T
      CO=RLO/T
      UCOI=UI/CO
      DLOI=DSTI/RLO
      AI=UCOI*UCOI/DLOI
```

```
      .BI=DLOI/UCOI
       DX=0.01
       X=0

c loop 80: smallest solution of Eqn (2.39)
80     X=X+DX
       IF(X.GT.10)THEN
       WRITE(6,*)'the wave cannot travel against the current'
       STOP
       ENDIF
       F1=X*TANH(DPG*X)
       F2=AI*(X-BI)**2
       IF(F1.LT.F2)GO TO 80
       X=X-DX
       DX=DX/10.
       IF(DX.GT.2.E-5)GO TO 80
       RLCI=DSTI/X
       RKCI=DPG/RLCI
       RKCIV(I)=RKCI

c DI=di, UI=ui, SI=si, DSTI =di^, RLCI=lci, RKCI=kci

c step 3): definitions (2.41–2.51)
       OI=1./(OM-UI*RKCI)
       COSA=COSH(RKCI*DSTI)
       CHI=COSA*COSA
       SHI=SINH(2.*RKCI*DSTI)
       IF(RKCI*DSTI.LT.10)THEN
       AD1=(1./16.)*9.8*OI*OI*UI*RKCI*RKCI*DSTI/CHI
       AD2=(1./32.)*9.8*((2.*RKCI*DSTI+SHI)/CHI)*OI*(1.+UI*RKCI*OI)
       RKI=AD1+AD2+UI/8.
       ELSE

c the asymptotic form of KI -Eqn (2.44)- as kci di^ --> inf
       AD1=0
       AD2=(1./32.)*9.8*2.*OI*(1.+UI*RKCI*OI)
       RKI=AD1+AD2+UI/8.
       ENDIF
       AI=((1./16.)*9.8*HO*HO/OM-0.5*PG*SI*HO*HO/T)/RKI
       BI=(2.*SI*UI-Q)/RKI
       CI=-HO*HO/16.+0.5*PG*(UI/9.8)*HO*HO/T
       DI=1./16.+(1./8.)*9.8*OI*OI*RKCI*RKCI*DSTI/CHI
       EI=-3.*SI
       FI=CI+AI*DI
       GI=BI*DI+EI

c store on memory the values of AI, BI, FI, GI
       AV(I)=AI
       BV(I)=BI
```

```
     .FV(I)=FI
      GV(I)=GI
100   CONTINUE

c step 4): obtain the sequence deltai from i=N-1 to i=1
      I=N
      DELTAV(N)=0
200   I=I-1
      DI=DV(I)
      DI1=DV(I+1)
      DELTAI1=DELTAV(I+1)
      FI=FV(I)
      FI1=FV(I+1)
      GI=GV(I)
      GI1=GV(I+1)

c rnum = numerator, den = denominator on the RHS of Eqn (2.52)
      RNUM=0.5*(DI+DI1)*DELTAI1-FI+FI1+GI1*DELTAI1
      DEN=GI+0.5*(DI+DI1)
      DELTAV(I)=RNUM/DEN
      IF(I.EQ.1)GO TO 201
      GO TO 200
201   CONTINUE

c step 5): obtain wave height H on the given water depth d
      DELTA1=DELTAV(1)
      A1=AV(1)
      B1=BV(1)

c H proceeds from Eqn (2.53)
      H=SQRT(A1+B1*DELTA1)

c delta1 is the wave set-down (or set-up) on the given water depth d
      WRITE(6,7003)DELTA1
7003  FORMAT(/,1X,'DELTA ',F7.3)

c particle acceleration of waves on current
      RKCI=RKCIV(1)
      DSTI=DSTIV(1)
      RLCI=DPG/RKCI
      ATTC=COSH(RKCI*ZITAC)/COSH(RKCI*DSTI)
      AYC=9.8*0.5*H*RKCI*ATTC

c ay (AYC) is given by Eqn (1.54)
      ATTC1=SINH(RKCI*ZITAC)/COSH(RKCI*DSTI)
      AZC=9.8*0.5*H*RKCI*ATTC1

c az (AZC) is given by Eqn (1.55)
```

```
c Froude-Krylov force on the submerged tunnel:
      FYC=RO*AREA*AYC/1.E3
      FZC=RO*AREA*AZC/1.E3

c particle acceleration without the current
      RLO=1.56*T*T
      RLI1=RLO
70    RLI=RLO*TANH(DPG*D/RLI1)
      TEST=ABS(RLI-RLI1)/RLI
      RLI1=RLI
      IF(TEST.GT.1.E-4)GO TO 70
      RL=RLI
      RK=DPG/RL
      SINA=SINH(2.*RK*D)
      TANA=TANH(RK*D)
      ARG=SINA/(TANA*(SINA+2.*RK*D))
      CSHO=SQRT(ARG)

c CSHO shoaling coefficient
      HH=HO*CSHO
      ATT=COSH(RK*ZITAC)/COSH(RK*D)
      AY=9.8*0.5*HH*RK*ATT
      ATT1=SINH(RK*ZITAC)/COSH(RK*D)
      AZ=9.8*0.5*HH*RK*ATT1

c Froude-Krylov force on the submerged tunnel, without the current:
      FY=RO*AREA*AY/1.E3
      FZ=RO*AREA*AZ/1.E3

      WRITE(6,*)

      write(6,*)'   with the current   without current'
      WRITE(6,2000)FYC,FY
2000  FORMAT(15X,'fy',7X,F7.0,7X,F7.0)
      WRITE(6,2001)FZC,FZ
2001  FORMAT(15X,'fz',7X,F7.0,7X,F7.0)
      WRITE(6,2002)H,HH
2002  FORMAT(15X,'H',10X,F6.1,8X,F6.1)
      WRITE(6,2003)RKCI,RK
2003  FORMAT(15X,'k',7X,F7.4,7X,F7.4)
      WRITE(6,2004)ATTC,ATT
2004  FORMAT(15X,'AF(ø)',3X,F7.4,7X,F7.4)
      WRITE(6,*)
      WRITE(6,*)'(ø) AF=attenuation factor'
      END
```

The results are

$\Delta = -0.030$ m;

	With the Current	Without the Current
f_y (kN/m)	419	344
f_z (kN/m)	409	321
H (m)	19.5	14.8
k (m^{-1})	0.0363	0.0282
AF (°)	0.2383	0.3339

(°) AF = Depth attenuation factor.

The conclusion is that the Froude–Krylov force on the submerged tunnel grows of about the 25% because of the current. The Froude–Krylov force tends to grow for two reasons: the increase of the wave height and the increase of the wave number. On the opposite, the Froude–Krylov force tends to decrease because of the depth attenuation factor, which decreases with an adverse current.

2.5 CONCLUSION

Wave refraction was of central interest in the scientific literature of the years after the Second World War (Munk and Traylor, 1947; Arthur et al., 1952; Dorrestein, 1960). The effects of currents on wave direction were covered in particular by Johnson (1947), Jonsson and Wang (1980), and Gonzalez (1984). The two-dimensional problem of shoaling and set-down (or set-up) of waves and current on a sloping seabed was given an approximate solution by Jonsson et al. (1970). This solution was deeply re-examined in my book (2000), because of its potential utility for what we could call an "Engineering of the Straits."

REFERENCES

Arthur, R.S., Munk, W.H., Isaacs, J.D., 1952. The direct construction of wave rays. Trans. Am. Geophys. Union 33, 855–865.

Boccotti, P., 2000. Wave Mechanics for Ocean Engineering. Elsevier, Amsterdam, 495 pp.

Dorrestein, R., 1960. Simplified method of determining refraction coefficients for sea waves. J. Geophys. Res. 65 (2), 637–642.

Gonzalez, F.I., 1984. A case-study of wave-current-bathymetry interactions at the Columbia river entrance. J. Phys. Oceanogr. 14 (6), 1065–1078.

Johnson, J.W., 1947. The refraction of surface waves by currents. Trans. Am. Geophys. Union 28 (6), 867–874.

Jonsson, I.G., Skougaard, C., Wang, J.D., 1970. Interaction between waves and current. In: Proc. 12th Conf. Coastal Eng. ASCE, pp. 489–507.

Jonsson, I.G., Wang, J.D., 1980. Current-depth refraction of water waves. Ocean. Eng. 7 (1), 153–171.

Munk, W.H., Traylor, M.A., 1947. Refraction of ocean waves: a process linking underwater topography to beach erosion. J. Geol. LV (1), 1–26.

Chapter 3

Random Wind-Generated Waves: Basic Concepts

CHAPTER OUTLINE

3.1 SEA STATE, SIGNIFICANT WAVE HEIGHT, SPECTRUM, AUTOCOVARIANCE

3.1.1 The Concept of "Sea State"

Usually a sequence of 100–200 waves in the sea is

1. short enough that it may belong to a stationary random process;
2. long enough so that its average characteristics are close to the average characteristics of the stationary random process.

Wave Mechanics and Wave Loads on Marine Structures. http://dx.doi.org/10.1016/B978-0-12-800343-5.00003-2

The stationary random process is called "sea state." According to the linear theory of sea states, the surface elevation $\eta(t)$ at some fixed point represents a stationary Gaussian random process of time. This may be expressed in the form

$$\eta(t) = \sum_{i=1}^{N} a_i \cos(\omega_i t + \varepsilon_i) \tag{3.1}$$

with the assumptions that:

N tends to infinity,
a_i are infinitesimal of the same order,
ω_i are all different from one another,
ε_i are distributed uniformly in $(0,2\pi)$,
ε_i are stochastically independent from one another.

3.1.2 The Significant Wave Height

The first characteristic of a sea state is the so called "significant wave height":

$$H_s \equiv 4\sigma \tag{3.2}$$

where σ is the root mean square (RMS) surface elevation

$$\sigma \equiv \sqrt{\langle \eta^2(t) \rangle} \tag{3.3}$$

3.1.3 Definition of the Frequency Spectrum

The frequency spectrum, $E(\omega)$, shows how the wave energy is distributed over the frequency domain:

$$E(\omega)\delta\omega \equiv \sum_i \frac{1}{2} a_i^2 \quad \text{for } i \text{ such that} \quad \omega - \delta\omega/2 < \omega_i < \omega + \delta\omega/2 \tag{3.4}$$

The peak period (T_p) is the period associated with the dominant frequency of the spectrum:

$$T_p \equiv \frac{2\pi}{\omega_p} \tag{3.5}$$

Spectral moments

$$m_j \equiv \int_0^\infty \omega^j E(\omega) \mathrm{d}\omega \tag{3.6}$$

are commonly used.

3.1.4 Relationship between Autocovariance and Spectrum

The definition of autocovariance $\psi(T)$ is

$$\psi(T) \equiv \langle \eta(t)\eta(t+T) \rangle \tag{3.7}$$

where T is an arbitrary time lag. With Eqn (3.1) of $\eta(t)$, Eqn (3.7) becomes

$$\psi(T) = \sum_{i=1}^{N} \sum_{j=1}^{N} a_i a_j \langle \cos(\omega_i t + \varepsilon_i) \cos\left[\omega_j (t+T) + \varepsilon_j\right] \rangle \tag{3.8}$$

where the order temporal mean and summation have been changed. Then, applying the addition formula to the second cosine, we obtain

$$\begin{aligned} \psi(T) = \sum_{i=1}^{N} \sum_{j=1}^{N} a_i a_j \big[& \cos(\omega_j T) \langle \cos(\omega_i t + \varepsilon_i) \cos(\omega_j t + \varepsilon_j) \rangle \\ & - \sin(\omega_j T) \langle \cos(\omega_i t + \varepsilon_i) \sin(\omega_j t + \varepsilon_j) \rangle \big] \end{aligned} \tag{3.9}$$

Here, the first temporal mean is equal to 1/2 if $i = j$, and is equal to 0 if $i \neq j$; and the second temporal mean is equal to 0, whichever the i and j, and therefore

$$\psi(T) = \sum_{i=1}^{N} \frac{1}{2} a_i^2 \cos(\omega_i T) \tag{3.10}$$

Let us consider the summation on the RHS of this equation. Since

$$\begin{aligned} & \left\{ \text{contribution to } \sum_{i=1}^{N} \frac{1}{2} a_i^2 \cos(\omega_i T) \text{ from the harmonics whose} \right. \\ & \left. \text{frequency } \omega_i \text{ is between } \omega - \delta\omega/2 \text{ and } \omega + \delta\omega/2 \right\} \\ & = \left\{ \cos(\omega T) \sum_{i} \frac{1}{2} a_i^2 \text{ for } i \text{ such that } \omega - \delta\omega/2 < \omega_i < \omega + \delta\omega/2 \right\} \\ & = \cos(\omega T) E(\omega) \delta\omega \end{aligned} \tag{3.11}$$

we have

$$\sum_{i=1}^{N} \frac{1}{2} a_i^2 \cos(\omega_i T) = \int_0^\infty E(\omega) \cos(\omega T) \mathrm{d}\omega \tag{3.12}$$

that together with Eqn (3.10) implies

$$\psi(T) = \int_0^\infty E(\omega) \cos(\omega T) \mathrm{d}\omega \tag{3.13}$$

3.1.5 Alternative Ways to Express the Variance of the Surface Elevation

From Eqn (3.1), it follows that

$$\langle \eta^2(t) \rangle = \sum_{i=1}^{N} \frac{1}{2} a_i^2 \tag{3.14}$$

This equation and the definition (Eqn (3.4)) of the spectrum imply

$$\langle \eta^2(t) \rangle = \int_0^\infty E(\omega) \mathrm{d}\omega \tag{3.15}$$

With this equation and Eqn (3.3) of σ, Eqn (3.2) of H_s, Eqn (3.6) of m_j, and Eqn (3.13) of $\psi(T)$, we obtain the following multiple equalities

$$\langle \eta^2(t) \rangle = \sigma^2 = \frac{H_s^2}{16} = m_0 = \int_0^\infty E(\omega) \mathrm{d}\omega = \psi(0) \tag{3.16}$$

3.2 THE CONCEPT OF "VERY NARROW SPECTRUM"

Let us consider the spectrum of Fig. 3.1: a very high triangle with a very small base $\delta\omega$, and a finite area m_0. The surface elevation at a fixed time, t_o, can be written in the form

$$\eta(t_o) = \sum_{i=1}^{N} a_i \cos\left[F_i(t_o)\right] \quad \text{with} \quad F_i(t_o) = \omega_p t_o + \delta\omega_i t_o + \varepsilon_i \tag{3.17}$$

where

$$\delta\omega_i \equiv \omega_i - \omega_p \tag{3.18}$$

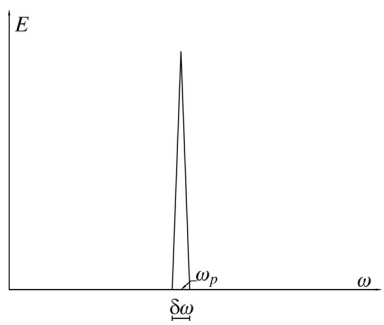

■ FIGURE 3.1 Very narrow spectrum.

The surface elevation at the instant $t_o + n\,T_p$, with n an arbitrary integer, can be written as

$$\eta(t_o + nT_p) = \sum_{i=1}^{N} a_i \cos\left[F_i(t_o + nT_p)\right] \quad \text{with} \quad F_i(t_o + nT_p)$$
$$= \omega_p t_o + \delta\omega_i t_o + \varepsilon_i + n2\pi + n\frac{\delta\omega_i}{\omega_p}2\pi \tag{3.19}$$

Hence

$$\frac{\eta(t_o + nT_p)}{\eta(t_o)} \cong 1 \tag{3.20}$$

provided that

$$n \ll \frac{\omega_p}{\delta\omega} \tag{3.21}$$

Equation (3.20) proceeds straightforwardly from Eqns (3.17) and (3.19); it suffices to note that $F_i(t_o + nT_p)$ differs from $F_i(t_o)$ of $n2\pi$, plus a term smaller than $n\left(\frac{\delta\omega}{2}/\omega_p\right)2\pi$.

As an example, let us assume

$$\omega_p/\delta\omega = 10^6, \quad n = 10 \tag{3.22}$$

Then, the difference between the F_i of the summation Eqn (3.19) and the F_i of the summation Eqn (3.17) will be smaller than $\pi/10^5$ (as can be easily verified). This means that $\eta(t_o + 10T_p)$ will be nearly coincident with $\eta(t_o)$. Naturally, even more so, the conclusion holds for $\eta(t_o + T_p)$, $\eta(t_o + 2T_p)$,…,$\eta(t_o + 9T_p)$. Through the same reasoning, we may easily realize that $\eta(t_o + 10^6 T_p)$ will be generally different from $\eta(t_o)$. Being t_o arbitrary, we may conclude that $\eta(t)$ will locally approach a sinusoidal wave of period T_p. The difference with respect to a pure sinusoidal wave is that each wave shows a small random variation from the preceding one, and the sum of these small variations, after a very large number of waves, can give rise to some large variation of the wave height.

In conclusion, a sea state with a very narrow spectrum would be similar to a sequence of sinusoidal waves. However, there would be a substantial difference as the wave height would vary largely, although very gradually. Clearly, the narrower the spectrum, the closer the waves would be to this ideal condition. Vice versa, the wider the spectrum, the more irregular the waves, that is, the greater the differences among consecutive waves.

Here, we may realize the utility of bandwidth (or narrow bandedness) parameters aimed to quantify the degree of difference of a sea state from the ideal sea state with a very narrow spectrum. We shall deal with such parameters in the following section. Before doing this, we must deduce the autocovariance associated with a very narrow spectrum.

We must execute the integral on the RHS of Eqn (3.13). The integrand is the product of two functions $E(\omega)$ and $\cos(\omega T)$ where $E(\omega)$—Fig. 3.1—is different from zero only in a very small interval $(\omega_p - \delta\omega/2,\ \omega_p + \delta\omega/2)$. In this interval, $\cos(\omega T)$ may be substituted by $\cos(\omega_p T)$, with the result that

$$\psi(T) = \cos\left(\omega_p T\right) \int_{\omega_p - \delta\omega/2}^{\omega_p + \delta\omega/2} E(\omega)\mathrm{d}\omega \tag{3.23}$$

and hence

$$\psi(T) = \cos\left(\omega_p T\right)\psi(0) \tag{3.24}$$

3.3 BANDWIDTH AND NARROW-BANDEDNESS PARAMETERS

Usually a bandwidth parameter approaches zero for a very narrow spectrum, and should approach 1 for very broad spectra.

Cartwright and Longuet–Higgins (1956) used the bandwidth parameter

$$\varepsilon \equiv \sqrt{1 - \frac{m_2^2}{m_0 m_4}} \tag{3.25}$$

which really is not always efficient, in that it is too sensitive to the high frequency noise. Let us see why with an example. The moments of the spectrum of Fig. 3.2 are

$$m_0 = m_{01} + m_{01}/n = m_{01}\left(1 + n^{-1}\right) \tag{3.26}$$

$$m_2 = m_{01}\omega_p^2 + (m_{01}/n)n^2\omega_p^2 = m_{01}\omega_p^2(1+n) \tag{3.27}$$

$$m_4 = m_{01}\omega_p^4 + (m_{01}/n)n^4\omega_p^4 = m_{01}\omega_p^4\left(1+n^3\right) \tag{3.28}$$

and hence

$$\varepsilon = \sqrt{1 - \frac{(1+n)^2}{(1+n^{-1})(1+n^3)}} \tag{3.29}$$

Thus, ε approaches 1 as $n \to \infty$, which suggests the idea of an extreme difference with respect to the case of the very narrow spectrum. Really,

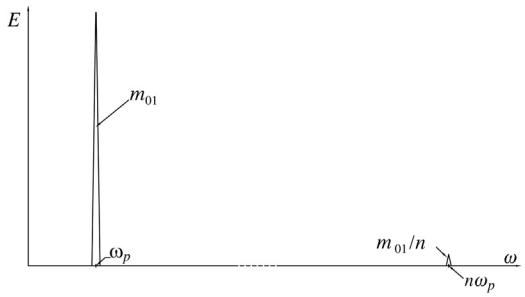

■ **FIGURE 3.2 The spectrum used for the analysis of the bandwidth parameters.**

as $n \to \infty$, the waves with this spectrum are practically the same as the waves with the very narrow spectrum. With the naked eye, these waves look exactly like the waves of the very narrow spectrum, and only if we use a magnifier should we find that their surface is pitted with a lot of very small ripples. Thus, in this case ε misses the mark. The fact is that resorting to ε is equivalent to judging by the number of the local maxima (or minima) being present in each wave; the greater this number, the greater the difference from the very narrow spectrum. With the spectrum of Fig. 3.2, each wave has an infinitely large number of local maxima due to the very small noise on the wave surface, and this is why ε gets the upper limit. For the same reason, ε is equal to one also for spectra of wind seas. Indeed these seas are affected by a high frequency noise of very small amplitude. The noise is due to the high frequency tail of the spectrum, which approaches zero as ω^{-5} as $\omega \to \infty$, as we shall see in the next section. Consequently m_4 tends to infinity and ε approaches 1, just like in the example of Fig. 3.2.

In 1975, Longuet–Higgins used a new bandwidth parameter:

$$\nu \equiv \sqrt{\frac{m_0 m_2}{m_1^2} - 1} \tag{3.30}$$

whose range is $(0, \infty)$. This new parameter has the same kind of inconveniences of ε (even though in a more attenuated form), and indeed for the spectrum of Fig. 3.2, it tends to infinity.

In a previous book (2000), the author suggested to consider

$$\psi^* \equiv |\psi(T^*)/\psi(0)| \tag{3.31}$$

where

$$T^* \equiv \text{ abscissa of the absolute minimum of the autocovariance function.} \tag{3.32}$$

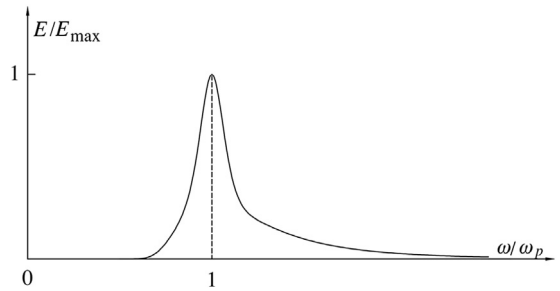

■ FIGURE 3.3 The mean JONSWAP spectrum.

If the spectrum is very narrow, the autocovariance approaches a cosine, and thus ψ^* approaches 1. As the bandwidth grows, ψ^* gets smaller and smaller approaching 0. Therefore, ψ^* is a narrow bandedness parameter, i.e., it is the one's complement of a bandwidth parameter.

Using ψ^*, we shall not be muddled by the high frequency noise. For example, the autocovariance of the spectrum of Fig. 3.2 is

$$\psi(T) = m_{01} \cos\left(\omega_p T\right) + \frac{1}{n} m_{01} \cos\left(n\omega_p T\right) \tag{3.33}$$

As $n \to \infty$, this $\psi(T)$ is a cosine affected by a very small noise. Therefore, ψ^* approaches 1 as in the case of the very narrow spectrum; that is, ψ^* correctly classifies the waves with this spectrum as very close to the waves with the very narrow spectrum.

3.4 CHARACTERISTIC SPECTRA OF WIND SEAS

3.4.1 The JONSWAP Spectrum

When a local wind generates waves, these are called "wind sea." If the wind is constant and the water is deep, the spectrum is like that of Fig. 3.3 where $E(\omega)$ approaches rapidly zero on the left side, and approaches zero more gradually on the right side. A mathematical form suggested for describing this characteristic spectrum shape is

$$E(\omega) = Ag^2\omega^{-5} \exp\left[-\frac{5}{4}\left(\frac{\omega_p}{\omega}\right)^4\right] \exp\left\{\ln \chi_1 \exp\left[-\frac{\left(\omega-\omega_p\right)^2}{2\chi_2^2\omega_p^2}\right]\right\} \tag{3.34}$$

This is the so called JONSWAP spectrum (Hasselmann et al., 1973), which as said is effective with deep water:

$$d > \frac{1}{2} L_{p0} \tag{3.35}$$

The JONSWAP spectrum was the final result of a work developed in the 1950s and 1964. Phillips was the first to observe in the 1950s that the spectrum approaches zero, for large ω, as ω^{-5}. The term $A\,g^2\omega^{-5}$ in the formula (3.34) is due to him (1958). The form

$$E(\omega) = Ag^2\omega^{-5}\exp\left[-\frac{5}{4}\left(\frac{\omega_p}{\omega}\right)^4\right] \tag{3.36}$$

was introduced by Pierson and Moskowitz in the 1960s. The last improvement, that is the introduction of the second exponential function, was due to the JONSWAP project in the early 1970s.

According to the researchers of the JONSWAP project, the more characteristic values of the shape parameters χ_1 and χ_2 are

$$\chi_1 = 3.3, \quad \chi_2\begin{cases} = 0.07 & \text{if} \quad \omega \le \omega_p \\ = 0.09 & \text{if} \quad \omega > \omega_p \end{cases} \tag{3.37}$$

but we may as well assume

$$\chi_1 = 3, \quad \chi_2 = 0.08 \tag{3.38}$$

with some negligible consequences. The spectrum with values (3.37) of parameters χ_1 and χ_2 is called the mean JONSWAP. It is shown by Fig. 3.3 in the nondimensional form $E(\omega)/E(\omega_p)$ as a function of ω/ω_p. It should be noted that such a nondimensional form depends only on the values of χ_1 and χ_2. Therefore, Fig. 3.3 represents the mean JONSWAP spectrum, whatever the peak frequency ω_p and energy scale parameter A.

As to parameter A, it depends on the characteristics of the wave generation: the smaller is the fetch $\mathscr{Y}$ and the greater is the wind speed u, the larger is A. Typical values are

$$0.008 < A < 0.014 \ \text{ with } \ 2\cdot 10^3 < \frac{g\,\mathscr{Y}}{u^2} < 2\cdot 10^4 \tag{3.39}$$

3.4.2 The Autocovariance Relevant to the JONSWAP Spectrum

From Eqn (3.13) between autocovariance and spectrum, and Eqn (3.34) of the JONSWAP spectrum, it follows that

$$\begin{aligned}\psi(T) = \int_0^\infty & Ag^2\omega^{-5}\exp\left[-\frac{5}{4}\left(\frac{\omega_p}{\omega}\right)^4\right] \\ & \times \exp\left\{\ln\chi_1\exp\left[-\frac{(\omega-\omega_p)^2}{2\chi_2^2\omega_p^2}\right]\right\}\cos(\omega T)\mathrm{d}\omega\end{aligned} \tag{3.40}$$

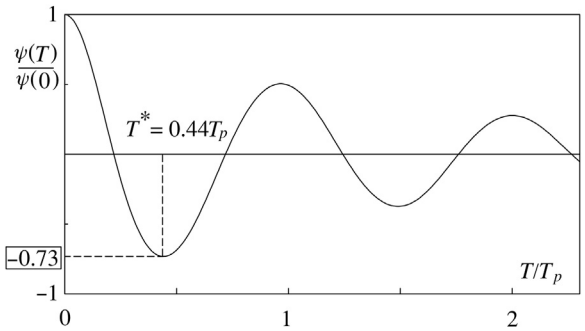

■ **FIGURE 3.4 Autocorrelation relevant to the mean JONSWAP spectrum.**

Then, replacing ω with $w = \omega/\omega_p$, we arrive at

$$\frac{\psi(T)}{\psi(0)} = \frac{\int_0^\infty \mathscr{E}(w)\cos\left(2\pi w\frac{T}{T_p}\right)\mathrm{d}w}{\int_0^\infty \mathscr{E}(w)\mathrm{d}w} \tag{3.41}$$

where

$$\mathscr{E}(w) \equiv w^{-5}\exp\left(-\frac{5}{4}w^{-4}\right)\exp\left\{\ln\chi_1\exp\left[-\frac{(w-1)^2}{2\chi_2^2}\right]\right\} \tag{3.42}$$

Please note that the autocorrelation (normalized autocovariance)

$$\frac{\psi(T)}{\psi(0)} \quad \text{vz} \quad \frac{T}{T_p}$$

depends only on the shape parameters χ_1, χ_2. The autocorrelation relevant to the mean JONSWAP spectrum is shown in Fig. 3.4.

3.4.3 The Relationship $T_p(H_s)$ Based on the JONSWAP Spectrum

Reasoning like in the previous section, we get

$$m_0 = Ag^2\omega_p^{-4}\int_0^\infty \mathscr{E}(w)\mathrm{d}w \tag{3.43}$$

from which it follows that

$$T_p = \frac{1}{\sqrt[4]{A\int_0^\infty \mathscr{E}(w)\mathrm{d}w}}\pi\sqrt{\frac{H_s}{g}} \tag{3.44}$$

(for the step from (3.43) to (3.44), bear in mind that $m_0 = H_s^2/16$ and $T_p = 2\pi/\omega_p$). Equations (3.44) may be rewritten in the form

$$T_p = \frac{K_0}{\sqrt[4]{A}}\pi\sqrt{\frac{H_s}{g}} \tag{3.45}$$

where

$$K_0 = \frac{1}{\sqrt[4]{\int_0^\infty \mathscr{E}(w)\mathrm{d}w}} \tag{3.46}$$

With the mean JONSWAP spectrum this yields

$$T_p = \frac{1.345}{\sqrt[4]{A}}\pi\sqrt{\frac{H_s}{g}} \tag{3.47}$$

3.4.4 The TMA Spectrum

The TMA spectrum (Bouws et al., 1985), founded on the work of Kitaigorodskii et al. (1975), Bouws et al. (1985) and Young and Verhagen (1996), is obtained on multiplying the JONSWAP spectrum by a transformation function:

$$\text{TMA } E(\omega) = \text{JONSWAP } E(\omega)\ \text{TFU}\ (\omega, d) \tag{3.48}$$

where

$$\text{TFU}\ (\omega, d) = \tanh^2(kd)\frac{\sinh(2kd)}{[\sinh(2kd) + 2kd]} \tag{3.49}$$

The TMA spectrum generalizes the applicability of the JONSWAP spectrum from deep water to arbitrary water depth.

For mathematical applications of the TMA, it is convenient defining the dimensionless wave number $\mathscr{k}_w$:

$$\mathscr{k}_w = \frac{k}{\omega_p^2/g} = \frac{k}{2\pi/L_{p0}} \tag{3.50}$$

From this definition and the dispersion relationship, the following equation proceeds

$$\mathscr{k}_w \tanh\left(2\pi\mathscr{k}_w d/L_{p0}\right) = w^2 \tag{3.51}$$

which admits a unique solution for $\mathscr{k}_w$, for given d/L_{p0} and w.

The dimensionless spectrum $\mathscr{E}(w)$ changes from the form (Eqn (3.42)), that here will be called $\underset{0}{\mathscr{E}}(w)$, to

$$\mathscr{E}(w) = \underset{0}{\mathscr{E}}(w)\tanh^2\left(2\pi \mathscr{k}_w d/L_{p0}\right)\frac{\sinh\left(4\pi \mathscr{k}_w d/L_{p0}\right)}{\left[\sinh\left(4\pi \mathscr{k}_w d/L_{p0}\right)+4\pi \mathscr{k}_w d/L_{p0}\right]} \quad (3.52)$$

where use has been made of the definition (Eqn (3.50)).

3.5 HOW TO OBTAIN THE FREQUENCY SPECTRUM

3.5.1 The Fourier Series

Given an odd number n of data $(\eta_1, \eta_2, \ldots, \eta_n)$, whose average is zero, being sampled at a constant interval Δt_{samp}, that is to say recorded at instants

$$t_1 = 0,\ t_2 = \Delta t_{\text{samp}}, \ldots,\ t_n = (n-1)\Delta t_{\text{samp}} \quad (3.53)$$

the function

$$\eta_F(t) = \sum_{i=1}^{N} a_i' \cos(\omega_i t) + a_i'' \sin(\omega_i t) \quad (3.54)$$

with

$$N = (n-1)/2,\ \ \omega_i = \frac{2\pi}{\Delta t_{\text{samp}}}\frac{i}{n},\ \ a_i' = \frac{2}{n}\sum_{j=1}^{n}\eta_j \cos\left(\omega_i t_j\right),$$
$$a_i'' = \frac{2}{n}\sum_{j=1}^{n}\eta_j \sin\left(\omega_i t_j\right) \quad (3.55)$$

is such that

$$\eta_F(t_1) = \eta_1, \eta_F(t_2) = \eta_2, \ldots, \eta_F(t_n) = \eta_n \quad (3.56)$$

$\eta_F(t)$ is the Fourier series, which is periodical of period $T_F = n\Delta t_{\text{samp}}$:

$$\eta_F(t + T_F) = \eta_F(t) \quad (3.57)$$

The Fourier series may be given the form (Eqn (3.1)), with the a_i and ε_i that are related to the coefficient of the series a_i', a_i'' by

$$a_i = \sqrt{a_i'^2 + a_i''^2},\ \ \cos\varepsilon_i = a_i'/a_i,\ \ \sin\varepsilon_i = -a_i''/a_i \quad (3.58)$$

From the a_i and ω_i of the Fourier series, we can re-obtain the spectrum of the sea state. However, there is a problem: the frequency resolution

$$\Delta\omega = \omega_{i+1} - \omega_i \quad (3.59)$$

is smaller in the actual sea state than in the Fourier series (indeed, it is assumed that the number of frequencies of the sea state tends to infinity). Therefore, the spectrum obtained from the Fourier series approaches the actual spectrum of the sea state the better the smaller the $\Delta\omega$ is. In order

to reduce $\Delta\omega$, there is only one thing to do: increasing the duration of the wave record.

3.5.2 Effects of the Duration of the Wave Record

Let us imagine that two persons A and B perform the following sort of play. Person A does a numerical simulation of a sea state, by means of Eqn (3.1) for a given frequency spectrum. Person B does not know the number N of harmonic wave components used by A, nor the triplets a_i, ω_i, ε_i. From the knowledge of n values (η_1, η_2, …, η_n) of the numerical simulation sampled at a sampling interval Δt, person B must discover which is the spectrum used by person A.

Person A simulates a sea state with the Pierson and Moskowitz spectrum, with a H_s of 5.6 m and a T_p of 10.1 s. As to the number N on the RHS of (3.1), this is taken of 1250, and the 1250 frequencies ω_i cover uniformly the range ($0.6\omega_p$, $3.1\omega_p$).

Person B fixes a sample interval of 0.4 s, and a duration of the wave record (DWR) of 1200 s. Hence, he obtains $n = 3001$ samples of the surface elevation, at time instants $t_1 = 0$, $t_2 = 0.4$ s, …, $t_n = 1200$ s. By means of Eqn (3.55), he obtains the ω_i and the a_i of the Fourier series, and hence the spectrum $\tilde{E}(\omega)$ relevant to the Fourier series (we use the symbol $\tilde{E}$ for the spectrum obtained by person B, whereas with E we denote the spectrum used by person A). Fig. 3.5 shows the spectrum $E(\omega)$ used by person A for his numerical simulation, and the spectrum $\tilde{E}(\omega)$ obtained by person B through the Fourier series. Now let us see which is the result obtained by person B, if DWR grows from 1200 to 8000 s (n grows from 3001 to 20,001), and hence $\Delta\omega$ is reduced from $2\pi/(3001 \cdot 0.4)$ to $2\pi/(20001 \cdot 0.4)$. The result

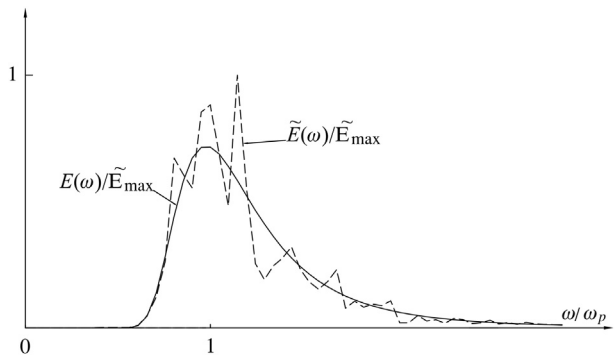

■ **FIGURE 3.5 Sea state: $H_s = 5.6$ m, $T_p = 10.1$ s.** Continuous line: given spectrum. Dashed line: spectrum obtained with a DWR of 20 min and sampling interval of 0.4 s.

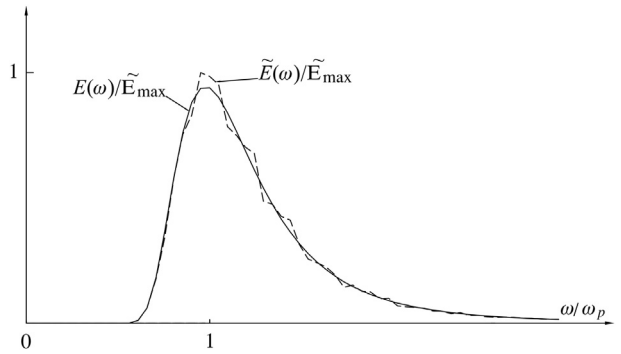

■ **FIGURE 3.6 Same as in Fig. 3.5 with the only difference that the DWR has been increased from 20 min to 2.2 h.**

is shown in Fig. 3.6 where the agreement between the spectrum obtained through the Fourier series and the actual spectrum appears with evidence.

Figure 3.7 shows the autocorrelation $\psi(T)/\psi(0)$ obtained by means of Eqn (3.13) from the actual spectrum $E(\omega)$, and the autocorrelation $\tilde{\psi}(T)/\tilde{\psi}(0)$ obtained by means of Eqn (3.13) from the spectrum $\tilde{E}(\omega)$ of Fig. 3.5. Notwithstanding the great difference between $\tilde{E}$ and E, which appears from Fig. (3.5), the difference between $\tilde{\psi}(T)/\tilde{\psi}(0)$ and $\psi(T)/\psi(0)$ is negligible! This is at least for the core of the autocorrelation, which consists in the central wave of this function. However, the fact that the core of the autocorrelation of the spectrum $\tilde{E}$ is nearly the same as the core of the autocorrelation of the spectrum E is important. Indeed we shall see in the next chapter that the main statistical properties of waves in sea states depend only on the configuration of the core of the autocorrelation.

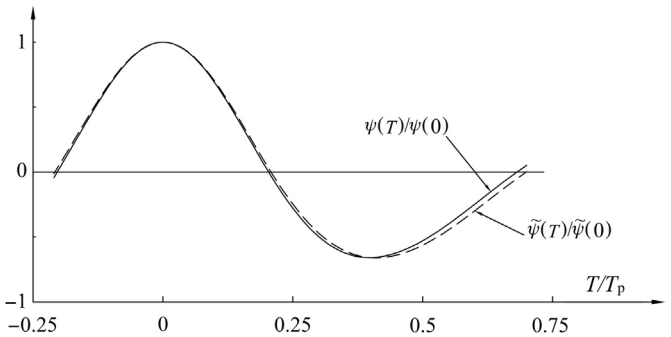

■ **FIGURE 3.7 Core of the autocorrelation relevant to the continuous spectrum of Fig. 3.5 versus core of the autocorrelation relevant to the dashed spectrum of Fig. 3.5.**

As said, the $\tilde{E}(\omega)$ of Fig. 3.5 was obtained with a DWR of 1200 s, which in our example corresponds to a sequence of about 150 individual waves. With this DWR, we obtain carefully what more counts for wave statistics that is the configuration of the core of the autocorrelation.

3.6 WAVE RECORD ANALYSIS

At sea, a typical DWR is 20 min (1200 s), and a typical sampling interval may be $\Delta t = 0.4$ s. With wind seas of H_s ranging between about 3 m and 15 m, a record of this duration may include from about 100 to 200 individual waves.

A routine analysis of a wave record ($n = 3001$, $\Delta t = 0.4$ s) may be:

1. Values of $\eta(t)$
   $\eta_1, \eta_2, \ldots, \eta_{3001}$ are the time series data of the surface elevation at a fixed point; the average $(\eta_1 + \eta_2 + \ldots + \eta_{3001})/3001$ must be equal to 0.
2. Calculation of H_s

$$\langle \eta^2(t) \rangle = \left(\eta_1^2 + \eta_2^2 + \ldots + \eta_{3001}^2\right)/3001$$

$$H_s = 4\sqrt{\langle \eta^2(t) \rangle}$$

3. Calculation of $\psi(T)$
   As an example, for $T = 1.2$ s, we have

$$\psi(1.2\text{ s}) = (\eta_1\eta_4 + \eta_2\eta_5 + \ldots + \eta_{2998}\eta_{3001})/2998$$

4. Calculation of $E(\omega)$

$$N = (3001 - 1)/2 = 1500$$

$$\Delta\omega = 2\pi/(3001 \cdot 0.4) = 5.234 \cdot 10^{-3}\text{ rad/s}$$

$$\omega_i = i\,5.234 \cdot 10^{-3}\text{ rad/s}$$

$$a_i' = (2/3001)\sum_{j=1}^{3001} \eta_j \cos\left[\omega_i \Delta t\,(j-1)\right]$$

$$a_i'' = (2/3001)\sum_{j=1}^{3001} \eta_j \sin\left[\omega_i \Delta t\,(j-1)\right]$$

As an example: the area of the spectrum between 0.30 rad/s and 0.33 rad/s:

$$0.5[E(0.30\text{ rad/s}) + E(0.33\text{ rad/s})]0.03\text{ rad/s}$$
$$= 0.5\left(a_{58}'^2 + a_{58}''^2 + a_{59}'^2 + a_{59}''^2 + a_{60}'^2 + a_{60}''^2 + a_{61}'^2 + a_{61}''^2 + a_{62}'^2 + a_{62}''^2 + a_{63}'^2 + a_{63}''^2\right)$$

Here, note that the interval 0.30 rad/s $< \omega <$ 0.33 rad/s contains the angular frequencies from $\omega_{58} = 0.3036$ rad/s to $\omega_{63} = 0.3297$ rad/s.

If one aims to obtain the basic parameters of a sea state (H_s, configuration of the core of the autocorrelation) this routine analysis usually is effective. This routine is also useful to get an overall idea of the spectrum. For example, in the case of Fig. 3.5, the spectrum $\tilde{E}$ obtained from the Fourier series coincides with the actual spectrum E on low frequencies; the high frequency tail is essentially the same for $\tilde{E}$ and E; the location and overall size of the bulk of the spectrum is essentially the same with E and $\tilde{E}$. The difference is in the great random noise that affects this bulk in $\tilde{E}(\omega)$. If one aims to deeply investigate the shape of the spectra, this person must search for some special records wherein the sea remains stationary for some long time interval. Indeed, increasing the DWR enables one to reduce $\Delta\omega$, and to better fit the spectrum. Alternatively, one may consider the average of some dimensionless spectra of similar sea states.

3.7 SMALL-SCALE FIELD EXPERIMENTS

There are two kinds of experimental activity concerning sea waves. The first one deals with measurement campaigns in the field. The second one consists in experiments performed in the laboratory. The following is the main conceptual difference between these two kinds of activity. In a measurement campaign, we do not know the characteristics of the sea state (often knowing these characteristics is the very goal of the campaign); in laboratories, the characteristics of the sea state are prescribed (and there may be a lot of goals: studying the distribution of wave heights, or the loads exerted on some kind of structure, etc.). Typically in a laboratory experiment, we shall have an array of wave gauges at some prescribed distance from one another, with these distances being related to L_p (the dominant wavelength relevant to the given water depth). Not so in the field, wherein typically there is a unique instrument (e.g., a heave buoy, or pitch-and-roll buoy, or wave staff).

Of course, there have been most famous field measurements with an array of instruments; however, these were aimed to study how the characteristics of sea states do vary with $g\mathscr{Y}/u^2$ ($\mathscr{Y}$ fetch, u wind speed). The matter is radically different in laboratories where the distance between two points in a wave tank or waveflume is so small that the effect of the variation of $g\mathscr{Y}/u^2$ is negligible.

A small-scale field experiment (SSFE) is a laboratory experiment being performed in the field rather than in a wavetank or waveflume. This requires

1. to have a small astronomical tide amplitude at the selected site;
2. to have waves of rather small size;
3. to be reasonably sure that a sea state with some prescribed characteristics will occur after a short waiting time at this site;
4. to value the prescribed sea state (item iii) to be one of interest for engineering.

As to (1) off the shore of Reggio Calabria (Eastern coast of the Straits of Messina) the astronomical tide amplitude is typically within 0.15 m. This tide amplitude yields a variability of d (the water depth) that has proved to be either effectless or useful: effectless in the SSFEs on deep water; useful in the other SSFEs (for example, in the SSFE on wave load on vertical breakwaters, which will be quoted in Chapter 14, the effect of tide helped to study the dependence of wave load on d/L_{p0}).

As to requirement (2), off the shore at Reggio Calabria, there are typically wind seas being generated by a local wind, with H_s ranging between 0.15 and 1.0 m, and T_p ranging from 1.6 to 3.8 s.

As to requirement (3), it is worthwhile telling a recent experience. The experiment was aimed to verify the theoretical distribution of wave heights in the space domain in a sea state of given spectrum: an array of 26 wave gauges was positioned. The configuration of the gauges was expected to be effective, under the assumption of: unimodal spectrum (like JONSWAP), angle between the orthogonal to the coastline and the dominant direction being within 20°; T_h (the characteristic period of the largest waves, which will be dealt with in the next chapter) between 2.0 and 2.2 s. History of the experiment: gauges and electronic station were ready on May 3, 2012; after five days (May 8, 2012) we had obtained more than 500 5-min records of sea states with the prescribed characteristics. This was notwithstanding the complex set of prescriptions, and especially the very narrow window allowed for the variability of T_h: only 0.20 s! Of course, after more than 20 years of work in the sea of Reggio Calabria, we know that in late spring, sea states with these characteristics are common at that site. However, this is a proof that, at least at some sites, requirement (3) for the SSFEs is fulfilled.

As to requirement (4), a most typical sea state off the beach at Reggio Calabria is a wind sea with a spectrum close to the mean JONSWAP, with $H_s = 0.35$ m and $A = 0.01$. With Eqn (3.47), this gives $T_p = 2.52$ s.This sea state with

$$H_s = 0.35 \text{ m}, \quad T_p = 2.52 \text{ s}$$

may be thought of as the 1:22.5 small-scale model of a full-scale sea state of

$$H_s = 7.87 \text{ m}, \quad T_p = 11.95 \text{ s}$$

or as the 1:45 small-scale model of

$$H_s = 15.75 \text{ m}, \quad T_p = 16.90 \text{ s}$$

in the Froude dynamic similarity. These two full-scale sea states are meaningful, respectively, of a design sea state for some areas of the Mediterranean Sea, and of a design sea state for some oceanic areas. Sometimes in the sea area of Reggio Calabria, the spectrum exhibits a secondary peak on some low frequency (e.g., on $\omega = 0.10$ rad/s). In this case, the full-scale sea state in the Froude dynamic similarity is no longer meaningful as a design sea state (e.g., in the 1:45 scale we would have wind waves of 16.90 s T_p being superimposed on a swell of 42 s!). All the same, these sea states may fulfill requirement(4). As an example, several SSFEs which will be quoted in the next chapters, re. the distribution of the wave height in the time domain, the directional spectrum, and the Morison equation were done for the largest possible variety of the spectrum. Hence. the spectrum with the peak on the low frequency was welcome for these experiments. Again, with respect to requirement (4), the variety of sea states of a natural location like Reggio Calabria was fully appreciated only with an SSFE on wave energy absorption-conversion, which will be quoted in Chapters 15 and 16. In fact, often at that site there are swells with a T_p between 3.0 and 6.0 s and a steepness markedly smaller than that of the wind seas. Of course, these are useless as small-scale model of design sea states. However, these small-scale sea states are useful to test the performances of converters with swells (which is a crucial item given that most of the wave energy that every year reaches coasts worldwide is carried by swells).

The NOEL (Natural Ocean Engineering Laboratory) has been constituted to perform SSFEs, regularly, in an area of sea of 5000 m^2 off the beach at Reggio Calabria.

3.8 CONCLUSION

The first small-scale field experiment (1990) was conceived and directed by the author with the aim to verify the quasi-determinism theory (Boccotti et al., 1993). According to Holthuijsen (2007), that of function $E(f)$ is the single most important concept in his book. In fact, it is not easy to explain the meaning of the continuous function $E(f)$ (or $E(\omega)$). I believe that an effective (and perhaps pleasant) way should be the sort of play of Section 3.5.2, which may be played by two teams of students: team A in place of person A of Section 3.5.2; and team B in place of person B.

REFERENCES

Boccotti, P., Barbaro, G., Mannino, L., 1993. A field experiment on the mechanics of irregular gravity waves. J. Fluid Mech. 252, 173–186.

Boccotti, P., 2000. Wave Mechanics for Ocean Engineering. Elsevier, Amsterdam, 495 pp.

Bouws, E., Gunther, H., Rosenthal, W., Vincent, C.L., 1985. Similarity of the wind wave spectrum in finite depth water. 1. Spectral form. J. Geophys. Res. 90 (C1), 975–986.

Cartwright, D.E., Longuet-Higgins, M.S., 1956. The statistical distribution of the maxima of a random function. Proc. R. Soc. Lond. A 237, 213–232.

Hasselmann, K., Barnett, T.P., Bouws, E., Carlson, H., Cartwright, D.E., Enke, E., Ewing, J.A., Gienapp, H., Hasselmann, D.E., Krusemann, P., Meerburg, A., Müller, P., Olbers, D.J., Richter, K., Sell, W., Walden, H., 1973. Measurements of wind-wave growth and swell decay during the Joint North Sea Wave Project (JONSWAP). Dtsch. Hydrogr. Z. Suppl. A8 (12), 95.

Holthuijsen, L.H., 2007. Waves in Oceanic and Coastal Waters. Cambridge University Press, Cambridge, 387 pp.

Kitaigorodskii, S.A., Krasitskii, V.P., Zaslavskii, M.M., 1975. On Phillips' theory of equilibrium range in the spectra of wind-generated gravity waves. J. Phys. Oceanogr. 5 (7), 410–420.

Longuet-Higgins, M.S., 1975. On the joint distribution of the periods and amplitudes of sea waves. J. Geophys. Res. 80, 2688–2694.

Pierson, W.J., Moskowitz, L., 1964. A proposed spectral form for fully developed waves based on the similarity theory of S. A. Kitaigorodskii. J. Geophys. Res. 69, 5181–5190.

Phillips, O.M., 1958. The equilibrium range of the spectrum of wind-generated waves. J. Fluid Mech. 4, 426–434.

Young, I.R., Verhagen, L.A., 1996. The growth of fetch limited waves in water of finite depth. Part 2. Spectral evolution. Coast. Eng. 29, 79–99.

Chapter 4

Wave Statistics in Sea States

CHAPTER OUTLINE

Wave Mechanics and Wave Loads on Marine Structures. http://dx.doi.org/10.1016/B978-0-12-800343-5.00004-4

4.1 SURFACE ELEVATION AS A STATIONARY GAUSSIAN PROCESS

4.1.1 The Probability of the Surface Elevation

The random process (Eqn (3.1)) with the assumptions we have made on N, a_i, ω_i, and ε_i is stationary and Gaussian. This means that the probability $p(\eta(t) = w)\mathrm{d}w$ that $\eta(t)$ of a given realization of the random process falls in a fixed small interval $(w,w + \mathrm{d}w)$ is equal to the probability $p(\eta(t_o) = w)\mathrm{d}w$ that $\eta(t_o)$ at any fixed time instant t_o, in a realization taken at random, falls in the given interval $(w,w + \mathrm{d}w)$, and these have the following form:

$$p(\eta(t) = w) = p(\eta(t_o) = w) = \frac{1}{\sqrt{2\pi m_0}} \exp\left(-\frac{w^2}{2m_0}\right) \tag{4.1}$$

The probability $p(\eta(t) = w)\mathrm{d}w$ is equal to the ratio between the time in which $w < \eta(t) < w + \mathrm{d}w$ and the total time. The probability $p(\eta(t_o) = w)\mathrm{d}w$ is equal to the ratio between the number of realizations in which $w < \eta(t_o) < w + \mathrm{d}w$ and the total number of realizations.

Now let us see how Eqn (4.1) may be achieved. First, let us consider two arbitrary random variables V_1 and V_2. If

$$\overline{V_1^n} = \overline{V_2^n} \quad \forall n \tag{4.2}$$

reads "if the mean value of the nth power of V_1 is equal to the mean value of the nth power of V_2, whichever the n," then the two variables have the same probability density function, that is,

$$p(V_1 = w) = p(V_2 = w) \tag{4.3}$$

This rather intuitive property, which proceeds formally from the theorem of moments, will enable us to prove Eqn (4.1).

Before giving the proof, it is worthwhile to specify that we shall adopt two different symbols for the mean: one for the time average, the other one for the ensemble average. Specifically, $\langle \eta^n(t) \rangle$ will denote the average of the nth power of $\eta(t)$ in a given realization of the process, and $\overline{\eta^n(t_o)}$ will denote the average of the nth power of η at the fixed time t_o.

4.1.2 Proof Relevant to Any Given Realization

From Eqn (3.1) and the assumption that $\omega_i \neq \omega_j$, if $i \neq j$, it follows that

$$\langle \eta^4(t) \rangle = 3 \sum_{i=1}^{N} \sum_{j=1(j\neq i)}^{N} \frac{1}{4} a_i^2 a_j^2 + \sum_{i=1}^{N} \frac{3}{8} a_i^4 \tag{4.4}$$

Here, the assumptions of Section 4.2 on N and a_i come into play (N being infinitely large, a_i being of the same order of one another). Indeed, under these assumptions, Eqn (4.4) may be rewritten in the form,

$$\langle \eta^4(t) \rangle = 3 \sum_{i=1}^{N} \sum_{j=1}^{N} \frac{1}{4} a_i^2 a_j^2 \tag{4.5}$$

which implies

$$\langle \eta^4(t) \rangle = 3 \left\lfloor \langle \eta^2(t) \rangle \right\rfloor^2 = 3m_0^2 \tag{4.6}$$

Now, assuming that Eqn (4.1) is actually the probability of the surface elevation, we get the same value of $\langle \eta^4(t) \rangle$:

$$\langle \eta^4(t) \rangle = \int_{-\infty}^{+\infty} w^4 p(\eta(t) = w) \mathrm{d}w = \frac{1}{\sqrt{2\pi m_0}} \int_{-\infty}^{+\infty} w^4 \exp\left(-\frac{w^2}{2m_0} \right) \mathrm{d}w = 3m_0^2 \tag{4.7}$$

By the same way of reasoning, we can prove that whichever the n, $\langle \eta^n(t) \rangle$ takes on the same value if evaluated from Eqn (3.1) of $\eta(t)$ or from Eqn (4.1) of the probability of $\eta(t)$. The fact that

$$\langle \eta^n(t) \rangle \text{ obtained from Eqn (3.1)} = \langle \eta^n(t) \rangle \text{ obtained from Eqn (4.1)} \quad \forall n \tag{4.8}$$

implies that Eqn (4.1) is actually the probability of $\eta(t)$.

4.1.3 Proof Relevant to the Ensemble at a Fixed Time Instant

Fixing any time instant t_o, from Eqn (3.1), we have

$$\overline{\eta^4(t_o)} = \overline{\left[\sum_{i=1}^{N} a_i \cos(\widehat{\varepsilon}_i) \right]^4} \tag{4.9}$$

where

$$\widehat{\varepsilon}_i \equiv \varepsilon_i + \omega_i t_o \tag{4.10}$$

If the ε_i are distributed uniformly over the circle and are stochastically independent from one another, also the $\widehat{\varepsilon}_i$ are distributed uniformly over the circle and are stochastically independent from one another. Because of this property, it can be shown that

$$\overline{\eta^4(t_o)} = 3 \sum_{i=1}^{N} \sum_{j=1(j \neq i)}^{N} \frac{1}{4} a_i^2 a_j^2 + \sum_{i=1}^{N} \frac{3}{8} a_i^4 \tag{4.11}$$

Comparing this with Eqn (4.4) of $\langle \eta^4(t) \rangle$, we see that

$$\overline{\eta^4(t_o)} = \langle \eta^4(t) \rangle \tag{4.12}$$

Similarly, we can verify the equality

$$\overline{\eta^n(t_o)} = \langle \eta^n(t) \rangle \forall n \tag{4.13}$$

which implies that the probability of $\eta(t_o)$ (relevant to the ensemble at a fixed time) is equal to the probability of $\eta(t)$ relevant to any given realization.

4.2 JOINT PROBABILITY OF SURFACE ELEVATION

Let us define n random variables V_1, V_2, …, V_n, each of them representing the surface elevation η or a derivative of any order of η taken at some fixed instants generally different from one another. For example,

$$V_1 \equiv \eta(t_o), V_2 \equiv \dot{\eta}(t_o + T), \ldots, V_n \equiv \ddot{\eta}(t_o + T') \tag{4.14}$$

where the dot denotes the derivative, t_o is any fixed time instant, and T, T' are fixed time lags. The product

$$p(V_1 = w_1, V_2 = w_2, \ldots, V_n = w_n) \mathrm{d}w_1 \mathrm{d}w_2 \ldots \mathrm{d}w_n \tag{4.15}$$

represents the probability that V_1 falls in a fixed small interval $\mathrm{d}w_1$ including w_1; V_2 falls in a fixed small interval $\mathrm{d}w_2$ including w_2; and so on.

In Section 4.1, we have proven that $p[\eta(t_o) = w]$ is a Gaussian (normal) probability density function. Expanding the reasoning from the probability density of a single variable to the joint probability density of a set of random variables, we may prove that $p(V_1 = w_1, V_2 = w_2, \ldots, V_n = w_n)$ is multivariate Gaussian, that is to say

$$\begin{aligned} &p(V_1 = w_1, V_2 = w_2, \ldots, V_n = w_n) \\ &\quad = \frac{1}{(2\pi)^{n/2}\sqrt{M}} \exp\left[-\frac{1}{2M} \sum_{i=1}^{n} \sum_{j=1}^{n} M_{ij} w_i w_j \right] \end{aligned} \tag{4.16}$$

where

$$M_{ij} \equiv i,j \text{ cofactor}, \quad M \equiv \text{determinant} \tag{4.17}$$

of the covariance matrix (CM) of V_1, V_2, …, V_n:

$$\mathrm{CM} = \begin{pmatrix} \overline{V_1^2} & \overline{V_1 V_2} & \cdots & \overline{V_1 V_n} \\ \overline{V_2 V_1} & \overline{V_2^2} & \cdots & \overline{V_2 V_n} \\ \vdots & \vdots & & \vdots \\ \overline{V_n V_1} & \overline{V_n V_2} & \cdots & \overline{V_n^2} \end{pmatrix} \tag{4.18}$$

The entries of this matrix are ensemble averages like $\overline{\eta^4(t_o)}$ obtained in Section 4.1. Since the ensemble averages are equal to the temporal means, the entries of the CM may be obtained also from temporal means. This approach is advisable.

The CM of $\eta(t_o), \dot{\eta}(t_o)$ (where t_o is any fixed time instant) will serve in the next section. This is

$$\text{CM} = \begin{pmatrix} \overline{\eta^2(t_o)} & \overline{\eta(t_o)\dot{\eta}(t_o)} \\ \overline{\dot{\eta}(t_o)\eta(t_o)} & \overline{\dot{\eta}^2(t_o)} \end{pmatrix} = \begin{pmatrix} m_0 & 0 \\ 0 & m_2 \end{pmatrix} \tag{4.19}$$

Hereafter, as an example, the steps to obtain the 2,2 entry of this matrix:

$$\begin{aligned} \overline{[\dot{\eta}(t_o)]^2} &= \langle [\dot{\eta}(t)]^2 \rangle = \left\langle \left(-\sum_{i=1}^{N} a_i \omega_i \sin(\omega_i t + \varepsilon_i) \right)^2 \right\rangle \\ &= \sum_{i=1}^{N} \sum_{j=1}^{N} a_i a_j \omega_i \omega_j \langle \sin(\omega_i t + \varepsilon_i) \sin(\omega_j t + \varepsilon_j) \rangle \\ &= \sum_{i=1}^{N} 0.5\, a_i^2 \omega_i^2 = m_2 \end{aligned} \tag{4.20}$$

4.3 RICE'S PROBLEM (1958)

Let us call b_+ an up-crossing of some fixed threshold value b—see Fig. 4.1—and let us consider the probability that

1. a fixed small interval $\left(t_o - \frac{\mathrm{d}t}{2}, t_o + \frac{\mathrm{d}t}{2}\right)$ contains a b_+; and
2. the derivative of this b_+ falls in a fixed small interval $(w, w + \mathrm{d}w)$. This joint probability, that we shall call $p_+(b, w)\mathrm{d}t\mathrm{d}w$, is equal to the probability that
3. $\eta(t_o)$ belongs to the small interval $\left(b - w\frac{\mathrm{d}t}{2}, b + w\frac{\mathrm{d}t}{2}\right)$ and
4. $\dot{\eta}(t_o)$ belongs to the small interval $(w, w + \mathrm{d}w)$.

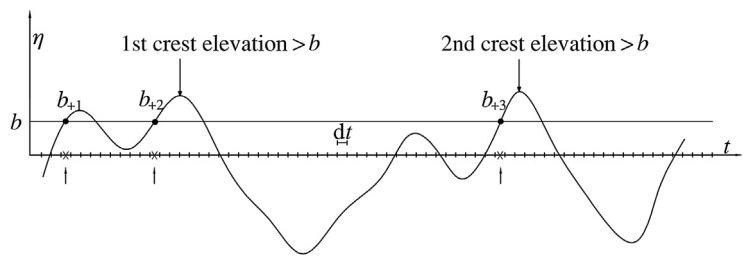

■ **FIGURE 4.1 A b_+ is an up-crossing of some fixed threshold b.** An individual wave is between two consecutive 0_+.

That is,

$$p_+(b,w)\mathrm{d}t\mathrm{d}w = p[\eta(t_o) = b, \dot{\eta}(t_o) = w]w\mathrm{d}t\mathrm{d}w \tag{4.21}$$

assuming that w is positive. (Figure 4.2 helps to realize that the probability of (1) and (2) is equal to the probability of (3) and (4).)

Now, let us consider the probability $p_+(b)\mathrm{d}t$ that the fixed small interval $\left(t_o - \frac{\mathrm{d}t}{2}, t_o + \frac{\mathrm{d}t}{2}\right)$ contains a b_+. This is related to the probability $p_+(b, w)$ $\mathrm{d}t\mathrm{d}w$ by

$$p_+(b)\mathrm{d}t = \int_0^\infty p_+(b,w)\mathrm{d}t\mathrm{d}w \tag{4.22}$$

Equations (4.21) and (4.22) yield

$$p_+(b) = \int_0^\infty p[\eta(t_o) = b, \dot{\eta}(t_o) = w]w\mathrm{d}w \tag{4.23}$$

That on the RHS is a joint Gaussian pdf:

$$p[\eta(t_o) = b, \dot{\eta}(t_o) = w] = \frac{1}{2\pi\sqrt{M}}\exp\left[-\frac{1}{2M}\left(M_{11}b^2 + M_{22}w^2 + 2M_{12}bw\right)\right] \tag{4.24}$$

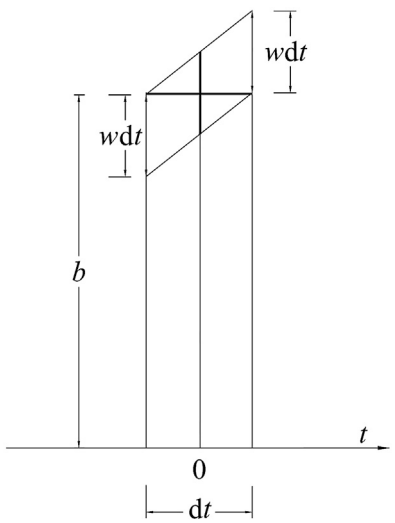

■ FIGURE 4.2 Graphic aid to understand Eqn (4.21).

where M and M_{ij} are, respectively, the determinant and the i,j cofactor of CM Eqn (4.19), that is,

$$M = m_0 m_2, \quad M_{11} = m_2, \quad M_{22} = m_0, \quad M_{12} = 0 \tag{4.25}$$

so that

$$p[\eta(t_o) = b, \dot{\eta}(t_o) = w] = \frac{1}{2\pi\sqrt{m_0 m_2}} \exp\left[-\frac{1}{2m_0 m_2}\left(m_2 b^2 + m_0 w^2\right)\right] \tag{4.26}$$

Equations (4.23) and (4.26) yield

$$p_+(b) = \int_0^\infty \frac{1}{2\pi\sqrt{m_0 m_2}} \exp\left[-\frac{1}{2m_0 m_2}\left(m_2 b^2 + m_0 w^2\right)\right] w \mathrm{d}w \tag{4.27}$$

At this point, we have arrived to the solution for $p_+(b)$, which is useful because

$$\mathscr{N}_+(b;\mathscr{T}) = p_+(b)\mathscr{T} \tag{4.28}$$

where $\mathscr{N}_+(b;\mathscr{T})$ is the expected number of b_+ in a very large time interval $\mathscr{T}$.

Solving the integral on the RHS of Eqn (4.27) by substitution, from the two last equations we get

$$\mathscr{N}_+(b;\mathscr{T}) = \frac{1}{2\pi}\sqrt{\frac{m_2}{m_0}} \exp\left(-\frac{b^2}{2m_0}\right)\mathscr{T} \tag{4.29}$$

4.4 COROLLARIES OF RICE'S PROBLEM

4.4.1 Probability of Crest Height and Wave Height

In general, we have

$$\mathscr{N}_{cr}(b;\mathscr{T}) \leq \mathscr{N}_+(b;\mathscr{T}) \tag{4.30}$$

where $\mathscr{N}_{cr}(b;\mathscr{T})$ is the expected number of wave crests higher than a fixed threshold b in time interval $\mathscr{T}$. (Figure 4.1 helps to realize this inequality.) However, in the limit as $b/\sigma \to \infty$, inequality Eqn (4.30) becomes an equality. Therefore,

$$P(C > b) = \frac{\mathscr{N}_+(b;\mathscr{T})}{\mathscr{N}_+(0;\mathscr{T})} \quad \text{as} \quad b/\sigma \to \infty \tag{4.31}$$

where $P(C > b)$ represents the probability that a wave crest be higher than a given threshold b. Equations (4.29) and (4.31) yield

$$P(C > b) = \exp\left(-\frac{b^2}{2m_0}\right) \quad \text{as} \quad b/\sigma \to \infty \tag{4.32}$$

which holds for every spectrum.

Inequality Eqn (4.30) becomes an equality for every b if the spectrum is very narrow. This is because each wave approaches a sinusoidal wave. Hence,

$$P(C > b) = \exp\left(-\frac{b^2}{2m_0}\right) \tag{4.33}$$

for every b if the spectrum is very narrow. Moreover, if the spectrum is very narrow, the wave height is twice the height of the wave crest, so that

$$P(\text{wave height} > H) = P(C > H/2) \tag{4.34}$$

The last two equations lead to

$$P(\text{wave height} > H) = \exp\left(-\frac{H^2}{8}\right) \tag{4.35}$$

4.4.2 The Mean Wave Period

The mean wave period is given by the quotient between the very large time interval $\mathscr{T}$ and the number $\mathscr{N}_+(0;\mathscr{T})$ of zero up-crossings in this interval:

$$T_m = \mathscr{T}/\mathscr{N}_+(0;\mathscr{T}) \tag{4.36}$$

(bearing in mind that the number of waves is equal to the number of zero up-crossings). With Eqn (4.29) of $\mathscr{N}_+(b;\mathscr{T})$, Eqn (4.36) becomes

$$T_m = 2\pi\sqrt{\frac{m_0}{m_2}} \tag{4.37}$$

that is-the formula of the mean wave period.

With the JONSWAP spectrum, we have

$$\frac{m_0}{m_2} = \frac{Ag^2\omega_p^{-4}\displaystyle\int_0^\infty \mathscr{E}(w)\mathrm{d}w}{Ag^2\omega_p^{-2}\displaystyle\int_0^\infty w^2\,\mathscr{E}(w)\mathrm{d}w} \tag{4.38}$$

where $\mathscr{E}(w)$ is defined by Eqn (3.42), and hence

$$T_m = T_p\sqrt{\frac{\displaystyle\int_0^\infty \mathscr{E}(w)\mathrm{d}w}{\displaystyle\int_0^\infty w^2\,\mathscr{E}(w)dw}} \tag{4.39}$$

The two integrals may be numerically evaluated for given values of the shape parameters χ_1 andχ_2 in the expression of $\mathscr{E}(w)$, and with the values of the mean JONSWAP spectrum ($\chi_1 = 3.3$, $\chi_2 = 0.08$), the result is

$$T_m = 0.78T_p \tag{4.40}$$

4.5 CONSEQUENCES OF THE QD THEORY ONTO WAVE STATISTICS

4.5.1 Period T_h of a Very Large Wave

Let us consider the set of the waves with a given height H, say $H = 3\sigma$, in a stationary Gaussian random process. The waves of this set will be different, even very different, from one another.

If we fixed a larger H, say $H = 8\sigma$, we would find that the waves contained in the set differ much less from one another. Also, in the limit as $H/\sigma \to \infty$, all the waves of the set, apart from a negligible share, would prove to be equal to one another. More specifically, each wave of the set would occupy the center of a well-defined group that is the sum of a deterministic framework and a residual random noise of a smaller order. The form of the deterministic component is

$$\overline{\eta}(T) = \frac{\psi(T) - \psi(T - T^*)}{\psi(0) - \psi(T^*)} \frac{H}{2} \tag{4.41}$$

where T^* is the abscissa of the absolute minimum, being assumed to be also the first minimum, of the autocovariance. As a consequence, it follows that, most probably, a wave of given height H very large has a well-defined period. This is

$$T_h = \text{period of the central wave of the group Eqn (4.41)} \tag{4.42}$$

where the subscript h stands for *high wave*.

With the JONSWAP spectrum, the deterministic wave group Eqn (4.41) becomes

$$\frac{\overline{\eta}(T)}{H} = \frac{1}{2} \frac{\displaystyle\int_0^\infty \mathscr{E}(w)\left\{\cos\left(2\pi w \frac{T}{T_p}\right) - \cos\left[2\pi w\left(\frac{T}{T_p} - \frac{T^*}{T_p}\right)\right]\right\} \mathrm{d}w}{\displaystyle\int_0^\infty \mathscr{E}(w)\left\{1 - \cos\left(2\pi w \frac{T^*}{T_p}\right)\right\} \mathrm{d}w} \tag{4.43}$$

For obtaining T_h, we must plot the function of T/T_p on the RHS of this equation. This function represents a dimensionless wave group. The period of the central wave of this group is equal to T_h/T_p (see Fig. 4.3).

4.5.2 The Wave Height Probability under General Bandwidth Assumptions

Figure 4.4(a) shows two possibilities of waves with a given height H. These possibilities are ∞^2 because the crest elevation may take on any value within 0 and H and the time interval between the crest and trough may take on any positive value. The situation is suitably represented in a

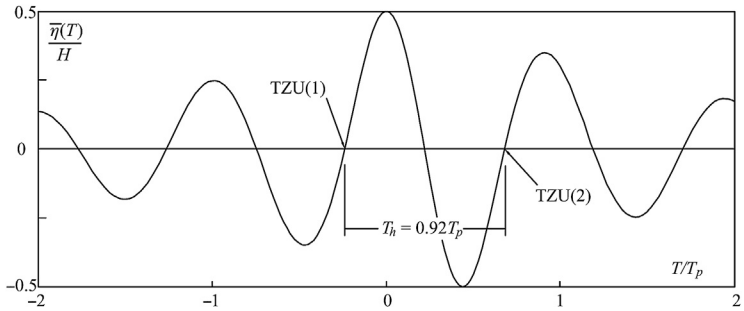

■ **FIGURE 4.3 Function (Eqn 4.41) obtained with the mean JONSWAP spectrum.**

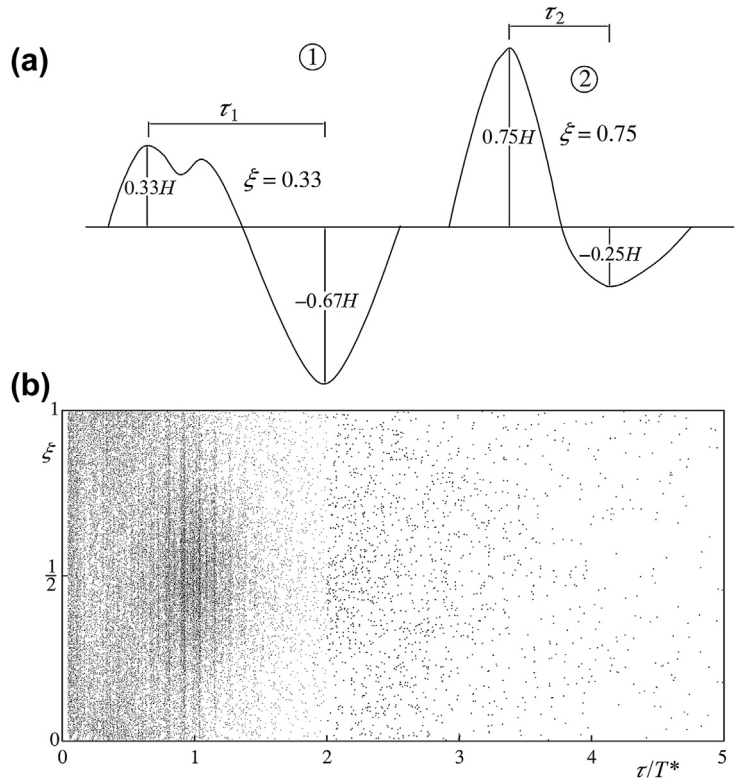

■ **FIGURE 4.4 The waves with a fixed height *H* generally show a large variety of ξ and τ: two examples are shown in panel** (a). Plotting ξ versus τ; generally we get a wide cloud of points (panel (b)).

plane τ-ξ, where τ is the crest-trough lag and ξ is the quotient between crest elevation and crest-to-trough wave height. In particular, the two waves (1) and (2) of Fig. 4.4(a) are represented by two distinct points in the plane τ-ξ.

Let us suppose to examine a very large time interval $\mathscr{T}$, to gather all the waves whose height is in a fixed small interval H, $H + \mathrm{d}H$, and to mark the points representative of these waves in the plane τ-ξ. If H/σ is finite, the marked points would spread over the plane τ-ξ, as we see in Fig. 4.4(b). On the contrary, as $H/\sigma \to \infty$, we would look at a great concentration: all the points but a negligible share would fall in an open 2-ball with center at $T^*, \frac{1}{2}$ and radius of order $(H/\sigma)^{-1}$. In the paper (1989) I obtained a number of these points (see also Sections 9.6–9.10 of my book (2000)). This led to the closed form solution for the asymptotic form of the probability of wave heights in the limit as $H/\sigma \to \infty$. This is

$$P(\text{wave height} > H) = K_1 \exp\left(-\frac{H^2}{K_2 m_0}\right), \quad \text{as } H/\sqrt{m_0} \to \infty \tag{4.44}$$

where

$$K_1 = \frac{(1+\ddot{\psi}^*)}{\sqrt{2\ddot{\psi}^*(1+\psi^*)}} \tag{4.45}$$

$$K_2 = 4(1+\psi^*) \tag{4.46}$$

with

$$\psi^* = \left|\frac{\psi(T^*)}{\psi(0)}\right|, \quad \ddot{\psi}^* = \left|\frac{\ddot{\psi}(T^*)}{\ddot{\psi}(0)}\right| \tag{4.47}$$

With the JONSWAP spectrum, T^*/T_p and ψ^* are obtained directly from the function $\psi(T)/\psi(0)$ versus T/T_p—Eqn (3.41). As to $\ddot{\psi}^*$ it is given by

$$\ddot{\psi}^* = \frac{\left|\int_0^\infty \mathscr{E}(w) w^2 \cos\left(2\pi w \frac{T^*}{T_p}\right) \mathrm{d}w\right|}{\int_0^\infty \mathscr{E}(w) w^2 \mathrm{d}w} \tag{4.48}$$

The probability Eqn (4.44) is used also in the form

$$P(\alpha > \overline{\alpha}) = K_1 \exp\left(-\frac{\overline{\alpha}^2}{K_2}\right), \quad \text{as } \overline{\alpha} \to \infty \tag{4.49}$$

where $P(\alpha > \overline{\alpha})$ represents the probability that

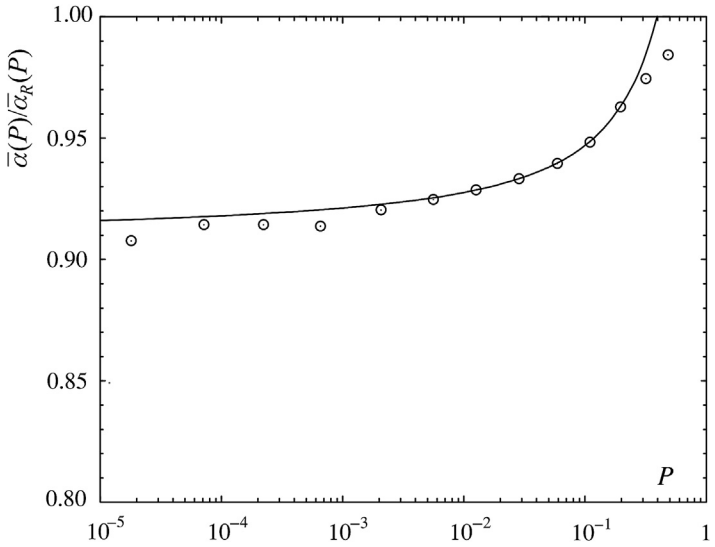

■ **FIGURE 4.5** Abscissa: the probability of exceedance; ordinate: the quotient between the wave height and the wave height with a very narrow spectrum. *Data points from numerical simulations of stationary Gaussian processes by Forristall (1984).*

$$\alpha = \text{wave height}/\sigma \tag{4.50}$$

exceeds some fixed threshold $\overline{\alpha}$. Equation (4.49) holds as $\overline{\alpha}$ tends to infinity, that is, as P approaches zero. However, with characteristic spectra of wind seas, it proves to be effective for P smaller than about 0.3, as we may see in Fig. 4.5. This figure shows the ratio

$$\overline{\alpha}(P)/\overline{\alpha}_R(P) \text{ versus } P \tag{4.51}$$

where $\overline{\alpha}(P)$ is the value of $\overline{\alpha}$ that has a given probability P to be exceeded, in a random process with a given spectrum, and $\alpha_R(P)$ is the value of $\overline{\alpha}$ that has a given probability P to be exceeded in the random process with the very narrow spectrum. The continuous line has been obtained with the asymptotic Eqn (4.49), which gives

$$\overline{\alpha}(P)/\overline{\alpha}_R(P) = \sqrt{K_2 \frac{\ln(K_1/P)}{8\ln(1/P)}} \tag{4.52}$$

The data points are from numerical simulations of stationary Gaussian processes by Forristall (1984).

4.6 FIELD VERIFICATION

4.6.1 An Experiment on Wave Periods

Let us obtain the pairs $\alpha_i, \tilde{T}_i$ for $i = 1, N$ with N being the number of waves of a record: α_i is the ratio between the height of the ith wave and the σ of the sea state, and $\tilde{T}_i$ is the ratio between the period of the ith wave and the T_h of the sea state. Let us gather the pairs $\alpha_i, \tilde{T}_i$ of a number of records from sea states, generally different from one another, and let us plot these pairs: each pair is represented by one point whose abscissa is α_i and whose ordinate is $\tilde{T}_i$. We shall obtain a cloud of points like that of Fig. 4.6. From the quasi-determinism (QD) theory, we expect that the rightmost points of the cloud have ordinates close to 1, and this is what typically happens.

4.6.2 The Random Variable β

In view of a verification of the distribution of wave heights in sea states, it is convenient defining a new random variable

$$\beta = \sqrt{8\left(\frac{\alpha^2}{K_2} - \ln K_1\right)} \tag{4.53}$$

β is a monotonic growing function of α, and the inverse function

$$\alpha = \sqrt{K_2\left(\frac{\beta^2}{8} + \ln K_1\right)} \tag{4.54}$$

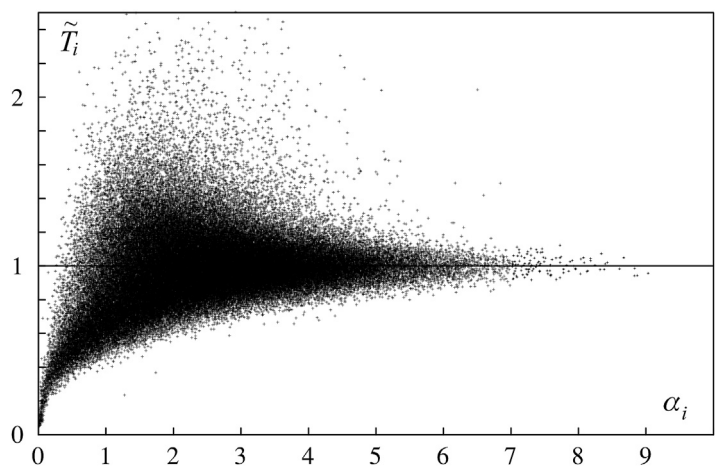

■ **FIGURE 4.6 Dimensionless wave period versus dimensionless wave height.** *Data points from a small scale field experiment of 1990, described in Chapter 9.*

is a monotonic growing function of β. From Eqn (4.54), it follows that

$$P(\beta > \overline{\beta}) = P\left(\alpha > \sqrt{K_2\left(\frac{\overline{\beta}^2}{8} + \ln K_1\right)}\right) \tag{4.55}$$

where $\overline{\beta}$ is an arbitrary threshold. Finally, from Eqns (4.49) and (4.55), it follows that

$$P(\beta > \overline{\beta}) = \exp\left(-\frac{\overline{\beta}^2}{8}\right), \quad \text{as } \overline{\beta} \to \infty \tag{4.56}$$

If the distribution of α is given by Eqn (4.49), the distribution of β is given by Eqn (4.56), and vice versa. As we may see, the asymptotic distribution of the random variable β does not depend on the spectrum shape.

A clear confirmation of Eqn (4.56) is given by Fig. 4.7, where the data points were obtained from more than six million individual waves from sea states with a large variety of spectra (Boccotti, 2012). We see that the convergence of the data points onto the asymptotic form Eqn (4.56) is very fast: the agreement between data points and asymptotic form being nearly perfect for $\overline{\beta} > 2$.

The same strict agreement between data points and asymptotic form Eqn (4.56) emerges from a new small-scale field experiment (SSFE) of

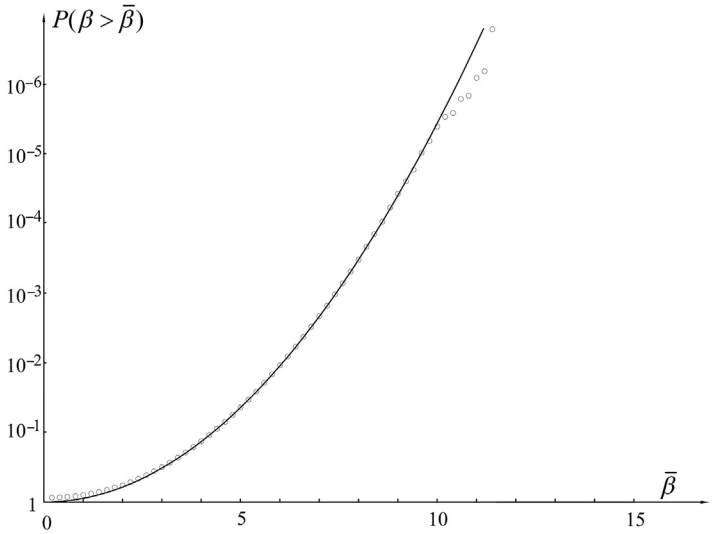

■ **FIGURE 4.7** $P(\beta > \overline{\beta})$ from a small-scale field experiment of 2010 on a very large variety of spectra, with a total number of 6,300,000 individual waves.

2012 on the distribution of wave heights in the space domain (Boccotti, 2013). This represents a strong test of the theory given that the range of values of K_1, K_2 for the waves in the space domain is different from the range of values of K_1, K_2 characteristic of the waves in the time domain. As an example, in the SSFE of 2012:

K_1 (1.1, 2.5) in the space domain → K_1 (1.0, 1.4) in the time domain.
K_2 (4.1, 6.8) in the space domain → K_2 (5.9, 7.6) in the time domain.

4.7 MAXIMUM EXPECTED WAVE HEIGHT AND CREST HEIGHT IN A SEA STATE OF GIVEN CHARACTERISTICS

4.7.1 The Maximum Expected Wave Height

Let us consider N consecutive waves of a sea state of given significant height. The probability that the largest wave height of this set of N waves is smaller than a given threshold H is equal to the probability that all the N wave heights are smaller than H, that is,

$$\mathscr{P}(H_{\max} < H) = [1 - P(\text{wave height} > H)]^N \tag{4.57}$$

which implies

$$P(H_{\max} > H) = 1 - [1 - P(\text{wave height} > H)]^N \tag{4.58}$$

Equations (4.57) and (4.58) are based on the assumption that the wave heights are stochastically independent of one another. Given that this assumption is not fully satisfied, Eqn (4.58) is slightly conservative, in that it slightly overpredicts the probability of exceedance of $H_{\max}$ (see Section 5.10.1 of Boccotti, 2000).

The mean value of a positive random variable V, like $H_{\max}$, is related to the probability of exceedance $P(V > x)$ by

$$\overline{V} = \int_0^\infty P(V > x)\mathrm{d}x \tag{4.59}$$

Hence, in the special case that $V = H_{\max}$, we have

$$\overline{H_{\max}} = \int_0^\infty P(H_{\max} > H)\mathrm{d}H \tag{4.60}$$

In order to understand the meaning of $\overline{H_{\max}}$, let us imagine taking n sets each of N consecutive waves from a sea state. The first set will have a

maximum wave height $H_{\max 1}$, the second set will have a maximum wave height $H_{\max 2}$ generally different from $H_{\max 1}$, and so on as far as the nth set whose maximum wave height will be $H_{\max n}$. $\overline{H_{\max}}$ represents the average of $H_{\max 1}$, $H_{\max 2}$, etc. Equations (4.44), (4.58), and (4.60) yield

$$\overline{H_{\max}} = \int_0^\infty 1 - \left[1 - K_1 \exp\left(-\frac{H^2}{K_2 m_0}\right)\right]^N \mathrm{d}H \tag{4.61}$$

The use of the asymptotic form Eqn (4.44) of P(wave height $> H$) is justified because the integrand in Eqn (4.60) gets appreciably different from 1 for H/σ definitely greater than 4 wherein the asymptotic form proves to be fully efficient.

4.7.2 Maximum Expected Crest Height

The reasoning done for $\overline{H_{\max}}$ may be repeated for obtaining $\overline{b_{\max}}$, the maximum expected height of a wave crest. We have

$$\overline{b_{\max}} = \int_0^\infty P(b_{\max} > b)\mathrm{d}b \tag{4.62}$$

that is,

$$\overline{b_{\max}} = \int_0^\infty 1 - [1 - P(C > b)]^N \mathrm{d}b \tag{4.63}$$

and, with the asymptotic form Eqn (4.32) of $P(C > b)$:

$$\overline{b_{\max}} = \int_0^\infty 1 - \left[1 - \exp\left(-\frac{b^2}{2m_0}\right)\right]^N \mathrm{d}b \tag{4.64}$$

$\overline{b_{\max}}$ proves to be greater than $\overline{H_{\max}}/2$.

4.8 FORTRAN PROGRAMS FOR THE MAXIMUM EXPECTED WAVE IN A SEA STATE OF GIVEN CHARACTERISTICS

The characteristics of a sea state are H_s, duration, and spectrum shape. Here, we assume to know these characteristics and aim to estimate height and period of the maximum expected wave. The following FORTRAN programs serve for this aim.

4.8.1 A Program for the Basic Parameters on Deep Water

Program SUMMARY calculates T^*/T_p and ψ^* (Eqn (3.41)), K_0 (Eqn (3.46)), T_m/T_p (Eqn (4.39)), T_h/T_p (Eqn (4.43)), $\ddot{\psi}^*$ (Eqn (4.48)), K_1 (Eqn (4.45)), and K_2 (Eqn (4.46)) with the JONSWAP spectrum. The equations of these parameters have been obtained throughout Chapters 3 and 4; hence, the title SUMMARY of the program. With the JONSWAP spectrum these parameters depend only on function $\mathscr{E}(w)$ defined by Eqn (3.42), which calls for two shape parameters χ_1, χ_2.

```
      PROGRAM SUMMARY
      DIMENSION EW(500),WV(500)
      DIMENSION TAUV(200),ETADET(200),TZU(5)
      PG=3.141592
      DPG=2.*PG
      WRITE(6,*)'chi1,chi2'
      READ(5,*)CHI1,CHI2
      C1=ALOG(CHI1)
      C2=2*CHI2*CHI2
      WIN=0.5
      WMAX=5

c calculation of E(w) -Eqn (3.42)-
      DW=0.02
      W=WIN-DW/2
      I=0
90    W=W+DW
      IF(W.GT.WMAX)GO TO 91
      I=I+1
      WM1=W-1
      W2=W*W
      W4=W2*W2
      W5=W4*W
      ARG3=WM1*WM1/C2
      E3=EXP(-ARG3)
      ARG2=C1*E3
      E2=EXP(ARG2)
      ARG1=1.25/W4
      E1=EXP(-ARG1)

c values of w and E(w) stored on memory
      WV(I)=W
      EW(I)=E1*E2/W5
      GO TO 90
91    CONTINUE
      IMAX=I
```

```
c calculation of T*/Tp and psi*
       PSIMIN=0
       DTAU=0.01
       TAU=-DTAU
70     TAU=TAU+DTAU
c Loop 70 tau (=T/Tp) from 0 to 1
       IF(TAU.GT.1) GO TO 71
c SOMT integral, numerator of the RHS of Eqn (3.41)
c SOM0 integral, denominator of the RHS of Eqn (3.41)
       SOMT=0
       SOM0=0
       DO 75 I=1,IMAX
c Loop 75 over the stored values of w and E(w)
       W=WV(I)
       COSA=COS(DPG*W*TAU)
       SOMT=SOMT+EW(I)*COSA*DW
       SOM0=SOM0+EW(I)*DW
75     CONTINUE
       PSI=SOMT/SOM0
c PSI=psi(T)/psi(0)
       IF(PSI.LT.PSIMIN)THEN
       PSIMIN=PSI
       TAUMI=TAU
       ENDIF
       GO TO 70
71     CONTINUE
       TASTP=TAUMI
       PSIAS=ABS(PSIMIN)
c TASTP=T*/Tp
c PSIAS=psi*

c calculation of K0 - Eqn (3.46)-
       SOM0=0
c SOM0 integral on the RHS of Eqn (3.46)
       DO I=1,IMAX
       SOM0=SOM0+EW(I)*DW
       ENDDO
       RK0=1./SOM0**0.25

c calculation of Tm/Tp - Eqn (4.39) -
c SOM0 integral, numerator of the RHS of Eqn (4.39)
c SOM2 integral, denominator of the RHS of Eqn (4.39)

       SOM0=0
       SOM2=0
       DO I=1,IMAX
       W=WV(I)
```

```
     .SOM0=SOM0+EW(I)*DW
      SOM2=SOM2+EW(I)*W*W*DW
      ENDDO
      TMTP=SQRT(SOM0/SOM2)

c TMTP=Tm/Tp
c calculation of Th/Tp
      DTAU=0.01
      TAUI=-0.5
      TAUF=1
      TAU=TAUI-DTAU
      J=0
80    TAU=TAU+DTAU
c Loop 80: TAU=T/Tp from -0.5 to 1
      IF(TAU.GT.TAUF)GO TO 81
      J=J+1
c SOM1 integral, numerator of the RHS of Eqn (4.43)
c SOM2 integral, denominator of the RHS of Eqn (4.43)
      SOM1=0
      SOM2=0
      DO I=1,IMAX
      W=WV(I)
      ARG1=DPG*W*TAU
      ARG2=DPG*W*(TAU-TASTP)
      ARG3=DPG*W*TASTP
      SOM1=SOM1+EW(I)*(COS(ARG1)-COS(ARG2))*DW
      SOM2=SOM2+EW(I)*(1-COS(ARG3))*DW
      ENDDO
      ETADET(J)=0.5*SOM1/SOM2
      TAUV(J)=TAU
c ETADET(J) = eta deterministic(tau)/H - Eqn (4.43) -
c TAUV(J)=T/Tp

      GO TO 80
81    CONTINUE
      JMAX=J

      NZU=0
      DO 65 J=2,JMAX

c Loop 65 over the stored values of eta deterministic(tau)/H - Eqn (4.43) -2
      TAU=TAUV(J)
      IF(ETADET(J).GE.0.AND.ETADET(J-1).LT.0)THEN
      NZU=NZU+1
      E1=-ETADET(J-1)
      E2=ETADET(J)
      TZU(NZU)=TAU-DTAU+DTAU*E1/(E1+E2)
```

```
      .ENDIF
65     CONTINUE
       THTP=TZU(2)-TZU(1)
c THTP=Th/Tp
c calculation of psi..* - Eqn (4.48) -
c SOM1 integral, numerator of the RHS of Eqn (4.48)
c SOM2 integral, denominator of the RHS of Eqn (4.48)
       SOM1=0
       SOM2=0
       DO I=1,IMAX
       W=WV(I)
       W2=W*W
       ARG=DPG*W*TASTP
       COSA=COS(ARG)
       SOM1=SOM1+EW(I)*W2*COSA*DW
       SOM2=SOM2+EW(I)*W2*DW
       ENDDO
       PSIS=ABS(SOM1/SOM2)
c PSIS=psi..*
c calculation of K1 -Eqn (4.45)-
       RNUM=1+PSIS
       RDEN=SQRT(2.*PSIS*(1.+PSIAS))
       RK1=RNUM/RDEN

c calculation of K2 -Eqn (4.46)-
       RK2=4.*(1.+PSIAS)

       WRITE(6,1001)TASTP
       WRITE(6,1002)PSIAS
       WRITE(6,1003)RK0
       WRITE(6,1004)TMTP
       WRITE(6,1005)THTP
       WRITE(6,1006)RK1
       WRITE(6,1007)RK2
1001   FORMAT(2X,'T*/Tp ',f7.2)
1002   FORMAT(2X,'psi* ',f7.2)
1003   FORMAT(2X,'K0 ',f7.3)
1004   FORMAT(2X,'Tm/Tp ',f7.2)
1005   FORMAT(2X,'Th/Tp ',f7.2)
1006   FORMAT(2X,'K1 ',f7.2)
1007   FORMAT(2X,'K2 ',f7.2)
       END
```

In this program, TAU is the ratio T/T_p. The function of TAU on the RHS of Eqn (4.43) is calculated from TAUI $= -0.5$ to TAUF $= 1$ with a step DTAU $= 0.01$ and is stored on the vector ETADET. Then the program

Table 4.1 Values of Some Basic Parameters in Sea States with the Mean JONSWAP Spectrum

T^*/T_p	0.44
ψ^*	0.73
K_0	1.345
$\overline{T}/T_p$	0.78
T_h/T_p	0.92
K_1	1.16
K_2	6.91

searches the two zero up-crossings of this function, in the domain (TAUI, TAUF). The TAU of the first zero up-crossing is TZU(1), and the TAU of the second zero up-crossing is TZU(2)—see Fig. 4.3. T_h/T_p is equal to the interval (TZU(2) − TZU(1)). With the mean JONSWAP spectrum ($\chi_1 = 3.3$, $\chi_2 = 0.08$), the program gives the values of Table 4.1.

4.8.2 A Program for the Basic Parameters on a Finite Water Depth, Using the Shape of the TMA Spectrum

A program for finite water, which we shall call SUMM1, may be obtained with the following changes from SUMMARY:

1. d and T_p must be supplied as inputs (hence the part of the program concerning K_0 may be canceled), and T_p may be obtained running SUMMARY for deep water;
2. the dimensionless spectrum $\mathscr{E}(w)$ must be multiplied by the transformation function TFU (see Section 3.4.6); specifically the line

```
EW(I)=E1*E2/W5
```

must be changed into

```
EW(I)=TFU(W,DLP0)*E1*E2/W5
```

where DLP0 is the ratio d/L_{p0}.

The transformation function is listed here:

```
FUNCTION TFU(w,DLP0)
PG=3.141592
DPG=2.*PG
```

```
c calculation of the dimensionless wave number - Eqn (3.51)-
      W2=W*W
      DX=1
      X=0
110   X=X+DX
      F=X*TANH(DPG*X*DLPO)
      IF(F.LT.W2)GO TO 110
      X=X-DX
      DX=DX/10.
      IF(DX.GT.2.E4)GO TO 110
      RKW=X
c RKW=kw
c calculation of TFU: function on the RHS of Eqn (3.52) divided by E0(w)
      ARG=4.*PG*RKW*DLPO
      IF(ARG.LT.30.)THEN
      SI2=SINH(ARG)
      DEN=SI2+ARG
      RMOL=SI2/DEN
      ARG=ARG/2
      TA=TANH(ARG)
      TFU=TA*TA*RMOL
      ELSE
      TFU=1
      ENDIF
      RETURN
      END
```

4.8.3 A Program for the Maximum Expected Wave Height

The third program is HMAX. It calculates $\overline{H_{\max}}$ in a sequence of N waves of given H_s and given spectrum:

```
      PROGRAM HMAX
      DOUBLE PRECISION UPH,PC,PDBLE
      CHARACTER*64 NOMEC
      NOMEC='PROHMAX'
      OPEN(UNIT=66,FILE=NOMEC)
      WRITE(6,*)'Hs,N'
      READ(5,*)HS,N
      WRITE(6,*)'K1,K2'
      READ(5,*)RK1,RK2
      SIG=HS/4.
      RMO=SIG*SIG
      DH=0.10
      HMA=0
c HMA value of the integral to be executed in the loop 90
      H=-DH/2.
```

```
      .90H=H+DH

c Loop 90: integral with respect to H on the RHS of Eqn (4.61)
      IF(H.GT.3.*HS)GO TO 91
      ARG=H*H/(RK2*RM0)
      EE=EXP(-ARG)
      PH=RK1*EE
      UPH=1.-DBLE(PH)
      PC=UPH**N
      PDBLE=1.-PC
      P=PDBLE
c P=P(Hmax>H)
      WRITE(66,1010)H,P
1010  FORMAT(2X,F7.2,2X,E12.4)
      HMA=HMA+P*DH
      GO TO 90
91    CONTINUE
      WRITE(6,1000)HMA
1000  FORMAT(2X,'Hmax ',f7.2)
      WRITE(6,*)'read file prohmax'
      END
```

4.8.4 **Worked Example**

Deep water sea state: $H_s = 8$ m, duration $= 5$ h, spectrum: mean JONSWAP with $A = 0.01$.

1. Calculation of T_p by means of Eqn (3.47):

$$T_p = \frac{1.345}{\sqrt[4]{0.01}}\pi\sqrt{8/9.8} = 12.1 \text{ s}$$

2. Calculation of T_m:

$$T_m = 0.78T_p = 9.4 \text{ s}$$

3. Calculation of the number of waves in the sea state:

$$N = \text{duration}/T_m = 5 \cdot 3600/9.4 = 1915$$

4. The run of program HMAX with input data $H_s = 8$ m, $N = 1915$, $K_1 = 1.16$, $K_2 = 6.91$ gives

$$\overline{H_{\max}} = 15.1 \text{ m}$$

5. Calculation of T_h:

$$T_h = 0.92T_p = 11.1 \text{ s}$$

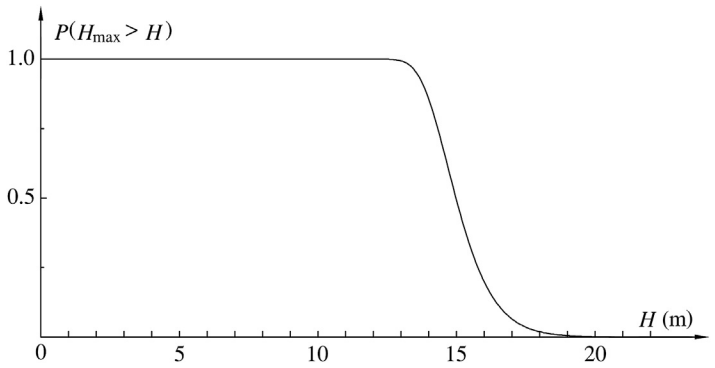

■ **FIGURE 4.8 Worked example of Section 4.8.4:** Probability P (ordinate) that the maximum wave height in a given sea state exceeds a given threshold H (abscissa). The maximum expected wave height in the sea state is the integral of this function on $(0, \infty)$.

Conclusion: the maximum expected wave in the given sea state has a height of 15.1 m and a period of 11.1 s. Figure 4.8 shows the probability $P(H_{max} > H)$, which is written by program HMAX on file PROHMAX (H: first column; P: second column).

4.9 CONCLUSION

I introduced Eqns (4.42) and (4.44) (or Eqn (4.49)), respectively, in the papers (1984) and (1989), as corollaries of the QD theory. Various comparisons of the asymptotic distribution (Eqn (4.49)) with oceanic data (Tayfun and Fedele, 2007; Casas–Prat and Holthuijsen, 2010) tend to support the effectiveness of this distribution, also under the effects of second-order corrections. The effects of third-order corrections may be of some relevance in wind seas, wherein the spectrum exhibits significant variability in space and/or time. These effects were dealt with under the narrowband assumption, by Tayfun and Lo (1990), Mori and Janssen (2006), Tayfun and Fedele (2007), Cherneva et al. (2009, 2013), Fedele et al. (2010). Resorting to Gram–Charlier series expansions was convenient, and the Gram–Charlier series approximation for the distribution of the wave heights (under narrowband assumption) proved to be (Tayfun and Fedele, 2007)

$$P(\alpha > \overline{\alpha}) = \exp\left(-\frac{\overline{\alpha}^2}{8}\right)\left[1 + \frac{\Lambda}{1024}\overline{\alpha}^2\left(\overline{\alpha}^2 - 16\right)\right] \tag{4.65}$$

where

$$\Lambda = \lambda_{40} + 2\lambda_{22} + \lambda_{04} \tag{4.66}$$

and

$$\lambda_{40} = \left\langle (\eta(t)/\sigma)^4 \right\rangle - 3 \tag{4.67}$$

$$\lambda_{22} = \left\langle (\eta(t)/\sigma)^2 (\widehat{\eta}(t)/\sigma)^2 \right\rangle - 1 \tag{4.68}$$

$$\lambda_{04} = \left\langle (\widehat{\eta}(t)/\sigma)^4 \right\rangle - 3 \tag{4.69}$$

with $\widehat{\eta}(t)$ being the Hilbert transform of $\eta(t)$. The fourth-order cumulants λ_{40}, λ_{22}, and λ_{04} are indexes of the differences between $\eta(t)$ and a stationary Gaussian process for which these cumulants are equal to zero. Then Alkhalidi and Tayfun (2013) suggested to generalize Eqn (4.49) into the form

$$P(\alpha > \overline{\alpha}) = K_1 \exp\left(-\frac{\overline{\alpha}^2}{K_2}\right)\left[1 + \frac{\Lambda}{16}\left(\frac{\overline{\alpha}^2}{K_2}\right)\left(\frac{\overline{\alpha}^2}{K_2} - 2\right)\right]$$

This form proved to be able to fit rather well even artificially created wave-flume conditions with rather large value of Λ due to fully developed third-order free−wave interactions.

REFERENCES

Alkhalidi, M.A., Tayfun, M.A., 2013. Generalized Boccotti distribution for nonlinear wave heights. Ocean Eng. 74, 101−106.

Boccotti, P., 1984. Sea waves and quasi-determinism of rare events in random processes. Atti Accad. Naz. Lincei Rendi. 76, 119−127.

Boccotti, P., 1989. On mechanics of irregular gravity waves. Atti Accad. Naz. Lincei Mem. VIII 19, 111−170.

Boccotti, P., 2000. Wave Mechanics for Ocean Engineering. Elsevier, Amsterdam, p. 495.

Boccotti, P., 2012. A new property of distributions of the heights of wind-generated waves. Ocean Eng. 54, 110−118.

Boccotti, P., 2013. On the distribution of wave heights in the space domain. Ocean Eng. 69, 54−59.

Casas-Prat, M., Holthuijsen, L.H., 2010. Short-term statistics of waves observed in deep water. J. Geophys. Res. 115, 5742−5761.

Cherneva, Z., Tayfun, M.A., Guedes Soares, C., 2009. Statistics of nonlinear waves generated in an offshore wave basin. J. Geophys. Res. 114, 5332−5339.

Cherneva, Z., Tayfun, M.A., Guedes Soares, C., 2013. Statistics of waves with different steepness simulated in a wave basin. Ocean Eng. 60, 186−192.

Fedele, F., Cherneva, Z., Tayfun, M.A., Guedes Soares, C., 2010. Nonlinear Schrodinger invariants and wave statistics. Phys. Fluids 22.

Forristall, G.Z., 1984. The distribution of measured and simulated heights as a function of spectra shape. J. Geophys. Res. 89, 10547−10552.

Mori, N., Janssen, P.A.E.M., 2006. On kurtosis and occurrence probability of freak waves. J. Phys. Ocean. 36, 1471−1483.

Rice, S.O., 1958. Distribution of the duration of fades in radio transmission. Bell Syst. Tech. J. 37, 581–635.

Tayfun, M.A., Lo, J.-M., 1990. Non-linear effects on wave envelope and phase. J. Waterw. Port Coast. Ocean Eng. 116, 79–100.

Tayfun, M.A., Fedele, F., 2007. Wave-height distribution and nonlinear effects. Ocean Eng. 34, 1631–1649.

Chapter 5

Design Wave

CHAPTER OUTLINE

Wave Mechanics and Wave Loads on Marine Structures. http://dx.doi.org/10.1016/B978-0-12-800343-5.00005-6

5.1 DISTRIBUTION OF H_S FOR A GIVEN GEOGRAPHIC LOCATION

5.1.1 Definition and Characteristic Form of the Distribution

Let us imagine we take a continuous record of the surface elevation $\eta(t)$ at a fixed location. We shall call $H_s(t)$ the significant wave height of the sea state being present at an instant t:

$$H_s(t) = 4\sqrt{\frac{1}{\Delta t}\int_{t-\Delta t/2}^{t+\Delta t/2}\eta^2(t')\mathrm{d}t'} \tag{5.1}$$

where Δt is the duration of a record. $H_s(t)$ is a random continuous function that is gradually variable, has a mean value that depends on the location, is not stationary because of a seasonal component, and has a strong statistical asymmetry with respect to the mean.

The probability of exceedance $P(H_s > h)$ is the ratio between the time in which H_s is greater than some fixed threshold h and the total time:

$$P(H_s > h) = \frac{1}{\mathscr{T}}\sum_i \Delta t_i(h) \tag{5.2}$$

where $\Delta t_i(h)$ are the time intervals in which H_s exceeds h at the fixed location, and $\mathscr{T}$ is the total time (see Fig. 5.1). The probability $p(H_s = h)\mathrm{d}h$ that $H_s(t)$ falls in a fixed small interval $(h,h+\mathrm{d}h)$ is equal to the ratio between the time in which $h < H_s < h+\mathrm{d}h$ and the total time:

$$p(H_s = h)\mathrm{d}h = \frac{1}{\mathscr{T}}\sum_i \mathrm{d}t_i(h;\mathrm{d}h) \tag{5.3}$$

where $\mathrm{d}t_i(h;\mathrm{d}h)$ is the ith time interval in which $h < H_s < h+\mathrm{d}h$ (see Fig. 5.2).

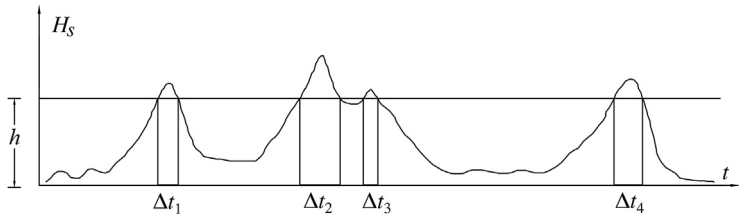

■ **FIGURE 5.1** $P(H_s > h)$ **is the quotient between summation** $(\Delta t_1 + \Delta t_2 + \ldots)$ **and total time.** Clearly, it can strongly change from one location to another.

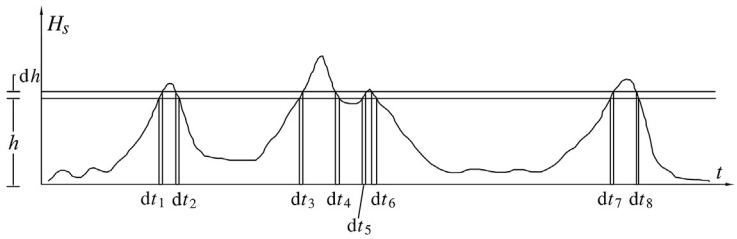

■ **FIGURE 5.2** $p(H_s = h)\mathrm{d}h$ **is the quotient between summation** $(\mathrm{d}t_1 + \mathrm{d}t_2 + \ldots)$ **and total time.**

The functions $P(H_s > h)$ and $p(H_s = h)$ are related to each other by

$$P(H_s > h) = \int_h^\infty p(H_s = h')\mathrm{d}h' \tag{5.4}$$

$$p(H_s = h) = -\frac{\mathrm{d}P(H_s > h)}{\mathrm{d}h} \tag{5.5}$$

which proceed from the definitions of these two functions.

Let us image we have 20,000 H_s data uniformly distributed over the seasons of the year, and let us suppose 2000 out of these 20,000 H_s data exceed 2.5 m. We shall have

$$P(H_s > 2.5\ \mathrm{m}) = \frac{2000}{20,000} = 0.10 \tag{5.6}$$

Similarly, we shall obtain $P(H_s > 3\ \mathrm{m})$, $P(H_s > 3.5\ \mathrm{m})$, and so on.

The data points of $P(H_s > h)$ are fitted by some theoretical form. In particular, in a previous book (2000) it was shown in some detail that a Weibull 2-parameter distribution

$$P(H_s > h) = \exp\left[-\left(\frac{h}{w}\right)^u\right] \tag{5.7}$$

is effective to fit the asymptotic distribution of many locations of the central Mediterranean Sea, as well as of some oceanic locations. Alternatively, $P(H_s > h)$ is commonly fitted by a Weibull or by a log-normal, since the pioneering work by Battjes (1972).

5.2 THE "EQUIVALENT TRIANGULAR STORM"

5.2.1 Maximum Expected Wave Height in a Given Storm

Let us consider a sea storm of given history $H_s(t)$. Let us subdivide the function $H_s(t)$ in steps of length Δt: h_i will be the H_s of the ith step. The probability that the maximum wave height ($H_{\max}$) in this storm is smaller than a

given threshold H is equal to the product of (probability that all the waves of the first step will be smaller than H) × (probability that all the waves of the second step will be smaller than H) × …… × (probability that all the waves of the Nth step will be smaller than H), with N being the number of steps. Accordingly, we have (Borgman, 1973)

$$\mathscr{P}(H_{\max} < H) = \prod_{i=1}^{N} [1 - P(H; H_s = h_i)]^{\frac{\Delta t}{T_{m_i}}} \tag{5.8}$$

where $P(H; H_s = h)$ is the probability that a wave height exceeds a fixed threshold H in a sea state of $H_s = h$; and

$$\prod_{i=1}^{N} A_i \equiv A_1 A_2 \cdots\cdots A_N \tag{5.9}$$

From Eqn (5.8) it follows that

$$P(H_{\max} > H) = 1 - \prod_{i=1}^{N} [1 - P(H; H_s = h_i)]^{\frac{\Delta t}{T_{m_i}}} \tag{5.10}$$

The Δt of the step function should be small so as to fit the given $H_s(t)$ of the actual sea storm. Δt within 5−10 min proves to be adequate for the estimate of $P(H_{\max} > H)$.

After having obtained $P(H_{\max} > H)$ (as a function of H), we may compute the maximum expected wave height of the storm. It suffices to recall that the mean value of a nonnegative random variable, like $H_{\max}$, is equal to the integral over $(0, \infty)$ of its probability of exceedance. The physical interpretation of $\overline{H_{\max}}$ is as follows. Let us consider n storms with the same time history. The maximum wave height of the first storm will be $H_{\max\,1}$, the maximum wave height of the second storm will be $H_{\max\,2}$, and so on. $\overline{H_{\max}}$ is the average of $H_{\max\,1}$, $H_{\max\,2}$, and so on.

5.2.2 Definition and Property of Equivalent Triangular Storm

We can associate with each actual sea storm an equivalent triangular storm (ETS) so defined:

1. the height a of the triangle is equal to the maximum significant wave height in the actual storm;
2. the base b of the triangle (that is, the duration of the ETS) is such that the maximum expected wave height of the triangular storm is equal to the maximum expected wave height of the actual storm.

According to this definition, the height of the triangle is immediately obtained, while the base will be obtained after a few attempts. It is convenient to fix a small base (duration of the triangular storm). Thus we shall find the maximum expected wave height of the triangular storm to be smaller than the maximum expected wave height of the actual storm. Then we shall gradually widen the base until the maximum expected wave height of the triangular storm will be equal to the maximum expected wave height of the actual storm.

We should expect that $P(H_{\max} > H)$ of the ETS is generally different from $P(H_{\max} > H)$ of the actual storm, and only their integrals over $(0, \infty)$ are equal to each other (since these integrals represent $\overline{H_{\max}}$). Unexpectedly, the two $P(H_{\max} > H)$ prove to be nearly coincident to each other. This is a general property that was found on comparing to each other the two $P(H_{\max} > H)$, the one of the ETS and the one of the actual storm, for several scores of locations (see an example in Fig. 5.3).

In conclusion, the actual storms have some irregular histories generally different from one another. However, an ETS can be associated with each actual storm. The equivalence between this ETS and the actual storm is full, since they have the same maximum value of the significant wave height and the same probability that the maximum wave height exceeds *any* fixed threshold H. Clearly, dealing with the ETS rather than with the actual storms simplifies the mathematical approach.

In the next section we shall deal with the equivalent sea consisting of the sequence of the ETS, and we shall obtain the solution for the return period of sea storms of given characteristics. For this job we have to consider the $P(H_s > h)$ relevant to the sequence of ETS. This proves to be essentially the same as the actual $P(H_s > h)$ in the range of practical interest, that is, for $h > 1.5-2.0$ times the average annual $H_s(t)$.

5.2.3 Regression Base Height of the ETS

Let us define a_{10} and b_{10} as, respectively, the average height a and the average base b of the 10 heaviest ETS in a year. Let us define

$$\tilde{a} = \frac{a}{a_{10}}, \quad \tilde{b} = \frac{b}{b_{10}} \tag{5.11}$$

In a previous book (Boccotti, 2000) the following form was suggested for fitting the regression of $\tilde{b}$ versus $\tilde{a}$:

$$\bar{\tilde{b}}(\tilde{a}) = K' \exp(K''\tilde{a}) \tag{5.12}$$

with values of K' and K'' peculiar to some wide areas of the globe (see Table 5.1).

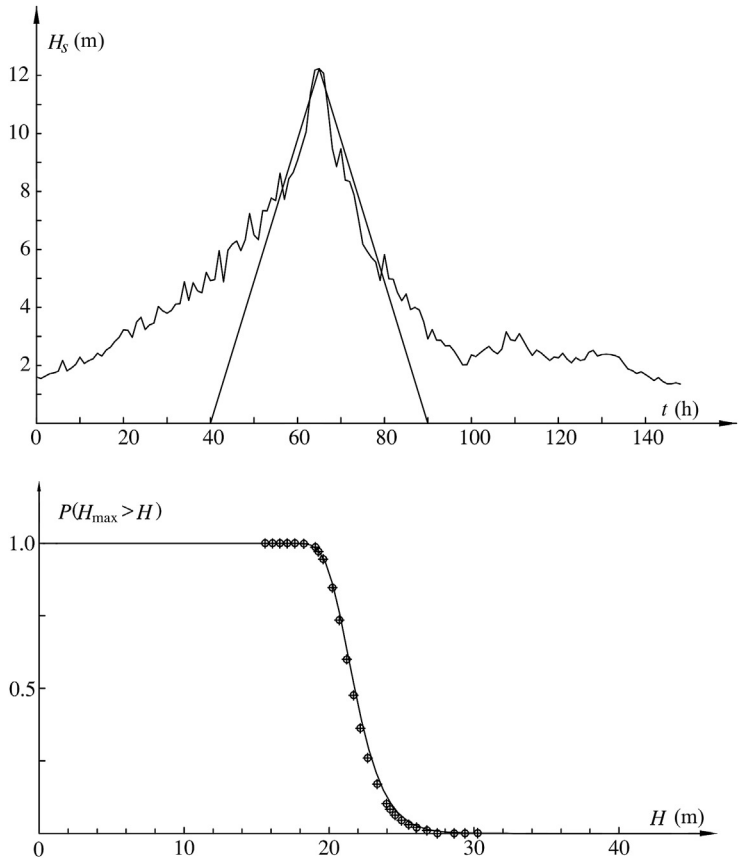

■ **FIGURE 5.3 A sea storm of September 2011 in the Atlantic Ocean, and its ETS.** We see that the $P(H_{max} > H)$ of the ETS (points) nearly coincides with the $P(H_{max} > H)$ of the actual storm (continuous line). The data of the actual storm are available at NOAA-National Data Buoy Center Web site (NDBC buoy 41048).

As to a_{10} and b_{10}, some typical values are: $a_{10} = 7.5-8.5$ m, $b_{10} = 60$ h for the Northeastern Pacific; $a_{10} = 6-7$ m, $b_{10} = 50-55$ h for the Northwestern Atlantic; $a_{10} = 3.0-3.5$ m, $b_{10} = 65-75$ h for the Central Mediterranean (off the western Sardinia coast a_{10} reaches 5 m and b_{10} 90 h).

Table 5.1 Parameters of Eqns (5.12) and (5.13)

	K'	K''
Northeastern Pacific	1.80	−0.59
Northwestern Atlantic	1.40	−0.46
Central Mediterranean	1.12	−0.11

Equation (5.12) in dimensional form becomes

$$\overline{b}(a) = K' b_{10} \exp\left(K'' \frac{a}{a_{10}}\right) \tag{5.13}$$

Note that the $\overline{b}(a)$ is decreasing (K'' being negative), and the rate of decrease is greater in the Pacific Ocean than in the Atlantic Ocean, and greater in the Atlantic Ocean than in the Mediterranean Sea. This phenomenon is due to the occurrence of sharp peaks of $H_s(t)$ in the largest storms, especially in the oceans.

5.3 RETURN PERIOD AND AVERAGE PERSISTENCE

The return period $R(H_s > h)$ of a sea storm wherein the H_s exceeds some given threshold at a given location represents the average time interval between the occurrences of two such sea storms at this location. The average persistence $\overline{D}(h)$ represents the average duration of time in which H_s remains above the given threshold h in the aforementioned sea storms.

5.3.1 Formal Solution for the Return Period $R(H_s > h)$

We shall write "triangle," "triangle height," "base of a triangle" in place of "ETS," "maximum H_s in an ETS," "duration of an ETS."

Let us define

$$p_A(a) \equiv \text{pdf of the triangle height} \tag{5.14}$$

$$p_B(b|A = a) \equiv \text{conditional pdf of the triangle base given the triangle height} \tag{5.15}$$

$$\mathcal{N}(\mathcal{T}) \equiv \text{number of triangles being present in a very large time interval } \mathcal{T} \tag{5.16}$$

$$\delta t(h, \mathrm{d}h, a, b) \equiv \text{time in which } H_s \text{ falls within a fixed small interval } (h, h + \mathrm{d}h) \text{ in a triangle of height } a \text{ and base } b \tag{5.17}$$

Using these definitions, we write

$$p_A(a)\,\mathrm{d}a\,\mathcal{N}(\mathcal{T}) = \text{number of triangles during } \mathcal{T}, \text{ the height of which belongs to a given interval } (a, a + \mathrm{d}a) \tag{5.18}$$

$$p_A(a)\,\mathrm{d}a\,\mathcal{N}(\mathcal{T})\,p_B(b|a)\mathrm{d}b = \text{number of triangles during } \mathcal{T}, \text{ the height of which belongs to a given interval } (a, a + \mathrm{d}a), \text{ and the base of which belongs to a given interval } (b, b + \mathrm{d}b) \tag{5.19}$$

$$[p_A(a)\,\mathrm{d}a\,\mathcal{N}(\mathcal{T})\,p_B(b|a)\mathrm{d}b]\delta t(h,\mathrm{d}h,a,b) \;=\; \text{time during } \mathcal{T}\text{, in which } H_s \text{ belongs to a given interval } (h, h+\mathrm{d}h)\text{, in the triangles the height of which is between } a \text{ and } a+\mathrm{d}a \text{ and the base of which is between } b \text{ and } b+\mathrm{d}b \tag{5.20}$$

It will have been noted that the LHS of the first equality, that is, $p_A(a)\,\mathrm{d}a\,\mathcal{N}(\mathcal{T})$, multiplied by $p_B(b|a)\mathrm{d}b$ becomes the LHS of the second equality, which in turn, multiplied by $\delta t(h,\mathrm{d}h,a,b)$, becomes the LHS of the third equality. In practice, the equalities (Eqns (5.18)–(5.20)) make a sequence. This sequence enables us to gradually trace the steps leading to Eqn (5.20), which is the true starting point of our analysis. It implies

$$\Delta t(h,\mathrm{d}h,\mathcal{T}) \;=\; \int_0^\infty \int_0^\infty p_A(a)\mathcal{N}(\mathcal{T})p_B(b|a)\delta t(h,\mathrm{d}h,a,b)\,\mathrm{d}b\,\mathrm{d}a \tag{5.21}$$

where $\Delta t(h,\mathrm{d}h,\mathcal{T})$ denotes *the time, during* $\mathcal{T}$*, in which* H_s *is within a small fixed interval* $(h, h+\mathrm{d}h)$.

As to $\delta t(h,\mathrm{d}h,a,b)$, its expression derives at once from its definition. It suffices to note that δt is zero for triangles like ① of Fig. 5.4 where $a < h$, while δt is equal to $(\mathrm{d}h/a)b$ for triangles like ②. Therefore

$$\delta t(h,\mathrm{d}h,a,b)\begin{cases} = (\mathrm{d}h/a)b & \text{if } a > h \\ = 0 & \text{if } a \le h \end{cases} \tag{5.22}$$

Substituting this expression of δt in Eqn (5.21), we obtain

$$\Delta t(h,\mathrm{d}h,\mathcal{T}) \;=\; \int_h^\infty \int_0^\infty p_A(a)\mathcal{N}(\mathcal{T})p_B(b|A=a)\frac{\mathrm{d}h}{a}b\,\mathrm{d}b\,\mathrm{d}a \tag{5.23}$$

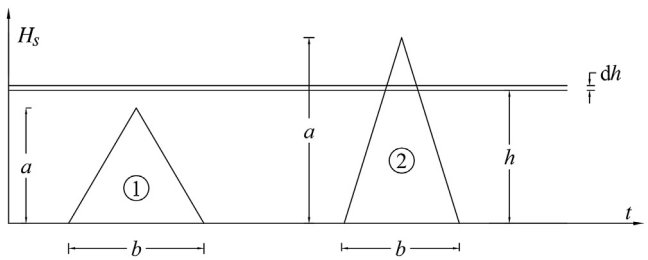

■ **FIGURE 5.4 Time duration of H_s within a fixed small interval $(h,h+\mathrm{d}h)$, in an ETS of height a and base b.** This duration is equal to $(\mathrm{d}h/a)b$ if $a > h$, while it is zero if $a < h$.

Note that the lower limit of the first integral passes from 0 in Eqn (5.21) to h in Eqn (5.23), as a consequence of the fact that $\delta t(h, \mathrm{d}h, a, b) = 0$ for $a \leq h$. Clearly, for the linearity property, the terms $\mathcal{N}(\mathcal{T})$ and $\mathrm{d}h$ in Eqn (5.23) may be put outside the integral. Then we may use the equality

$$\int_0^\infty p_B(b|a) b \mathrm{d}b \; = \; \overline{b}(a) \tag{5.24}$$

where $\overline{b}(a)$, introduced in Section 5.2.3, represents the mean base amplitude of the triangles with a given height a. Therefore Eqn (5.23) may be rewritten in the form

$$\Delta t(h, \mathrm{d}h, \mathcal{T}) \; = \; \mathcal{N}(\mathcal{T}) \mathrm{d}h \int_h^\infty p_A(a) \frac{1}{a} \overline{b}(a) \, \mathrm{d}a \tag{5.25}$$

More simply, $\Delta t(h, \mathrm{d}h, \mathcal{T})$ could have been written at once in the form

$$\Delta t(h, \mathrm{d}h, \mathcal{T}) \; = \; p(H_s \; = \; h) \mathrm{d}h \mathcal{T} \tag{5.26}$$

which proceeds from the definition of $p(H_s = h)$ (cf. Section. 5.1.1).

Equation (5.25) gives Δt in terms of the pdf $p_A(a)$, and Eqn (5.26) gives the same Δt in terms of the pdf $p(H_s = h)$. Hence equating the RHS of the two Eqns (5.25) and (5.26), we obtain the relation between the unknown function $p_A(a)$ and the known function $p(H_s = h)$:

$$\mathcal{N}(\mathcal{T}) \int_h^\infty p_A(a) \frac{1}{a} \overline{b}(a) \, \mathrm{d}a \; = \; p(H_s \; = \; h) \mathcal{T} \tag{5.27}$$

Here, differentiating with respect to h on both sides of the equation, we get

$$-\mathcal{N}(\mathcal{T}) p_A(h) \frac{1}{h} \overline{b}(h) \; = \; \frac{\mathrm{d}p(H_s \; = \; h)}{\mathrm{d}h} \mathcal{T} \tag{5.28}$$

and hence

$$p_A(a) \; = \; - \frac{\mathcal{T}}{\mathcal{N}(\mathcal{T})} \frac{a}{\overline{b}(a)} \frac{\mathrm{d}p(H_s \; = \; a)}{\mathrm{d}a} \tag{5.29}$$

(The change of variable from h in Eqn (5.28) to a in Eqn (5.29) is simply formal, h and a playing the role of dummy variables.)

The number of triangles whose height is greater than some fixed threshold h, in the time interval $\mathcal{T}$, is

$$\mathcal{N}(h, \mathcal{T}) \; = \; \mathcal{N}(\mathcal{T}) \int_h^\infty p_A(a) \, \mathrm{d}a \tag{5.30}$$

The return period $R(H_s > h)$, that is to say, the average time interval between two consecutive triangles with height exceeding h, is related to $\mathcal{N}(h, \mathcal{T})$ by

$$R(H_s > h) = \frac{\mathcal{T}}{\mathcal{N}(h, \mathcal{T})} \tag{5.31}$$

The last two equations yield

$$R(H_s > h) = \frac{\mathcal{T}}{\mathcal{N}(\mathcal{T}) \int_h^\infty p_A(a)\, \mathrm{d}a} \tag{5.32}$$

which, with the formula (Eqn (5.29)) of $p_A(a)$, becomes

$$R(H_s > h) = \frac{1}{-\int_h^\infty \frac{a}{\overline{b}(a)} \frac{\mathrm{d}p(H_s = a)}{\mathrm{d}a}\, \mathrm{d}a} \tag{5.33}$$

The convergence of the integral in the last equation is quick and, on the contrary, $\overline{b}(a)$ is a very gradually varying function. Hence, we achieve an excellent approximate form assuming $\overline{b}(a)$ to be constant on the interval of integration, that is, assuming

$$\overline{b}(a) = \overline{b}(h) \tag{5.34}$$

With this assumption, the expression of $R(H_s > h)$ becomes

$$R(H_s > h) = \frac{\overline{b}(h)}{-\int_h^\infty a \frac{\mathrm{d}p(H_s = a)}{\mathrm{d}a}\, \mathrm{d}a} \tag{5.35}$$

from which, integrating by parts, we arrive at

$$R(H_s > h) = \frac{\overline{b}(h)}{hp(H_s = h) + P(H_s > h)} \tag{5.36}$$

Finally, with the formula (Eqn (5.7)) of $P(H_s > h)$, we obtain the following simple formula for the return period:

$$R(H_s > h) = \frac{\overline{b}(h)}{1 + u\left(\frac{h}{w}\right)^u} \exp\left(\frac{h}{w}\right)^u \tag{5.37}$$

5.3.2 Corollary: The Equation of the Average Persistence

We have

$$P(H_s > h)\mathcal{T} = \text{time duration in which } H_s > h, \text{ in the long interval } \mathcal{T} \tag{5.38}$$

$$\mathscr{T}/R(H_s > h) = \text{number of storms in which } H_s \text{ exceeds the threshold } h, \text{ during } \mathscr{T} \tag{5.39}$$

from which it follows that

$$\overline{D}(h) = \frac{P(H_s > h)\mathscr{T}}{\mathscr{T}/R(H_s > h)} = P(H_s > h)R(H_s > h) \tag{5.40}$$

If $P(H_s > h)$ is given by Eqn (5.7), $\overline{D}(h)$ takes the form

$$\overline{D}(h) = \frac{\overline{b}(h)}{1 + u\left(\frac{h}{w}\right)^{\overline{u}}} \tag{5.41}$$

5.4 THE ENCOUNTER PROBABILITY OF A SEA STORM WITH SOME GIVEN CHARACTERISTICS

The encounter probability $\mathscr{P}(L, R)$ is the probability that at least one occurrence of a natural event of given return period R takes place during the lifetime L of a structure.

5.4.1 The Poisson Process

Let us consider a very large time interval $\mathscr{T}$ and subdivide it into a sequence of small intervals dt, as in Fig. 5.5. Let us get $\mathscr{T}/\mathrm{d}t$ white balls, and blacken $\mathscr{T}/R$ of these balls. Then let us put all the balls in a box, shuffle the balls, and draw them at random. Each draw is coupled with a new small interval dt: the first draw with the first small interval, the second draw with the second small interval, and so on. If the drawn ball is black we mark a point in the small interval, otherwise we do not. The points so marked represent a Poisson random point process (RPP). At the end, we shall have marked $\mathscr{T}/R$ points, as many points as black balls, and consequently the mean value of the inter-arrival times T_i will be

$$\overline{T_i} = \frac{\mathscr{T}}{\mathscr{T}/R} = R \tag{5.42}$$

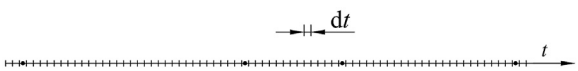

■ **FIGURE 5.5** How to generate a Poisson process: subdivide the time axis into a very large number of small intervals dt, and draw at random from a box containing white balls and black balls (one draw for each small interval). If the drawn ball is black, mark a point in the small interval.

Each point represents an occurrence of a natural event of given return period R. The probability $1 - \mathscr{P}(L, R)$ that no point occurs in the lifetime L is equal to

$$1 - \mathscr{P}(L, R) = \left(1 - \frac{\mathrm{d}t}{R}\right)^{L/\mathrm{d}t} \tag{5.43}$$

Here note that $(1 - \mathrm{d}t/R)$ is the probability that a given small interval $\mathrm{d}t$ does not contain a point; and $(L/\mathrm{d}t)$ is the number of small intervals $\mathrm{d}t$ being present in the lifetime L. Multiplying and dividing by R the exponent on the RHS of Eqn (5.43), and applying the limit

$$\lim_{w \to 0} (1 - w)^{\frac{1}{w}} = e^{-1} \tag{5.44}$$

we get

$$\mathscr{P}(L, R) = 1 - \exp\left(-\frac{L}{R}\right) \tag{5.45}$$

5.4.2 A General Inequality for the Encounter Probability

Let us consider a very long time interval of length $\mathscr{T}$, and a partition that determines a number of subintervals of length L. Whatever the RPP, we have

$$\begin{aligned} \mathscr{P}(L, R) &= \frac{\text{number of subintervals containing at least one point of the RPP}}{\text{number of subintervals}} \\ &\leq \frac{\text{number of points of the RPP}}{\text{number of subintervals}} \end{aligned} \tag{5.46}$$

The number of points of the RPP in the interval $\mathscr{T}$ is equal to $\mathscr{T}/R$, and the number of subintervals is equal to $\mathscr{T}/L$. Hence, it follows

$$\mathscr{P}(L, R) \leq \frac{\mathscr{T}/R}{\mathscr{T}/L} \tag{5.47}$$

that is,

$$\mathscr{P}(L, R) \leq \frac{L}{R} \tag{5.48}$$

5.5 THE DESIGN SEA STATE FOR GIVEN LIFETIME AND ENCOUNTER PROBABILITY

The design data are lifetime L and encounter probability $\mathscr{P}$. The minimum allowable value of L and the maximum allowable value of $\mathscr{P}$ are prescribed

for various classes of marine structures. Usually, R is obtained from $L, \mathscr{P}$, with the relationship valid for the Poisson process:

$$R(L, \mathscr{P}) = L \Big/ \ln\left(\frac{1}{1-\mathscr{P}}\right) \tag{5.49}$$

which proceeds from Eqn (5.45).

Then we obtain the function $R(H_s > h)$, and we get the value of the abscissa $h(R)$ related to the given value of the ordinate R. $h(R)$ is the threshold that is exceeded on average once in R years, and the persistence of H_s above this threshold is a random variable whose mean value $\overline{D}[h(R)]$ is given by Eqn (5.40). This means that once in R years we have a stage of a storm of a duration of $2\overline{D}[h(R)]$ wherein the average H_s is equal to $h(R)$. Figure 5.6 is helpful to realize this concept. Accordingly, we may take as design sea state one with

$$H_s = h(R), \quad \text{duration} = 2\overline{D}[h(R)] \tag{5.50}$$

If, conservatively, we assume the maximum value of R for given L and $\mathscr{P}$, from Eqn (5.48) we have

$$R = L/\mathscr{P} \tag{5.51}$$

and the value of $h(R)$ may increase within about the 3%, and in most cases of practical interest within only the 1%, so that the consequences on the design sea state are small.

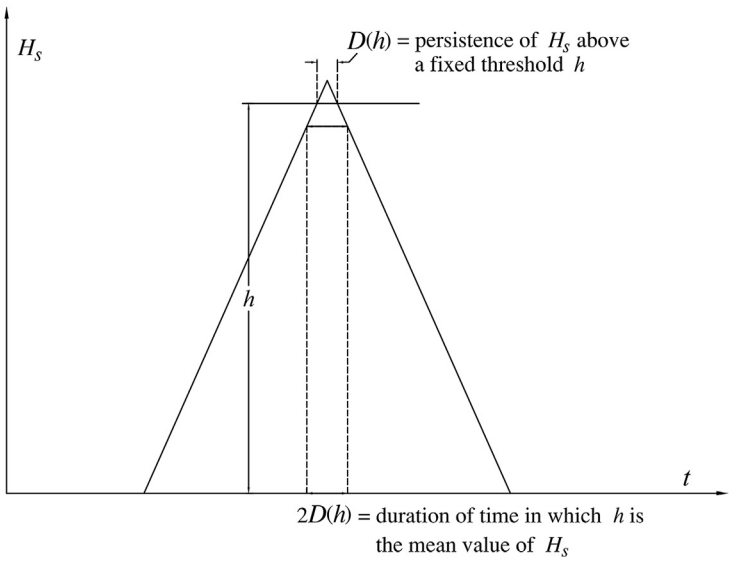

■ **FIGURE 5.6 Graphic aid to realize Eqn (5.50).**

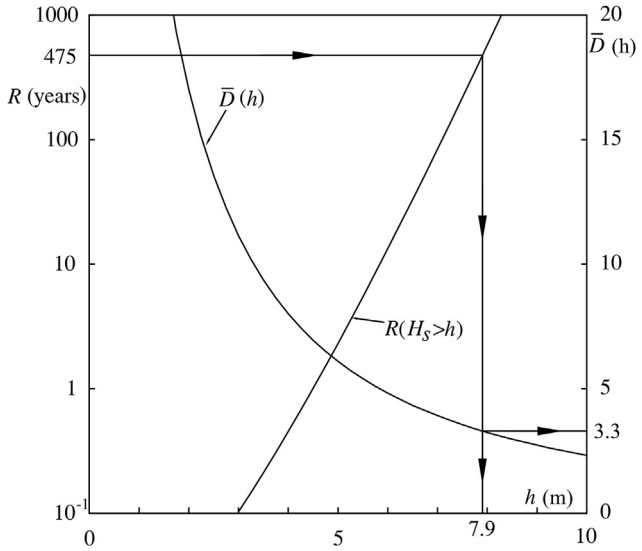

■ **FIGURE 5.7 Worked example of Section 5.5: obtaining $h(R)$ and $\overline{D}(h)$, for $R = 475$ years.**

5.5.1 Worked Example

Calculation of the design sea state for an offshore platform in the Mediterranean Sea:

1. Lifetime: $L = 50$ years;
2. Encounter probability: $\mathscr{P} = 0.10$;
3. $R = 50/\ln(1/1-0.10) = 475$ years;
4. $P(H_s > h)$ Eqn (5.7) with $w = 0.874$ m, $u = 1.200$;
5. $\overline{b}(a)$ Eqn (5.13) with $K' = 1.12$, $K'' = -0.11$, $a_{10} = 3.4$ m, $b_{10} = 70$ h;
6. $R(H_s > h)$ is calculated by means of Eqn (5.37) and is plotted in Fig. 5.7; $h(R)$ is the value of the abscissa corresponding to the ordinate $R = 475$ years: $h(475 \text{ years}) = 7.90$ m;
7. $\overline{D}(h)$ is calculated by means of Eqn (5.41) and is plotted in Fig. 5.7, from which we find that $\overline{D}(7.90 \text{ m}) = 3.3$ h;
8. Conclusion: design sea state: $H_s = 7.90$ m, duration $= 6.6$ h.

5.6 ESTIMATE OF THE LARGEST WAVE HEIGHT IN THE LIFETIME

5.6.1 The Design Sea State Pattern

A simple way to estimate the largest wave height in the lifetime is to assume it equal to the maximum expected wave height in the design sea

state. The worked example of Section 5.5 has just shown how to calculate H_s and the duration of the design sea state. The worked example of Section 4.8.4 had shown how to calculate the maximum expected wave height in a sea state of given H_s and duration. The sequence of operations of the two worked examples enables one to make an estimate of the largest wave height in the lifetime.

5.6.2 An Advanced Approach

This consists of calculating

1. $P(H_{\max}(L) > H)$, which is the probability that the maximum wave height in the lifetime exceeds a fixed threshold H;
2. $p(H_s = h; H_{\max} = x)$, which is the pdf of the H_s of the sea state in which the maximum wave height in the lifetime, of given height x, will occur. The formal solutions for these two probability functions, with the ETS model, may be found in Chapter 7 of a previous book by the author (2000). The equations of probability functions (1) and (2) are

$$P\left[H_{\max}(L) > H\right] = 1 - \exp\left\{ -L \int_H^\infty \int_0^\infty \frac{1}{T_m(h)} p(x; H_s = h) \times \int_h^\infty -\frac{\mathrm{d}p(H_s = a)}{\mathrm{d}a} \cdot \exp\left[\frac{\overline{b}(a)}{a} \int_0^a \frac{1}{T_m(h')} \times \ln[1 - P(x; H_s = h')]\mathrm{d}h' \right] \mathrm{d}a\, \mathrm{d}h\, \mathrm{d}x \right\} \quad (5.52)$$

$$p(H_s = h; H_{\max} = x) = K \frac{1}{T_m(h)} p(x; H_s = h) \int_h^\infty -\frac{\mathrm{d}p(H_s = a)}{\mathrm{d}a} \times \exp\left[\frac{\overline{b}(a)}{a} \int_0^a \frac{1}{T_m(h')} \ln[1 - P(x; H_s = h')]\mathrm{d}h' \right] \mathrm{d}a \quad (5.53)$$

where

$$P(x; H_s = h) = P(\text{wave height} > x) \text{ in a sea state of given } H_s = h \quad (5.54)$$

$$p(x; H_s = h) = -\frac{\mathrm{d}P(x; H_s = h)}{\mathrm{d}x} \quad (5.55)$$

and K in Eqn (5.53) is a normalizing factor.

Hereafter the FORTRAN program PHL is listed, which serves for calculating $P(H_{max}(L) > H)$ as a function of H. The value x of H is found such that

$$P(H_{max}(L) > x) = \mathscr{P} \tag{5.56}$$

that is, the probability prescribed for the design. The output (x) of the first part of PHL becomes the input of the second part of this program, which calculates $p(H_s = h; H_{max} = x)$ as a function of h. In Section 7.7.3 of the previous edition of this some hints were given for the calculation of the integrals in Eqns (5.52) and (5.53). These hints, which concern the limits and the steps of integration, are used in the following program. As to $P(H_s > h)$, Eqn (5.7) is used, so that the equation of the pdf is

$$p(H_s = h) = \frac{u}{w}\left(\frac{h}{w}\right)^{(u-1)} \exp\left[-\left(\frac{h}{w}\right)^{u}\right] \tag{5.57}$$

and the derivative in Eqns (5.52) and (5.53) is

$$\frac{\mathrm{d}p(H_s = a)}{\mathrm{d}a} = \left[\left(\frac{u}{w^u}\right)(u-1)a^{(u-2)} - \left(\frac{u^2}{w^{2u}}\right)a^{(2u-2)}\right]\exp\left[-\left(\frac{a}{w}\right)^{u}\right] \tag{5.58}$$

and is implemented in the function DERI. The solution for the pdf of the triangle heights carried out in Section 5.3.1 calls for the derivative $\mathrm{d}p(H_s = a)/\mathrm{d}a$ to be negative (see Eqn (5.29)). This condition is satisfied in all cases of practical interest. However, for the sake of completeness function DERI is provided with a control: if $\mathrm{d}p(H_s = a)/\mathrm{d}a$ were positive the program would be stopped.

```
      PROGRAM PHL
      CHARACTER*64 NOMEC
      DIMENSION HPV(3000),FHV(3000),SHV(3000)
      COMMON ALPHA,TMTP,RK0,RK1,RK2,W,U,RKP,RKS,A10,B10
      NOMEC='PDFHS'
      OPEN(UNIT=60,FILE=NOMEC)
      PG=3.141592
      DPG=2.*PG
C _____________________________________________________________
c spectrum
      ALPHA=0.01
      TMTP=0.78
      RK0=1.345
      RK1=1.16
```

```
        .RK2=6.91
c _____________________________________________________________
c local wave climate
        W=2.685
        U=1.555
        RKP=1.80
        RKS=-0.59
        A10=8.0
        B10=60
c _____________________________________________________________
c design prescription
        PROBA=0.10
        RL=50
        RLS=RL*365.*24.*3.6E3
c _____________________________________________________________

c first part of the program: probability of the largest
c wave height in the lifetime (RL)

        DDH=1
        DX=0.5
        DHP=0.5
        DA=0.5
        DHPP=0.5
        WRITE(6,*)'range of H: minimum value'
        READ(5,*)HI
        H=HI-DDH

c loop 800 calculates the function of H on the LHS of Eqn (5.52)
c for various values of H, starting on HI, with step DDH

800     H=H+DDH

c SOM is the 3-fold integral, with respect to x,h, and a,
c on the RHS of Eqn (5.52)

        SOM=0
        X=H-0.5*DX
        X2=2.*H
c loop 100: integral with respect to x
100     X=X+DX
        IF(X.GT.X2)GO TO 101
        HP1=0.3*X
        HP2=0.8*X
        HP=HP1-0.5*DHP
c loop 200: integral with respect to h (HP)
```

```
200     HP=HP+DHP
        IF(HP.GT.HP2)GO TO 100
        T1=TM(HP)
        P1=PP(X,HP)
        A1=HP
        A2=1.5*HP
        A=A1-0.5*DA
c loop 300: integral with respect to a (A)
300     A=A+DA
        IF(A.GT.A2)GO TO 200
        BB=BMED(A)
        HPP1=0.5*A
        HPP2=A
        HPP=HPP2+0.5*DHPP
c S4 is the integral with respect to h' inside the exponential function
        S4=0
c loop 400: integral with respect to h' (HPP)
400     HPP=HPP-DHPP
        IF(HPP.LT.HPP1)GO TO 401
        P3=P(X,HPP)
        T2=TM(HPP)
        AA=ALOG(1.-P3)
        S4=S4+AA/T2
        GO TO 400
401     S4=S4*DHPP
        ARG=(BB/A)*S4
        EE=EXP(ARG)
        SOM=SOM+(1./T1)*P1*(-DERI(A))*EE*DA*DHP*DX
        GO TO 300
101     CONTINUE
        PROB=1.-EXP(-RLS*SOM)
        WRITE(6,7000)H,PROB
7000    FORMAT(2X,'H ',F7.2,6X,'PROB ',E12.3)
c it looks for the H for which PROB is equal to the prescribed value (PROBA).
c this value of H is found with an approximation of 0.01m.
        IF(PROB.GT.PROBA)GO TO 800
        H=H-DDH
        DDH=DDH/10.
        IF(DDH.GT.5.E-3)GO TO 800
        X=H
c ____________________________________________________________
c second part of the program: distribution of the Hs of the sea state
c wherein the wave of height x (largest in the lifetime) will occur
        DHP=0.05
        HP1=0.3*X
        N1=IFIX(HP1/DHP)
        HP1=FLOAT(N1)*DHP
```

```
      .HP2=0.7*X
       HP=HP1-DHP
       I=0

c loop 210 calculates the function of h (HP) on the LHS of Eqn (5.53)
c for various values of h,with step DHP

210    HP=HP+DHP
       IF(HP.GT.HP2)GO TO 211
       T1=TM(HP)
       P1=PP(X,HP)
       A1=HP
       A2=1.5*HP

c SOMA is the integral with respect to a on the RHS of Eqn (5.53)
       SOMA=0
       A=A1-0.5*DA
c loop 310: integral with respect to a (A)
310    A=A+DA
       IF(A.GT.A2)GO TO 311
       BB=BMED(A)
       HPP1=0.5*A
       HPP2=A
       HPP=HPP2+0.5*DHPP
c S4 is the integral with respect to h' inside the exponential function
       S4=0
410    HPP=HPP-DHPP
       IF(HPP.LT.HPP1)GO TO 411
       P3=P(X,HPP)
       T2=TM(HPP)
       AA=ALOG(1.-P3)
       S4=S4+AA/T2
       GO TO 410
411    S4=S4*DHPP
       ARG=(BB/A)*S4
       EE=EXP(ARG)
       SOMA=SOMA-DERI(A)*EE*DA
       GO TO 310
311    CONTINUE
       FH=(1./T1)*P1*SOMA
       I=I+1
       HPV(I)=HP
       FHV(I)=FH
c FHV is the pdf on the LHS of Eqn (5.53), unless a constant
       IF(FH.GT.FHMAX)FHMAX=FH
       IF(I.GE.2)THEN
       ADDI=0.5*(FHV(I-1)+FHV(I))
       SHV(I)=SHV(I-1)+ADDI
```

```
c SHV is the probability distribution, unless a constant
       ENDIF
       GO TO 210
211    CONTINUE
       IMAX=I
       STOT=SHV(IMAX)
       DO I=2,IMAX
       HP=HPV(I)
       FH=FHV(I)/FHMAX
       SH=SHV(I)/STOT
c FH is the normalized pdf on the LHS of Eqn (5.53)
c SH is the probability distribution
       WRITE(60,1300)HP,FH,SH
1300   FORMAT(2X,F7.2,3X,F7.4,3X,F7.4)
       ENDDO
       WRITE(6,*)
       WRITE(6,*)'read file PDFHS'
       END

FUNCTION TM(HP)
c mean wave period in a sea state of given Hs=HP
       COMMON ALPHA,TMTP,RK0,RK1,RK2,W,U,RKP,RKS,A10,B10
       PG=3.141592
       ARG=HP/9.81
       COSTA=RK0/ALPHA**0.25
       TP=COSTA*PG*SQRT(ARG)
       TM=TMTP*TP
       RETURN
       END

FUNCTION P(X,HP)
c probability that a wave height be greater than a fixed X in a sea
c state with a given Hs=HP
       COMMON ALPHA,TMTP,RK0,RK1,RK2,W,U,RKP,RKS,A10,B10
       RM0=HP*HP/16
       ARG=X*X/(RK2*RM0)
       P=RK1*EXP(-ARG)
       RETURN
       END

FUNCTION PP(X,HP)
c pdf of the wave height in a sea state of given Hs=HP
       COMMON ALPHA,TMTP,RK0,RK1,RK2,W,U,RKP,RKS,A10,B10
       RM0L=RK1*2./RK2
       RM0=HP*HP/16.
       ARG=X*X/(RK2*RM0)
```

```
      .EE=EXP(-ARG)
       PP=RMOL*(X/RMO)*EE
       RETURN
       END

FUNCTION BMED(A)
c regression base-height of the ETS
       COMMON ALPHA,TMTP,RKO,RK1,RK2,W,U,RKP,RKS,A10,B10
       BMED=RKP*B10*EXP(RKS*A/A10)
       BMED=BMED*3.6E3
       RETURN
       END

FUNCTION DERI(A)
c derivative of the pdf of the Hs at the given geographic location
       COMMON ALPHA,TMTP,RKO,RK1,RK2,W,U,RKP,RKS,A10,B10
       RM1=U*(U-1)/W**U
       RM2=U*U/W**(2.*U)
       AD1=RM1*A**(U-2)
       AD2=RM2*A**(2*U-2)
       ARG=(A/W)**U
       EE=EXP(-ARG)
       DERI=(AD1-AD2)*EE
       IF(DERI.GT.0)THEN
       WRITE(6,*)'dp(Hs=a)/da > 0. Give a greater minimum value when
       1 the program asks range of H: minimum value'
       STOP
       ENDIF
       RETURN
       END
```

5.6.3 **Worked Example**

Let us consider a point on deep water of the northeastern Pacific with the $P(H_s > h)$ given by Eqn (5.7) with

$$w = 2.685 \text{ m}, \quad u = 1.555$$

and the regression $\overline{b}(a)$ of the ETS being given by Eqn (5.13) with the values of the parameters characteristic of that area, that is to say (see Section 5.2.3)

$$K' = 1.80, \quad K'' = -0.59, \quad a_{10} = 8.0 \text{ m}, \quad b_{10} = 60 \text{ h}$$

Let us estimate the largest wave height in the lifetime, for

$$L = 50 \text{ years}, \quad \mathscr{P} = 0.10$$

The first solution of the problem (design sea state pattern (DSSP), Section 5.6.1):

1. $R(H_s > h)$ as a function of h is calculated by means of Eqn (5.37);
2. $\overline{D}(h)$ is calculated by means of Eqn (5.41);
3. $R(H_s > h)$ and $\overline{D}(h)$ are plotted as in Fig. 5.7;
4. Equation (5.49) with the input data ($L = 50$ years, $\mathscr{P} = 0.10$) yields $R = 475$ years;
5. we enter the plot of item (3) and read $h(R = 475 \text{ years}) = 15.2$ m, $\overline{D}(15.2 \text{ m}) = 1.5$ h;
6. conclusion: design sea state

$$H_s = 15.2 \text{ m}, \quad \text{duration} = 3 \text{ h}$$

With the mean JONSWAP spectrum with $A = 0.01$ (see Eqn (3.45) and Section 4.8.1) we have

$$T_p = 16.6 \text{ s}, \quad T_m = 13.0 \text{ s}$$

from which it follows that the number of waves of the design sea state is

$$N = 830$$

Finally, the run of program HMAX (Section 4.8.3) with input data $H_s = 15.20$ m, $N = 830$, $K_1 = 1.16$, $K_2 = 6.91$ gives

$$\overline{H}_{\max} = 27.2 \text{ m}$$

The conclusion is that the largest wave height, with the given lifetime and encounter probability, is

$$H_1 = 27.2 \text{ m}$$

and occurs in a sea state of

$$H_{s_1} = 15.2 \text{ m}$$

where the subscript 1 stands for first solution.

The second solution of the problem (advanced approach, Section 5.6.2): The values of the parameters of the spectrum and the local wave climate must be loaded at the beginning of program PHL. Of course, they are the same values we used for the first solution. Program PHL writes H and $P(H_{\max}(L) > H)$ for H growing from HI (suggested value: 10 m) with initial step of 1 m. The program looks for the value of H such that $P(H_{\max}(L) > H) = 0.1$ (the prescribed value of the encounter probability that in the program is denoted by PROBA). In our case PHL shows that

$$P(H_{\max}(L) > H = 28.6 \text{ m}) = 0.10$$

that is, the searched value of H is 28.6 m. This value is called x. Then the second part of the program writes h, the normalized pdf $p(H_s = h;$

$H_{\max} = x$), which is calculated by means of Eqn (5.53), and the relevant cumulative distribution. This writing is done from $h = 0.3x$ to $h = 0.7x$ with step $\mathrm{d}h = 0.05$ m, and is stored on file PDFHS. The mode of this pdf turns out to be $h_m = 13.30$ m. The conclusion is that the largest wave height, with the given lifetime and encounter probability, is

$$H_2 = 28.6 \text{ m}$$

and the greatest probability is that it occurs in a sea state of

$$H_{s_2} = 13.3 \text{ m}$$

where the subscript 2 stands for second solution.

5.6.4 Comment on the Advanced Approach and the DSSP

With reference to the worked example, there is a 10% probability (the prescribed value) that the largest wave height in 50 years (the prescribed lifetime) at the given location exceeds 28.6 m. Should the largest wave height in the 50 years of the lifetime be equal to 28.6 m, then the greatest probability is that this wave height will occur in a sea state of 13.30 m H_s. In addition to this, we know the probability of the H_s of the sea state wherein this largest wave height of 28.6 m will occur. As an example, with 90% probability this wave will occur in sea states with H_s between 11.20 and 15.75 m. We realize that the advanced approach enables us to answer exhaustively the typical questions of engineering for what concerns wave prediction. As for the DSSP, notwithstanding its greater simplicity, it yields an estimate that may be effective for preliminary design purposes. Some graphs of the worked example are shown in Fig. 5.8.

5.7 CONCLUSION

The "peak-over-threshold" (POT) approach is commonly used. The probability of exceedance

$$P_A(h) = \int_h^\infty p_A(a)\mathrm{d}a \tag{5.59}$$

(with the symbols of this book) is extrapolated from the data on the percentage of sea storms whose $H_{s_{\max}}$ exceeds any given threshold h, at a given location (see Ferreira and Guedes Soares, 1998; Caires and Sterl, 2005). Then the return period $R(H_s > h)$ is obtained by means of Eqn (5.32), with $\mathscr{T}/\mathscr{N}(h, \mathscr{T})$ being the average interval between all storms. For obtaining the average persistence of H_s above a given threshold h, one has to resort

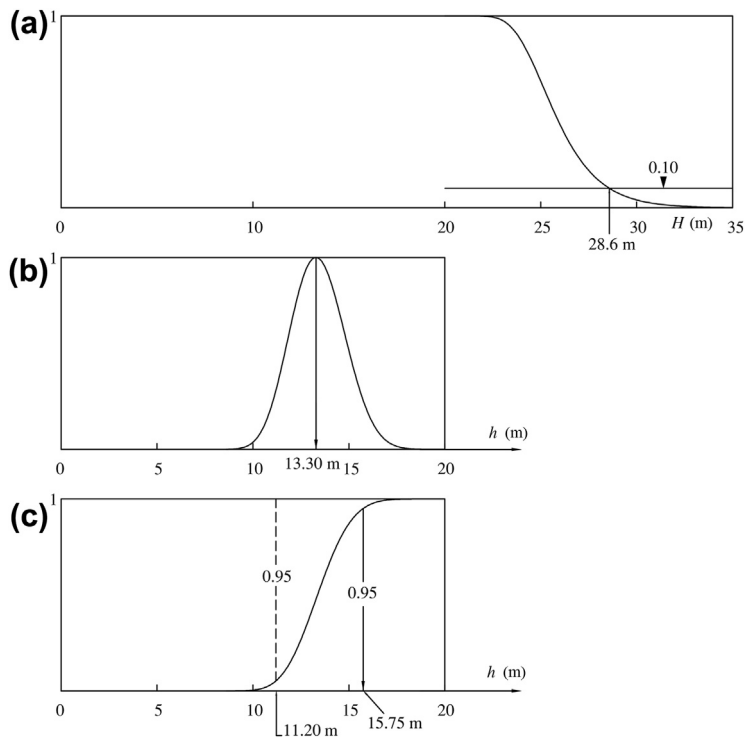

■ **FIGURE 5.8 Worked example of Section 5.6: (a) $P(H_{max}(50\ \text{years}) > H)$; (b) $p(H_s = h | H_{max}(50\ \text{years}) = 28.6\ \text{m})$; (c) probability distribution relevant to (b).**

to a new extrapolation of data; in particular one may obtain $P(H_s > h)$ from which $\overline{D}(h)$ proceeds by means of Eqn (5.40). Some solutions for engineering, such as the probability that the maximum wave height in the lifetime occurs in a sea state of given H_s (dealt with in our FORTRAN program and worked example), are beyond the possibility of the POT approach. The ETS theory with the solutions of Sections 5.3 and 5.6 was introduced in works (1986) and (2000) by the author. This kind of approach has been developed in subsequent years by Arena and Pavone (2006, 2009) and by Fedele and Arena (2010).

REFERENCES

Arena, F., Pavone, D., 2006. Return period of nonlinear high wave crests. J. Geophys. Res. 111, C08004.

Arena, F., Pavone, D., 2009. A generalized approach for long-term modelling of extreme crest-to-trough wave heights. Ocean Modell. 26, 217–225.

Battjes, J.A., 1972. Long-term wave height distributions at seven stations around the British Isles. Dtsch. Hydrogr. Z. 25 (4), 179–189.

Boccotti, P., 1986. On coastal and offshore structure risk analysis. Excerpta Ital. Contrib. Field Hydraul. Eng. 1, 19–36.

Boccotti, P., 2000. Wave Mechanics for Ocean Engineering. Elsevier, Amsterdam, 495 pp.

Borgman, L.E., 1973. Probabilities for highest wave in hurricane. J. Waterw. Harbors Coastal Eng. Div. ASCE 99 (WW2), 185–207.

Caires, S., Sterl, A., 2005. 100-year return value estimates for ocean wind speeds and significant wave height from the ERA-data. J. Clim. 18, 1032–1048.

Fedele, F., Arena, F., 2010. Long-term statistics and extreme waves in sea storms. J. Phys. Oceanogr. 1106–1117.

Ferreira, J.A., Guedes Soares, C., 1998. An application of the peak over threshold method to predict extremes of significant wave height. J. Offshore Mech. Arct. Eng. ASME 120, 165–176.

Chapter 6

Space—Time Theory of Sea States

CHAPTER OUTLINE

6.1 WAVE FIELD IN THE OPEN SEA

6.1.1 Concept of Homogeneous Wave Field

Let us imagine that a constant wind blows over deep water perpendicularly to a straight and infinitely long coastline. With a given wind speed u and fetch $\mathscr{Y}$ (the distance to the upwind coastline), after a certain duration of the wind a stationary condition (sea state) is reached. A relationship between the H_s, T_p of this sea state and the $\mathscr{Y}$, u (being defined as the wind speed at an elevation of 10 m above the mean sea surface) is given by the following equations:

$$\frac{gH_s}{u^2} = A_1\left\{\tanh\left[B_1\left(\frac{g\mathscr{Y}}{u^2}\right)^{C_1}\right]\right\}^{D_1} \tag{6.1}$$

Wave Mechanics and Wave Loads on Marine Structures. http://dx.doi.org/10.1016/B978-0-12-800343-5.00006-8

$$\frac{gT_p}{u} = A_2\left\{\tanh\left[B_2\left(\frac{g\mathscr{Y}}{u^2}\right)^{C_2}\right]\right\}^{D_2} \tag{6.2}$$

with

$$A_1 = 0.24,\ B_1 = 4.14\cdot 10^{-4},\ C_1 = 0.79,\ D_1 = 0.572 \tag{6.3}$$
$$A_2 = 7.69,\ B_2 = 2.77\cdot 10^{-7},\ C_2 = 1.45,\ D_2 = 0.187 \tag{6.4}$$

which are based on the work by Pierson and Moskowitz (1964), Kahma and Calkoen (1992), and Young and Verhagen (1996), being revised by Breugem and Holthuijsen (2007) and cf. Holthuijsen (2007).

Let us consider the percent variation of H_s in one dominant wave length along the wind direction. This is

$$\Delta \equiv 100\frac{\frac{dH_s}{d\mathscr{Y}}L_{p0}}{H_s} \tag{6.5}$$

and may be rewritten in the form

$$\Delta \equiv \frac{100}{2\pi}\frac{d\left(\frac{gH_s}{u^2}\right)}{d\left(\frac{g\mathscr{Y}}{u^2}\right)}\left(\frac{gT_p}{u}\right)^2 \Big/ \frac{gH_s}{u^2} \tag{6.6}$$

where the derivative of gH_s/u^2 with respect to $g\mathscr{Y}/u^2$ proceeds straightforwardly from Eqn (6.1). This derivative is a function of $g\mathscr{Y}/u^2$, so that also Δ is a function of $g\mathscr{Y}/u^2$. Calculation shows that

$$0.02 < \Delta < 0.2 \quad \text{on} \quad 100 < \frac{g\mathscr{Y}}{u^2} < 10000 \tag{6.7}$$

with the largest Δ corresponding to the smallest $g\mathscr{Y}/u^2$. That is, the H_s varies by less than the 0.2% in one wave length, because of the wind action (and this is the largest variation; that is, the variation in the wind direction).

Conclusion: in an open sea the variations of H_s from one point to another, due to the wind action, in a square with sides of 10 wave lengths, are negligible. Hence, such a square may be regarded as a homogeneous random wave field.

6.1.2 Random Surface Elevation and Velocity Potential

A steady and homogeneous wave field is thought of as the sum of a very large number N of harmonic wave components, with amplitudes, frequencies, and phases obeying the assumptions of Section 3.1. The directions

of these harmonic wave components are assumed to be generally different from one another. Accordingly, the mathematical form to the first order in a Stokes expansion is

$$\eta(x,y,t) = \sum_{i=1}^{N} a_i \cos(k_i x \sin\theta_i + k_i y \cos\theta_i - \omega_i t + \varepsilon_i) \tag{6.8}$$

$$\phi(x,y,z,t) = g\sum_{i=1}^{N} a_i \omega_i^{-1} \frac{\cosh\left[k_i(d+z)\right]}{\cosh\left(k_i \mathrm{d}\right)} \sin(k_i x \sin\theta_i + k_i y \cos\theta_i - \omega_i t + \varepsilon_i) \tag{6.9}$$

where the relation between the wave number k_i and the angular frequency ω_i is

$$k_i \tanh\left(k_i d\right) = \frac{\omega_i^2}{g} \tag{6.10}$$

The ith term of the sum Eqn (6.8) gives the surface elevation (and the ith term of the sum Eqn (6.9) gives the velocity potential) of a periodic wave of amplitude a_i, frequency ω_i, and phase ε_i, whose direction of advance makes an angle θ_i with the y-axis.

The surface elevation at any fixed point x, y is given by

$$\eta(t) = \sum_{i=1}^{N} a_i \cos\left(\omega_i t + \tilde{\varepsilon}_i\right) \tag{6.11}$$

where

$$\tilde{\varepsilon}_i \equiv -(\varepsilon_i + k_i x \sin\theta_i + k_i y \cos\theta_i) \tag{6.12}$$

The $\tilde{\varepsilon}_i$, like the ε_i, are distributed uniformly on the circle and are stochastically independent of one another, so that Eqn (6.11) represents a stationary Gaussian process (the proof is the same as given in Section 4.1).

6.2 MAXIMUM EXPECTED WAVE HEIGHT AT A GIVEN ARRAY OF POINTS IN THE DESIGN SEA STATE

Let us consider two points A and B in a homogeneous random wave field. If the two points are far from each other, the wave heights at A will be stochastically independent of the wave heights at B. As a consequence, the maximum expected wave height in two sequences of N waves, taken contemporarily at the two points, will be equal to the maximum expected wave height in a sequence of $2N$ waves taken at one fixed point. However, if the two points are very close to each other, the maximum expected wave

height in two sequences of N waves, taken contemporarily at the two points, will be equal to the maximum expected wave height in a sequence of N waves taken at one fixed point.

Let us define: $\overline{\alpha_{\max}}(N)$, the ratio between the maximum expected wave height $\overline{H_{\max}}$ in a sequence of N waves, and $\sqrt{m_0}$; $\overline{\alpha_{\max}}(N, n, \Delta x)$, the ratio $\overline{H_{\max}}/\sqrt{m_0}$, with $\overline{H_{\max}}$ being the maximum expected wave height in n sequences of N waves taken contemporarily at n points aligned on the x-axis sensibly orthogonal to the wave direction, at some distance Δx from each other.

Figure 6.1 shows $\overline{\alpha_{\max}}(N)$, $\overline{\alpha_{\max}}(N, 2, L_{p0}/6)$, $\overline{\alpha_{\max}}(N, 2, L_{p0}/2)$, $\overline{\alpha_{\max}}(2N)$. (The data points were taken from a small-scale field experiment (SSFE) of 1990 described in Chapter 9.) The dataset consists of wind seas on deep water. The figure shows that $\overline{\alpha_{\max}}(N, 2, L_{p0}/2)$ is close to $\overline{\alpha_{\max}}(2N)$, which suggests that the maximum expected wave height in a sequence of N waves at n points sensibly aligned with the orthogonal to the wave direction may be calculated as the maximum expected wave height in a sequence of n N waves at one point, provided that distance Δx between

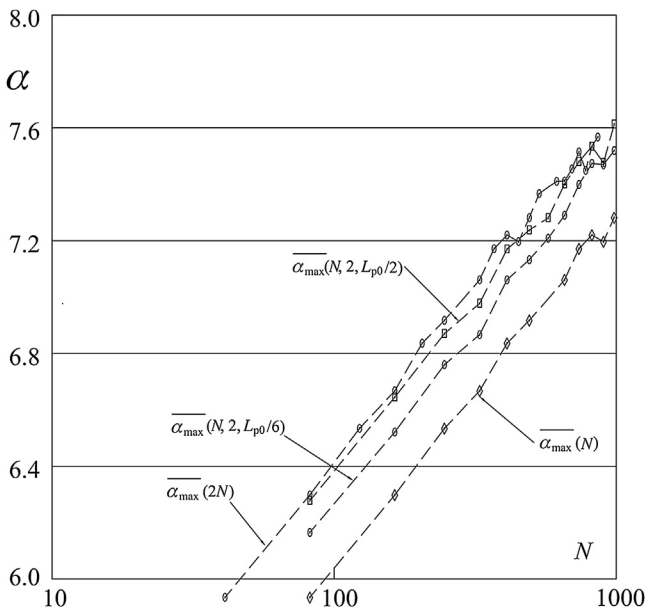

■ **FIGURE 6.1** $\overline{\alpha_{\max}}$ in sequences of N and $2N$ waves at a single point; $\overline{\alpha_{\max}}$ in two sequences of N waves taken contemporarily at two different points sensibly aligned with the orthogonal to the wave direction. The figure helps in understanding the suggestion given at the end of Section 6.2.

two consecutive points is greater than $L_{p0}/2$. This suggestion will be applied in Chapter 13 for estimating the maximum expected wave height at the piers of a submerged tunnel.

6.3 DIRECTIONAL SPECTRUM: DEFINITION AND CHARACTERISTIC SHAPE

The amplitudes, frequencies, and directions of the harmonic wave components give rise to a directional spectrum:

$$S(\omega,\theta)\delta\omega\delta\theta \equiv \sum_i \frac{1}{2}a_i^2 \quad \text{for } i \text{ such that } \omega < \omega_i < \omega + \delta\omega \text{ and } \theta < \theta_i < \theta + \delta\theta \tag{6.13}$$

In words: the product $2S(\omega, \theta)\delta\omega\delta\theta$ represents the sum of the square amplitudes of the harmonic wave components whose frequencies ω_i and angles θ_i fall in the small rectangle $(\omega, \omega + \delta\omega; \theta, \theta + \delta\theta)$. The definitions Eqn (6.13) of $S(\omega, \theta)$ and (3.4) of $E(\omega)$ yield

$$E(\omega) = \int_0^{2\pi} S(\omega,\theta)\mathrm{d}\theta \tag{6.14}$$

The directional spectrum is generally given in the form

$$S(\omega,\theta) = E(\omega)D(\theta;\omega) \tag{6.15}$$

where $D(\theta; \omega)$ is the directional distribution. Clearly, Eqns (6.14) and (6.15) imply

$$\int_0^{2\pi} D(\theta;\omega)\mathrm{d}\theta = 1 \tag{6.16}$$

The directional distribution of a wind sea with a constant wind exhibits a typical shape that usually is fitted by the cosine-power function

$$D(\theta;\omega) = K(n)\cos^{2n}\left[\frac{1}{2}(\theta - \theta_d)\right] \quad \text{with} \quad n = n(\omega) \tag{6.17}$$

where $\cos^{2n}$ is understood to be the nth power of the square cosine, $K(n)$ is the normalizing factor

$$K(n) \equiv \left[\int_0^{2\pi} \cos^{2n}\frac{1}{2}\theta\mathrm{d}\theta\right]^{-1} \tag{6.18}$$

being necessary to comply with Eqn (6.16), and θ_d is the angle that the dominant direction makes with the y-axis. Mitsuyasu et al. (1975) suggested

$$n\begin{cases} = n_p\left(\omega/\omega_p\right)^5 & \text{if} \quad \omega \le \omega_p \\ = n_p\left(\omega_p/\omega\right)^{2.5} & \text{if} \quad \omega > \omega_p \end{cases} \tag{6.19}$$

where n_p grows with $g\mathscr{Y}/u^2$. Eqn (6.19) implies that the directional spreading is minimum with the peak frequency ω_p, which has obtained several confirmations (see, in particular, Young et al., 1996; Ewans, 1998).

6.4 CLASSIC APPROACH: OBTAINING THE DIRECTIONAL DISTRIBUTION

The classic approach, due to the work of Longuet-Higgins et al. (1963) and Cartwright (1963), was conceived for measurements of pitch and roll. However, this approach is also applied with other kinds of measurements. The classic approach consists of finding a directional distribution for each frequency ω_i through a best-fit procedure. Let us see this approach here below.

Let us consider the surface elevation and its space derivatives at some fixed point x,y. The surface elevation is given by Eqn (6.11), and the space derivatives are

$$\eta_x(t) \equiv \frac{\partial}{\partial x}\eta(x,y,t) = \sum_{i=1}^{N} a_i k_i \sin\theta_i \sin\left(\omega_i t + \tilde{\varepsilon}_i\right) \tag{6.20}$$

$$\eta_y(t) \equiv \frac{\partial}{\partial y}\eta(x,y,t) = \sum_{i=1}^{N} a_i k_i \cos\theta_i \sin\left(\omega_i t + \tilde{\varepsilon}_i\right) \tag{6.21}$$

Let us obtain the relation between the average product $\langle \eta_x(t)\eta_y(t)\rangle$ and the directional spectrum. We have

$$\left\langle \eta_x(t)\eta_y(t)\right\rangle = \sum_{i=1}^{N}\frac{1}{2}a_i^2 k_i^2 \sin\theta_i \cos\theta_i = \int_0^{\infty}\int_0^{2\pi} S(\omega,\theta)k^2 \sin\theta\cos\theta \mathrm{d}\theta\mathrm{d}\omega \tag{6.22}$$

This average product may be obtained also from the time series data of pitch and roll. For this aim it is convenient to resort to the Fourier series of $\eta_x(t)$ and $\eta_y(t)$:

$$\eta_x(t) = \sum_{i=1}^{N} a'_{xi}\cos\omega_i t + a''_{xi}\sin\omega_i t \tag{6.23}$$

$$\eta_y(t) = \sum_{i=1}^{N} a'_{yi}\cos\omega_i t + a''_{yi}\sin\omega_i t \tag{6.24}$$

(Note that N in Eqns (6.20) and (6.21) stands for the number (very large) of harmonic components forming the sea state, while N in Eqns (6.23) and (6.24) is the number of frequencies in the Fourier series, which depends upon record length and sampling rate.)

From Eqns (6.23) and (6.24) we get

$$\langle \eta_x(t)\eta_y(t)\rangle = \sum_{i=1}^{N} \frac{1}{2}\left(a'_{xi}a'_{yi} + a''_{xi}a''_{yi}\right) \tag{6.25}$$

And from Eqns (6.22) and (6.25) we conclude that

$$\Delta\omega \int_0^{2\pi} S(\omega_i,\theta)k_i^2 \sin\theta\cos\theta \mathrm{d}\theta = \frac{1}{2}\left(a'_{xi}a'_{yi} + a''_{xi}a''_{yi}\right) \tag{6.26}$$

The two sides of this equation represent the contribution to the average product $\langle \eta_x(t)\eta_y(t)\rangle$ from the components whose frequency is within $\omega_i - \Delta\omega/2$ and $\omega_i + \Delta\omega/2$ ($\Delta\omega$ being the frequency resolution of the Fourier series).

Using Eqn (6.15) we can rewrite Eqn (6.26) in the form

$$\int_0^{2\pi} D(\theta;\omega_i)\sin 2\theta \mathrm{d}\theta = \frac{a'_{xi}a'_{yi} + a''_{xi}a''_{yi}}{\Delta\omega E(\omega_i)k_i^2} \tag{6.27}$$

where the terms on the right-hand side (RHS) are all known (they proceed from the time series data of $\eta(t)$, $\eta_x(t)$, and $\eta_y(t)$).

Of course, Eqn (6.27) alone is not enough to obtain univocally the unknown function $D(\theta;\omega_i)$. However, some further relations of the same kind can be obtained from an analysis of the following averages:

$$\langle \eta(t)\eta_x^*(t)\rangle, \langle \eta(t)\eta_y^*(t)\rangle, \left\langle \eta_y^2(t) - \eta_x^2(t)\right\rangle$$

where

$$\eta_x^*(t) \equiv \eta_x(t) \text{ with each component advanced of } 90^\circ \text{ in phase,} \tag{6.28}$$

$$\eta_y^*(t) \equiv \eta_y(t) \text{ with each component advanced of } 90^\circ \text{ in phase.} \tag{6.29}$$

The further relations are

$$\int_0^{2\pi} D(\theta;\omega_i)\sin\theta \mathrm{d}\theta = \frac{a'_i a''_{xi} - a''_i a'_{xi}}{2\Delta\omega E(\omega_i)k_i} \tag{6.30}$$

$$\int_0^{2\pi} D(\theta;\omega_i)\cos\theta \mathrm{d}\theta = \frac{a'_i a''_{yi} - a''_i a'_{yi}}{2\Delta\omega E(\omega_i)k_i} \tag{6.31}$$

$$\int_0^{2\pi} D(\theta;\omega_i)\cos 2\theta \mathrm{d}\theta = \frac{\left(a_{yi}'^2 + a_{yi}''^2\right) - \left(a_{xi}'^2 + a_{xi}''^2\right)}{2\Delta\omega E(\omega_i)k_i^2} \tag{6.32}$$

where a_i', a_i'' are the Fourier coefficients of $\eta(t)$.

These relationships are for a perfect surface-following buoy. Tucker (1989) worked out these equations, taking account of buoy response. The result is a set of equations conceptually similar to Eqns (6.27) and (6.30)—(6.32), in which appear the amplitudes and phases of heave and tilt response. Here, for simplicity, we shall continue making reference to the set of the perfect surface-following buoy, because of their conceptual equivalence to the Tucker equations. From these equations we may obtain the first and second angular harmonics of the directional distribution, e.g., follow this logic sequence:

1. Consider the integral

$$\int_0^{2\pi} D(\theta;\omega_i)\cos\theta \mathrm{d}\theta$$

2. This integral (1) has the known value that proceeds from Eqn (6.31).
3. Write the directional distribution in terms of its angular harmonics (cf. Tucker and Pitt, 2001).
4. The integral of item (1), when executed with the series of angular harmonics, proves to be equal to the cosine-amplitude of the first angular harmonic.
5. As a consequence of (2) and (4), obtain the value of the cosine-amplitude of the first angular harmonic.

Likewise, from the known value of the integral on the left-hand side (LHS) of Eqn (6.30) we obtain the sine-amplitude of the first angular harmonic. Then from the known values of the integrals on the LHS of Eqns (6.31) and (6.27) we obtain, respectively, the cosine-amplitude and the sine-amplitude of the second angular harmonic. Then, the classic assumption of Cartwright (1963) is that the directional distribution follows the form (Eqn (6.17)) for every ω_i, that is,

$$D(\theta;\omega_i) = K(n_i)\cos^{2n_i}\left[\frac{1}{2}(\theta - \theta_{d_i})\right] \tag{6.33}$$

is made; and the two independent parameters of this equation, that is to say n_i and θ_{d_i} (K serves to fulfill condition (6.16)), may be estimated from either the first or the second angular harmonic of the directional distribution. The values of the parameters generally prove to depend on the angular harmonic that is used for the estimate, and of course this introduces some uncertainty.

6.5 NEW APPROACH: OBTAINING INDIVIDUAL ANGLES θ_I

6.5.1 The Algorithm

An alternative approach introduced by the author (2004) provides the angle θ_i associated with each frequency ω_i. The method is based on measurements of the surface elevation. However, it may be adapted to work with some different kinds of measurements. This approach is reproposed here in a more detailed form.

With reference to the scheme of Fig. 6.2(a), from Eqn (6.8) of the random surface elevation of a sea state, we have

$$\eta_A(t) = \sum_{i=1}^{N} a_i \cos(-\omega_i t + \varepsilon_i) \tag{6.34}$$

$$\eta_B(t) = \sum_{i=1}^{N} a_i \cos(k_i X \sin\theta_i - \omega_i t + \varepsilon_i) \tag{6.35}$$

Hereafter we shall use the compact notation

$$C_i = k_i X \sin\theta_i \tag{6.36}$$

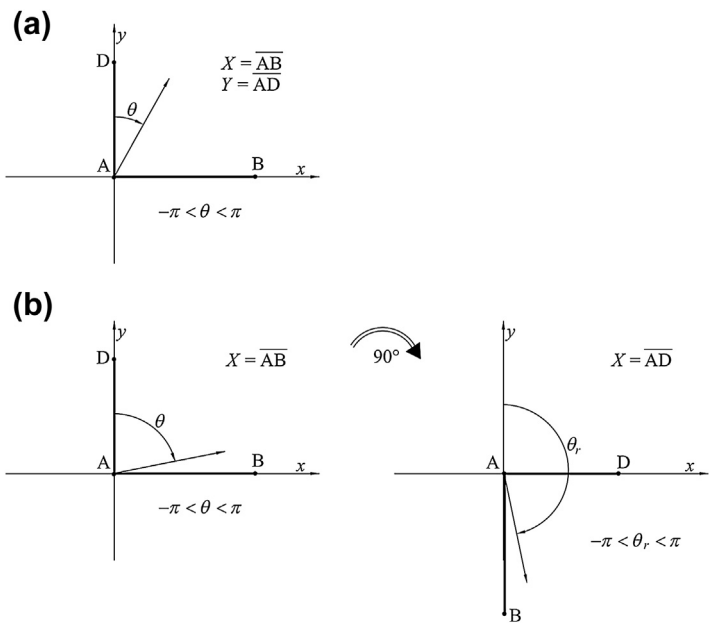

■ **FIGURE 6.2** (a) Reference scheme for obtaining the directional spectrum. (b) If θ is close to 90° (or −90°), obtaining θ from the phase angle between A and B implies a small degree of precision. Then it is convenient to obtain θ_r from the phase angle between A and D.

Let us assume that we have gotten two records of the surface elevation: one at point A and one at point B. From these two records we obtain the Fourier series, as shown in Section 3.5.1:

$$\eta_A(t) = \sum_{i=1}^{N} A_i' \cos(\omega_i t) + A_i'' \sin(\omega_i t) \tag{6.37}$$

$$\eta_B(t) = \sum_{i=1}^{N} B_i' \cos(\omega_i t) + B_i'' \sin(\omega_i t) \tag{6.38}$$

We know the N quadruplets A_i', A_i'', B_i', B_i'' and the N angular frequencies ω_i, and we aim to obtain the N triplets a_i, ε_i, θ_i. From Eqns (6.34) and (6.37) it follows that

$$A_i' = a_i \cos \varepsilon_i \tag{6.39}$$

$$A_i'' = a_i \sin \varepsilon_i \tag{6.40}$$

which yields straightforwardly the N pair a_i, ε_i.

From Eqns (6.35) and (6.38) it follows that

$$A_i' \cos C_i - A_i'' \sin C_i = B_i' \tag{6.41}$$

$$A_i'' \cos C_i + A_i' \sin C_i = B_i'' \tag{6.42}$$

where use has been made of definition (Eqn (6.36)) of C_i, and of the two equalities (Eqns (6.39) and (6.40)).

Now let us multiply

1. the LHS and the RHS of Eqn (6.41) by A_i';
2. the LHS and the RHS of Eqn (6.41) by A_i'';
3. the LHS and the RHS of Eqn (6.42) by A_i';
4. the LHS and the RHS of Eqn (6.42) by A_i''.

The result is

$$A_i'^2 \cos C_i - A_i' A_i'' \sin C_i = A_i' B_i' \tag{6.43}$$

$$A_i' A_i'' \cos C_i - A_i''^2 \sin C_i = A_i'' B_i' \tag{6.44}$$

$$A_i' A_i'' \cos C_i + A_i'^2 \sin C_i = A_i' B_i'' \tag{6.45}$$

$$A_i''^2 \cos C_i + A_i' A_i'' \sin C_i = A_i'' B_i'' \tag{6.46}$$

Respectively, from Eqns (6.43) and (6.46), and from Eqns (6.44) and (6.45) we arrive at

$$\cos C_i \left(A_i'^2 + A_i''^2\right) = A_i' B_i' + A_i'' B_i'' \tag{6.47}$$

$$\sin C_i \left(A_i'^2 + A_i''^2\right) = A_i' B_i'' - A_i'' B_i' \tag{6.48}$$

This may be rewritten in the form

$$\tan C_i = \frac{A_i' B_i'' - A_i'' B_i'}{A_i' B_i' + A_i'' B_i''} \tag{6.49}$$

$$\sin C_i \left(A_i' B_i'' - A_i'' B_i'\right) > 0 \tag{6.50}$$

$$\cos C_i \left(A_i' B_i' + A_i'' B_i''\right) > 0 \tag{6.51}$$

A sufficient condition for Eqns (6.49)–(6.51) to yield a unique solution for C_i is that

$$|C_i| < \pi \tag{6.52}$$

From definition (Eqn (6.36)) of C_i, it follows that a further sufficient condition is that

$$k_i X < \pi \tag{6.53}$$

that is,

$$X < \frac{L_i}{2} \tag{6.54}$$

where L_i is the wavelength relevant to angular frequency ω_i. A unique solution for C_i implies that also sin (θ_i) has a unique solution.

If points A and B are near a coast where $-\pi/2 < \theta_i < \pi/2$ the solution for sin (θ_i) closes the problem. If points A and B are in the open sea, the question remains whether cos (θ_i) is positive or negative. In order to answer this question we have to compare to each other the time series at points A and D on the y-axis (see Fig. 6.2(a)). We write the Fourier series at the two points in the form

$$\eta_A(t) = \sum_{i=1}^{N} A_i \cos\left(\omega_i t + \alpha_i\right) \tag{6.55}$$

$$\eta_D(t) = \sum_{i=1}^{N} D_i \cos\left(\omega_i t + \beta_i\right) \tag{6.56}$$

with the α_i and β_i in $(0,2\pi)$. Therefore the time instants t_A and t_D of the maximum of the ith harmonic component in the time interval $(-T_i,0)$ (with $T_i = 2\pi/\omega_i$) at points A and D are, respectively:

$$t_A = -\frac{\alpha_i}{\omega_i} \tag{6.57}$$

$$t_D = -\frac{\beta_i}{\omega_i} \tag{6.58}$$

and there are the following four alternatives:

$$1. \quad |t_D - t_A| < \frac{T_i}{2} \text{ and } t_D > t_A \Rightarrow \cos\left(\theta_i\right) > 0 \tag{6.59}$$

$$2.\quad |t_D - t_A| < \frac{T_i}{2} \text{ and } t_D < t_A \Rightarrow \cos(\theta_i) < 0 \tag{6.60}$$

$$3.\quad |t_D - t_A| > \frac{T_i}{2} \text{ and } t_D > t_A \Rightarrow \cos(\theta_i) < 0 \tag{6.61}$$

$$4.\quad |t_D - t_A| > \frac{T_i}{2} \text{ and } t_D < t_A \Rightarrow \cos(\theta_i) > 0 \tag{6.62}$$

This is provided that the distance Y fulfills the inequality

$$Y < \frac{L_i}{2} \tag{6.63}$$

so that the time needed to cover the distance from A to D (or from D to A) must be smaller than $T_i/2$.

6.5.2 The Base of the New Approach

If the $\omega_i (i = 1,\ldots, N)$ of Eqns (6.37) and (6.38) were the same as the ω_i of Eqns (6.34) and (6.35), the algorithm that we have just given would yield the N exact solutions for the triplets $a_i,\varepsilon_i,\theta_i$. However, the ω_i of Eqns (6.37) and (6.38) will be the ones of a Fourier series and will be generally different from the actual ω_i of Eqns (6.34) and (6.35) representing the sea state. Thus, the algorithm of Section 6.5.1 will not yield the actual a_i,ε_i, and θ_i of the sea state. However, the frequency spectrum and the directional spectrum that we shall obtain will be similar, respectively, to the actual frequency spectrum and the actual directional spectrum. Usually, the smaller the frequency resolution $\omega_{i+1} - \omega_i$ (that is, the greater the duration of a wave record (DWR)), the closer should be the agreement between the calculated spectra and the actual spectra. Note that a few θ_i will remain indeterminate in that sin (θ_i) will not fulfill the inequality

$$|\sin(\theta_i)| < 1 \tag{6.64}$$

However, the energy of the harmonic components with indeterminate θ_i is typically a small share of the total energy of the spectrum, so that we can discard these components.

6.6 SUBROUTINES FOR CALCULATION OF THE DIRECTIONAL SPECTRUM WITH THE NEW METHOD

6.6.1 Subroutine FOUR

The input ETA(N,1), ETA(N,2), ETA(N,3) (N = 1, NMAX) are the time series data of the surface elevation, respectively, at points A, B, and D.

The subroutine performs the Fourier transform and yields the Fourier coefficients:

AIP(I, 1) $= a_i'$, AIS(I, 1) $= a_i''$ at point A; AIP(I, 2) $= a_i'$, AIS(I, 2) $= a_i''$ at point B; AIP(I, 3) $= a_i'$, AIS(I, 3) $= a_i''$ at point D; for I = 1,IMA (IMA cannot exceed (NMAX-1)/2).

```
      SUBROUTINE FOUR(ETA,AIP,AIS,OVF,AIV)
      COMMON NMAX,IMA,DT
      DIMENSION ETA(300001,3),OVF(150000),AIV(150000)
      DIMENSION AIP(150000,3),AIS(150000,3)
      PG=3.141592
      DPG=2.*PG
      DUR=DT*FLOAT(NMAX)
      DOMI=DPG/DUR
      IULT=3*IMA
      ITOT=0
      WRITE(6,*)
      WRITE(6,*)'subroutine FOUR'

c Loop 200: L = 1 -> point A, L = 2 -> point B, L = 3 -> point D
c I = 1,IMA; IMA = number of the Fourier frequencies being employed

      DO 200 L=1,3
      DO 200 I=1,IMA
      ITOT=ITOT+1
      OMI=DOMI*FLOAT(I)
      OVF(I)=OMI
      IF((ITOT/1000)*1000.EQ.ITOT)THEN
      WRITE(6,2666)ITOT, IULT
2666  FORMAT(2X,'done ',I6,5X,'total ',I6)
      ENDIF
      AIP(I,L)=0
      AIS(I,L)=0.
c Loop 210: for calculation of ai',ai''
      DO 210 J=1,NMAX
      TJ=DT*FLOAT(J-1)
      AIP(I,L)=AIP(I,L)+ETA(J,L)*COS(OMI*TJ)
      AIS(I,L)=AIS(I,L)+ETA(J,L)*SIN(OMI*TJ)
210   CONTINUE
      AIP(I,L)=AIP(I,L)*2./FLOAT(NMAX)
      AIS(I,L)=AIS(I,L)*2./FLOAT(NMAX)
200   CONTINUE
      DO I=1,IMA
      AI1=AIP(I,1)
      AI2=AIS(I,1)
      AIV(I)=SQRT(AI1*AI1+AI2*AI2)
      ENDDO
```

```
      .RETURN
       END
```

6.6.2 Subroutine SDI

Subroutine SDI employs the Fourier coefficients obtained by Subroutine FOUR, and applies the algorithm of Section 6.5.1 to obtain the θ_i. These are stored on vector TETV1(I), whose range is $(-180°, 180°)$. If θ_i proves to be indeterminate (inequality 6.64 not satisfied), this θ_i is given the conventional value 999.

```
      SUBROUTINE SDI(TETV1)
      COMMON NMAX,IMA,DT,AB,AD,DEPTH
      COMMON AIP(150000,3),AIS(150000,3),OVF(150000),
      AIV(150000)
      DIMENSION TETV1(150000)
      X=AB
      Y=AD
      PG=3.141592
      DPG=2.*PG

      DO 600 I=1,IMA
      OMI=OVF(I)
      PEI=DPG/OMI
      RLI=WLENGTH(DEPTH,PEI)
      RKI=DPG/RLI
      AI1=AIP(I,1)
      AI2=AIS(I,1)
      BI1=AIP(I,2)
      BI2=AIS(I,2)
      DI1=AIP(I,3)
      DI2=AIS(I,3)
      SCI=AI1*BI2-AI2*BI1
      CCI=AI1*BI1+AI2*BI2
      ARG=SCI/CCI
c ARG is the RHS of Eqn (6.49)
      CI=ATAN(ARG)
c CI is defined by Eqn (6.36)
c the domain of CI is (-PG,PG)
      IF(SCI.GT.0.AND.CCI.LT.0)CI=PG+CI
      IF(SCI.LT.0.AND.CCI.LT.0)CI=-(PG-CI)
      SI=CI/(RKI*X)
c SI = sin(tetai)
c_____________________________________________________________

c here the calculation of sin(thetai) is completed
c now the subroutine starts the calculation of the sign of
cos(thetai)
c_____________________________________________________________
```

```
c ALFAI is alphai on the RHS of Eqn (6.55)
c BETAI is betai on the RHS of Eqn (6.56)
c the domain of alphai is 0,DPG
c the domain of betai is 0,DPG
      ARG=-AI2/AI1
      ALFAI=ATAN(ARG)
      ARG=-DI2/DI1
      BETAI=ATAN(ARG)
      IF(-AI2.GT.0.AND.AI1.LT.0)ALFAI=PG+ALFAI
      IF(-AI2.LT.0.AND.AI1.LT.0)ALFAI=PG+ALFAI
      IF(-AI2.LT.0.AND.AI1.GT.0)ALFAI=DPG+ALFAI
      IF(-DI2.GT.0.AND.DI1.LT.0)BETAI=PG+BETAI
      IF(-DI2.LT.0.AND.DI1.LT.0)BETAI=PG+BETAI
      IF(-DI2.LT.0.AND.DI1.GT.0)BETAI=DPG+BETAI
c TA = tA Eqn (6.57)
c TD = tD Eqn (6.58)
      TA=-ALFAI/OMI
      TD=-BETAI/OMI
      DIFF=ABS(TD-TA)
      TI=DPG/OMI
      TI2=TI/2.
c the following are the four alternatives given by
Eqns (6.59)–(6.62)
      IF(DIFF.LT.TI2.AND.TD.GT.TA)CO=1
      IF(DIFF.LT.TI2.AND.TD.LT.TA)CO=-1
      IF(DIFF.GT.TI2.AND.TD.GT.TA)CO=-1
      IF(DIFF.GT.TI2.AND.TD.LT.TA)CO=1
c CO=1 -> cos(thetai)>0
c CO=-1 -> cos(thetai)<0
      IF(ABS(SI).GT.1)THEN
      TETV1(I)=999
      GO TO 600
      ENDIF
      TETI=ASIN(SI/CO)
      IF(CO.LT.0.AND.SI.LT.0)TETI=-PG+TETI
      IF(CO.LT.0.AND.SI.GT.0)TETI=PG+TETI
      TETV1(I)=TETI*180./PG
c TETV1(I) = thetai
c The domain of TETV1(I) is (-180ø,180ø)
600   CONTINUE
      RETURN
      END
```

6.6.3 **Subroutine SDIR**

On rotating the x,y-axis 90° clockwise we can calculate angles θ_{r_i} of the ith component (see Fig. 6.2(b)). The algorithm is essentially the same as that of Subroutine SDI, with the difference that sin (θ_{r_i}) is obtained from the time series data at points A and D, instead of A and B; and the sign of

$\cos(\theta_{r_i})$ is obtained from the time series data at points A and B, instead of A and D. The conversion from θ_{r_i} to θ_i is obtained with the equations

$$\theta_i = \theta_{r_i} - 90^\circ \quad \text{if} \quad \theta_{r_i} - 90^\circ > -180^\circ \tag{6.65}$$

$$\theta_i = \theta_{r_i} + 270^\circ \quad \text{otherwise} \tag{6.66}$$

SDI cannot be accurate if θ_i is close to 90° (or -90°), given that the wave direction is nearly parallel to the line AB. Similarly, SDIR is not accurate if θ_i is close to 0°, or 180° or -180°. Therefore, it is advisable to use SDIR if $|\theta_i|$ is close to 90° and SDI if $|\theta_i|$ is close to 0° or 180°. Otherwise, one may use SDI or SDIR at his or her choice. The values of θ_i obtained by means of SDIR are stored on TETV2(I).

```
      SUBROUTINE SDIR(TETV2)
      COMMON NMAX,IMA,DT,AB,AD,DEPTH
      COMMON AIP(150000,3),AIS(150000,3),OVF(150000),
      AIV(150000)
      DIMENSION TETVR(150000),TETV2(150000)
      X=AD
      Y=AB
      PG=3.141592
      DPG=2.*PG

      DO 600 I=1,IMA
      OMI=OVF(I)

      RKI=OMI*OMI/9.8
      AI1=AIP(I,1)
      AI2=AIS(I,1)
      BI1=AIP(I,2)
      BI2=AIS(I,2)
      DI1=AIP(I,3)
      DI2=AIS(I,3)
      SCI=AI1*DI2-AI2*DI1
      CCI=AI1*DI1+AI2*DI2
      ARG=SCI/CCI
      CI=ATAN(ARG)
      IF(SCI.GT.0.AND.CCI.LT.0)CI=PG+CI
      IF(SCI.LT.0.AND.CCI.LT.0)CI=CI-PG
      SI=CI/(RKI*X)
c SI = sin(thetari)
c_____________________________________________________________
c here the calculation of sin(thetari) is completed
c now the subroutine starts the calculation of the sign of
cos(thetari)
c_____________________________________________________________
      ARG=-AI2/AI1
      ALFAI=ATAN(ARG)
      ARG=-BI2/BI1
      BETAI=ATAN(ARG)
```

```
     .IF(-AI2.GT.0.AND.AI1.LT.0)ALFAI=PG+ALFAI
      IF(-AI2.LT.0.AND.AI1.LT.0)ALFAI=PG+ALFAI
      IF(-AI2.LT.0.AND.AI1.GT.0)ALFAI=DPG+ALFAI
      IF(-BI2.GT.0.AND.BI1.LT.0)BETAI=PG+BETAI
      IF(-BI2.LT.0.AND.BI1.LT.0)BETAI=PG+BETAI
      IF(-BI2.LT.0.AND.BI1.GT.0)BETAI=DPG+BETAI
      TA=-ALFAI/OMI
      TB=-BETAI/OMI
      DIFF=ABS(TB-TA)
      TI=DPG/OMI
      TI2=TI/2.
      IF(DIFF.LT.TI2.AND.TB.GT.TA)CO=-1
      IF(DIFF.LT.TI2.AND.TB.LT.TA)CO=1
      IF(DIFF.GT.TI2.AND.TB.GT.TA)CO=1
      IF(DIFF.GT.TI2.AND.TB.LT.TA)CO=-1
      IF(ABS(SI).GT.1)THEN
      TETV2(I)=999
      GO TO 600
      ENDIF
      TETIR=ASIN(SI/CO)
      IF(CO.LT.0.AND.SI.LT.0)TETIR=-PG+TETIR
      IF(CO.LT.0.AND.SI.GT.0)TETIR=PG+TETIR
      TETVR(I)=TETIR*180./PG
c TETVR(I) = thetari
c The domain of TETVR(I) is (-180ø,180ø)

c conversion thetari --> thetai (Eqns (6.65) and (6.66))
      TEST=TETVR(I)-90
      IF(TEST.GT.-180)THEN
      TETV2(I)=TETVR(I)-90
      ELSE
      TETV2(I)=TETVR(I)+270
      ENDIF
c TETV2(I) = thetai
c The domain of TETV2(I) is (-180ø,180ø)
600   CONTINUE
      RETURN
      END
```

6.6.4 **Program TESTDS**

Program TESTDS enables us to test the subroutines for the directional spectrum. The first part of the program generates the time series data ETA(N,1), ETA(N,2), and ETA(N,3) at the given points A, B, and D through a numerical simulation of a sea state with a given directional spectrum consisting of NK prisms: base of the *k*th prism: O1V(k)-O2V(k), TE1V(k)-TE2V(k); ratio

between the volume of the kth prism and the total volume of the spectrum: FRAIN(k); number of harmonic components = number of frequencies of the kth prism = NDOV(k); number of angles of the kth prism = NTEV(k). For the generation of random phase angles ε_i use is made of a routine from the book by Press et al. (1992).

The second part of the program aims to obtain the directional spectrum from the three time series data by means of subroutines FOUR, SDI, and SDIR. The spectrum is obtained with the definition (Eqn (6.13)), from the triplets a_i, θ_i.

Note: the largest angular frequency considered is $\omega_{i_{\max}} = \pi$ rad/s, so that the smallest wavelength is $L_i = 6.24$ m (deep water), and AB = $X = 2$ m, AD = $Y = 2$ m fulfill conditions (Eqns (6.54) and (6.63)).

```
      PROGRAM TESTDS
      CHARACTER*64 NOMEC
      COMMON NMAX,IMA,DT,AB,AD,DEPTH
      COMMON AIP(150000,3),AIS(150000,3),OVF(150000),
      AIV(150000)
      DIMENSION ETA(300001,3)
      DIMENSION TETV(150000),TETV1(150000),TETV2(150000)
      DIMENSION OV(50000),TV(50000),EPS(50000),A1V(50000)
      DIMENSION O1V(50),O2V(50),TE1V(50),TE2V(50),AA(50)
      DIMENSION FRAIN(50),NDOV(50),NTEV(50)
      REAL ran0,AM
      PARAMETER (IA=16807,IM=2147483647,AM=1./IM,IQ=127773,
      IR=2836,
     *MASK=123459876)
      NOMEC='DOMAINS'
      OPEN(UNIT=50,STATUS='OLD',FILE=NOMEC,ERR=233)
      GO TO 234
233   STOP
234   CONTINUE

      NOMEC='OUTSP'
      OPEN(UNIT=65,FILE=NOMEC)

      PG=3.141592
      DPG=2.*PG
      PG4=PG/4.
      WRITE(6,*)'d'
      READ(5,*)DEPTH
      WRITE(6,*)'NK'
      READ(5,*)NK
      RM0=1
      IMAX=0
      DO K=1,NK
```

```
     .READ(50,*)
      O1V(K),O2V(K),TE1V(K),TE2V(K),FRAIN(K),NDOV(K),NTEV(K)
      IMAX=IMAX+NDOV(K)
      RMOP=RM0*FRAIN(K)
      RMOPP=RMOP/FLOAT(NDOV(K))
      AA(K)=SQRT(2.*RMOPP)
      ENDDO
      I=0
c Loop 280, wherein I runs from 1 to IMAX, generates
c amplitudes AIV(I), angular frequencies OV(I), and angles
c of the wave direction of the harmonic wave components
      DO 280 K=1,NK
      O1=O1V(K)
      O2=O2V(K)
      TE1=(PG/180.)*TE1V(K)
      TE2=(PG/180.)*TE2V(K)
      NDIV=NDOV(K)
      DO=(O2-O1)/FLOAT(NDIV)
      DTE=(TE2-TE1)/FLOAT(NTEV(K))
      O=O1-DO/2.
      TE=TE1-DTE
90    O=O+DO
      IF(O.GT.O2)GO TO 91
      I=I+1
      TE=TE+DTE
      IF(TE.GT.TE2)TE=TE1+DTE/2.
      OV(I)=O
      TV(I)=TE
      A1V(I)=AA(K)
      GO TO 90
91    CONTINUE
280   CONTINUE

c Loop 281 generates the IMAX random phase angles of the
c harmonic wave components
      IDUM=1
      DO 281 I=1,IMAX
      IDUM=IEOR(IDUM,MASK)
      K=IDUM/IQ
      IDUM=IA*(IDUM-K*IQ)-IR*K
      IF (IDUM.LT.0) IDUM=IDUM+IM
      RAN0=AM*IDUM
      IDUM=IEOR(IDUM,MASK)
      EPS(I)=DPG*RAN0
281   CONTINUE

      AB=2.
      AD=2.
```

```
      .DT=0.4
       WRITE(6,*)'duration sea state in hours'
       READ(5,*)DUR
       DUR=DUR*3.6E3
       NMAX=1+DUR/DT
       N=0
100    N=N+1
       IF(N.GT.NMAX)GO TO 101
       IF((N/1000)*1000.EQ.N)WRITE(6,*)'random wave simulation ',N,NMAX
       T=DT*FLOAT(N-1)

       DO L=1,3
       ETA(N,L)=0
       ENDDO

       DO I=1,IMAX
       OM=OV(I)
       PE=DPG/OM
       RL=WLENGTH(DEPTH,PE)
       RK=DPG/RL
       TE=TV(I)
       EP=EPS(I)
       A1=A1V(I)
       ARGA=-OM*T+EP
       ARGB=RK*AB*SIN(TE)+ARGA
       ARGD=RK*AD*COS(TE)+ARGA
       COSA=COS(ARGA)
       COSB=COS(ARGB)
       COSD=COS(ARGD)
       ETA(N,1)=ETA(N,1)+A1*COSA
       ETA(N,2)=ETA(N,2)+A1*COSB
       ETA(N,3)=ETA(N,3)+A1*COSD
       ENDDO
       GO TO 100
101    CONTINUE
c_____________________________________________________________

c the random time series at points A,B,D have been generated;
c hereafter the directional spectrum will be obtained from
c these three time series
c_____________________________________________________________
       DOMI=DPG/DUR
       OMAX=PG
       IMA=OMAX/DOMI

       CALL FOUR(ETA,AIP,AIS,OVF,AIV)
       CALL SDI(TETV1)
       CALL SDIR(TETV2)
```

```
     .RMO1=0
      ERR=0
      DO I=1,IMA
      TW1=TETV1(I)
      TW2=TETV2(I)
      AMP=AIV(I)
      ADD=AMP*AMP/2.
      ITI=2
      IF(TW1.GT.-180.AND.TW1.LT.-120)ITI=1
      IF(TW1.GT.-60.AND.TW1.LT.60)ITI=1
      IF(TW1.GT.120.AND.TW1.LT.180)ITI=1
      IF(ITI.EQ.1)THEN
      TETV(I)=TW1
      ELSE
      TETV(I)=TW2
      ENDIF
      IF(TETV(I).EQ.999)ERR=ERR+ADD
      RMO1=RMO1+ADD
      ENDDO
      ERR=ERR/RMO1
      WRITE(6,1000)ERR
1000  FORMAT(2X,'indeterminate ',E12.4)
c ERR is the share of the wave energy of the spectrum, for which,
c inequality Eqn (6.64) is not fulfilled
      WRITE(6,*)'O1,O2,DOM'
      READ(5,*)O1,O2,DOM
      WRITE(6,*)'TE1,TE2,DTE'
      READ(5,*)TE1,TE2,DTE
      O2M=O2-DOM
      TE2M=TE2-DTE
      O=O1-DOM
      I=0
150   O=O+DOM
      IF(O.GT.O2M+DOM/10.)GO TO 160
      I=I+1
      TE=TE1-DTE
      J=0
140   TE=TE+DTE
      IF(TE.GT.TE2M+DTE/10.)GO TO 150
      J=J+1
      SOMT=0
      SOMTP=0
c the following loop considers all the harmonic wave components used for
c the numerical simulation based on the given directional spectrum;
c and sums the square amplitude of those whose angular
c frequency falls in (O,O+DOM) and angle theta falls in (TE,TE+DTE)
```

```
      DO N=1,IMAX
      AX=A1V(N)
      OO=OV(N)
      TT=TV(N)*180./PG
      SOMT=SOMT+0.5*AX*AX
      IF(OO.GT.O.AND.OO.LT.O+DOM.AND.TT.GT.TE.AND.TT.LT.
      TE+DTE)THEN
      SOMTP=SOMTP+0.5*AX*AX
      ENDIF
      ENDDO


      SOMS=0
      SOMSP=0
c the following loop considers all the harmonics of the Fourier series
c at point A, and sums the square amplitude of those whose angular
c frequency falls in (O,O+DOM) and angle theta falls in (TE,TE+DTE)
      DO N=1,IMA
      AX=AIV(N)
      OO=OVF(N)
      TT=TETV(N)
      IF(TT.EQ.999)GO TO 888
      SOMS=SOMS+0.5*AX*AX
      IF(OO.GT.O.AND.OO.LT.O+DOM.AND.TT.GT.TE.AND.TT.LT.
      TE+DTE)THEN
      SOMSP=SOMSP+0.5*AX*AX
      ENDIF
888   CONTINUE
      ENDDO
      RT=100.*SOMTP/SOMT
      RS=100.*SOMSP/SOMS
c RT represents the percent energy of the actual spectrum on the
c domain (O,O+DOM),(TE,TE+DTE)
c Rs represents the percent energy of the output spectrum on the
c domain (O,O+DOM),(TE,TE+DTE)
      OO1=O
      OO2=O+DOM
      TT1=TE
      TT2=TE+DTE
      WRITE(6,7000)OO1,OO2,TT1,TT2,RT,RS
      WRITE(65,7000)OO1,OO2,TT1,TT2,RT,RS
7000  FORMAT(2X,F7.2,1X,F7.2,2X,F6.0,1X,F6.0,1X,F6.1,1X,F6.1)
      GO TO 140
160   CONTINUE
      WRITE(6,*)
      WRITE(6,*)'READ FILE OUTSP'
      END
```

6.6.5 Function WLENGTH

In order to speed up calculation it is convenient to resort to the equation

$$L = \left(1 - \frac{2\pi}{6}\frac{d}{L_0}\right)\sqrt{gd}\,T \tag{6.67}$$

which yields the wavelength with an error within the 0.25% on the range $d/L_0 < 0.20$ (see Boccotti, 2000, Section 1.5.5). The following function applies to Eqn (6.67) if $d/L_0 < 0.20$ and sequence (1.25) if $d/L_0 > 0.20$.

```
      FUNCTION WLENGTH(D,T)
      PG=3.141592
      DPG=2.*PG
      RLO=(9.8/DPG)*T*T
      DLO=D/RLO
      IF(DLO.LT.0.20)THEN
      RL=(1-(DPG/6)*(D/RLO))*SQRT(9.8*D)*T
      ELSE
      RLP=RLO
144   RL=RLO*TANH(DPG*D/RLP)
      TEST=ABS(RL-RLP)/RL
      RLP=RL
      IF(TEST.GT.2.5E-3)GO TO 144
      ENDIF
      WLENGTH=RL
      RETURN
      END
```

6.7 WORKED EXAMPLE OF OBTAINING A DIRECTIONAL SPECTRUM

A directional spectrum consists of three distinct prisms (NK = 3) with the characteristics given in Table 6.1.

Table 6.1 Worked Example: The Directional Spectrum Consists of Three Prisms with These Characteristics

	ω_1 (rad/s)	ω_2 (rad/s)	θ_1 (degrees)	θ_2 (degrees)	Percent Wave Energy
1	0.4	0.6	0	20	30%
2	1.0	1.2	60	80	40%
3	1.4	1.6	−140	−120	30%

Program TESTDS reads file DOMAINS that contains the data of this table as well as the number of frequencies ω_i and angles θ_i to be used for the numerical simulation. File DOMAINS used here is the following:

```
File DOMAINS
0.4     0.6     0       20      0.30    1040    40
1.0     1.2     60      80      0.40    1120    40
1.4     1.6     −140    −120    0.30    1026    38
```

A numerical simulation of a sea state on 100 m water depth with this spectrum is performed with the first part of program TESTDS. Then, with a DWR of 20 min and a sampling rate of 0.4 s (NMAX = 3001), by means of subroutines FOUR, SDI, and SDIR we obtain the directional spectrum represented in Fig. 6.3(a). With a DWR of 10 h we obtain the directional spectrum of Fig. 6.3(b). The share of wave energy whose direction remains indeterminate is equal to $5 \cdot 10^{-4}$ with the DWR of 20 min, and is reduced to about 10^{-5} with the DWR of 10 h.

What counts is that, even with the DWR of 20 min, we are able to catch the essential features of the directional spectrum: the energy of the actual spectrum is distributed (30%, 40%, and 30%, respectively) on three domains of (0.2 rad/s·20°), and the energy of the spectrum obtained from the time records, on these domains, is 28%, 40%, and 25%, respectively. With the DWR of 10 h, the directional spectrum calculated proves to be close to the actual one.

Note that if one is given the values of the four integrals on the LHS of Eqns (6.27) and (6.30−6.32), as with the classic method, one can obtain only the first and the second angular harmonic components of the directional distribution. Here, the $D(\theta;\omega)$ is a rectangle and requires a greater number of angular harmonic components to be satisfactorily approximated (see Fig. 6.4). Thus we may realize why the classic method needs some further informations, besides the values of the four aforementioned integrals. These additional informations must concern the very shape of the directional distribution. In our particular case, one should a priori know that this distribution has a rectangular shape.

Note that the result of program TESTDS is given in file OUTSP wherein the first two columns give the range of ω in rad/s, the 3rd and the 4th columns give the range of θ in degree, the 5th and the 6th columns give the percentage of the energy of the spectrum. The 5th column is for the actual spectrum, the 6th column is for the spectrum obtained with the new method. Note that the actual spectrum is obtained with the a_i, ω_i, and θ_i used for the numerical simulation (as such it may somewhat differ from the given spectrum). The

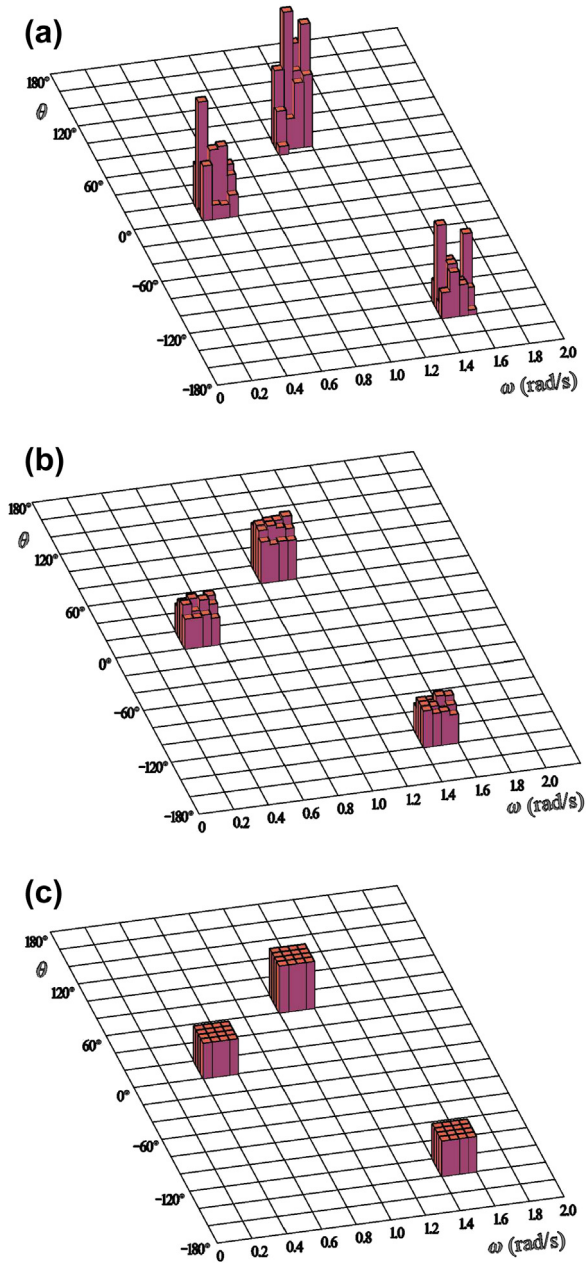

■ **FIGURE 6.3** Worked example: (a) result obtained with a 20 min DWR; (b) result obtained with a 10 h DWR; (c) the given directional spectrum.

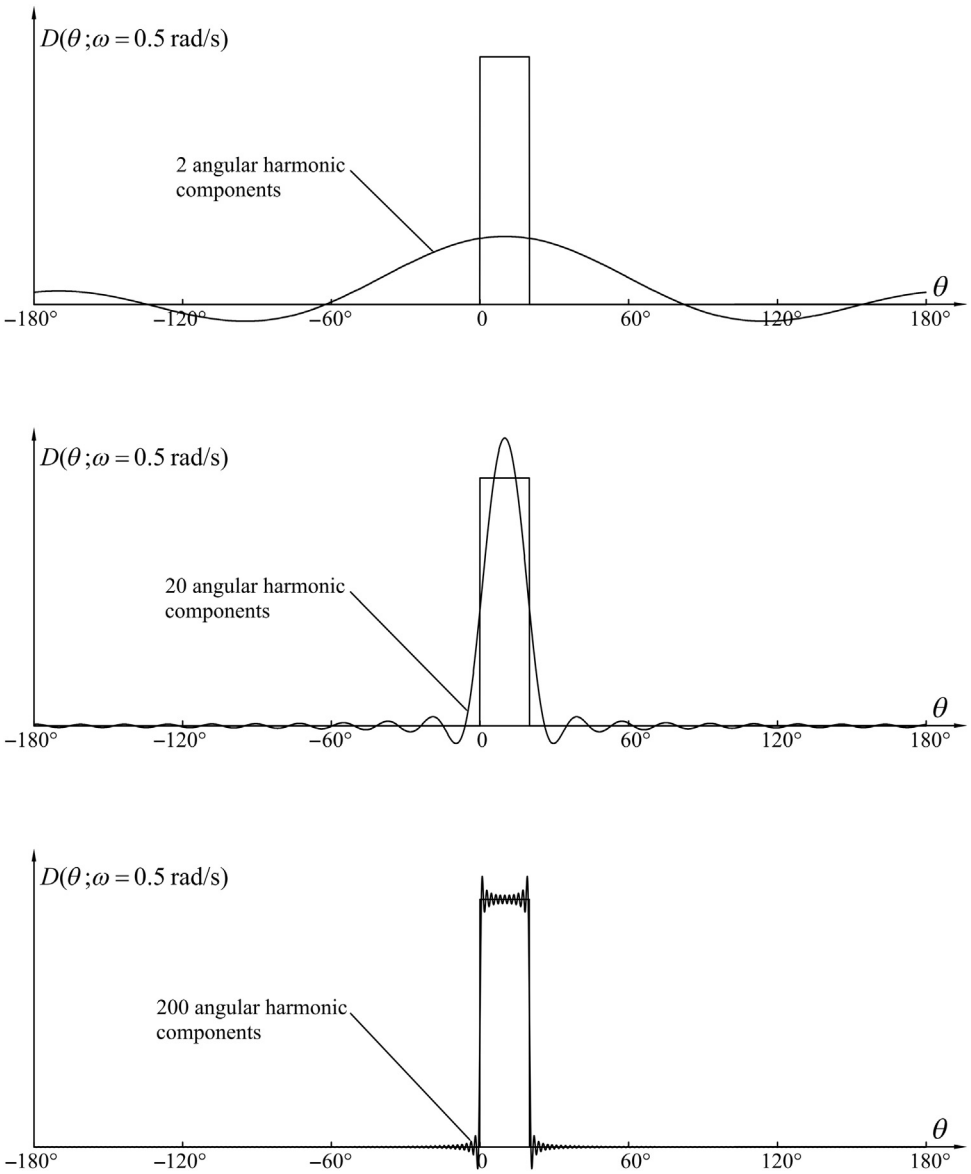

■ **FIGURE 6.4** The directional distribution of the first wave family of the directional spectrum of the worked example, and what is obtained with some increasing number of angular harmonic components.

inputs from console for Fig. 6.3(a) and (b) were: O1=0, O2=2, DOM=0.05; TE1=−180, TE2=180, DTE=5. For obtaining the energy content on rectangles of 0.2 rad × 20°, DOM and DTE must be changed, respectively, into 0.2 and 20.

6.8 CONCLUSION

The classic method (Eqns (6.27) and (6.30)−(6.32)) does not enable us to discover the form of the actual spectrum, starting from some time series data. In particular, the classic method does not enable us to discover that the directional spectrum of a sea state is that of Fig. 6.3(c). Besides time series data, the classic method needs some general information on the configuration of the directional distribution to be found. With wind seas, this information consists of the Cartwright equation; that is, the directional distribution is expected to have the general form (Eqn (6.33)). The new method (Eqns (6.49)−(6.51) and (6.59)−(6.62)) does not need this kind of information, and can work with only the time series data at three points (two points in the proximity of a coast). It succeeds in discovering the configuration of the directional spectrum without receiving any clue on this configuration, as we have seen in the worked example. However, this capability has been proven only in sea states consisting of families of waves with generally distinct directions provided that these families have also some distinct ranges of frequencies (as with the case of Fig. 6.3). With a typical DWR (20 min for a full-scale sea state), I have always found that the new method is able to yield an essential overall picture of the directional spectrum of this kind of sea state. Having the original FORTRAN program available, the reader is invited to check and deepen this conclusion.

Obtaining the directional spectrum near a coast with the new method was the object of an SSFE described by Boccotti et al. (2011).

The classic approach based on the work of Longuet-Higgins et al. (1963) and Cartwright (1963) is correctly developed from Eqn (6.8) of the random surface elevation. However, the fact that the output is $D(\theta;\omega_i)$ may be misleading and may suggest the idea of a variety of angles with a unique frequency; that is, the idea of a surface elevation having the form

$$\eta(x,y,t) = \sum_{i=1}^{N}\sum_{j=1}^{M} a_{ij}\cos\left(k_i x\sin\theta_j + k_i y\cos\theta_j - \omega_i t + \varepsilon_{ij}\right) \qquad (6.68)$$

in place of the form of Eqn (6.8). Whether or not the cause is in the approach to the directional spectrum, it is a matter of fact that form (Eqn (6.68)) is disseminated in the literature (cf. Eqn (22) of Massel and Brinkman

(1998), or Eqns (3.1) and (3.2) of Jensen (2005)). Here, pay attention: wave field (Eqn (6.68)) does not comply with the condition of spatial homogeneity. Indeed, the variance of the surface elevation proves to be

$$\langle \eta^2(t) \rangle = \sum_{i=1}^{N} \sum_{j=1}^{M} \frac{a_{ij}^2}{2} + \sum_{i=1}^{N} \sum_{j=1}^{M} \sum_{\substack{k=1 \\ k \neq j}}^{M} \frac{a_{ij} a_{ik}}{2} \cos \left(k_i x \sin \theta_j + k_i y \cos \theta_j + \varepsilon_{ij} - k_i x \sin \theta_k - k_i y \cos \theta_k - \varepsilon_{ik} \right) \tag{6.69}$$

And, as such, it is a random function of x, y.

REFERENCES

Boccotti, P., 2000. Wave Mechanics for Ocean Engineering. Elsevier, Amsterdam pp. 1—495.

Boccotti, P., 2004. A method to obtain the directional wave spectrum. Ocean Eng. 31, 539—545.

Boccotti, P., Arena, F., Fiamma, V., Romolo, A., Barbaro, G., 2011. Estimation of mean spectral directions in random seas. Ocean Eng. 38, 509—518.

Breugem, W., Holthuijsen, L., 2007. Generalized shallow water wave growth from Lake George. J. Waterw. Port Coast. Ocean Eng. 133 (3), 173—182.

Cartwright, D.E., 1963. The use of directional spectra in studying the output of a wave recorder on a moving ship. In: Ocean Wave Spectra. Prentice Hall, New York, pp. 203—218.

Ewans, K.C., 1998. Observations of the directional spectrum of fetch-limited waves. J. Phys. Oceanogr. 28 (3), 495—512.

Holthuijsen, L.H., 2007. Waves in Oceanic and Coastal Waters. Cambridge University Press, Cambridge, 387 pp.

Jensen, J.J., 2005. Conditional second-order short-crested water waves applied to extreme wave episodes. J. Fluid Mech. 545, 29—40.

Kahma, K.K., Calkoen, C.J., 1992. Reconciling discrepancies in the observed growth of wind-generated waves. J. Phys. Oceanogr. 22 (12), 1389—1405.

Longuet-Higgins, M.S., Cartwright, D.E., Smith, N.D., 1963. Observations of the directional spectrum of sea waves using the motions of a floating buoy. In: Ocean Wave Spectra. Prentice Hall, New York, pp. 111—136.

Massel, S.R., Brinkman, R.M., 1998. On the determination of directional wave spectra for practical applications. Appl. Ocean Res. 20, 357—374.

Mitsuyasu, H., Tasai, F., Suhara, T., Mizuno, S., Ohkusu, M., Honda, T., Rikiishi, K., 1975. Observations of the directional spectrum of ocean waves using a cloverleaf buoy. J. Phys. Oceanogr. 5 (10), 750—760.

Pierson, W.J., Moskowitz, L., 1964. A proposed spectral form for fully developed waves based on the similarity theory of S. A. Kitaigorodskii. J. Geophys. Res. 69, 5181—5190.

Press, W.H., Teukoisky, S.A., Vetterling, W.T., Flannery, B.P., 1992. Numerical Recipes in FORTRAN 77: The Art of Scientific Computing. Cambridge University Press.

Tucker, M.J., 1989. Interpreting directional data from large pitch-roll-heave buoys. Ocean Eng. 16, 173–192.

Tucker, M.J., Pitt, E.G., 2001. Waves in Ocean Engineering. Elsevier, Amsterdam, p. 521.

Young, I.R., Verhagen, L.A., 1996. The growth of fetch limited waves in water of finite depth. Part 1. Total energy and peak frequency. Coast. Eng. 29, 47–78.

Young, I.R., Verhagen, L.A., Shatri, S.K., 1996. The growth of fetch limited waves in water of finite depth. Part 3. Directional spectra. Coast. Eng. 29, 101–122.

Chapter 7

Complements of Space—Time Theory of Sea States*

CHAPTER OUTLINE

7.1 CROSS-COVARIANCES: HOMOGENEOUS RANDOM WAVE FIELD

The quasi-determinism (QD) theory uses the cross-covariance of the surface elevation:

$$\Psi(X,Y,T;x_o,y_o) \equiv \langle \eta(x_o,y_o,t)\eta(x_o+X,y_o+Y,t+T)\rangle \tag{7.1}$$

With Eqn (6.8) of $\eta(x,y,t)$ we have

$$\Psi(X,Y,T;x_o,y_o) = \sum_{i=1}^{N}\sum_{j=1}^{N} a_i a_j \langle \cos\,(A_i(t))\cos\,(A_j(t)+B_j)\rangle \tag{7.2}$$

where we have resorted to the compact notations

*These Complements Are Needed for the QD Theory.

Wave Mechanics and Wave Loads on Marine Structures. http://dx.doi.org/10.1016/B978-0-12-800343-5.00007-X

$$A_i(t) = k_i x_o \sin\theta_i + k_i y_o \cos\theta_i - \omega_i t \tag{7.3}$$

$$B_j = k_j X \sin\theta_j + k_j Y \cos\theta_j - \omega_j T \tag{7.4}$$

The average in Eqn (7.2) may be rewritten in the form

$$\langle . \rangle = \langle \cos(A_i(t)) \cos(A_j(t)) \cos B_j \rangle - \langle \cos(A_i(t)) \sin(A_j(t)) \sin B_j \rangle \tag{7.5}$$

The second average on the right-hand side (RHS) of Eqn (7.5) is zero whichever the i, j; the first average is zero if $i \neq j$, and is equal to 0.5 $cos\ B_i$ if $i = j$. Hence, Eqn (7.2) is reduced to

$$\Psi(X, Y, T; x_o, y_o) = \sum_{i=1}^{N} \frac{1}{2} a_i^2 \cos B_i \tag{7.6}$$

and replacing B_i with its expression (Eqn 7.4):

$$\Psi(X, Y, T; x_o, y_o) = \sum_{i=1}^{N} \frac{1}{2} a_i^2 \cos(k_i X \sin\theta_i + k_i Y \cos\theta_i - \omega_i T) \tag{7.7}$$

With the definition Eqn (6.13) of directional spectrum this becomes

$$\Psi(X, Y, T; x_o, y_o) = \int_0^{\infty} \int_0^{2\pi} S(\omega, \theta) \cos(kX \sin\theta + kY \cos\theta - \omega T) \mathrm{d}\theta \mathrm{d}\omega \tag{7.8}$$

The QD theory also uses the cross-covariance of the surface elevation and the velocity potential:

$$\Phi(X, Y, z, T; x_o, y_o) \equiv \langle \eta(x_o, y_o, t) \phi(x_o + X, y_o + Y, z, t + T) \rangle \tag{7.9}$$

On replacing η with its expression (6.8) and ϕ with its expression (6.9), and doing essentially the same steps as we have done for Ψ, we arrive at

$$\Phi(X, Y, z, T; x_o, y_o) = g \int_0^{\infty} \int_0^{2\pi} S(\omega, \theta) \omega^{-1} \frac{\cosh[k(d+z)]}{\cosh(kd)} \times \sin(kX \sin\theta + kY \cos\theta - \omega T) \mathrm{d}\theta \mathrm{d}\omega \tag{7.10}$$

7.2 SEA STATES NONHOMOGENEOUS IN SPACE

7.2.1 Sea States Near Breakwaters

The surface elevation $\eta(x,y,t)$ and the velocity potential $\phi(x,y,z,t)$ of a periodic wave before a vertical reflecting wall are given by Eqns (1.68, 1.69). Hence, η and ϕ of a sea state, which is the sum of a very large number N of small periodic waves, are given by

$$\eta(x,y,t) = 2\sum_{i=1}^{N} a_i \cos(k_i x \sin\theta_i - \omega_i t + \varepsilon_i)\cos(k_i y \cos\theta_i) \tag{7.11}$$

$$\begin{aligned}\phi(x,y,z,t) = {} & 2g\sum_{i=1}^{N} a_i \omega_i^{-1} \frac{\cosh[k_i(d+z)]}{\cosh(k_i d)} \\ & \times \sin(k_i x \sin\theta_i - \omega_i t + \varepsilon_i)\cos(k_i y \cos\theta_i)\end{aligned} \tag{7.12}$$

In other words: if we put a vertical reflecting wall in the plane $y = 0$, the random wave field Eqns (6.8, 6.9) take on the form Eqns (7.11) and (7.12).

If we put a semi-infinite vertical wall in the plane $y = 0$, with the origin at $x = 0$, the wave field Eqns (6.8, 6.9) becomes

$$\eta(r,\beta,t) = \sum_{i=1}^{N} a_i [F(r,\beta;\omega_i,\theta_i)\cos(\omega_i t + \varepsilon_i) + G(r,\beta;\omega_i,\theta_i)\sin(\omega_i t + \varepsilon_i)] \tag{7.13}$$

$$\begin{aligned}\phi(r,\beta,z,t) = {} & g\sum_{i=1}^{N} a_i \omega_i^{-1} \frac{\cosh[k_i(d+z)]}{\cosh(k_i d)} [G(r,\beta;\omega_i,\theta_i)\cos(\omega_i t + \varepsilon_i) \\ & - F(r,\beta;\omega_i,\theta_i)\sin(\omega_i t + \varepsilon_i)]\end{aligned} \tag{7.14}$$

where r and β are the polar coordinates (see the definition sketch of Fig. 1.8). The ith terms of these two summations represent the flow field due to an incident wave of amplitude a_i, frequency ω_i, phase ε_i, whose direction makes an angle θ_i with the y-axis. The functions $F(r,\beta;\omega,\theta)$ and $G(r,\beta;\omega,\theta)$ were defined in Section 1.8.1.

The surface elevation at every fixed point of both wave fields Eqns (7.11) and (7.13) represents a stationary Gaussian process (as usually, the proof exploits the assumptions on the a_i, ω_i, ε_i, and N). A big novelty with respect to the random wave field Eqn (6.8) in the open sea is that here the wave field is no longer homogeneous in space. It is nonhomogeneous because of the diffraction induced by the breakwater. Indeed, the variance of the surface elevation of wave field Eqn (7.11) is

$$\sigma^2(y) = 4\sum_{i=1}^{N} \frac{1}{2} a_i^2 \cos^2(k_i y \cos\theta_i) \tag{7.15}$$

and the variance of wave field Eqn (7.13) is

$$\sigma^2(r,\beta) = \sum_{i=1}^{N} \frac{1}{2} a_i^2 \left[F^2(r,\beta;\omega_i,\theta_i) + G^2(r,\beta;\omega_i,\theta_i)\right] \tag{7.16}$$

7.2.2 Diffraction Coefficients before a Long Upright Breakwater

With the definition of directional spectrum, Eqn (7.15) may be rewritten in the form

$$\sigma^2(y) = 4\int_0^{\infty}\int_0^{2\pi} S(\omega,\theta)\cos^2(ky\cos\theta)\mathrm{d}\theta\mathrm{d}\omega \tag{7.17}$$

Figure 7.1 shows the function $\sigma^2(y)/\sigma^2(0)$ obtained by means of Eqn (7.17) with a characteristic spectrum of wind seas for the case of orthogonal wave attack (i.e., the dominant direction of the incident waves is orthogonal to the wall). For a comparison, the figure shows also

$$\frac{\sigma^2(y)}{\sigma^2(0)} = \cos^2\left(2\pi\frac{y}{L}\right) \tag{7.18}$$

of the periodic waves (for the same condition of wave attack orthogonal to the wall).

As we may see, the difference between wind seas and periodic waves is great. The variance of the periodic waves fluctuates between maxima equal to the maximum at the wall and minima equal to zero, and the fluctuations go on as far as an infinite distance from the wall. The variance of the wind-generated waves is a damped oscillatory function of the distance from the

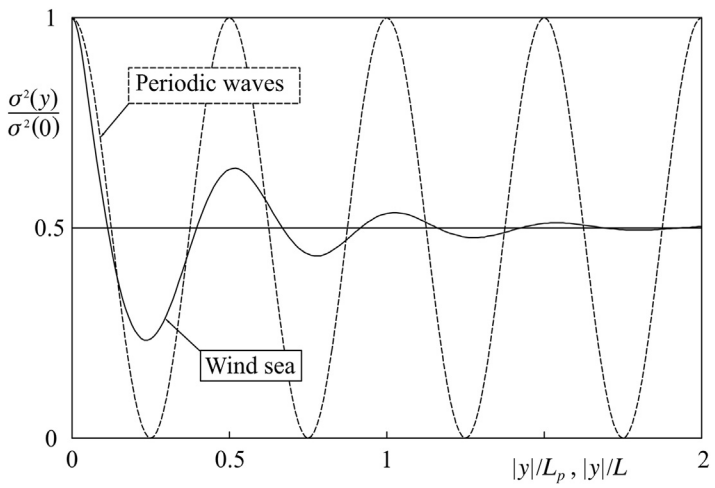

■ **FIGURE 7.1** Variance of the surface elevation as a function of the distance from the wall for an orthogonal wave attack.

wall; and, at only one or two wavelengths from the wall, it approaches a constant value being equal to half of the value at the wall.

The diffraction coefficient C_d of the waves interacting with some solid obstacle is defined as the ratio between the root mean square (RMS) surface elevation at a given point and the RMS surface elevation of the incident waves (for the periodic waves, C_d coincides with the ratio between the wave height at the given point and the height of the incident waves, as we saw in Chapter 1). In the case of the long breakwater it is convenient to write

$$C_d(y) \equiv \frac{\sigma(y)}{\sigma} = \frac{\sigma(y)}{\sigma(0)} \frac{\sigma(0)}{\sigma} \tag{7.19}$$

where σ is the RMS surface elevation of the wave field Eqn (6.8) that would be there without the wall. Indeed, the quotient $\sigma(0)/\sigma$ is equal to 2 for whichever be the spectrum, and hence we have the relationship

$$C_d(y) = 2\frac{\sigma(y)}{\sigma(0)} \tag{7.20}$$

that enables us to deduce C_d from the function $\sigma^2(y)/\sigma^2(0)$ of Fig. 7.1. At the wall C_d is equal to 2, and starting on about one wavelength from the wall, approaches $2\sqrt{\frac{1}{2}} = \sqrt{2}$.

7.2.3 Diffraction Coefficients in the Lee of an Upright Breakwater

With the definition of directional spectrum, Eqn (7.16) of the variance of the surface elevation becomes

$$\sigma^2(r,\beta) = \int_0^{\infty} \int_0^{2\pi} S(\omega,\theta)\left[F^2(r,\beta;\omega,\theta) + G^2(r,\beta;\omega,\theta)\right] \mathrm{d}\theta \mathrm{d}\omega \tag{7.21}$$

and hence the diffraction coefficient is given by

$$C_d(r,\beta) = \sqrt{\frac{\int_0^{\infty} \int_0^{2\pi} S(\omega,\theta)[F^2(r,\beta;\omega,\theta) + G^2(r,\beta;\omega,\theta)]d\theta d\omega}{\int_0^{\infty} \int_0^{2\pi} S(\omega,\theta) d\theta d\omega}} \tag{7.22}$$

Figure 7.2 shows the values of C_d for a case of an orthogonal attack ($\theta_d = 0$) and for the case of an inclined attack ($\theta_d = 45°$). This figure should be compared with Fig. 1.10. The comparison shows that:

1. in the more sheltered area of the geometric shadow the C_d of a wind sea is practically coincident with the C_d of the periodic waves;

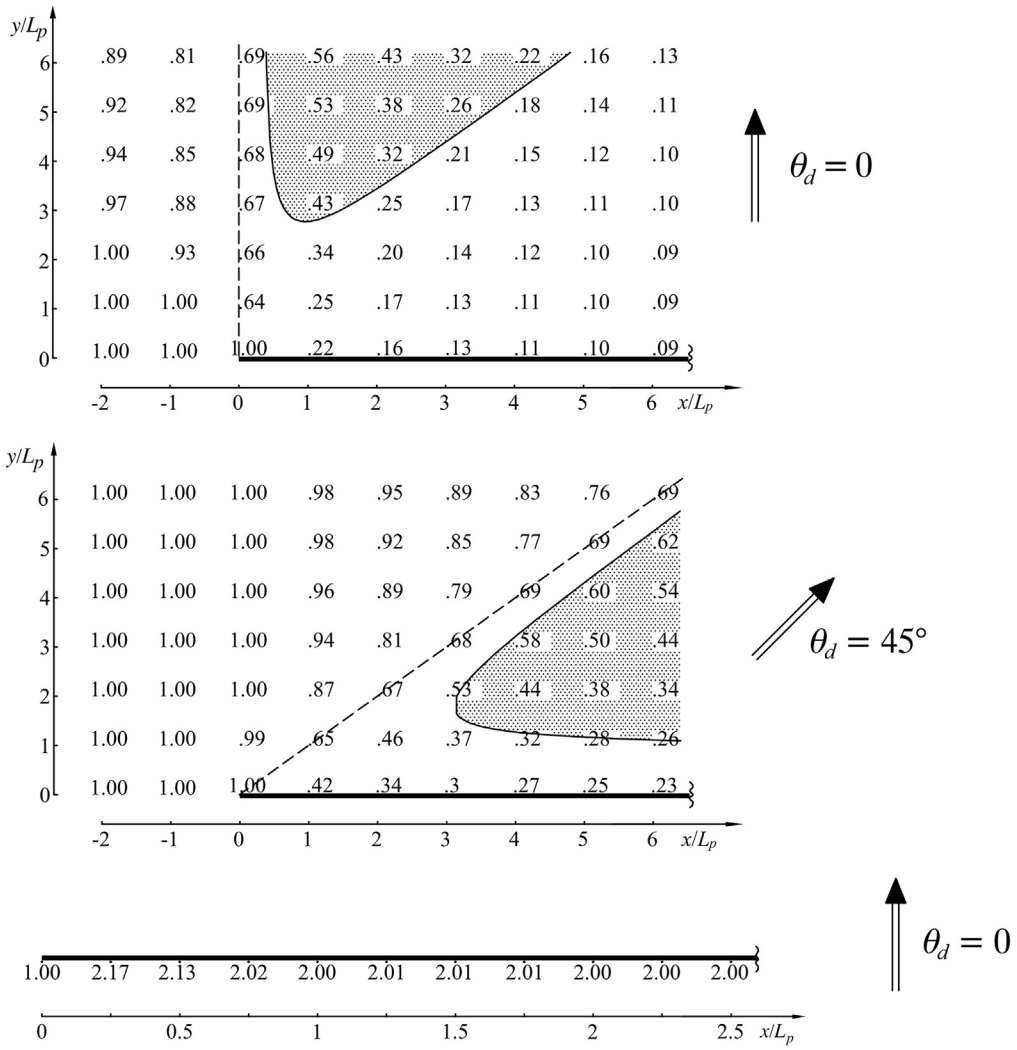

■ **FIGURE 7.2** Diffraction coefficient of wind seas (mean JONSWAP spectrum, directional distribution of Mitsuyasu et al. with $n_p = 20$). Comparing this figure with Fig. 1.10, it may be noted that the C_d of the wind seas, in the dark areas, is at least 50% greater than the C_d of the periodic waves.

2. within the dark area of the geometric shadow (see Fig. 7.2) the C_d of the wind sea is at least 50% greater than the C_d of the periodic waves;
3. along the wave-beaten wall, the C_d of the wind sea settles on the constant value 2 at a short distance from the breakwater's tip, while the C_d of the periodic waves exhibits an infinite sequence of local maxima greater than 2 and local minima smaller than 2.

It is apparent that the really important matter is point (2) above; that is, the large difference between the C_d of wind seas and the C_d of periodic waves in the "dark area" in the lee of a breakwater.

7.3 CROSS-COVARIANCES: NONHOMOGENEOUS RANDOM WAVE FIELDS

7.3.1 Before a Long Upright Breakwater

For obtaining Ψ for a sea state before a long breakwater, η in Eqn (7.1) must be replaced by its Eqn (7.11), and the result may be written in the form

$$\Psi(X,Y,T;x_o,y_o) = 4\sum_{i=1}^{N}\sum_{j=1}^{N} a_i a_j C_i D_j \langle \cos(A_i(t))\cos\left(A_j(t)+B_j\right)\rangle \quad (7.23)$$

with the definitions

$$C_i = \cos(k_i y_o \cos\theta_i) \quad (7.24)$$

$$D_i = \cos[k_i(y_o+Y)\cos\theta_i] \quad (7.25)$$

$$A_i(t) = k_i x \sin\theta_i - \omega_i t + \varepsilon_i \quad (7.26)$$

$$B_i = k_i X \sin\theta_i - \omega_i T \quad (7.27)$$

The average on the RHS of Eqn (7.23) is equal to 0.5 $\cos B_i$ if $i=j$ and otherwise is zero, so that

$$\Psi(X,Y,T;x_o,y_o) = 4\sum_{i=1}^{N}\frac{1}{2}a_i^2 C_i D_i \cos B_i \quad (7.28)$$

and, with the definition of directional spectrum,

$$\Psi(X,Y,T;x_o,y_o) = 4\int_0^{\infty}\int_0^{2\pi} S(\omega,\theta)\cos(ky_o\cos\theta)\cos[k(y_o+Y)\cos\theta] \cdot\cos(kX\sin\theta-\omega T)\mathrm{d}\theta\mathrm{d}\omega \quad (7.29)$$

With the same sequence of steps we obtain the expression of Φ for the wave field before the long breakwater; we have to replace η with its Eqn (7.11) and ϕ with Eqn (7.12) in Eqn (7.9), with the result:

$$\Phi(X,Y,z,T;x_o,y_o) = 4g\int_0^{\infty}\int_0^{2\pi} S(\omega,\theta)\omega^{-1}\frac{\cosh[k(d+z)]}{\cosh(kd)}\cos(ky_o\cos\theta) \cdot\cos[k(y_o+Y)\cos\theta]\sin(kX\sin\theta-\omega T)\mathrm{d}\theta\mathrm{d}\omega \quad (7.30)$$

7.3.2 In the Lee of an Upright Breakwater

For the wave field Eqn (7.13) we must work with polar coordinates, and hence the definitions of Ψ and Φ are slightly different.

We have

$$\Psi(R,\beta,T;r_o,\beta_o) \equiv \langle \eta(r_o,\beta_o,t)\eta(R,\beta,t+T)\rangle \tag{7.31}$$

(see Fig. 7.3), so that Eqn (7.13) of $\eta(r,\beta,t)$ yields

$$\begin{aligned}\Psi(R,\beta,T;r_o,\beta_o) \equiv \sum_{i=1}^{N}\sum_{j=1}^{N} a_i a_j \big\langle &[F_{o_i}\cos(A_i(t)) + G_{o_i}\sin(A_i(t))] \\ &\cdot\left[F_j\cos\left(A_j(t)+B_j\right) + G_j\sin\left(A_j(t)+B_j\right)\right]\big\rangle\end{aligned} \tag{7.32}$$

where

$$F_{o_i} = F(r_o,\beta_o;\omega_i,\theta_i) \tag{7.33}$$

$$G_{o_i} = G(r_o,\beta_o;\omega_i,\theta_i) \tag{7.34}$$

$$F_i = F(R,\beta;\omega_i,\theta_i) \tag{7.35}$$

$$G_i = G(R,\beta;\omega_i,\theta_i) \tag{7.36}$$

$$A_i(t) = \omega_i t + \varepsilon_i \tag{7.37}$$

$$B_i = \omega_i T \tag{7.38}$$

The average on the RHS of Eqn (7.32) is equal to zero if $i \neq j$, and is

$$\langle . \rangle = \frac{1}{2}(F_{o_i}F_i + G_{o_i}G_i)\cos(B_i) + \frac{1}{2}(F_{o_i}G_i - G_{o_i}F_i)\sin(B_i) \tag{7.39}$$

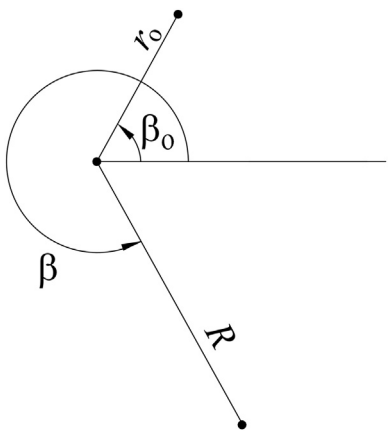

■ **FIGURE 7.3** Reference scheme for the cross-covariance in polar coordinates.

if $i = j$. Hence Eqn (7.32) is reduced to

$$\Psi(R,\beta,T;r_o,\beta_o) \equiv \sum_{i=1}^{N}\frac{1}{2}a_i^2[(F_{o_i}F_i + G_{o_i}G_i)\cos(B_i) + (F_{o_i}G_i - G_{o_i}F_i)\sin(B_i)] \tag{7.40}$$

and, with the definition of directional spectrum:

$$\begin{aligned}\Psi(R,\beta,T;r_o,\beta_o) = \int_0^{\infty}\int_0^{2\pi} S(\omega,\theta)\{&[F(r_o,\beta_o;\omega,\theta)F(R,\beta;\omega,\theta) \\ &+ G(r_o,\beta_o;\omega,\theta)\cdot G(R,\beta;\omega,\theta)]\cos(\omega T) \\ &+ [F(r_o,\beta_o;\omega,\theta)G(R,\beta;\omega,\theta) \\ &- G(r_o,\beta_o;\omega,\theta)F(R,\beta;\omega,\theta)]\cdot\sin(\omega T)\}\mathrm{d}\theta\mathrm{d}\omega\end{aligned} \tag{7.41}$$

Similarly, we obtain

$$\begin{aligned}\Phi(R,\beta,z,T;r_o,\beta_o) = g\int_0^{\infty}\int_0^{2\pi} S(\omega,\theta)\omega^{-1}\frac{\cosh[k(d+z)]}{\cosh(kd)} \\ \{-[F(r_o,\beta_o;\omega,\theta)F(R,\beta;\omega,\theta) \\ + G(r_o,\beta_o;\omega,\theta)G(R,\beta;\omega,\theta)]\sin(\omega T) \\ + [F(r_o,\beta_o;\omega,\theta)G(R,\beta;\omega,\theta) \\ - G(r_o,\beta_o;\omega,\theta)\cdot F(R,\beta;\omega,\theta)]\cos(\omega T)\}\mathrm{d}\theta\mathrm{d}\omega\end{aligned} \tag{7.42}$$

7.3.3 Cross-correlation of the Surface Elevation

In the deduction of the QD theory (Chapter 8) it is convenient to resort to the cross-correlation, defined as

$$\widehat{\Psi}(X,Y,T;x_o,y_o) \equiv \langle\widehat{\eta}(x_o,y_o,t)\widehat{\eta}(x_o+X,y_o+Y,t+T)\rangle \tag{7.43}$$

where

$$\widehat{\eta}(x,y,t) = \frac{\eta(x,y,t)}{\sigma(x,y)} \tag{7.44}$$

$\widehat{\Psi}$ ranges from -1 to 1. It is -1 or 1, respectively, if for every t

$$\eta(x_o+X,y_o+Y,t+T) = -K\eta(x_o,y_o,t) \tag{7.45}$$

or

$$\eta(x_o+X,y_o+Y,t+T) = K\eta(x_o,y_o,t) \tag{7.46}$$

where K is any positive constant. If $\eta(x_o+X,y_o+Y,t+T)$ is stochastically independent from $\eta(x_o,y_o,t)$, $\widehat{\Psi}$ is 0.

7.4 MAXIMUM EXPECTED WAVE HEIGHT IN A NONHOMOGENEOUS SEA STATE

Preliminarily it is convenient rewriting Eqn (4.61) in the form

$$\overline{H_{\max}} = \sigma \int_0^\infty \left\{1 - \left[1 - K_1 \exp\left(-\frac{u^2}{K_2}\right)\right]^N\right\} \mathrm{d}u \tag{7.47}$$

where the dimensional variable H has been replaced by $u = H/\sigma$. For a nonhomogeneous wave field, like Eqn (7.11) or (7.13), where the RMS surface elevation and the spectrum vary in general from one point to another, Eqn (7.47) may be reproposed in the form

$$\overline{H_{\max}}(x,y) = C_d(x,y)\,\sigma \int_0^\infty \left\{1 - \left[1 - K_1(x,y)\exp\left(-\frac{u^2}{K_2(x,y)}\right)\right]^N\right\} \mathrm{d}u \tag{7.48}$$

where σ is the RMS surface elevation of the incident waves. Calculations show that usually

$$\overline{H_{\max}}(x,y) \cong C_d(x,y)\,\overline{H_{\max}} \tag{7.49}$$

7.5 CONCLUSION

The diffraction coefficient of a random wave field is generally obtained with the equation

$$C_d(x,y) = \left(\int_0^\infty \int_0^{2\pi} S(\omega,\theta)\, C_d^2(x,y;\omega,\theta)\mathrm{d}\theta\mathrm{d}\omega \Big/ \int_0^\infty \int_0^{2\pi} S(\omega,\theta)\mathrm{d}\theta\mathrm{d}\omega\right)^{1/2} \tag{7.50}$$

where $C_d(x,y;\omega,\theta)$ is the diffraction coefficient of a periodic wave wherein ω is the angular frequency and θ is the angle between the direction and y-axis. Probably the first application of this equation was due to Goda et al. (1978). It was a nice application to port engineering. Equation (7.50) implies that, for obtaining the diffraction coefficient of a random nonhomogeneous wave field, it is sufficient to know the directional spectrum of the incident waves and diffraction coefficients of periodic unidirectional waves. In other words, it is not necessary to work with functions of surface elevation like Eqns (7.11)–(7.14). However, this kind of work becomes necessary in view of the application of the QD theory. Indeed, as we shall see in the next chapters, the QD theory calls for the cross-covariances Ψ and Φ. The first time this

work was done is presumed to be in my paper (1988). Then this work was done by Filianoti (see Filianoti, 2000) for the case of the detached breakwater and the breakwater gap.

REFERENCES

Boccotti, P., 1988. Refraction, reflection and diffraction of irregular gravity waves. Excerpta Ital. Contrib. Field Hydraul. Eng. 3, 47–89.

Filianoti, P., 2000. Diffraction of random wind-generated waves by detached breakwater or breakwater gap. Ocean. Eng. 27 (11), 1249–1263.

Goda, Y., Takayama, T., Suzuki, Y., 1978. Diffraction diagrams for directional random waves. Proc.16th Conf. Coast. Eng., 628–650.

Chapter 8

The Theory of Quasi-Determinism

CHAPTER OUTLINE

8.1 THE NECESSARY AND SUFFICIENT CONDITION FOR THE OCCURRENCE OF A WAVE CREST OF GIVEN VERY LARGE HEIGHT

The condition

$$\eta(t_o) = b \tag{8.1}$$

where t_o is a given time instant and b is a given positive value, in the limit as $b/\sigma \to \infty$, and is not only necessary but also sufficient in probability for the occurrence of a wave crest of given height b. ("A is sufficient in probability for the occurrence of B" means that "given A, the probability approaches 1 that B occurs.")

Wave Mechanics and Wave Loads on Marine Structures. http://dx.doi.org/10.1016/B978-0-12-800343-5.00008-1

Actually, the necessary and sufficient condition in probability is

$$\eta(t_o) = b, \quad \dot{\eta}(t_o) = 0 \tag{8.2}$$

However, the reasoning we are going to do is the same whether starting from condition (8.1) or from condition (8.2), and the conclusion is exactly the same. The advantage in dealing with condition (8.1) rather than with condition (8.2) is that one works with a 2×2 covariance matrix rather than 3×3, so the mathematical steps are lighter.

In order to prove that condition (8.1) is sufficient, let us consider the conditional probability of the surface elevation at any fixed time instant $t_o + T$ given condition (8.1). We have

$$p[\eta(t_o + T) = u | \eta(t_o) = b] = \frac{p[\eta(t_o) = b, \eta(t_o + T) = u]}{p[\eta(t_o) = b]} \tag{8.3}$$

From Section 4.2 we know that

$$\begin{aligned} p[\eta(t_o) &= b, \eta(t_o + T) = u] \\ &= \frac{1}{2\pi\sqrt{M}} \exp\left[-\frac{1}{2M} \left(M_{11} b^2 + 2M_{12} bu + M_{22} u^2 \right) \right] \end{aligned} \tag{8.4}$$

$$p[\eta(t_o) = b] = \frac{1}{\sqrt{2\pi m_0}} \exp\left(-\frac{b^2}{2m_0} \right) \tag{8.5}$$

Hence, it follows that

$$p[\eta(t_o + T) = u | \eta(t_o) = b] = \sqrt{\frac{m_0}{2\pi M}} \exp[F(u)] \tag{8.6}$$

where $F(u)$ denotes the function

$$F(u) = -\frac{1}{2M} \left(M_{11} b^2 + 2M_{12} bu + M_{22} u^2 \right) + \frac{b^2}{2m_0} \tag{8.7}$$

which may be rewritten in the form

$$F(u) = -\frac{M_{22}}{2M} (u - u_m)^2 + F(u_m) \tag{8.8}$$

where u_m is the abscissa of the maximum:

$$u_m = -\frac{M_{12}}{M_{22}} b \tag{8.9}$$

(The determinant and the i,i cofactors of a covariance matrix are positive, and this is why we have concluded that the function $F(u)$ has a maximum.) From Eqns (8.6) and (8.8) we get

$$p[\eta(t_o + T) = u | \eta(t_o) = b] = \sqrt{\frac{m_0}{2\pi M}} \exp[F(u_m)] \exp\left[-\frac{M_{22}}{2M} (u - u_m)^2 \right] \tag{8.10}$$

Now let us obtain the cofactors M_{ij} and the determinant M. The random variables here are $\eta(t_o)$ and $\eta(t_o + T)$ and hence the covariance matrix is

$$CM = \begin{pmatrix} m_0 & \psi(T) \\ \psi(T) & m_0 \end{pmatrix} \tag{8.11}$$

so that

$$M_{11} = m_0, \quad M_{22} = m_0, \quad M_{12} = -\psi(T), \quad M = m_0^2 - \psi^2(T) \tag{8.12}$$

Here, it can be proven that $F(u_m) = 0$. However, this proof is not strictly necessary for our goal, so that we limit ourselves to note that the random variable $\eta(t_o + T)$, given condition (8.1), has the following:

$$\text{CONDITIONAL AVERAGE} = u_m \tag{8.13}$$

$$\text{CONDITIONAL STANDARD DEVIATION} = \sqrt{\frac{M}{M_{22}}} \tag{8.14}$$

which implies

$$\text{CONDITIONAL AVERAGE} = \frac{\psi(T)}{\psi(0)} b \tag{8.15}$$

$$\text{CONDITIONAL STANDARD DEVIATION} < \sigma \tag{8.16}$$

The conditional average is a deterministic function of T; that is,

$$\overline{\eta}(t_o + T) = \frac{\psi(T)}{\psi(0)} b \tag{8.17}$$

Since the standard deviation of the random surface elevation with respect to this deterministic function is smaller than σ, the random function $\eta(t_o + T)$ is asymptotically equal to the deterministic function $\overline{\eta}(t_o + T)$, if b/σ tends to infinity. Finally, given that $\overline{\eta}(t_o + T)$ has its absolute maximum at t_o, and this maximum is b, we conclude that condition (8.1) is sufficient for the occurrence of a wave crest of given height b, if $b/\sigma \to \infty$.

8.2 A SUFFICIENT CONDITION FOR THE OCCURRENCE OF A WAVE OF GIVEN VERY LARGE HEIGHT

The condition

$$\eta(t_o) = \frac{H}{2}, \quad \eta(t_o + T^*) = -\frac{H}{2} \tag{8.18}$$

where t_o is a given time instant and H is a given positive value, in the limit as $H/\sigma \to \infty$ is sufficient and necessary in probability for the occurrence of a wave of given height H. Actually, this is not exactly the sufficient and necessary condition in probability. As to being sufficient: given condition (8.18)

(with $H/\sigma \to \infty$) the probability approaches 1 to have the occurrence of a wave height H plus a very small random difference of order $(H/\sigma)^{-1}\sigma$. As to being necessary: given a very large wave height H, the probability approaches 1 that the following occur:

$$\eta(t_o) = \left(\frac{1}{2} + \delta\xi\right)H, \quad \eta(t_o + T^*) = \left(-\frac{1}{2} + \delta\xi\right)H \tag{8.19}$$

with $\delta\xi$ being a very small random difference of order $(H/\sigma)^{-1}$. However, these very small random differences are negligible for the conclusions of this chapter. (They become nonnegligible in the problem of the probability of wave heights leading to Eqn (4.44). Sections 9.7−9.10 of a previous book by the author (2000) may serve to deepen this item.)

In order to prove that condition (8.18) is sufficient, let us consider the conditional probability of the surface elevation at any fixed time instant $t_o + T$ given condition (8.18). We have

$$\begin{aligned} &p\left[\eta(t_o + T) = u \middle| \eta(t_o) = \frac{H}{2}, \eta(t_o + T^*) = -\frac{H}{2}\right] \\ &= \frac{p\left[\eta(t_o) = \frac{H}{2}, \eta(t_o + T^*) = -\frac{H}{2}, \eta(t_o + T) = u\right]}{p\left[\eta(t_o) = \frac{H}{2}, \eta(t_o + T^*) = -\frac{H}{2}\right]} \end{aligned} \tag{8.20}$$

From Section 4.2 we know that

$$\begin{aligned} &p\left[\eta(t_o) = \frac{1}{2}H, \eta(t_o + T^*) = -\frac{1}{2}H, \eta(t_o + T) = u\right] \\ &= \frac{1}{(2\pi)^{3/2}\sqrt{M}} \exp\left\{-\frac{1}{2M}\left[M_{33}u^2 + 2(M_{13} - M_{23})\frac{1}{2}Hu \right.\right. \\ &\qquad \left.\left. + (M_{11} + M_{22} - 2M_{12})\frac{1}{4}H^2\right]\right\}, \end{aligned} \tag{8.21}$$

$$\begin{aligned} &p\left[\eta(t_o) = \frac{1}{2}H, \eta(t_o + T^*) = -\frac{1}{2}H\right] \\ &= \frac{1}{2\pi\sqrt{\tilde{M}}} \exp\left[-\frac{1}{2\tilde{M}}\left(\tilde{M}_{11} + \tilde{M}_{22} - 2\tilde{M}_{12}\right)\frac{1}{4}H^2\right], \end{aligned} \tag{8.22}$$

where M_{ij} and M are the i,j cofactor and the determinant of the covariance matrix of $\eta(t_o)$, $\eta(t_o + T^*)$, $\eta(t_o + T)$; that is,

$$CM = \begin{pmatrix} \psi(0) & \psi(T^*) & \psi(T) \\ \psi(T^*) & \psi(0) & \psi(T - T^*) \\ \psi(T) & \psi(T - T^*) & \psi(0) \end{pmatrix}, \tag{8.23}$$

and $\tilde{M}_{ij}$ and $\tilde{M}$ are the i,j cofactor and the determinant of the covariance matrix of $\eta(t_o)$, $\eta(t_o + T^*)$. (Note that $\tilde{M}$ is equal to M_{33}.) Hence, it follows that

$$p\left[\eta(t_o+T) = u \middle| \eta(t_o) = \frac{H}{2}, \eta(t_o+T^*) = -\frac{H}{2}\right] = \sqrt{\frac{M_{33}}{2\pi M}}\exp[F(u)] \tag{8.24}$$

where $F(u)$ here denotes the function

$$F(u) = -\frac{1}{2M}\left[M_{33}u^2 + 2(M_{13}-M_{23})\frac{1}{2}Hu + (M_{11}+M_{22}-2M_{12})\frac{1}{4}H^2 - \frac{M}{M_{33}}\left(\tilde{M}_{11}+\tilde{M}_{22}-2\tilde{M}_{12}\right)\frac{H^2}{4}\right] \tag{8.25}$$

which may be rewritten in the form

$$F(u) = -\frac{M_{33}}{2M}(u-u_m)^2 + F(u_m) \tag{8.26}$$

where u_m is the abscissa of the maximum:

$$u_m = \frac{M_{23}-M_{13}}{M_{33}}\frac{H}{2} \tag{8.27}$$

From Eqns (8.24) and (8.26) we get

$$p\left[\eta(t_o+T) = u \middle| \eta(t_o) = \frac{H}{2}, \eta(t_o+T^*) = -\frac{H}{2}\right] = \sqrt{\frac{M_{33}}{2\pi M}}\exp[F(u_m)]\cdot\exp\left[-\frac{M_{33}}{2M}(u-u_m)^2\right] \tag{8.28}$$

Now let us obtain the cofactors M_{ij} and the determinant M of the covariance matrix Eqn (8.23). When dealing with large covariance matrices it is convenient to resort to some compact symbols for the entries of these matrices. In this case let us define

$$a = \psi(0), \quad b = \psi(T^*), \quad c = \psi(T), \quad d = \psi(T-T^*) \tag{8.29}$$

so that the covariance matrix and the relevant cofactors are reduced to

$$CM = \begin{pmatrix} a & b & c \\ b & a & d \\ c & d & a \end{pmatrix} \tag{8.30}$$

$$M_{11} = a^2 - d^2 \tag{8.31}$$
$$M_{12} = cd - ab \tag{8.32}$$
$$M_{13} = bd - ac \tag{8.33}$$
$$M_{23} = bc - ad \tag{8.34}$$

$$M_{33} = a^2 - b^2 \tag{8.35}$$

$$M = a\left(a^2 - d^2\right) + b(cd - ab) + c(bd - ac) \tag{8.36}$$

Here, it can be proven that $F(u_m) = 0$. However, this proof is not strictly necessary for our goal, so that we limit ourselves to note that the random variable $\eta(t_o + T)$, given condition (8.18), has

$$\text{CONDITIONAL AVERAGE} = u_m \tag{8.37}$$

$$\text{CONDITIONAL STANDARD DEVIATION} = \sqrt{\frac{M}{M_{33}}} \tag{8.38}$$

which implies

$$\text{CONDITIONAL AVERAGE} = \frac{c - d}{a - b}\ \frac{H}{2} \tag{8.39}$$

$$\text{CONDITIONAL STANDARD DEVIATION} < \sigma \tag{8.40}$$

Later we shall prove the inequality Eqn (8.40).

The conditional average is a deterministic function of T, that is,

$$\overline{\eta}(t_o + T) = \frac{\psi(T) - \psi(T - T^*)}{\psi(0) - \psi(T^*)}\ \frac{H}{2} \tag{8.41}$$

Since the standard deviation of the random surface elevation with respect to this deterministic function is smaller than σ, the random function $\eta(t_o + T)$ is asymptotically equal to the deterministic function $\overline{\eta}(t_o + T)$, if H/σ tends to infinity. Since

1. $\overline{\eta}(t_o + T)$ has its absolute maximum at t_o, and this maximum is $H/2$;
2. $\overline{\eta}(t_o + T)$ has its absolute minimum at $t_o + T^*$, and this minimum is $-H/2$.

we conclude that condition (8.18) is sufficient for the occurrence of a wave of given height H, if $H/\sigma \to \infty$. This is provided that the wave crest at t_o and the wave trough at $t_o + T^*$ in the deterministic wave $\overline{\eta}(t_o + T)$ are the crest and trough of the same wave. Whether or not this condition is satisfied depends on the shape of the spectrum. This condition is satisfied with characteristic spectra of wind seas like JONSWAP or Pierson and Moskowitz.

It remains to prove the inequality Eqn (8.40). We must prove that

$$\frac{a(a^2 - d^2) + b(cd - ab) + c(bd - ac)}{a^2 - b^2} < a \tag{8.42}$$

This may be rewritten in the form

$$a\left[1-\frac{c^2+d^2-2cd\left(\frac{b}{a}\right)}{a^2-b^2}\right]<a \tag{8.43}$$

that is proven if we succeed in proving that

$$c^2+d^2-2cd\left(\frac{b}{a}\right)>0 \tag{8.44}$$

Here we note that

$$-1<\frac{b}{a}<0 \tag{8.45}$$

(b/a being the ratio between the absolute minimum and the absolute maximum of the autocovariance); as to the product cd it may be either positive or negative (according to the value of T). If $cd>0$, the inequality is satisfied because the term $-2cd(b/a)$ is greater than zero. If $cd<0$ it follows that

$$c^2+d^2-2cd\left(\frac{b}{a}\right)>c^2+d^2+2cd=(c+d)^2>0 \tag{8.46}$$

which completes the proof.

8.3 A NECESSARY CONDITION FOR THE OCCURRENCE OF A WAVE OF GIVEN VERY LARGE HEIGHT

We shall prove that condition (8.18) is necessary in probability for the occurrence of a wave of given height H, as $H/\sigma\rightarrow\infty$.

8.3.1 General Necessary Condition

A general necessary condition for the occurrence of a wave of given height H is that the surface elevation is ξH, with ξ in (0,1), at a time instant t_o, and is $(\xi-1)H$ at a later time instant t_o+T (t_o being the instant of the wave crest and t_o+T the instant of the wave trough). The mathematical form of this general necessary condition is

$$\eta(t_o)=\xi H,\quad \eta(t_o+T)=(\xi-1)H\quad \text{with } 0<\xi<1 \tag{8.47}$$

For focusing the general necessary condition, look at Fig. 4.4(a) (see Chapter 4), which shows two waves with a fixed height H and different values of ξ and $T(=\tau)$.

8.3.2 The Probability $P(H,T,\xi)$

Let us consider the probability that the surface elevation at an instant t_o falls between

$$\xi H \quad \text{and} \quad \xi H + \mathrm{d}\eta_1$$

and, at a later time $t_o + T$, falls between

$$(\xi - 1)H \quad \text{and} \quad (\xi - 1)H + \mathrm{d}\eta_2$$

t_o, H, T, ξ being arbitrarily fixed, and $\mathrm{d}\eta_1$, $\mathrm{d}\eta_2$ being two fixed small intervals. The probability under examination is given by

$$\mathrm{P}(H,T,\xi) = \frac{1}{2\pi\sqrt{M}} \cdot \exp\left\{-\frac{1}{2M}\left[M_{11}\xi^2H^2 + M_{22}(\xi-1)^2H^2 + 2\,M_{12}\xi(\xi-1)H^2\right]\right\}\mathrm{d}\eta_1\mathrm{d}\eta_2 \tag{8.48}$$

Here M_{ij} and M are, respectively, the i,j cofactor and the determinant of the covariance matrix of $\eta(t_o)$ and $\eta(t_o + T)$:

$$CM = \begin{pmatrix} \psi(0) & \psi(T) \\ \psi(T) & \psi(0) \end{pmatrix} \tag{8.49}$$

It is convenient to resort to the compact symbols

$$a = \psi(0), \quad c = \psi(T) \tag{8.50}$$

with which matrix and cofactors get the form

$$CM = \begin{pmatrix} a & c \\ c & a \end{pmatrix} \tag{8.51}$$

$$M_{11} = a, \quad M_{22} = a, \quad M_{12} = -c, \quad M = a^2 - c^2 \tag{8.52}$$

Let us rewrite Eqn (8.48) in the compact form

$$P(H,T,\xi) = \frac{1}{2\pi\sqrt{a^2-c^2}} \exp\left[-0.5f(T,\xi)\left(\frac{H}{\sigma}\right)^2\right]\mathrm{d}\eta_1\mathrm{d}\eta_2 \tag{8.53}$$

where

$$f(T,\xi) = \frac{a\left[a\xi^2 + a(\xi-1)^2 - 2c\xi(\xi-1)\right]}{a^2-c^2} \tag{8.54}$$

Let us develop the terms in the square parentheses on the right-hand side (RHS). We have

$$[.] = (2a - 2c)\xi^2 - (2a - 2c)\xi + a \tag{8.55}$$

that may be rewritten in the form

$$[.] = 2(a-c)(\xi-0.5)^2 + 0.5(a+c) \tag{8.56}$$

that together with Eqn (8.54) yields

$$f(T,\xi) = \frac{2a(a-c)(\xi-0.5)^2 + 0.5a(a+c)}{(a+c)(a-c)} \tag{8.57}$$

This may be rewritten in the form

$$f(T,\xi) = \frac{2a}{a+c}(\xi-0.5)^2 + \frac{a}{2(a-c)} \tag{8.58}$$

With the definitions (Eqn (8.50)) of the compact symbols a and c we arrive at

$$f(T,\xi) = 2\frac{\psi(0)}{\psi(0)+\psi(T)}\left(\xi-\frac{1}{2}\right)^2 + \frac{1}{2}\,\frac{\psi(0)}{\psi(0)-\psi(T)} \tag{8.59}$$

8.3.3 Analysis of the Function $f(T,\xi)$

The second term on the RHS of Eqn (8.59), that is to say

$$\frac{1}{2}\,\frac{\psi(0)}{\psi(0)-\psi(T)}$$

is independent of ξ, and its absolute minimum on the domain $T>0$ occurs at $T = T^*$ (given that T^* is the abscissa of the absolute minimum of $\psi(T)$). The first term on the RHS of Eqn (8.59), that is to say

$$2\frac{\psi(0)}{\psi(0)+\psi(T)}\left(\xi-\frac{1}{2}\right)^2$$

is zero if $\xi = \frac{1}{2}$, and is greater than zero if $\xi \neq \frac{1}{2}$. Therefore, the absolute minimum of the function $f(T,\xi)$ for T in $(0,\infty)$ and ξ in $(-\infty,\infty)$ occurs at $T = T^*$ and $\xi = \frac{1}{2}$.

8.3.4 Condition (8.18) Is Necessary

The fact that the absolute minimum of $f(T,\xi)$ occurs at $T = T^*$, $\xi = \frac{1}{2}$ implies

$$\frac{\mathrm{P}(H,T,\xi)}{\mathrm{P}\left(H,T^*,\frac{1}{2}\right)} \to 0 \quad \text{as } H/\sigma \to \infty, \tag{8.60}$$

for every fixed pair T,ξ with $T \neq T^*$ and/or $\xi \neq \frac{1}{2}$. In other words: as $H/\sigma \to \infty$, the probability that the surface elevation is ξH at an instant t_o

and is $(\xi - 1)H$ at an instant $t_o + T$, for any fixed pair T, ξ with $T \neq T^*$ and/or $\xi \neq \frac{1}{2}$, is negligible with respect to the probability that the surface elevation is $\frac{1}{2}H$ at t_o and is $-\frac{1}{2}H$ at $t_o + T^*$. Hence, as $H/\sigma \to \infty$, condition (8.18) becomes necessary in probability for the occurrence of a wave of given height H.

8.4 THE FIRST DETERMINISTIC WAVE FUNCTION IN SPACE AND TIME

"Given a very large wave crest of height b at a time instant t_o at a point x_o, y_o" is equivalent to given:

$$\eta(x_o, y_o, t_o) = b \tag{8.61}$$

This is what proceeds from Section 8.1. Here let us consider the conditional probability of the surface elevation at any fixed point $x_o + X$, $y_o + Y$ at time instant $t_o + T$, given condition (8.61). We have

$$\begin{aligned} &p[\eta(x_o + X, y_o + Y, t_o + T) = u | \eta(x_o, y_o, t_o) = b] \\ &\quad = \frac{p[\eta(x_o, y_o, t_o) = b, \eta(x_o + X, y_o + Y, t_o + T) = u]}{p[\eta(x_o, y_o, t_o) = b]} \end{aligned} \tag{8.62}$$

What is most important is that we make no restriction about whether the wave field is or is not homogeneous in space. For example, the wave field may be on the open sea, or before a long breakwater, or in the lee of a vertical breakwater.

Given that both $\eta(x_o, y_o, t_o)$ and $\eta(x_o + X, y_o + Y, t_o + T)$ represent stationary Gaussian processes of time, the steps to be done are the same leading from Eqns (8.1) to (8.10), and the result is

$$\begin{aligned} &p[\eta(x_o + X, y_o + Y, t_o + T) = u | \eta(x_o, y_o, t_o) = b] \\ &\quad = \sqrt{\frac{M_{22}}{2\pi M}} \exp\left[-\left(\frac{M_{22}}{2M}\right)(u - u_m)^2 \right] \end{aligned} \tag{8.63}$$

where

$$u_m = -\frac{M_{12}}{M_{22}} b \tag{8.64}$$

Now let us obtain the cofactors M_{ij} and the determinant M. The random variables here are $\eta(x_o, y_o, t_o)$ and $\eta(x_o + X, y_o + Y, t_o + T)$ and hence the covariance matrix is

$$CM = \begin{pmatrix} \sigma^2(x_o, y_o) & \Psi(X, Y, T; x_o, y_o) \\ \Psi(X, Y, T; x_o, y_o) & \sigma^2(x_o + X, y_o + Y) \end{pmatrix} \tag{8.65}$$

We have

$$M_{11} = \sigma^2(x_o + X, y_o + Y) \tag{8.66}$$

$$M_{22} = \sigma^2(x_o, y_o) \tag{8.67}$$

$$M_{12} = -\Psi(X, Y, T; x_o, y_o) \tag{8.68}$$

$$M = \sigma^2(x_o, y_o)\sigma^2(x_o + X, y_o + Y) - \Psi^2(X, Y, T; x_o, y_o) \tag{8.69}$$

The random surface elevation $\eta(x_o + X, y_o + Y, t_o + T)$, given that $\eta(x_o, y_o, t_o) = b$, has

$$\text{CONDITIONAL AVERAGE} = u_m \tag{8.70}$$

$$\text{CONDITIONAL STANDARD DEVIATION} = \sqrt{\frac{M}{M_{22}}} \tag{8.71}$$

which implies

$$\text{CONDITIONAL AVERAGE} = \frac{\Psi(X, Y, T; x_o, y_o)}{\sigma^2(x_o, y_o)} b \tag{8.72}$$

$$\text{CONDITIONAL STANDARD DEVIATION} < \sigma(x_o + X, y_o + Y) \tag{8.73}$$

The conditional average is a deterministic wave function of X, Y, T that may be rewritten in the form

$$\overline{\eta}(x_o + X, y_o + Y, t_o + T) = \widehat{\Psi}(X, Y, T; x_o, y_o)\left[\frac{b}{\sigma(x_o, y_o)}\right]\sigma(x_o + X, y_o + Y) \tag{8.74}$$

where $\widehat{\Psi}$ is the cross-correlation whose range is $(-1,1)$ (cf. Section 7.3.3). From Eqn (8.73) we know that the standard deviation of the random surface elevation with respect to this deterministic function is smaller than $\sigma(x_o + X, y_o + Y)$. Conclusion: the random surface elevation $\eta(x_o + X, y_o + Y, t_o + T)$ is asymptotically equal to the deterministic wave function $\overline{\eta}(x_o + X, y_o + Y, t_o + T)$, as $b/\sigma(x_o, y_o)$ tends to infinity.

It must be pointed out that there is no restriction on the ratio $\sigma(x_o + X, y_o + Y)/\sigma(x_o, y_o)$. In particular, x_o, y_o may be a point in the lee of a breakwater and $x_o + X, y_o + Y$ may be a point on the wave-beaten wall of the breakwater, so that the ratio $\sigma(x_o + X, y_o + Y)/\sigma(x_o, y_o)$ is very large. Nevertheless, if we know that at point x_o, y_o a wave crest occurs with a height b that is exceptionally large with respect to the root mean square surface elevation at this point, we may expect that the surface elevation at $x_o + X, y_o + Y$ will be close to a well-defined deterministic wave function given by Eqn (8.74). Hence, even if the wave crest recorded in the lee is much smaller than the waves at the outer wall, the fact of having found a wave crest that is exceptionally

large with respect to the average in the lee will enable us to predict how the waves are even at the outer wall.

8.5 THE VELOCITY POTENTIAL ASSOCIATED WITH THE FIRST DETERMINISTIC WAVE FUNCTION IN SPACE AND TIME

The form (Eqn (8.74)) of the deterministic wave function is effective for understanding the sense of the QD theory; however, for calculation, the form

$$\overline{\eta}(x_o + X, y_o + Y, t_o + T) = \frac{\Psi(X, Y, T; x_o, y_o)}{\sigma^2(x_o, y_o)} b \tag{8.75}$$

is more straightforward. Associated with this deterministic wave function is a distribution of velocity potential in the water, which to the lowest order in a Stokes expansion is given by

$$\overline{\phi}(x_o + X, y_o + Y, z, t_o + T) = \frac{\Phi(X, Y, T, z; x_o, y_o)}{\sigma^2(x_o, y_o)} b \tag{8.76}$$

The surface elevation (Eqn (8.75)) and the velocity potential (Eqn (8.76)) satisfy the linear flow equations. In particular, we shall prove that $\overline{\eta}$ and $\overline{\phi}$ satisfy the first linear flow equation under the hypothesis that η and ϕ satisfy this equation. That is to say, we shall prove that

$$\overline{\eta} = -\frac{1}{g}\left(\frac{\partial \overline{\phi}}{\partial T}\right)_{z=0} \tag{8.77}$$

provided that

$$\eta = -\frac{1}{g}\left(\frac{\partial \phi}{\partial t}\right)_{z=0} \tag{8.78}$$

With the formulas (8.75) and (8.76) of $\overline{\eta}$ and $\overline{\phi}$, the equality (8.77) (to be proved) takes on the form

$$\frac{\Psi(X, Y, T; x_o, y_o)}{\sigma^2(x_o, y_o)} b = -\frac{1}{g}\left[\frac{\partial}{\partial T}\Phi(X, Y, T, z; x_o, y_o)\frac{b}{\sigma^2(x_o, y_o)}\right]_{z=0} \tag{8.79}$$

where the term $b/\sigma^2(x_o, y_o)$ cancels. With the definitions (7.1) and (7.9) of Ψ and Φ, the equality to be proved becomes

$$\begin{aligned} &\langle \eta(x_o, y_o, t_o)\eta(x_o + X, y_o + Y, t + T)\rangle \\ &= -\frac{1}{g}\left[\frac{\partial}{\partial T}\langle \eta(x_o, y_o, t)\phi(x_o + X, y_o + Y, z, t + T)\rangle\right]_{z=0} \end{aligned} \tag{8.80}$$

wherein the order "derivative with respect to T," "average with respect to t" may be inverted, with the result that the equality to be proved becomes

$$\langle \eta(x_o, y_o, t_o)\eta(x_o + X, y_o + Y, t + T)\rangle = \left[\left\langle \eta(x_o, y_o, t)\left(-\frac{1}{g}\right)\frac{\partial}{\partial T}\phi(x_o + X, y_o + Y, z, t + T)\right\rangle\right]_{z=0}$$

and this equality is proved since

$$\eta(x_o + X, y_o + Y, t + T) = \left(-\frac{1}{g}\right)\frac{\partial}{\partial T}\phi(x_o + X, y_o + Y, z, t + T)_{z=0} \quad (8.81)$$

as a consequence of Eqn (8.78). Equation (8.81) says that random surface elevation η and the relevant velocity potential ϕ satisfy the linear flow Eqn (8.78) at point $x_o + X$, $y_o + Y$, at time instant $t + T$.

8.6 THE SECOND DETERMINISTIC WAVE FUNCTION IN SPACE AND TIME

"Given a very large wave of height H at a time instant t_o at a point x_o, y_o" is equivalent to

$$\eta(x_o, y_o, t_o) = \frac{H}{2}, \quad \eta(x_o, y_o, t_o + T^*) = -\frac{H}{2} \quad (8.82)$$

This is what proceeds from Sections 8.2 and 8.3.

Given condition (8.82) as $H/\sigma(x_o, y_o) \to \infty$, the random surface elevation $\eta(x_o + X,\ y_o + Y,\ t_o + T)$ is asymptotically equal to the deterministic function

$$\overline{\eta}(x_o + X, y_o + Y, t_o + T) = \frac{\Psi(X, Y, T; x_o, y_o) - \Psi(X, Y, T - T^*; x_o, y_o)}{\Psi(0, 0, 0; x_o, y_o) - \Psi(0, 0, T^*; x_o, y_o)}\frac{H}{2} \quad (8.83)$$

and the velocity potential associated with this deterministic wave function is

$$\overline{\phi}(x_o + X, y_o + Y, z, t_o + T) = \frac{\Phi(X, Y, z, T; x_o, y_o) - \Phi(X, Y, z, T - T^*; x_o, y_o)}{\Psi(0, 0, 0; x_o, y_o) - \Psi(0, 0, T^*; x_o, y_o)}\frac{H}{2} \quad (8.84)$$

The deterministic wave function (Eqn (8.83)) is obtained starting from condition (8.82) and reasoning as in Section 8.4. Then with the same reasoning done in Section 8.5, one can verify that deterministic wave function (Eqn (8.83)) and velocity potential (Eqn (8.84)) satisfy the linear flow equations.

8.7 COMMENT: A DETERMINISTIC MECHANICS IS BORN BY THE THEORY OF PROBABILITY

Given a wave with a known height H, if H/σ is very large, the conditional standard deviation of the random surface elevation is negligible with respect to the conditional average surface elevation. This conditional average represents a deterministic wave function of space and time. Hence, the actual (random) waves will be very close to this deterministic wave function. Associated with this deterministic wave function is a very precise distribution of velocity potential in the water.

The conclusion is that a deterministic mechanics consisting of the deterministic wave function (Eqn (8.83)) and the relevant velocity potential (Eqn (8.84)) is born by the theory of probability.

What the author finds exciting is that Eqns (8.83) and (8.84) hold for an arbitrary configuration of the solid boundary (of course, provided that the flow is frictionless). Only the relationship between functions Ψ and Φ and the directional spectrum $S(\omega,\theta)$ of the incident waves changes with the solid boundary (several examples of this relationship are given in Chapter 7).

The sense of the QD theory is the following: if a wave with an exceptionally large height H occurs at some point x_o, y_o at a time instant t_o, it is most probable that the occurrence of this wave happens in a very precise (deterministic) way.

Note that the assumption that given wave height H is very large with respect to σ of the sea state may be consistent with the Stokes assumption that the wave height is small with respect to the bottom depth and the wavelength. Of course, what has been said in this section regarding the wave of given height H conceptually holds also for the wave crest of given height b.

8.8 CONCLUSION

In the spring of 1980 the author realized that a wave with a given very large crest height in a Gaussian sea state is close to the autocovariance (Eqn (8.17)) and published this result in papers (1982, 1983). After this result the author wondered whether determinism can be born within a chaotic process. In fact, the result suggested two opposite conclusions. Let us review these conclusions in simple words; to do this we shall resort to the evidence of numbers. (The reader should bear in mind that we are dealing with a Gaussian random process of unlimited duration and unlimited wave height). Let us assume that the ψ^* of this stationary random Gaussian process is equal to 0.60. In this process, a wave with a crest height of $b = 100\sigma$ will

have a height H = 1.6 $100\sigma = 160\sigma$. Because of the statistical symmetry of the Gaussian process, a wave with an elevation of the trough of -100σ will have a profile opposite to that of the wave of crest height 100σ. Hence a consequence of Eqn (8.17) with our example is that

1. a wave of given crest height 100σ has a deterministic height of 160σ;
2. a wave of given height 160σ does not have a deterministic crest height: indeed, there is the same probability that this wave has a crest of 100σ or a trough of -100σ (which implies a crest of 60σ).

Item (1) suggests a positive conclusion: yes, determinism can be born within a chaotic process. Item (2) suggests the opposite conclusion. The author was able to solve this contradiction with the proof shown in Sections 8.2 and 8.3 of the present chapter: a wave of given very large height H is close to the deterministic wave function (8.41); what this implies, in our example, is that a wave of given height 160σ has a deterministic crest height of 80σ. This does not contradict what proceeds from Eqn (8.17), since the number of wave crests of 100σ is very small with respect to the number of wave heights of 160σ. In other words, the set of waves having the given height of 160σ consists of waves all with the crest height of 80σ, except for a very small fraction of anomalous elements of the set. This very small fraction includes the whole set of waves with the given crest height of 100σ. Hence, the general conclusion is: yes, determinism can be born within a chaotic process. This was called "quasi-determinism" because of the presence of the very small fractions of anomalous elements. The first time the term quasi-determinism appeared was in a paper by the author (1984), where Eqn (8.41) was also disclosed.

Some time later the author made substantial progress when Eqn (8.83) was applied to the space-time; this was in 1986, and the publication was in the paper (1989). Here, the author showed that a very large wave of given height H occurs at some fixed point x_o, y_o because this point is struck home by a well-defined wave group. This group has a deterministic (new) mechanics that we shall analyze in detail in the next chapter. Finally, in June 1987 the author applied Eqn (8.83) to Gaussian wave fields being nonhomogeneous in space (publication in the papers (1988) and (1997b)). It was an exciting experience! We shall see a few examples in Chapter 11. In particular, we shall see that a very large wave of given height occurs at a fixed point x_o, y_o far from a long breakwater, because of a collision of two wave groups. The logic is that of quasi-determinism: if a wave with a given very large height will occur at some fixed point, we can predict, with a probability approaching 1, the story of this occurrence. This result implies that "a deterministic mechanics can be born within a chaotic process," which is an

aspect of the possibility that determinism can be born within a chaotic process.

In the 1980s the author knew Rice's work (1944, 1945, 1958) on the analysis of stationary random Gaussian processes, and the author did not know some subsequent works on the same subject. In particular, Lindgren (1972) had shown that the behavior of $\eta_b(t)$ is well determined by the behavior of $\psi(t)$ as $b \to \infty$, where η_b is the random Gaussian function, given that at $t = 0$ there is a local maximum of ordinate b. This is essentially the same as Eqn (8.17). However, the approach was different from the author's: in his paper Lindgren focused on mathematical random functions, whereas in the papers (1982, 1983) the author focused on waves. If the author had not reobtained independently Eqn (8.17) through the approach focused on waves, the author would not have arrived at the QD theory. Professor Leon Borgman played an important role with an open-minded review of the author's early work (acknowledged in the paper (1983)).

The more difficult part of the basic proof of the QD theory is that concerning the necessary condition. The original forms the author gave in the 1980s were rather complicated, and only some years later (1997a) the author reached the simple form that is given in Section 8.3 of this chapter.

REFERENCES

Boccotti, P., 1982. On ocean waves with high crests. Meccanica 17, 16–19.
Boccotti, P., 1983. Some new results on statistical properties of wind waves. Appl. Ocean Res. 5 (3), 134–140.
Boccotti, P., 1984. Sea waves and quasi-determinism of rare events in random processes. Atti Accad. Naz. Lincei Rend. 76, 119–127.
Boccotti, P., 1988. Refraction, reflection and diffraction of irregular gravity waves. Excerpta Ital. Contrib. Field Hydraul. Eng. 3, 47–89.
Boccotti, P., 1989. On mechanics of irregular gravity waves. Atti Accad. Naz. Lincei Mem. VIII 19, 111–170.
Boccotti, P., 1997a. A general theory of three-dimensional wave groups. Part I: the formal derivation. Ocean Eng. 24 (3), 265–280.
Boccotti, P., 1997b. A general theory of three-dimensional wave groups. Part I: interaction with a breakwater. Ocean Eng. 24 (3), 281–300.
Boccotti, P., 2000. Wave Mechanics for Ocean Engineering. Elsevier, Amsterdam, 495 pp.
Lindgren, G., 1972. Local maxima of Gaussian fields. Archiv for Matematik 10, 195–218.
Rice, S.O., 1944. Mathematical analysis of random noise. Bell Syst. Tech. J. 23, 282–332.
Rice, S.O., 1945. Mathematical analysis of random noise. Bell Syst. Tech. J. 24, 46–156.
Rice, S.O., 1958. Distribution of the duration of fades in radio transmission. Bell Syst. Tech. J. 37, 581–635.

Chapter 9

Quasi-Determinism Theory: Mechanics of Wave Groups

CHAPTER OUTLINE

9.1 WHAT DOES THE DETERMINISTIC WAVE FUNCTION REPRESENT?

9.1.1 A Three-Dimensional Wave Group

With Eqn (7.8) of Ψ, Eqn (8.75) of the first deterministic wave function, and Eqn (8.83) of the second deterministic wave function become, respectively

$$\overline{\eta}(x_o + X, y_o + Y, t_o + T) = b \int_0^{\infty} \int_0^{2\pi} S(\omega, \theta) \times \cos(kX \sin\theta + kY \cos\theta - \omega T) \times \mathrm{d}\theta \mathrm{d}\omega \Big/ \int_0^{\infty} \int_0^{2\pi} S(\omega, \theta) \mathrm{d}\theta \mathrm{d}\omega \tag{9.1}$$

Wave Mechanics and Wave Loads on Marine Structures. http://dx.doi.org/10.1016/B978-0-12-800343-5.00009-3

$$\begin{aligned}\overline{\eta}(x_o + X, y_o + Y, t_o + T) = \frac{H}{2}\int_0^{\infty}\int_0^{2\pi} S(\omega,\theta)\{&\cos\,(kX\sin\theta + kY\cos\theta - \omega T)\\ &-\cos\,[kX\sin\theta + kY\cos\theta\\ &-\omega(T - T^*)]\,\}\mathrm{d}\theta\mathrm{d}\omega \Big/ \int_0^{\infty}\int_0^{2\pi} S(\omega,\theta)[1\\ &-\cos(\omega T^*)]\mathrm{d}\theta\mathrm{d}\omega\end{aligned} \tag{9.2}$$

Figure 9.1 shows some pictures of the deterministic wave function (9.2). Point x_o,y_o of the wave of given exceptionally large height H is at the center of the framed area. The input data are: deep water; spectrum: mean JONSWAP; directional distribution: Mitsuyasu et al. with $n_p = 20$; dominant direction

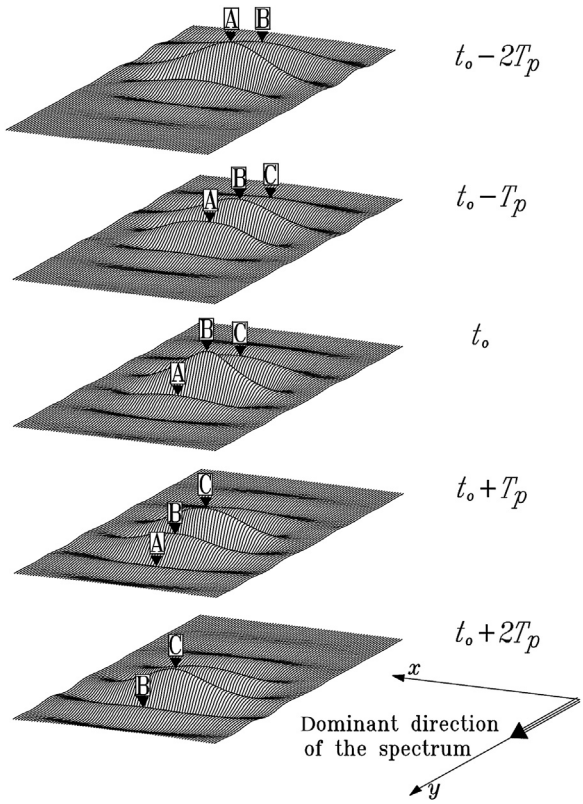

■ **FIGURE 9.1** In the open sea, deterministic wave function (8.83) represents a wave group that strikes home point x_o,y_o, at the apex of its development stage.

parallel to the y-axis. We see a three-dimensional wave group transiting x_o,y_o. Thus, the theory implicitly reveals the existence of a well-defined physical unit, that is, the three-dimensional wave group. The theory also reveals two basic features of this group. First, the individual waves have a propagation speed greater than the group velocity, so that each of them runs along the envelope from the tail where it is born to the head where it dies (follow wave B during its evolution). Second, the wave group has a development stage that is followed by a decay stage; in the development stage the three-dimensional envelope shrinks, so that the height of the central wave grows to a maximum.

As we may see, the answer of the theory is simple and clear. In words it says: "if you record an exceptionally large wave at a point at sea, you can expect that most probably it is the center of a well-defined group at the apex of its development."

The wave groups are similar to the human families. Let us think of the house of Medici of Florence. Throughout the fourteenth and fifteenth century this family had a development stage up to a maximum at the age of Lorenzo the Magnificent. Then during the two following centuries the family had a progressive decay. In the four centuries from 1300 AD to 1700 AD a lot of individuals of this family were born, grew up, and died. The same is true of the waves: the group is like the family, and the individual waves are like the members of the family. The wave group at the apex of the development stage is like the house of Medici at the age of Lorenzo the Magnificent, and the wave at the center of the group at the apex of its development is like Lorenzo the Magnificent in the years of his full maturity.

The propagation speed of the wave group is nearly equal to the group velocity c_G (cf. Section 1.10) associated with the period T_p, and the propagation speed of each individual wave is nearly equal to the phase speed c associated with T_p. Therefore, on deep water, the propagation speed of each individual wave is nearly twice the propagation speed of the wave group. The fact that each individual wave moves along the envelope leads to a few amazing transformations: the wave that goes to occupy the central position of the group at the apex of the development stage nearly doubles its height in a run of only one wavelength! Moreover, as an individual wave approaches the central position of the group, its wave period and wavelength reduce itself. As it leaves the central position, a compensating stretch occurs.

In Fig. 9.1 we see first the replacement of wave A by wave B at the envelope center, and then the replacement of wave B by wave C. At sea the replacement at the envelope center sometimes becomes well evident. This occurs if

a large wave like A in the first image of Fig. 9.1 is spilling near the crest. Then this wave leaves the central position (second image), it gets smaller, and it sheds its whitecap. Then the next wave (B) takes the central position, and it starts spilling near the crest. Then, wave B leaves the central position, which is occupied by the next wave (C), and this wave in its turn starts spilling near the crest. In these cases the whitecap is like a crown passing from one wave to the next one.

9.1.2 The Core of the Quasi-Determinism Theory

We shall call G1 the deterministic wave group given by Eqn (9.1), and G2 the deterministic wave group given by Eqn (9.2). The sequence of pictures of G1 looks essentially like the sequence of pictures of G2.

However, there are some differences. Figure 9.2 shows these two wave groups in the time domain at point x_o,y_o (they represent the records that would be done by an ideal gauge at point x_o,y_o at the center of the framed area). The reason for this difference is the following:

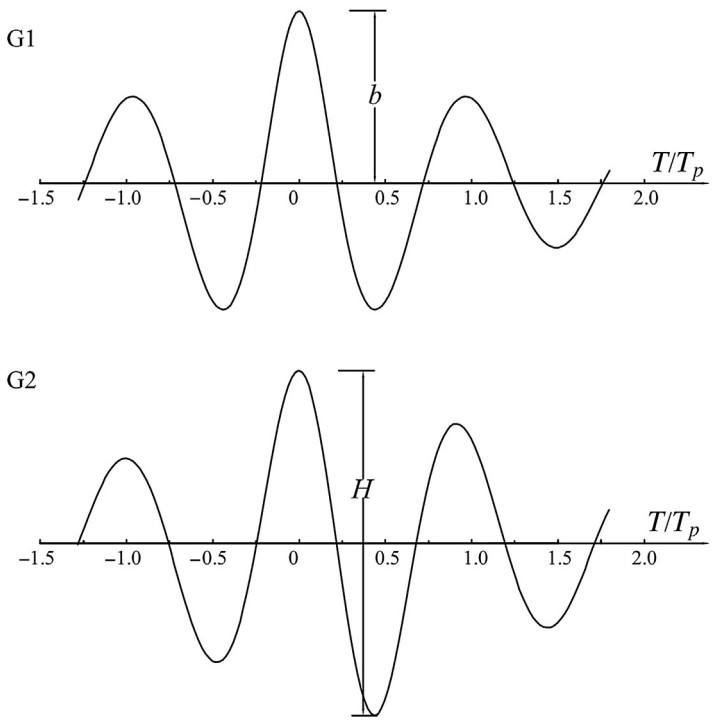

■ **FIGURE 9.2** Wave group G1 and wave group G2 at point x_o,y_o, in the time domain.

A wave group yields its maximum crest elevation at a point 1 and its maximum wave height at a point 2 somewhat after point 1. At point 1 the envelope center coincides with the wave crest. Then the wave crest is reduced because it leaves the envelope center, and the following trough grows because it approaches the envelope center. At point 2 the envelope center coincides with the zero between the crest and the trough. The quasi-determinism (QD) theory says "if you record a wave crest at a fixed point x_o,y_o, with a given exceptionally large height b, you may expect that most probably your point x_o,y_o is point 1"; and "if you record a wave at a fixed point x_o,y_o, with a given exceptionally large height H, you may expect that most probably your point x_o,y_o is point 2."

Is this the only difference between G2 and G1? It is not exactly so. We have seen that a wave group has a development stage in which the three-dimensional envelope shrinks, and a decay stage in which the three-dimensional envelope stretches. Well, wave group G1 gets the apex of its development stage at the very instant wherein the envelope center transits at point 1 (which gives a further small contribution to yield the exceptional crest elevation at point 1); whereas G2 gets the apex of its development stage at the instant wherein the envelope centre transits at point 2 (which gives a further small contribution to yield the exceptional wave height at point 2).

Thus the full response of the theory is, first: "if you record a wave crest at a fixed point x_o,y_o, with a given exceptionally large height b, you may expect that most probably your point x_o,y_o is point 1, and that the wave group has got the apex of its development at the very instant wherein the envelope center transits at point 1"; second: "if you record a wave at a fixed point x_o,y_o, with a given exceptionally large height H, you may expect that most probably your point x_o,y_o is point 2, and that the wave group has got the apex of its development at the very instant wherein the envelope center transits at point 2." Now we can appreciate the overall consistency between Eqns (8.17) and (8.41): the first represents wave group G1 in the time domain at point x_o,y_o; the second represents wave group G2 in the time domain at point x_o,y_o.

9.2 PARTICLE VELOCITY AND ACCELERATION IN WAVE GROUPS

The deterministic velocity potential associated to wave groups (8.75) and (8.83) is given, respectively, by Eqns (8.76) and (8.84). With Eqn (7.30) of the cross-covariance, $\overline{\phi}$ becomes, respectively

$$\overline{\phi}(x_o + X, y_o + Y, z, t_o + T) = gb \int_0^{\infty} \int_0^{2\pi} S(\omega, \theta)\omega^{-1} \frac{\cosh[k(d+z)]}{\cosh(kd)} \times \sin(kX \sin\theta + kY \cos\theta - \omega T) \times \mathrm{d}\theta \mathrm{d}\omega \Big/ \int_0^{\infty} \int_0^{2\pi} S(\omega, \theta) \mathrm{d}\theta \mathrm{d}\omega \tag{9.3}$$

$$\overline{\phi}(x_o + X, y_o + Y, z, t_o + T) = g\frac{H}{2} \int_0^{\infty} \int_0^{2\pi} S(\omega, \theta)\omega^{-1} \frac{\cosh[k(d+z)]}{\cosh(kd)} \times \{\sin(kX \sin\theta + kY \cos\theta - \omega T) - \sin[kX \sin\theta + kY \cos\theta - \omega(T - T^*)]\} \times \mathrm{d}\theta \mathrm{d}\omega \Big/ \int_0^{\infty} \int_0^{2\pi} S(\omega, \theta)[1 - \cos(\omega T^*)] \mathrm{d}\theta \mathrm{d}\omega \tag{9.4}$$

Particle velocity and acceleration in the wave groups proceed on differentiating these functions $\overline{\phi}$. We have:

Wave Group G1

$$\overline{v_x}(x_o + X, y_o + Y, z, t_o + T) = gb \int_0^{\infty} \int_0^{2\pi} S(\omega, \theta)k \sin\theta\omega^{-1} \frac{\cosh[k(d+z)]}{\cosh(kd)} \cdot \cos(kX \sin\theta + kY \cos\theta - \omega T) \times \mathrm{d}\theta \mathrm{d}\omega \Big/ \int_0^{\infty} \int_0^{2\pi} S(\omega, \theta) \mathrm{d}\theta \mathrm{d}\omega \tag{9.5}$$

$$\overline{v_y}(x_o + X, y_o + Y, z, t_o + T) = gb \int_0^{\infty} \int_0^{2\pi} S(\omega, \theta)k \cos\theta\omega^{-1} \frac{\cosh[k(d+z)]}{\cosh(kd)} \cdot \cos(kX \sin\theta + kY \cos\theta - \omega T) \times \mathrm{d}\theta \mathrm{d}\omega \Big/ \int_0^{\infty} \int_0^{2\pi} S(\omega, \theta) \mathrm{d}\theta \mathrm{d}\omega \tag{9.6}$$

$$\overline{v_z}(x_o+X,y_o+Y,z,t_o+T) = gb\int_0^{\infty}\int_0^{2\pi} S(\omega,\theta)k\omega^{-1}\frac{\sinh\,[k(d+z)]}{\cosh\,(kd)} \cdot\sin\,(kX\sin\theta+kY\cos\theta-\omega T) \times \mathrm{d}\theta\mathrm{d}\omega \Big/ \int_0^{\infty}\int_0^{2\pi} S(\omega,\theta)\mathrm{d}\theta\mathrm{d}\omega \tag{9.7}$$

$$\overline{a_x}(x_o+X,y_o+Y,z,t_o+T) = gb\int_0^{\infty}\int_0^{2\pi} S(\omega,\theta)k\sin\theta\frac{\cosh\,[k(d+z)]}{\cosh\,(kd)} \cdot\sin\,(kX\sin\theta+kY\cos\theta-\omega T) \times \mathrm{d}\theta\mathrm{d}\omega \Big/ \int_0^{\infty}\int_0^{2\pi} S(\omega,\theta)\mathrm{d}\theta\mathrm{d}\omega \tag{9.8}$$

$$\overline{a_y}(x_o+X,y_o+Y,z,t_o+T) = gb\int_0^{\infty}\int_0^{2\pi} S(\omega,\theta)k\cos\theta\,\frac{\cosh\,[k(d+z)]}{\cosh\,(kd)} \cdot\sin\,(kX\sin\theta+kY\cos\theta-\omega T) \times \mathrm{d}\theta\mathrm{d}\omega \Big/ \int_0^{\infty}\int_0^{2\pi} S(\omega,\theta)\mathrm{d}\theta\mathrm{d}\omega \tag{9.9}$$

$$\overline{a_z}(x_o+X,y_o+Y,z,t_o+T) = -gb\int_0^{\infty}\int_0^{2\pi} S(\omega,\theta)k\,\frac{\sinh\,[k(d+z)]}{\cosh\,(kd)} \cdot\cos\,(kX\sin\theta+kY\cos\theta-\omega T) \times \mathrm{d}\theta\mathrm{d}\omega \Big/ \int_0^{\infty}\int_0^{2\pi} S(\omega,\theta)\mathrm{d}\theta\mathrm{d}\omega \tag{9.10}$$

Wave Group G2

$$\overline{v_x}(x_o+X,y_o+Y,z,t_o+T) = g\frac{H}{2}\int_0^{\infty}\int_0^{2\pi} S(\omega,\theta)k\sin\theta\,\omega^{-1}\frac{\cosh\,[k(d+z)]}{\cosh\,(kd)} \cdot\Big\{\cos\,(kX\sin\theta+kY\cos\theta-\omega T) - \cos\,[kX\sin\theta+kY\cos\theta-\omega(T-T^*)]\Big\} \times \mathrm{d}\theta\mathrm{d}\omega \Big/ \int_0^{\infty}\int_0^{2\pi} S(\omega,\theta)[1-\cos\,(\omega T^*)]\mathrm{d}\theta\mathrm{d}\omega \tag{9.11}$$

$$\overline{v_y}(x_o+X,y_o+Y,z,t_o+T) = g\frac{H}{2}\int_0^{\infty}\int_0^{2\pi} S(\omega,\theta)k\cos\theta\omega^{-1}\frac{\cosh\left[k(d+z)\right]}{\cosh\left(kd\right)} \cdot\left\{\cos\left(kX\sin\theta+kY\cos\theta-\omega T\right) - \cos\left[kX\sin\theta+kY\cos\theta-\omega(T-T^*)\right]\right\} \times \mathrm{d}\theta\mathrm{d}\omega \Big/ \int_0^{\infty}\int_0^{2\pi} S(\omega,\theta)[1-\cos\left(\omega T^*\right)]\mathrm{d}\theta\mathrm{d}\omega \tag{9.12}$$

$$\overline{v_z}(x_o+X,y_o+Y,z,t_o+T) = g\frac{H}{2}\int_0^{\infty}\int_0^{2\pi} S(\omega,\theta)k\omega^{-1}\frac{\sinh\left[k(d+z)\right]}{\cosh\left(kd\right)} \cdot\left\{\sin\left(kX\sin\theta+kY\cos\theta-\omega T\right) - \sin\left[kX\sin\theta+kY\cos\theta-\omega(T-T^*)\right]\right\} \times \mathrm{d}\theta\mathrm{d}\omega \Big/ \int_0^{\infty}\int_0^{2\pi} S(\omega,\theta)[1-\cos\left(\omega T^*\right)]\mathrm{d}\theta\mathrm{d}\omega \tag{9.13}$$

$$\overline{a_x}(x_o+X,y_o+Y,z,t_o+T) = g\frac{H}{2}\int_0^{\infty}\int_0^{2\pi} S(\omega,\theta)k\sin\theta\frac{\cosh\left[k(d+z)\right]}{\cosh\left(kd\right)} \cdot\left\{\sin\left(kX\sin\theta+kY\cos\theta-\omega T\right) - \sin\left[kX\sin\theta+kY\cos\theta-\omega(T-T^*)\right]\right\} \times \mathrm{d}\theta\mathrm{d}\omega \Big/ \int_0^{\infty}\int_0^{2\pi} S(\omega,\theta)[1-\cos\left(\omega T^*\right)]\mathrm{d}\theta\mathrm{d}\omega \tag{9.14}$$

$$\overline{a_y}(x_o+X,y_o+Y,z,t_o+T) = g\frac{H}{2}\int_0^{\infty}\int_0^{2\pi} S(\omega,\theta)k\cos\theta\frac{\cosh\left[k(d+z)\right]}{\cosh\left(kd\right)} \cdot\left\{\sin\left(kX\sin\theta+kY\cos\theta-\omega T\right) - \sin\left[kX\sin\theta+kY\cos\theta-\omega(T-T^*)\right]\right\} \times \mathrm{d}\theta\mathrm{d}\omega \Big/ \int_0^{\infty}\int_0^{2\pi} S(\omega,\theta)[1-\cos\left(\omega T^*\right)]\mathrm{d}\theta\mathrm{d}\omega \tag{9.15}$$

$$\begin{aligned}\overline{a_z}(x_o+X,y_o+Y,z,t_o+T) = -g\frac{H}{2}\int_0^{\infty}\int_0^{2\pi} S(\omega,\theta)k\frac{\sinh\left[k(d+z)\right]}{\cosh\left(kd\right)}\\ \cdot\left\{\cos\left(kX\sin\theta+kY\cos\theta-\omega T\right)\right.\\ \left.-\cos\left[kX\sin\theta+kY\cos\theta-\omega(T-T^*)\right]\right\}\\ \times \mathrm{d}\theta\mathrm{d}\omega\Big/\int_0^{\infty}\int_0^{2\pi} S(\omega,\theta)[1-\cos\left(\omega T^*\right)]\mathrm{d}\theta\mathrm{d}\omega\end{aligned} \tag{9.16}$$

If the wave of the given height H very large is a zero down-crossing wave, both Eqn (9.2) of $\overline{\eta}$ and Eqns (9.11)–(9.16) of $\overline{v_x}$, $\overline{v_y}$, $\overline{v_z}$, $\overline{a_x}$, $\overline{a_y}$, $\overline{a_z}$ must be multiplied by (-1).

The knowledge of particle velocities and accelerations enables us to calculate the wave loads on cylinders of small diameter, by means of the Morison equation (as we shall see in Chapter 12). Then the knowledge of particle accelerations enables us to calculate the Froude-Krylov forces on isolated bodies. As we have already seen in Chapter 2, the Froude-Krylov force is the force acting on an ideal water body with the same volume and shape as the solid body. As such, the Froude-Krylov force is related to a_x, a_y, a_z by

$$\mathbf{F} = \int_W \rho\left(a_x\mathbf{i_x}+a_y\mathbf{i_y}+a_z\mathbf{i_z}\right)\mathrm{d}W \tag{9.17}$$

where W denotes the volume of the water body. Calculation of the Froude-Krylov force is a preliminary step that is necessary for calculating wave loads on large isolated bodies with an arbitrary shape. In Chapter 10 we shall see which calculation must be done for passing from the Froude-Krylov force to the actual wave force on the solid body. Then, in Chapter 13 we shall see some examples of calculations of wave loads on large isolated bodies.

Typically, we shall assume

$$H = H_{\max} \quad \text{or} \quad b = b_{\max} \tag{9.18}$$

where H_{max} and b_{max} are, respectively, the maximum expected wave height and the maximum expected crest elevation in the design sea state (Chapter 5). With Eqns (9.11)–(9.16) we shall be able to calculate the effect of the wave with the maximum expected height, and with Eqns (9.5)–(9.10) we shall be able to calculate the effect of the wave crest with the maximum expected height.

9.3 THE SUBROUTINE QD

The inputs are X, Y, z, T, and UD (if the wave of the given very large height H is a zero up-crossing $\rightarrow$ UD $= 1$; otherwise, UD $= -1$). NCALL must be 1, except for a preliminary call, as we shall see later.

The outputs are $\overline{\eta}$, $\overline{v_x}$, $\overline{v_y}$, $\overline{v_z}$, $\overline{a_x}$, $\overline{a_y}$, $\overline{a_z}$. The subroutine is specified for the mean JONSWAP spectrum, and the directional distribution of Mitsuyasu et al. However, for changing the spectrum or the directional distribution one has to operate on a small number of variables, which are those included between the two lines of asterisks.

The program must supply: d, H_s, H, A, θ_d, and n_p. (Alternatively, the program may give T_p in place of H_s and A. In this case one has to cancel a pair of lines from the subroutine, which serve to obtain T_p from H_s and A.)

A preliminary call of the subroutine must be done with NCALL $= 0$. This serves to compute the directional spectrum $S(\omega, \theta)$ with steps $d\omega$, $d\theta$ suitable for the numerical integrations. The values of $S(\omega, \theta)$ are stored on memory (SOT(I,J)) for the next calls of the subroutine.

The calculation is made with Eqns (9.2) and (9.11)–(9.16). All of the output variables are the result of the ratio of two integrals with respect to ω and θ. The integral in the denominator is the same for the whole set of variables and is denoted by DENOINT. The integral in the numerator is denoted ETAINT, VXINT, VYINT, etc.

Program EXAMPLE shows an easy application, with the inputs of subroutine QD being given from the console.

```
      SUBROUTINE QD(NCALL,UD,X,Y,Z,T,VX,VY,VZ,AX,AY,AZ,ETA)
      COMMON D,HS,H,TP,TST,ALPHA, TETAD,RNP
      COMMON IMAX,JMAX,OMV(300),TETV(150),RKV(300)
      COMMON SOT(300,150)
      DIMENSION EO(300),DTE(150)
      G=9.8
      G2=G*G
      PG=3.141592
      DPG=2.*PG
      IF(NCALL.GT.0)GO TO 500
c*****************************************
      RKO=1.345
      CHI1=3.3
      CHI2=0.08
      CST=0.44
c*****************************************
```

```
      COST=RKO/ALPHA**0.25
      TP=COST*PG*SQRT(HS/G)
      TST=CST*TP
      ALCHI1=ALOG(CHI1)
      CHI2Q=CHI2*CHI2
      OMP=DPG/TP
      DOMEGA=OMP/50.
      O1=0.5*OMP
      O2=3.*OMP
      OMPQ=OMP*OMP
      DTETA=PG/100.
      TE1=-PG/2.
      TE2=PG/2.
      OM=O1-DOMEGA/2.
      I=0
c Loop 90: the grid of values of the directional spectrum, being necessary
c for the execution of the double integrals, is loaded on memory
90    OM=OM+DOMEGA
      IF(OM.GT.O2)GO TO 91
      I=I+1
      OMV(I)=OM
c values of omega stored on OMV(I) (I=1,IMAX)
      PE=DPG/OM
      RLO=(G/DPG)*PE*PE
      DLO=D/RLO
      IF(DLO.GT.0.5)THEN
      RKV(I)=DPG/RLO
      ELSE
      RLP=RLO
300   RL=RLO*TANH(DPG*D/RLP)
      TES=ABS(RL-RLP)/RL
      RLP=RL
      IF(TES.GT.1.E-4)GO TO 300
      RKV(I)=DPG/RL
      ENDIF
c k(omega) stored on RKV(I)
      OMM5=1./OM**5
      ARG=(OM-OMP)**2/(2.*CHI2Q*OMPQ)
      E3=EXP(-ARG)
      ARG=ALCHI1*E3
      E2=EXP(ARG)
      ARG=1.25*(OMP/OM)**4
      E1=EXP(-ARG)
      EO(I)=ALPHA*G2*OMM5*E1*E2
c EO(I)=SSE(omega)
c*****************************************
```

```
      IF(OM.LE.OMP)THEN
      RN=RNP*(OM/OMP)**5
      ELSE
      RN=RNP*(OMP/OM)**2.5
      ENDIF
c*****************************************
      DN=2.*RN
      TE=TE1-DTETA/2
      J=0
80    TE=TE+DTETA
      IF(TE.GT.TE2)GO TO 81
      J=J+1
      TETV(J)=TE+TETAD
c values of theta stored on TETV(J) (J=1,JMAX)
      ABC=ABS(COS(TE/2.))
      DTE(J)=ABC**DN
      GO TO 80
81    CONTINUE
      JMAX=J
      SOMT=0
      DO J=1,JMAX
      SOMT=SOMT+DTE(J)*DTETA
      ENDDO
      RKN=1./SOMT
c RKN=K(n) (Eqn 6.18)
      DO J=1,JMAX
      DTE(J)=RKN*DTE(J)
c DTE(J)=D(theta;omega)
      SOT(I,J)=DTE(J)*EO(I)
c directional spectrum stored on SOT(I,J)
      ENDDO
      GO TO 90
91    CONTINUE
      IMAX=I
      IF(NCALL.EQ.0)GO TO 501
500   CONTINUE
c ETAINT=double integral numerator RHS of Eqn (9.2)
c VXINT=double integral numerator RHS of Eqn (9.5)
c VYINT=double integral numerator RHS of Eqn (9.6)
c VZINT=double integral numerator RHS of Eqn (9.7)
c AXINT=double integral numerator RHS of Eqn (9.8)
c AYINT=double integral numerator RHS of Eqn (9.9)
c AZINT=double integral numerator RHS of Eqn (9.10)
c DENOINT=double integral denominator RHS of Eqn (9.2) or (9.5)–(9.10)
      ETAINT=0
      VXINT=0
      VYINT=0
```

```
     .VZINT=0
      AXINT=0
      AYINT=0
      AZINT=0
      DENOINT=0
      DO I=1,IMAX
      DO J=1,JMAX
      OM=OMV(I)
      OM1=1./OM
      RK=RKV(I)
c A1 attenuation factor of horizontal components
c A2 attenuation factor of vertical components
c for large kd both A1 and A2 tend to exp(kz). This
c asymptotic form is used (for large kd) in order to avoid
c overflow errors in cosh(kd)
      IF(RK*D.GT.20)THEN
      A1=EXP(RK*Z)
      A2=A1
      ELSE
      A1=COSH(RK*(D+Z))/COSH(RK*D)
      A2=SINH(RK*(D+Z))/COSH(RK*D)
      ENDIF
      TE=TETV(J)
      S=SOT(I,J)
      ST=SIN(TE)
      CT=COS(TE)
      ARG1=RK*X*ST+RK*Y*CT-OM*T
      ARG2=RK*X*ST+RK*Y*CT-OM*(T-TST)
      CO1=COS(ARG1)
      CO2=COS(ARG2)
      SI1=SIN(ARG1)
      SI2=SIN(ARG2)
      ETAINT=ETAINT+S*(CO1-CO2)
      VXINT=VXINT+S*OM1*RK*A1*ST*(CO1-CO2)
      VYINT=VYINT+S*OM1*RK*A1*CT*(CO1-CO2)
      VZINT=VZINT+S*OM1*RK*A2*(SI1-SI2)
      AXINT=AXINT+S*RK*A1*ST*(SI1-SI2)
      AYINT=AYINT+S*RK*A1*CT*(SI1-SI2)
      AZINT=AZINT-S*RK*A2*(CO1-CO2)
      DENOINT=DENOINT+S*(1.-COS(OM*TST))
      ENDDO
      ENDDO
      ETA=UD*0.5*H*ETAINT/DENOINT
      VX=UD*0.5*G*H*VXINT/DENOINT
      VY=UD*0.5*G*H*VYINT/DENOINT
      VZ=UD*0.5*G*H*VZINT/DENOINT
      AX=UD*0.5*G*H*AXINT/DENOINT
```

```
     .AY=UD*0.5*G*H*AYINT/DENOINT
      AZ=UD*0.5*G*H*AZINT/DENOINT
501   CONTINUE
c the values of all the double integrals (ETAINT, VXINT,VYINT, VZINT,
c AXINT, AYINT,AZINT,DENOINT) should have been multiplied by the
c product DTETA*DOMEGA; however this product cancels on executing
c the ratios ETAINT/DENOINT, VXINT/DENOINT, etc
      RETURN
      END

      PROGRAM EXAMPLE
      COMMON D,HS,H,TP,TST,ALPHA,TETAD,RNP
      COMMON IMAX,JMAX,OMV(300),TETV(150),RKV(300)
      COMMON SOT(300,150)
      PG=3.141592
      DPG=2.*PG
      WRITE(6,*)'d,Hs,H'
      READ(5,*)D,HS,H
      WRITE(6,*)'alpha,thetad(degree),np'
      READ(5,*)ALPHA,TETAD,RNP
      WRITE(6,*)'zero up-crossing wave -> 1, down-crossing -> -1'
      READ(5,*)UD
      TETAD=TETAD*PG/180.
      CALL QD(NCALL,UD,X,Y,Z,T,VX,VY,VZ,AX,AY,AZ,ETA)
      NCALL=NCALL+1
500   WRITE(6,*)'X,Y,Z,T'
      READ(5,*)X,Y,Z,T
      CALL QD(NCALL,UD,X,Y,Z,T,VX,VY,VZ,AX,AY,AZ,ETA)
      WRITE(6,1000)ETA
      WRITE(6,1001)VX,VY,VZ
      WRITE(6,1001)AX,AY,AZ
1000  FORMAT(2X,F7.2)
1001  FORMAT(2X,3(F7.2,1X))
      GO TO 500
      END
```

9.4 EXPERIMENTAL VERIFICATION OF THE QUASI-DETERMINISM THEORY: BASIC CONCEPTS

9.4.1 Obtaining the Deterministic Wave Function from Time Series Data

Let us imagine two wave gauges at two points A and B in a sea area. We measure the surface elevation at these two points in the same time instants. The sample interval is Δt, and n is the number of samples per record per gauge. We wonder "what may we expect to happen at point B provided that a wave with a given height H, being exceptionally large with respect to the sea state, occurs at point A?" According to the QD theory, point A is x_o,y_o and point B is $x_o + X,y_o + Y$. The expected surface elevation at $x_o + X,y_o + Y$ is given by Eqn (8.83). Using the definition (7.1) of Ψ, Eqn (8.83) may be rewritten in the form

$$\overline{\eta_B}(t_o + T) = \frac{\langle \eta_A(t)\eta_B(t+T)\rangle - \langle \eta_A(t)\eta_B(t+T-T^*)\rangle}{\langle \eta_A^2(t)\rangle - \langle \eta_A(t)\eta_A(t+T^*)\rangle}\frac{H}{2} \tag{9.19}$$

where

$$\eta_A(t) = \eta(x_o, y_o, t) \tag{9.20}$$

$$\eta_B(t) = \eta(x_o + X, y_o + Y, t) \tag{9.21}$$

and T^* is the lag of the absolute minimum of the autocovariance

$$\psi(T) = \langle \eta_A(t)\eta_A(t+T)\rangle \tag{9.22}$$

The averages in Eqn (9.19) may be obtained from the time series data. As an example, let $\Delta t = 0.1$ s and $n = 3001$ as it is currently taken at the NOEL; then for obtaining $\overline{\eta}_B(t_o + T)$ with $T = 0.6$ s we shall have to perform the following average:

$$\langle \eta_A(t)\eta_B(t+0.6\text{s})\rangle = \frac{\eta_{A_1}\eta_{B_7} + \eta_{A_2}\eta_{B_8} + \cdots + \eta_{A_{2995}}\eta_{B_{3001}}}{2995} \tag{9.23}$$

where η_{A_i} denotes the ith sample value at point A.

9.4.2 Resorting to Time Series Data of Pressure Head Waves

Equation (9.19) holds also for pressure head waves at some depth beneath the water level. More generally, all that has been shown until now holds whether η is the surface elevation or the fluctuating pressure head at some fixed depth beneath the water level. Hence, one may test the theory either with surface waves or with pressure head waves, at one's own choice. Working with pressure head waves is preferable. Aside from the fact that the author attracted to pressure head waves, there is the fact that, at the NOEL, the cost of a small-scale field experiment (SSFE) on pressure head waves is an order of magnitude smaller than the cost of the same SSFE on surface waves.

9.4.3 A Typical Experiment Aimed to Verify the Theory

There is an array of gauges. The largest distance between two gauges is within a few wave lengths. These gauges record the surface elevation at the same time instants. Many records are taken in many sea states. The largest ratio H/σ is searched in each record. This is the largest value

of H/σ from all the zero up-crossing waves and all the zero down-crossing waves obtained by the whole array of gauges in the record. This will be called $(H/\sigma)_{\max\, i}$, where i denotes the number of the record. To fix the ideas let us think of these numbers:

number of gauges: 30
record duration: 300 s
number of records: 1000

Let us imagine that the largest value of the ratio $(H/\sigma)_{\max\, i}$ has occurred in the record $i = 600$ at $t_o = 200$ s, that the record was done by gauge number 25, and that the wave of this largest H/σ was a zero up-crossing wave. Then we apply Eqn (9.19) with A = point of gauge 25, and B = point of gauge 1, then B = point of gauge 2, and so on, until B = point of gauge 30. Of course, the time series data used for the averages in Eqn (9.19) will be those of record number 600. Thus, we obtain the $\overline{\eta}(t_o + T)$ at the 30 points of the wave gauges, as a function of the time lag T (T typically ranges from $-3T_p$ to $3T_p$). Finally, the deterministic $\overline{\eta}$ is compared to the random η in record number 600.

9.5 RESULTS OF SMALL-SCALE FIELD EXPERIMENTS

In an early SSFE in 1990 there were nine piles, each of which supported a wave gauge (the plan of the piles is shown in Fig. 9.3). The wave with the largest ratio H/σ was recorded at point 3. It was a zero down-crossing wave with a $H/\sigma = 9.6$.

Figure 9.4(a) shows the deterministic $\overline{\eta}(t_o + T)$ calculated with Eqn (9.19), and Fig. 9.4(b) shows the random $\eta(t)$ at the locations of the gauges. The

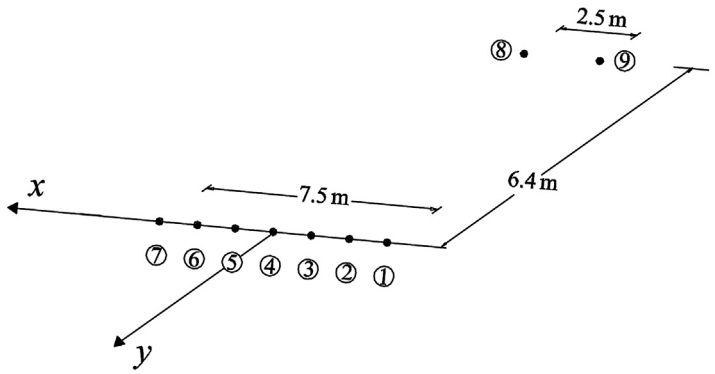

■ **FIGURE 9.3** Plan of the wave gauges in the SSFE of 1990 aimed to verify the QD theory. (The data acquisition system had eight channels so that one of the wave gauges had to be disconnected. In the stage of the experiment wherein the largest wave height occurred, the disconnected gauge was no. 6.)

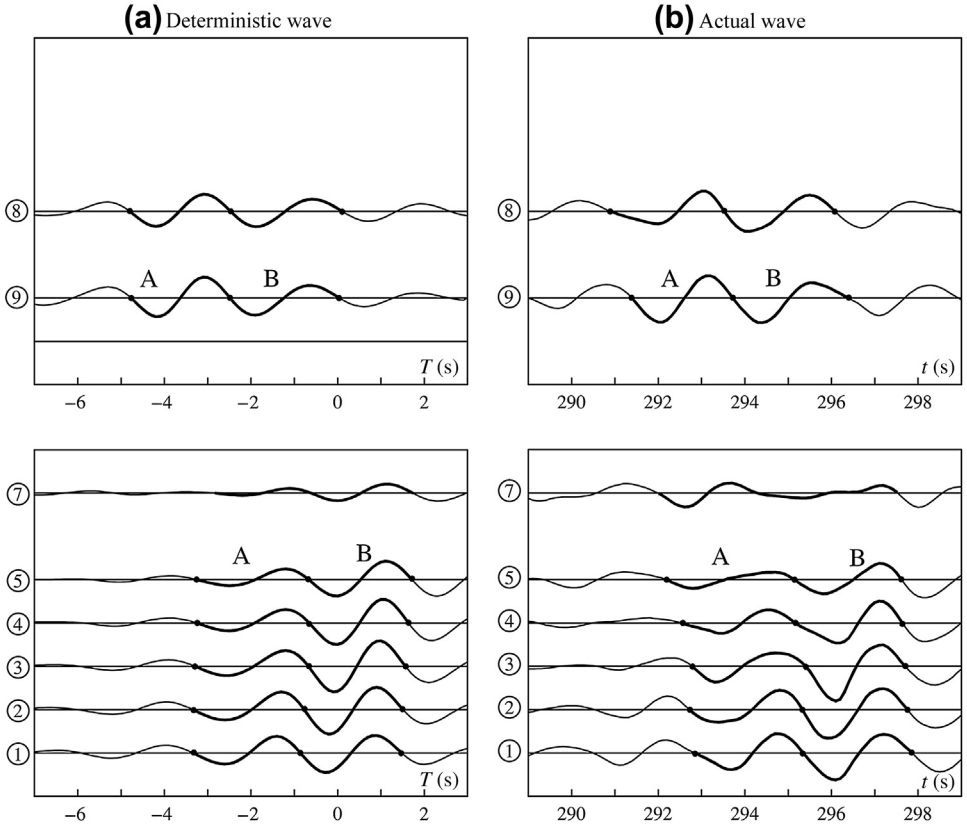

■ **FIGURE 9.4 SSFE of 1990** (see the plan of the gauges in Fig. 9.3). The figure compares the actual waves (b) with deterministic waves (a) when the wave with the largest H/σ was recorded (this was a zero down-crossing wave with $H/\sigma = 9.6$ recorded by gauge no. 3).

relative phases at the traverse of points 1−7 reveal that the angle between the direction of wave advance (of the deterministic wave) and the y-axis was about 10°. Hence, if the center of the wave crest passed at point 3 it had to pass very close to point 9. At point 9, A is at the center of the envelope, and B is in the envelope tail. At point 3, B is at the center of the envelope, and A is in the envelope head.

Of course, there are some differences between random η and deterministic $\overline{\eta}$ and indeed the QD theory states that η becomes asymptotically equal to $\overline{\eta}$ only as H/σ tends to infinity. Besides these main discrepancies due to residual randomness, there are some discrepancies due to nonlinearity effects, which produce some local distortion of the wave profile that cannot be foreseen by the linear QD theory. However, the overall closeness between the

random waves (η) and the deterministic waves ($\overline{\eta}$) was evident since that early experiment of 1990.

The more recent SSFEs deal with waves in the space-time domain. Besides time series at some fixed points, these experiments enable one to obtain wave profiles in the space domain. This is possible because the wave gauges are close to each other and sensibly aligned with the wave direction, as is shown in Fig. 9.5.

This novelty has made it possible to take a step forward into verification of the QD theory. Indeed, some cases were found wherein the overall closeness between random wave profiles and deterministic wave profiles is really amazing. In particular, look at Fig. 9.6, where the continuous lines represent the deterministic wave profiles and the dashed lines represent the random wave profiles, for a case of a ratio $H/\sigma = 9.22$. Figure 9.6 proves that the wave groups of the QD theory do exist in the field. The figure shows the transit of one of these groups over the gauge array (GA). In the first line of the figure ($t_o - 5$ s), on the right-hand side of the GA there is the near-calm that precedes the arrival of a wave group; on the left-hand side there is wave crest A, which is decreasing because it precedes the envelope center. On the opposite in the last line ($t_o + 6$ s), on the left-hand side of the GA there is the near-calm that follows the transit of a wave group; on the right-hand side there is wave crest E that is growing because it follows the envelope center, which has already left the GA. The envelope center is close to the locations of wave crests B, C, and D, respectively, at $t_o - 2$ s, $t_o + 1$ s, and $t_o + 4$ s. Wave crests B and C nearly complete their life cycle during the passage over the GA. In particular, wave crest B is in its growing stage from $t_o - 4$ s to $t_o - 2$ s and in the decay stage from $t_o - 2$ s to t_o; wave crest C is in its growing stage from $t_o - 2$ s to $t_o + 1$ s, and in the decay stage from $t_o + 1$ s to $t_o + 2$ s.

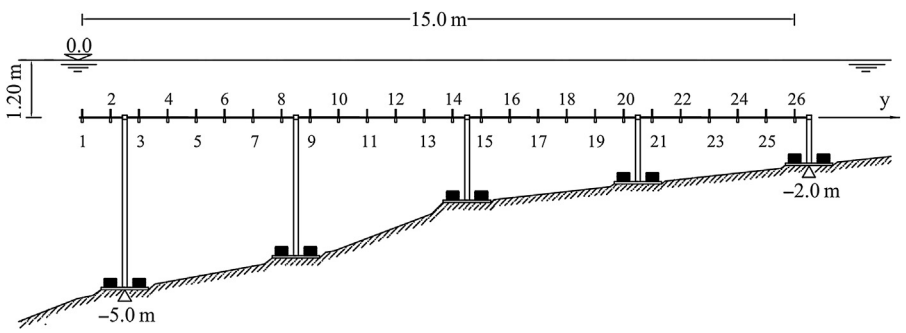

■ **FIGURE 9.5** The gauges of a recent SSFE (2010) aimed to verify the QD theory. There was an array of 26 pressure transducers, each of which was connected with a small vertical tube with a bending section (like a small periscope). Pressure head waves were measured 0.80 m beneath the mean water level.

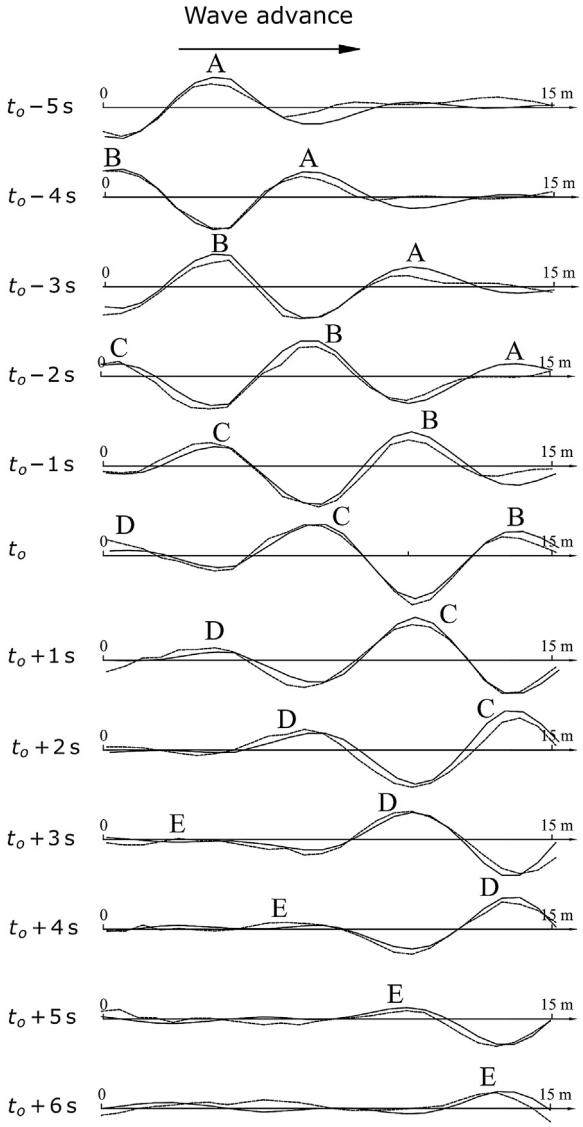

■ **FIGURE 9.6** Small-scale field experiment of 2010. What happened when a zero down-crossing wave of $H/\sigma = 9.22$ was recorded by gauge no. 18 (the location of this gauge is shown by a small vertical segment in the picture relevant to time instant t_o). Dashed line: actual (random) wave. Continuous line: deterministic wave.

9.6 CONCLUSION

The characteristic mechanics of wave groups shown in Section 9.1.1 were disclosed in a paper by the author (1989). Only some years later than the publication of the paper (1989) the author realized the overall physical consistency of the theory, which here has been called "core of the theory" (Section 9.1.2), and was disclosed in the book (2000). The SSFEs of 1990 and 2010 were described, respectively, by Boccotti et al. (1993) and Boccotti (2011).

Two full-scale field experiments on the configuration of wave group G1 near the exceptionally large wave crest were performed by Phillips et al. (1993a,b). Some nonlinearity effects on the wave groups were dealt with by Arena (2005), Arena and Fedele (2005), Fedele and Arena (2005), Arena et al. (2008), and Arena and Guedes Soares (2009). The QD theory has widened the view on sea wave groups: from statistics to mechanics. A wave group was dealt with in the time domain and defined as a sequence of waves with heights greater than some given (large) threshold. The analysis was purely in statistics: concerning the number of waves (Kimura, 1980; van Vledder, 1992; Medina and Huspeth, 1990), or the wave energy of the group (Medina and Hudspeth, 1994).

REFERENCES

Arena, F., 2005. On non-linear very large sea wave groups. Ocean Eng. 32, 1311−1331.

Arena, F., Fedele, F., 2005. Non-linear space-time evolution of wave groups with a high crest. ASME J. Offshore Mech. Artic Eng. 127, 1−10.

Arena, F., Ascanelli, A., Nava, A., Pavone, D., Romolo, A., 2008. Non-linear three-dimensional wave groups in finite water depth. Coastal Eng. 55 (12), 1052−1061.

Arena, F., Guedes Soares, C., 2009. Non linear high wave groups in bimodal sea states. J. Waterway Port Coastal Ocean Eng. 135 (3), 69−79.

Boccotti, P., 1989. On mechanics of irregular gravity waves. Atti Accad. Naz. Lincei Mem. VIII 19, 111−170.

Boccotti, P., 2000. Wave Mechanics for Ocean Engineering. Elsevier, Amsterdam, 1−495.

Boccotti, P., 2011. Field verification of quasi-determinism theory for wind waves in the space-time domain. Ocean Eng. 38, 1503−1507.

Boccotti, P., Barbaro, G., Mannino, L., 1993. A field experiment on the mechanics of irregular gravity waves. J. Fluid Mech. 252, 173−186.

Fedele, F., Arena, F., 2005. Weakly nonlinear statistics of high random waves. Phys. Fluids 17, 1−10.

Kimura, A., 1980. Statistical properties of random wave groups. In: Proc. 17th Conf. Coastal Engineering. ASCE, New York, pp. 2955−2973.

Medina, J.R., Hudspeth, R.T., 1990. A review of analyses of wave groups. Coastal Eng. 14, 515−542.

Medina, J.R., Hudspeth, R.T., Fassardi, C., 1994. Breakwater armor damage due to wave groups. J. Waterway Port Coastal Ocean Engrg. 120 (2), 179−198.

Phillips, O.M., Gu, D., Donelan, M., 1993a. On the expected structure of extreme waves in a Gaussian sea. I. Theory and SWADE buoy measurements. J. Phys. Oceanogr. 23, 992–1000.

Phillips, O.M., Gu, D., Walsh, E.J., 1993b. On the expected structure of extreme waves in a Gaussian sea. II. SWADE scanning radar altimeter measurements. J. Phys. Oceanogr. 23, 2297–2309.

van Vledder, G. Ph, 1992. Statistics of wave group parameters. In: Proc. 23th Conf. Coastal Engineering. ASCE, New York, pp. 946–959.

Chapter 10

QD Theory: Mechanics of Wave Forces on Large Isolated Bodies

CHAPTER OUTLINE

10.1 FURTHER PROOF THAT THE QD THEORY HOLDS FOR ARBITRARY CONFIGURATIONS OF THE SOLID BOUNDARY

It can be proved that the deterministic velocity potential $\overline{\phi}$ satisfies every boundary condition, provided that random velocity potential ϕ satisfies this boundary condition.

For simplicity, and without loss of generality, we shall assume the solid boundary to be a cylinder (see the reference scheme of Fig. 10.1). Provided that

$$\frac{\partial \phi}{\partial z} = \frac{\partial \phi}{\partial y}\tan\beta \quad \text{at } x = x_1,\ y = y_1,\ z = z_1 \tag{10.1}$$

Wave Mechanics and Wave Loads on Marine Structures. http://dx.doi.org/10.1016/B978-0-12-800343-5.00010-X

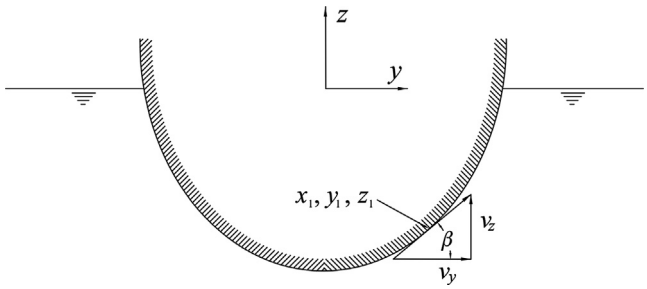

■ **FIGURE 10.1 Reference scheme: QD theory with an arbitrary solid boundary.**

where x_1, y_1, z_1 is an arbitrary point of the cylinder surface, we aim to prove that

$$\frac{\partial\overline{\phi}}{\partial z} = \frac{\partial\overline{\phi}}{\partial Y}\tan\beta \quad \text{at } X = x_1 - x_o,\ Y = y_1 - y_o,\ z = z_1 \tag{10.2}$$

That is, we aim to prove the following equality:

$$\left(\frac{\partial}{\partial z}\right) b\frac{\Phi(X,Y,z,T;x_o,y_o)}{\sigma^2(x_o,y_o)} = \left(\frac{\partial}{\partial Y}\right) b\frac{\Phi(X,Y,z,T;x_o,y_o)}{\sigma^2(x_o,y_o)}\tan\beta \quad \text{at } X = x_1 - x_o,\ Y = y_1 - y_o,\ z = z_1 \tag{10.3}$$

If the definition (Eqn (7.9)) of Φ is used, and $b/\sigma^2(x_o, y_o)$ is canceled from both the LHS and the RHS, the equality to be proved becomes

$$\frac{\partial}{\partial z}\langle\eta(x_o,y_o,t)\phi(x,y,z,t+T)\rangle = \frac{\partial}{\partial y}\langle\eta(x_o,y_o,t)\phi(x,y,z,t+T)\rangle\tan\beta \quad \text{at } x = x_1,\ y = y_1,\ z = z_1 \tag{10.4}$$

To prove this equality, one has to invert the order derivative-average both on the LHS and on the RHS, and use the equality Eqn (10.1).

10.2 DETERMINISTIC PRESSURE FLUCTUATIONS ON SOLID BODY

The pressure fluctuation $\overline{\Delta p}$ is related to velocity potential $\overline{\phi}$ by

$$\overline{\Delta p}(x_o + X, y_o + Y, z, t_o + T) = -\rho\frac{\partial\overline{\phi}(x_o + X, y_o + Y, z, t_o + T)}{\partial T} \tag{10.5}$$

which, with Eqn (8.76) of $\overline{\phi}$, becomes

$$\overline{\Delta p}(x_o + X, y_o + Y, z, t_o + T) = -\rho\left(\frac{\partial}{\partial T}\right) b \frac{\Phi(X, Y, z, T; x_o, y_o)}{\sigma^2(x_o, y_o)} \tag{10.6}$$

and with the definition (Eqn (7.9)) of Φ:

$$\overline{\Delta p}(x_o + X, y_o + Y, z, t_o + T) = -\rho\left(\frac{\partial}{\partial T}\right) \times b \frac{\langle \eta(x_o, y_o, t)\phi(x_o + X, y_o + Y, z, t + T)\rangle}{\sigma^2(x_o, y_o)} \tag{10.7}$$

Finally, on inverting the order derivative with respect to T—average with respect to t, we arrive at

$$\overline{\Delta p}(x_o + X, y_o + Y, z, t_o + T) = b \frac{\langle \eta(x_o, y_o, t)(-\rho \frac{\partial}{\partial T})\phi(x_o + X, y_o + Y, z, t + T)\rangle}{\langle \eta^2(x_o, y_o, t)\rangle} \tag{10.8}$$

and hence

$$\overline{\Delta p}(x_o + X, y_o + Y, z, t_o + T) = b \frac{\langle \eta(x_o, y_o, t)\Delta p(x_o + X, y_o + Y, z, t + T)\rangle}{\langle \eta^2(x_o, y_o, t)\rangle} \tag{10.9}$$

If a wave crest with a given height b occurs at point x_o, y_o at time instant t_o, and $b/\sigma(x_o, y_o) \to \infty$, the random wave pressure in space and time, in a neighborhood of x_o, y_o, will be asymptotically equal to this deterministic function.

If a wave with a given height H occurs at point x_o, y_o, and $H/\sigma(x_o, y_o) \to \infty$, the random wave pressure in space and time, in a neighborhood of x_o, y_o, will be asymptotically equal to the deterministic function

$$\begin{aligned}
&\overline{\Delta p}(x_o + X, y_o + Y, z, t_o + T) \\
&\quad = \frac{H}{2}[\langle \eta(x_o, y_o, t)\Delta p(x_o + X, y_o + Y, z, t + T)\rangle \\
&\quad - \langle \eta(x_o, y_o, t)\Delta p(x_o + X, y_o + Y, z, t + T - T^*)\rangle] \\
&\quad /[\langle \eta^2(x_o, y_o, t)\rangle - \langle \eta(x_o, y_o, t)\eta(x_o, y_o, t + T^*)\rangle]
\end{aligned} \tag{10.10}$$

which proceeds from the velocity potential (Eqn (8.84)).

These equations of $\overline{\Delta p}$ are valid for every point in the water, and thus in particular at the boundary of a solid body with an arbitrary configuration.

10.3 COMPARING WAVE PRESSURES ON AN ISOLATED SOLID BODY TO THE WAVE PRESSURES ON AN EQUIVALENT WATER BODY

In 1992 and 1993, two small-scale field experiments (SSFEs) were executed in the sea area of the NOEL, for comparing, in real time, wave forces on large isolated bodies to the Froude–Krylov force. The field laboratory of the 1992 experiment is shown in Fig. 10.2. The structure was the 1:50 scale model of an offshore gravity platform of the North Sea.

In the 1:50 scale, the typical sea states consisting of wind seas of about 0.30 m H_s corresponded to full-scale sea states of about 15 m H_s which are realistic design sea states for the North Sea. Wave pressures were recorded by an array of pressure transducers at several points (1, 2, 3, 4) at the boundary of the platform, and the surface elevation was recorded at point 0 above the center of platform's base, by means of an ultrasonic probe. The wave pressures were contemporarily recorded at points (1, 2, 3, 4) with the same spatial configuration of the points at the boundary of the platform, far away where the diffraction effects were negligible. Points (1, 2, 3, 4) may

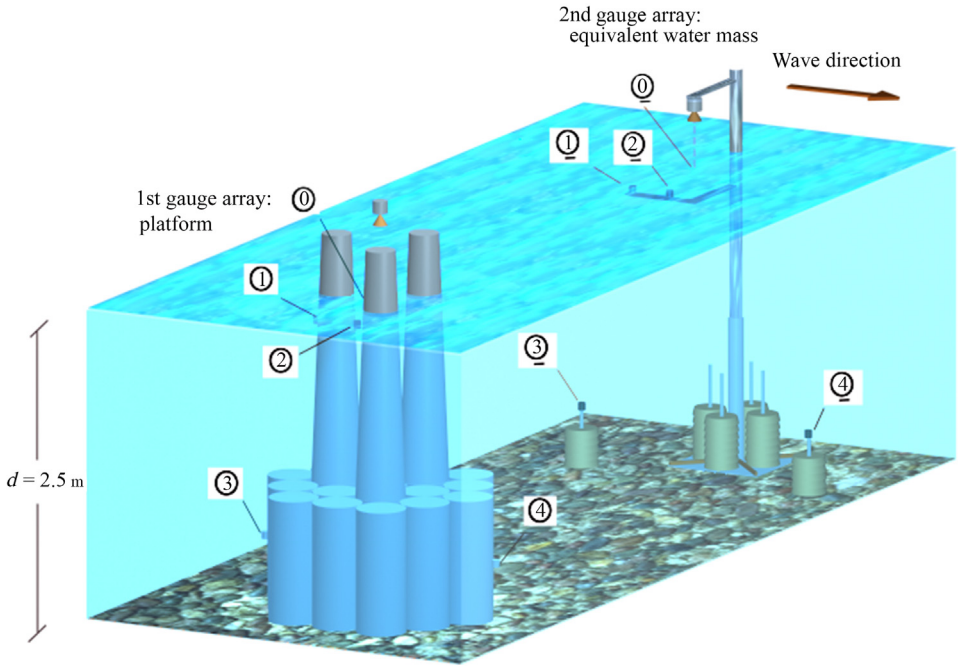

■ **FIGURE 10.2 A small-scale field experiment of 1992.** 1:50 scale model of supporting structure of a gravity offshore platform, and points where wave pressure or surface elevation was measured.

be thought of as points at the boundary of an ideal water platform with the same volume and shape as the solid platform. The surface elevation at point 0 above the center of the base of the equivalent water platform was recorded by a second ultrasonic probe.

The field laboratory of the 1993 experiment is shown in Fig. 10.3. The structure was the 1:30 scale model of a hypothesis of submerged tunnel across the Messina Straits. Here, the typical 0.30 m H_s corresponded to a full-scale H_s of 9 m, which is consistent with the H_s of the cautious design sea state. Here too, wave pressures were measured at a number of points (5, 12) of the boundary of the solid cylinder, and at the points (5, 12) with the same spatial configuration of the boundary of an ideal water cylinder with the same geometry as the solid cylinder (same radius, same immersion, same water depth, same orientation). The surface elevation was recorded at point 0 above the section of the solid cylinder with points (5, 12). The surface elevation was recorded also at point 0 above the section of the equivalent water cylinder with points (5, 12).

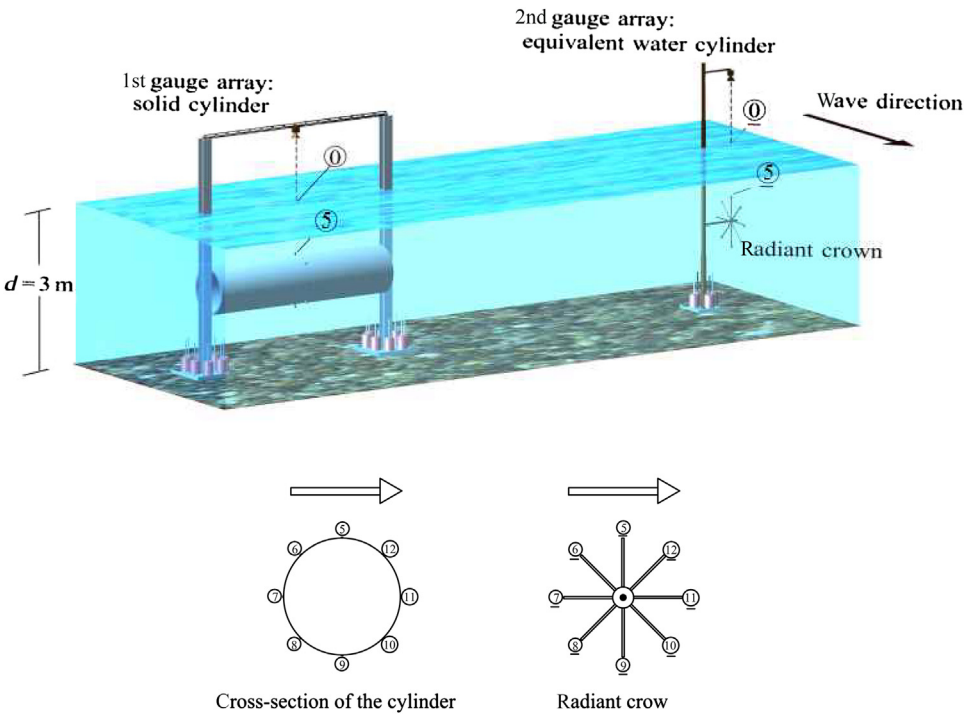

■ **FIGURE 10.3 A small-scale field experiment of 1993.** 1:30 scale model of a piece of floating tunnel, and points where surface elevation was measured.

10.4 THE REASON THE WAVE FORCE ON THE SOLID BODY IS GREATER THAN THE FROUDE–KRYLOV FORCE

Figure 10.4(a) shows the deterministic wave pressure $\overline{\Delta p_i}/\sigma_i$ at the points ($i = 1, 2, 3, 4$) at the boundary of the solid body of the first experiment. That is, the figure shows the ratio between

$$\overline{\Delta p_i}(t_o + T) = \frac{H}{2} \cdot \frac{\langle \eta_0(t)\Delta p_i(t+T)\rangle - \langle \eta_0(t)\Delta p_i(t+T-T^*)\rangle}{\langle \eta_0^2(t)\rangle - \langle \eta_0(t)\eta_0(t+T^*)\rangle} \tag{10.11}$$

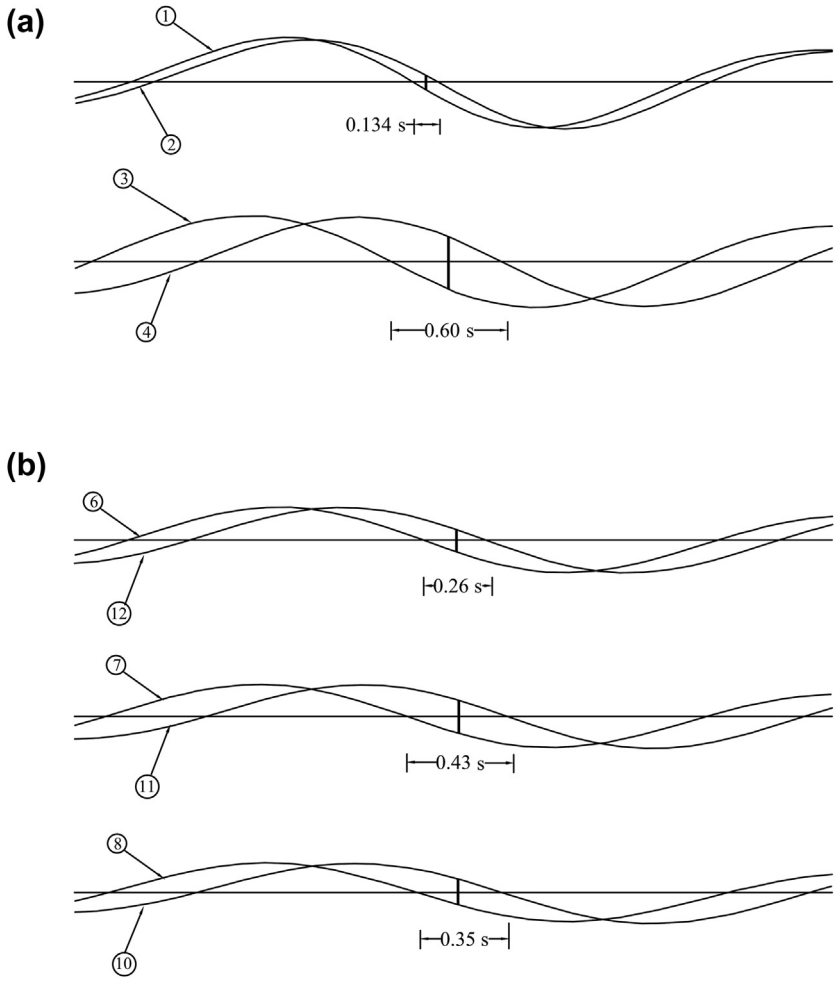

■ **FIGURE 10.4 Small-scale field experiments of 1992 and 1993.** (a) Wave pressures at various points of the platform if a wave of given very large height passes at central point 0; (b) wave pressures at various points of the horizontal cylinder if a wave of given very large height passes at point 0 above this cylinder; obtained on applying the algorithm of the QD theory with time series data.

and

$$\sigma_i = \sqrt{\langle \Delta p_i^2(t) \rangle} \tag{10.12}$$

Equation (10.11) is the same as Eqn (10.10) for the special case that point x_o, y_o is point 0 and point $x_o + X$, $y_o + Y$, z is point i. Figure 10.4(b) shows the deterministic wave pressure $\overline{\Delta p_i}/\sigma_i$ at the points $(i = 5,\ 6,\ldots,12)$ at the boundary of the solid body of the second experiment. Figure 10.5 is

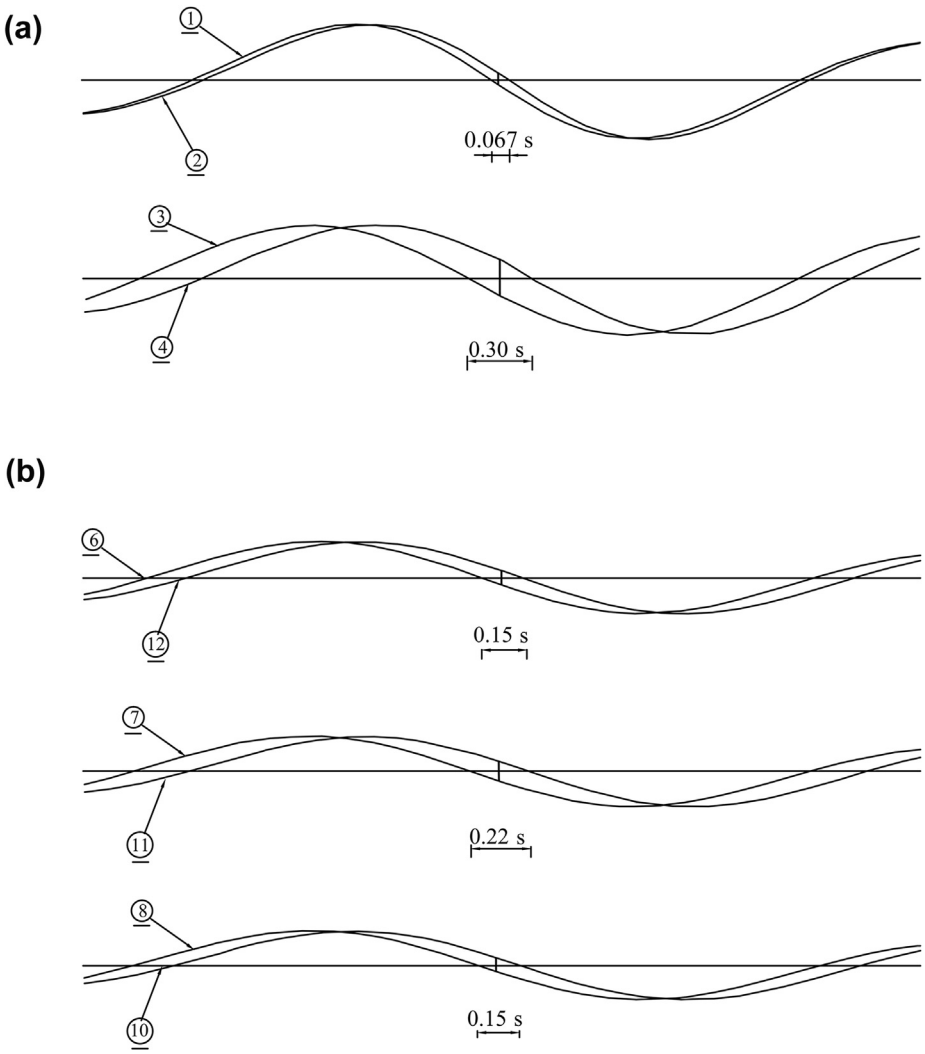

■ **FIGURE 10.5 Small-scale field experiments of 1992 and 1993.** (a) Wave pressures at various points of the water body equivalent to the platform if a wave of given very large height passes at central point 0; (b) wave pressures at various points of the water cylinder equivalent to the solid cylinder if a wave of given very large height passes at point 0 above this water cylinder, obtained on applying the algorithm of the QD theory with time series data.

the same as Fig. 10.4, with the only difference that the water body is considered in place of the solid body, and hence, the time series data of ($\underline{0}$, $\underline{1}$, $\underline{2}$,…) are used instead of (0, 1, 2,…).

On comparing Fig. 10.5 to Fig. 10.4, we see that the phase angle between a pair of points at the solid body is nearly twice the phase angle between the same pair of points at the water body. For example, the time shift between point 1 and point 2 at the column of the platform is 0.134 s, whereas the time shift between the same pair of points at the water body is 0.067 s.

Typically, a larger phase angle implies a larger pressure difference between the wave beaten half of a cylinder and the sheltered half, and this is the essential reason why the horizontal force on the solid cylinder is greater than the horizontal force on the water cylinder.

As to the effect of the amplitude of the pressure fluctuations, let us consider the RMS pressure fluctuation σ_i at various points. As to points like 3, 4 of the platform base and $\underline{3}$, $\underline{4}$ of the equivalent water body, σ_i is the same in 3, 4, $\underline{3}$, $\underline{4}$. Nearly the same holds also for points 1, 2, $\underline{1}$, $\underline{2}$ of the column and of its equivalent water body.

The σ_i at the tunnel are shown in Fig. 10.6. We see that, from the water cylinder to the solid cylinder, the σ_i grows on the upper half, and is decreased on the lower half. Of course, this is the reason the amplitude of the vertical wave force on the tunnel is greater than the amplitude of the vertical Froude−Krylov force.

On the opposite, we see that the average σ_i either on the wave-beaten half-cylinder or on the sheltered half cylinder has only a small change from the

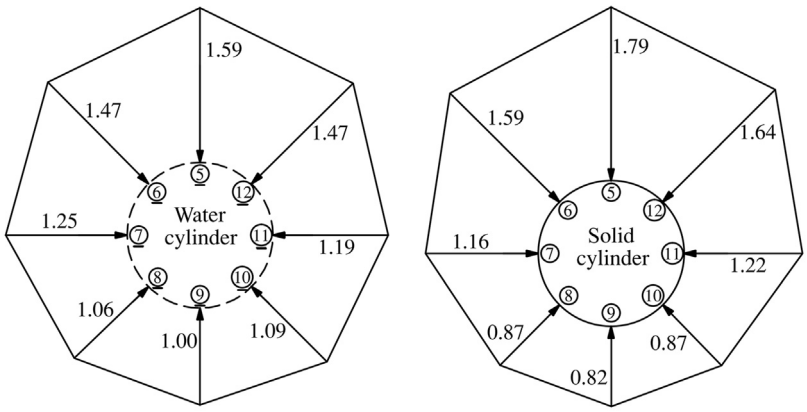

■ **FIGURE 10.6 Small-scale field experiment of 1993.** The polar diagram represents the average ratio $\sqrt{\frac{\langle \Delta p_i^2(t) \rangle}{\langle \Delta p_{\underline{i}}^2(t) \rangle}}$ in the whole set of records. Here, i denotes the location of the ith measurement point. The diagram on the left is relevant to the water cylinder. The diagram on the right is relevant to the solid cylinder.

water cylinder to the solid cylinder. This implies that the amplification of the horizontal wave force from the horizontal water cylinder to the horizontal solid cylinder depends essentially on the reduction of the propagation speed of the pressure head waves at the solid cylinder, just as it happens for the vertical cylinder.

10.5 COMPARING WAVE FORCE ON AN ISOLATED SOLID BODY TO THE FROUDE—KRYLOV FORCE

The *y*-*z* components of the sectional wave force on the tunnel were obtained by means of

$$F_y = \sum_{i=5}^{12} C_{y_i} \Delta p_i \tag{10.13}$$

$$F_z = \sum_{i=5}^{12} C_{z_i} \Delta p_i \tag{10.14}$$

where

$$C_{y_5} = 0,\ C_{y_6} = C_1,\ C_{y_7} = C_0,\ C_{y_8} = C_1,\ C_{y_9} = 0,\ C_{y_{10}} = -C_1,\ C_{y_{11}} = -C_0,\ C_{y_{12}} = -C_1 \tag{10.15}$$

$$C_{z_5} = -C_0,\ C_{z_6} = -C_1,\ C_{z_7} = 0,\ C_{z_8} = C_1,\ C_{z_9} = C_0,\ C_{z_{10}} = C_1,\ C_{z_{11}} = 0,\ C_{z_{12}} = -C_1 \tag{10.16}$$

$$C_0 = 2R\sin(\pi/8),\ C_1 = C_0\cos(\pi/4) \tag{10.17}$$

Equations of the form

$$F_y = \sum_{i=1}^{n} C_{y_i} \Delta p_i \tag{10.18}$$

$$F_z = \sum_{i=1}^{n} C_{z_i} \Delta p_i \tag{10.19}$$

$$\overline{F_y} = \sum_{i=1}^{n} C_{y_i} \overline{\Delta p_i} \tag{10.20}$$

$$\overline{F_z} = \sum_{i=1}^{n} C_{z_i} \overline{\Delta p_i} \tag{10.21}$$

may be used for calculating the random (actual) wave force and the deterministic wave force on a solid body with an arbitrary configuration. With Eqn (10.11) in Eqns (10.20) and (10.21), we get

$$\overline{F_y}(t_o + T) = \sum_{i=1}^{n} C_{y_i} \frac{H}{2} \cdot \frac{\langle \eta_0(t)\Delta p_i(t+T)\rangle - \langle \eta_0(t)\Delta p_i(t+T-T^*)\rangle}{\langle \eta_0^2(t)\rangle - \langle \eta_0(t)\eta_0(t+T^*)\rangle} \tag{10.22}$$

$$\overline{F_z}(t_o+T) = \sum_{i=1}^{n} C_{zi}\frac{H}{2}\cdot\frac{\langle\eta_0(t)\Delta p_i(t+T)\rangle - \langle\eta_0(t)\Delta p_i(t+T-T^*)\rangle}{\langle\eta_0^2(t)\rangle - \langle\eta_0(t)\eta_0(t+T^*)\rangle} \tag{10.23}$$

Finally, on inverting the order $\sum$ with respect to i—average with respect to t, we arrive at

$$\overline{F_y}(t_o+T) = \frac{\langle\eta_0(t)F_y(t+T)\rangle - \langle\eta_0(t)F_y(t+T-T^*)\rangle}{\langle\eta_0^2(t)\rangle - \langle\eta_0(t)\eta_0(t+T^*)\rangle}\cdot\frac{H}{2} \tag{10.24}$$

$$\overline{F_z}(t_o+T) = \frac{\langle\eta_0(t)F_z(t+T)\rangle - \langle\eta_0(t)F_z(t+T-T^*)\rangle}{\langle\eta_0^2(t)\rangle - \langle\eta_0(t)\eta_0(t+T^*)\rangle}\cdot\frac{H}{2} \tag{10.25}$$

which is the relationship between the deterministic wave force and the random (actual) wave force.

A property that emerged, on the whole, from the two SSFEs was the following:

$$\overline{F_y}(t_o+T) = C_{d_o}\underline{\overline{F}}_y(t_o+T) \tag{10.26}$$

$$\overline{F_z}(t_o+T) = C_{d_v}\underline{\overline{F}}_z(t_o+T) \tag{10.27}$$

where

$\overline{F}$ is the deterministic wave force on the solid cylinder;
$\underline{\overline{F}}$ is the deterministic wave force on the water cylinder;

and C_{d_o} and C_{d_v} are, respectively, the diffraction coefficient of the horizontal wave force, and the diffraction coefficient of the vertical wave force:

$$C_{d_o} = \sqrt{\frac{\langle F_y^2(t)\rangle}{\langle\underline{F}_y^2(t)\rangle}} \tag{10.28}$$

$$C_{d_v} = \sqrt{\frac{\langle F_z^2(t)\rangle}{\langle\underline{F}_z^2(t)\rangle}} \tag{10.29}$$

Both the experiments were concerned with wind seas, and y was close to the dominant wave direction; moreover, in the second experiment, y was also the orthogonal to the horizontal cylinder. A proof of properties (Eqns (10.28) and (10.29)) is shown in Fig. 10.7.

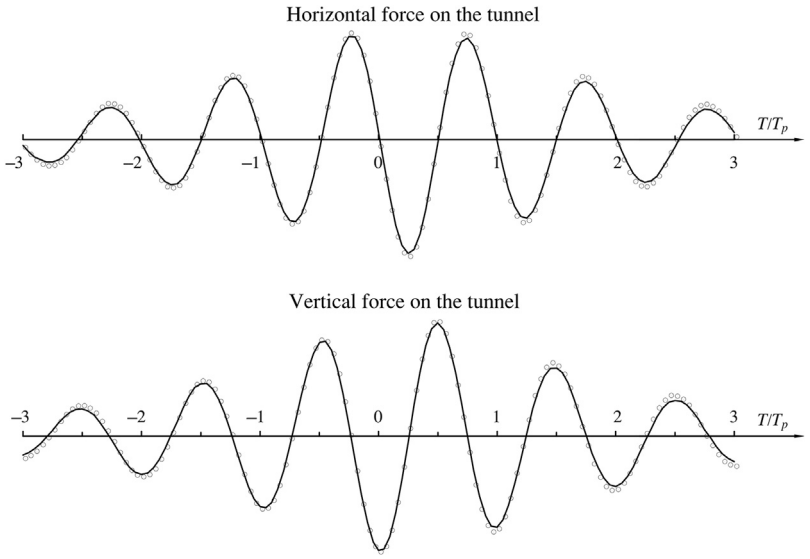

■ **FIGURE 10.7 Small-scale field experiment of 1993.** Solid line: deterministic wave force on the tunnel. Dashed line: product of the diffraction coefficient and the deterministic wave force on the equivalent water cylinder. Deterministic forces obtained on applying the algorithm of the QD theory with the time series data.

10.6 A GENERAL MODEL FOR CALCULATING THE DIFFRACTION COEFFICIENT OF WAVE FORCES

We refer to the sketch of Fig. 10.8 showing the cross-section of a vertical water cylinder. Let us think of the cylinder as being subjected to two horizontal wave forces $\underline{F'_o}(t)$ and $\underline{F''_o}(t)$, the first one acting on the left half-cylinder

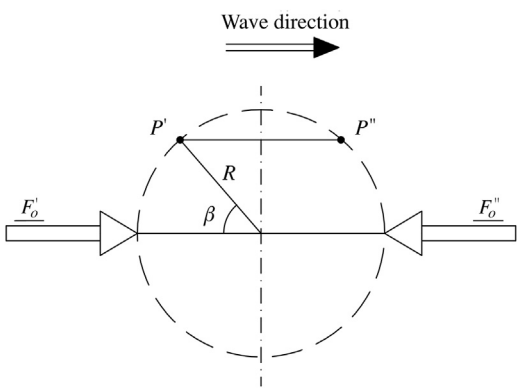

■ **FIGURE 10.8 Reference scheme for Eqns (10.30) and (10.31).**

(the wave beaten half) and the second one acting on the right half-cylinder (the sheltered half).

These forces are

$$\underline{F'_o}(t) = \int_{-\pi/2}^{\pi/2} \Delta p_{\max} \cos(-kR\cos\beta - \omega t) R\cos\beta \mathrm{d}\beta \tag{10.30}$$

$$\underline{F''_o}(t) = \int_{-\pi/2}^{\pi/2} \Delta p_{\max} \cos(kR\cos\beta - \omega t) R\cos\beta \mathrm{d}\beta \tag{10.31}$$

where $\Delta p_{\max}$ is the amplitude of the pressure fluctuation at the given depth. On passing from the water cylinder to the solid cylinder, what changes is only the phase angle: the phase angle of a pair of points like P', P'' grows

$$\text{from} \quad 2kR\cos\beta \quad \text{to} \quad \mathscr{F}_{\mathscr{R}}\, 2kR\cos\beta$$

and we have seen that the phase speed reduction factor $\mathscr{F}_{\mathscr{R}}$ is about 2.

Therefore, the forces F'_o and F''_o on the two halves of the solid cylinder are

$$F'_o(t) = \int_{-\pi/2}^{\pi/2} \Delta p_{\max} \cos(-\mathscr{F}_{\mathscr{R}}\, kR\cos\beta - \omega t) R\cos\beta \mathrm{d}\beta \tag{10.32}$$

$$F''_o(t) = \int_{-\pi/2}^{\pi/2} \Delta p_{\max} \cos(\mathscr{F}_{\mathscr{R}}\, kR\cos\beta - \omega t) R\cos\beta \mathrm{d}\beta \tag{10.33}$$

From Eqns (10.30) and (10.31) and Eqns (10.32) and (10.33), we get

$$\underline{F_y}(t) = \underline{F'_o}(t) - \underline{F''_o}(t) = -2\Delta p_{\max} R \int_{-\pi/2}^{\pi/2} \sin(kR\cos\beta)\sin(\omega t)\cos\beta \mathrm{d}\beta \tag{10.34}$$

$$F_y(t) = F'_o(t) - F''_o(t) = -2\Delta p_{\max} R \int_{-\pi/2}^{\pi/2} \sin(\mathscr{F}_{\mathscr{R}}\, kR\cos\beta)\sin(\omega t)\cos\beta \mathrm{d}\beta \tag{10.35}$$

and hence

$$C_{d_o} \equiv \frac{\sqrt{\langle F_y^2(t)\rangle}}{\sqrt{\langle \underline{F_y^2}(t)\rangle}} = \frac{\left| \int_{-\pi/2}^{\pi/2} \sin(\mathscr{F}_{\mathscr{R}}\, kR\cos\beta)\cos\beta \mathrm{d}\beta \right|}{\left| \int_{-\pi/2}^{\pi/2} \sin(kR\cos\beta)\cos\beta \mathrm{d}\beta \right|} \tag{10.36}$$

The following suggestions proceed from the experience of the two SSFEs of 1992 and 1993:

1. Equation (10.36) may be applied also with horizontal cylinders (provided that the wave attack is orthogonal to the cylinder axis);
2. k in Eqn (10.36) may be calculated with the peak period T_p;
3. $\mathscr{F}_{\mathscr{R}}$ may be taken as 1.75 for a base of a gravity platform, and 2 for columns of a gravity platform and tunnels.

As to C_{d_v} for submerged tunnels, it proved to be about 10% smaller than C_{d_o}. Equation (10.36) and the suggestions enable one to do a quick estimate of the diffraction coefficient. However, we recommend also doing a precise estimate. Then, with the same gauge array suitable for obtaining C_{d_o} and/or C_{d_v} one may also verify the crucial conclusions (Eqns (10.26) and (10.27)).

10.7 OVERALL SYNTHESIS

The conclusion of this chapter consists of Eqns (10.26), (10.27) and (10.36). Equations (10.26) and (10.27) say that extreme wave loads on large isolated bodies are equal to the Froude–Krylov force multiplied by the diffraction coefficient. Equation (10.36) may be used for calculating this coefficient. Equation (10.36) is based on the fact that the horizontal wave force on a large isolated body is greater than the horizontal Froude–Krylov force only because of a reduction of the propagation speed of pressure head waves at the solid body. Hereafter is a FORTRAN program to calculate C_{d_o} by means of Eqn (10.36).

```
      PROGRAM CODIF
      PG=3.141592
      DPG=2.*PG
      G=9.8
      WRITE(6,*)'d,diam,Tp'
      READ(5,*)D,DIAM,TP
      WRITE(6,*)'FR'
      READ(5,*)FR
      R=DIAM/2
      RLPO=(G/DPG)*TP*TP
c RLPO=dominant wavelength on deep water
      RLP=RLPO
75    RL=RLPO*TANH(DPG*D/RLP)
      TEST=ABS(RL-RLP)/RL
      RLP=RL
      IF(TEST.GT.1.E-4)GO TO 75
c RL=dominant wavelength on water depth d
      RK=DPG/RL
      DBETA=PG/200.
```

```
      .BETA1=-PG/2.
       BETA2=PG/2.
       BETA=BETA1-DBETA/2.
c RINTNUM=integral numerator RHS Eqn (10.36)
c RINTDEN=integral denominator RHS Eqn (10.36)
       RINTNUM=0
       RINTDEN=0
c Loop 90: integrals on the RHS of Eqn (10.36)
90     BETA=BETA+DBETA
       IF(BETA.GT.BETA2)GO TO 91
       ARG=FR*RK*R*COS(BETA)
       RINTNUM=RINTNUM+SIN(ARG)*COS(BETA)
       ARG=RK*R*COS(BETA)
       RINTDEN=RINTDEN+SIN(ARG)*COS(BETA)
       GO TO 90
91     CONTINUE
       CDO=ABS(RINTNUM)/ABS(RINTDEN)
       WRITE(6,1000)CDO
1000   FORMAT(2x,'Cdo=',F7.3)
       END
```

10.8 CONCLUSION

The SSFEs of 1992 and 1993 were described, respectively, by the author (1995) and (1996). These were unusual experiments, not only for their nature of SSFEs. For the first time, as far as is known, there was a real-time comparison between measured wave force and measured Froude-Krylov force. Then, the QD theory was exploited to evidence the relationship between actual wave forces and Froude−Krylov forces. In particular, it exploited the fact that the $\overline{\Delta p_i}$ obtained through QD Eqn (10.11) always looks regular, as in Figs 10.4 and 10.5, even though it is obtained from random time-series data of surface elevation and wave pressures. Recently, some experiments to verify the QD theory have been performed in a waveflume (Petrova et al., 2011). Notwithstanding their peculiarity, the SSFEs of 1992, 1993 could also be verified in a waveflume at one's choice.

REFERENCES

Boccotti, P., 1995. A field experiment on the small-scale model of a gravity offshore platform. Ocean Eng. 22, 615−627.

Boccotti, P., 1996. Inertial wave loads on horizontal cylinders: a field experiment. Ocean Eng. 23, 629−648.

Petrova, P., Arena, F., Guedes Soares, C., 2011. Space-time evolution of random wave groups with high waves based on the quasi-determinism theory. Ocean Eng. 38, 1640−1648.

Chapter 11

QD Theory: Mechanics of Reflected and Diffracted Wave Groups

CHAPTER OUTLINE

11.1 BEFORE A BREAKWATER

11.1.1 Equations of Deterministic Waves before an Upright Breakwater

The deterministic surface elevation before a long breakwater, provided that a very large wave of given height H occurs at some given point x_o,y_o, is given by Eqn (8.83) with Eqn (7.29) of Ψ:

$$\overline{\eta}(x_o+X, y_o+Y, t_o+T) = \frac{H}{2}\int_0^{\infty}\int_0^{2\pi} S(\omega,\theta)\cos(k\, y_o\cos\theta)\cos[k(y_o+Y)\cos\theta]\cdot\{\cos(kX\sin\theta-\omega T) - \cos[kX\sin\theta-\omega(T-T^*)]\}\mathrm{d}\theta\mathrm{d}\omega \Big/ \int_0^{\infty}\int_0^{2\pi} S(\omega,\theta)\cos^2(k\, y_o\cos\theta) \times[1-\cos(\omega T^*)]\mathrm{d}\theta\mathrm{d}\omega \tag{11.1}$$

Wave Mechanics and Wave Loads on Marine Structures. http://dx.doi.org/10.1016/B978-0-12-800343-5.00011-1

As to T^*, it is the lag of the minimum of

$$\Psi(0,0,T;x_o,y_o) = 4\int_0^{\infty}\int_0^{2\pi} S(\omega,\theta)\cos^2(k\,y_o\cos\theta)\cos(\omega T)\mathrm{d}\theta\mathrm{d}\omega \qquad (11.2)$$

The deterministic velocity potential $\overline{\phi}$ is given by Eqn (8.84) with Eqn (7.30) of Φ:

$$\begin{aligned}&\overline{\phi}(x_o+X,y_o+Y,z,t_o+T)\\&= g\frac{H}{2}\int_0^{\infty}\int_0^{2\pi} S(\omega,\theta)\omega^{-1}\frac{\cosh[k(d+z)]}{\cosh(kd)}\cos(k\,y_o\cos\theta)\cdot\cos[k(y_o+Y)\cos\theta]\\&\quad\times\{\sin(kX\sin\theta-\omega T)-\sin[kX\sin\theta-\omega(T-T^*)]\}\mathrm{d}\theta\mathrm{d}\omega/\\&\quad\int_0^{\infty}\int_0^{2\pi} S(\omega,\theta)\cos^2(k\,y_o\cos\theta)[1-\cos(\omega T^*)]\mathrm{d}\theta\mathrm{d}\omega\end{aligned} \qquad (11.3)$$

The deterministic wave pressure $\overline{\Delta p}$ proceeds on differentiating $\overline{\phi}$ with respect to time T, and multiplying by $(-\rho)$. The result is

$$\begin{aligned}&\overline{\Delta p}(x_o+X,y_o+Y,z,t_o+T)\\&= \rho g\frac{H}{2}\int_0^{\infty}\int_0^{2\pi} S(\omega,\theta)\frac{\cosh[k(d+z)]}{\cosh(kd)}\cos(k\,y_o\cos\theta)\cdot\cos[k(y_o+Y)\cos\theta]\\&\quad\times\{\cos(kX\sin\theta-\omega T)-\cos[kX\sin\theta-\omega(T-T^*)]\}\mathrm{d}\theta\mathrm{d}\omega/\\&\quad\int_0^{\infty}\int_0^{2\pi} S(\omega,\theta)\cos^2(ky_o\cos\theta)[1-\cos(\omega T^*)]\mathrm{d}\theta\mathrm{d}\omega\end{aligned} \qquad (11.4)$$

The horizontal particle velocity and acceleration proceed on differentiating $\overline{\phi}$ with respect to X or Y, and with respect to T and X or Y. The result is

$$\overline{v_x}(x_o + X, y_o + Y, z, t_o + T)$$
$$= g\frac{H}{2}\int_0^{\infty}\int_0^{2\pi} S(\omega,\theta)\omega^{-1}k\sin\theta\frac{\cosh[k(d+z)]}{\cosh(kd)}\cos(k\,y_o\cos\theta)$$
$$\cdot\cos[k(y_o + Y)\cos\theta]\{\cos(kX\sin\theta - \omega T) - \cos[kX\sin\theta - \omega(T - T^*)]\}\mathrm{d}\theta\mathrm{d}\omega/$$
$$\int_0^{\infty}\int_0^{2\pi} S(\omega,\theta)\cos^2(k\,y_o\cos\theta)[1 - \cos(\omega T^*)]\mathrm{d}\theta\mathrm{d}\omega \tag{11.5}$$

$$\overline{v_y}(x_o + X, y_o + Y, z, t_o + T)$$
$$= -g\frac{H}{2}\int_0^{\infty}\int_0^{2\pi} S(\omega,\theta)\omega^{-1}k\cos\theta\frac{\cosh[k(d+z)]}{\cosh(kd)}\cos(k\,y_o\cos\theta)$$
$$\cdot\sin[k(y_o + Y)\cos\theta]\{\sin(kX\sin\theta - \omega T) - \sin[kX\sin\theta - \omega(T - T^*)]\}\mathrm{d}\theta\mathrm{d}\omega/$$
$$\int_0^{\infty}\int_0^{2\pi} S(\omega,\theta)\cos^2(k\,y_o\cos\theta)[1 - \cos(\omega T^*)]\mathrm{d}\theta\mathrm{d}\omega \tag{11.6}$$

$$\overline{a_x}(x_o + X, y_o + Y, z, t_o + T)$$
$$= g\frac{H}{2}\int_0^{\infty}\int_0^{2\pi} S(\omega,\theta)k\sin\theta\frac{\cosh[k(d+z)]}{\cosh(kd)}\cos(k\,y_o\cos\theta)\cdot\cos[k(y_o + Y)\cos\theta]$$
$$\times\{\sin(kX\sin\theta - \omega T) - \sin[kX\sin\theta - \omega(T - T^*)]\}\mathrm{d}\theta\mathrm{d}\omega/$$
$$\int_0^{\infty}\int_0^{2\pi} S(\omega,\theta)\cos^2(k\,y_o\cos\theta)[1 - \cos(\omega T^*)]\mathrm{d}\theta\mathrm{d}\omega \tag{11.7}$$

$$\overline{a_y}(x_o + X, y_o + Y, z, t_o + T)$$
$$= g\frac{H}{2}\int_0^{\infty}\int_0^{2\pi} S(\omega,\theta)k\cos\theta\frac{\cosh[k(d+z)]}{\cosh(kd)}\cos(k\,y_o\cos\theta)\cdot\sin[k(y_o + Y)\cos\theta]$$
$$\times\{\cos(kX\sin\theta - \omega T) - \cos[kX\sin\theta - \omega(T - T^*)]\}\mathrm{d}\theta\mathrm{d}\omega/$$
$$\int_0^{\infty}\int_0^{2\pi} S(\omega,\theta)\cos^2(k\,y_o\cos\theta)[1 - \cos(\omega T^*)]\mathrm{d}\theta\mathrm{d}\omega \tag{11.8}$$

11.1.2 Occurrence of Exceptionally Large Waves before an Upright Breakwater

Figure 11.1 answers the question "what happens if a wave of a given, exceptionally large height, occurs at a point x_o,y_o at the breakwater?" This point is at the center of the framed part of the breakwater. The figure was obtained with Eqn (11.1), with the input data: deep water; spectrum: mean JONSWAP; directional distribution: Mitsuyasu et al. with $n_p = 20$. We see a wave group that approaches the breakwater, hits it, is reflected, and goes back seawards. It will have been noted that, while the wave group is approaching the wall, its envelope gradually shrinks, and, on the contrary, while the wave group goes back seawards, the envelope stretches. This means that the wave group is at the apex of its development stage when it arrives at the breakwater. In short, the answer is: if you record an exceptionally high wave at the wall, most probably, it is the central wave of a group hitting the breakwater, at the apex of its development stage.

Let us pass to a new question: what happens if a wave of a given, exceptionally large height, occurs at a point x_o,y_o, which is $3L_p$ before the breakwater? The answer is given in Fig. 11.2, which shows a big novelty: two groups! The first wave group hits the breakwater at time $T = -6T_p$, is reflected, goes back seawards, and collides with the second wave group approaching the breakwater.

The central waves of the two groups strike each other at the fixed point x_o,y_o, yielding the given, exceptionally large wave height. This wave height is very large because both wave groups reach the apex of their development when they come into collision. Thus, we realize why the maximum expected wave height far from the breakwater is smaller than the maximum expected wave height at the breakwater (on applying Eqn (7.49) one finds that $H_{\max}$ at any point distant from the wall more than $2L_p$ is about $1/\sqrt{2}$ times smaller than $H_{\max}$ at a point at the breakwater). The reason is that an exceptionally large wave far from the breakwater calls for an event that has a probability to occur, which is small in comparison to the probability of the event yielding an exceptionally large wave at the breakwater.

Finally, Fig. 11.3 shows what we may expect to happen if a wave of a given, exceptionally large height should occur at some given point of a breakwater, if the dominant wave direction of the incident waves makes a 20° angle with the wall-orthogonal. We see that the wave group travels in the dominant direction of the spectrum, hits the wall at the apex of the development stage, is subjected to specular reflection, and returns seawards.

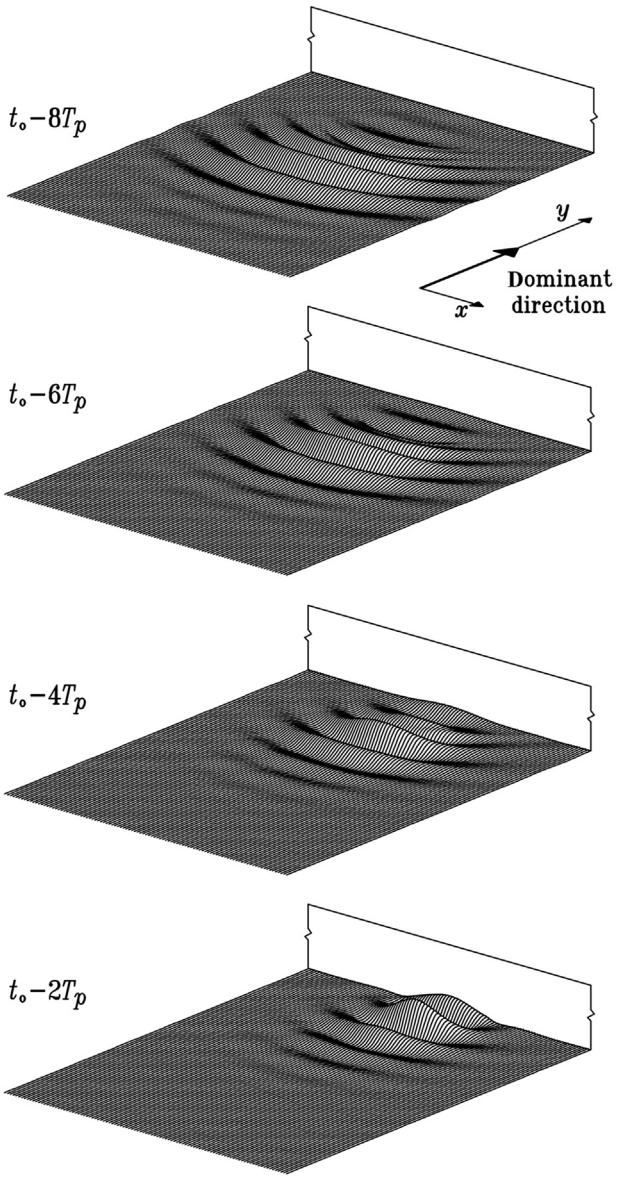

■ **FIGURE 11.1** If x_o, y_o is at an upright breakwater, deterministic wave function Eqn (8.83) represents a wave group that strikes this point, at the apex of its development stage.

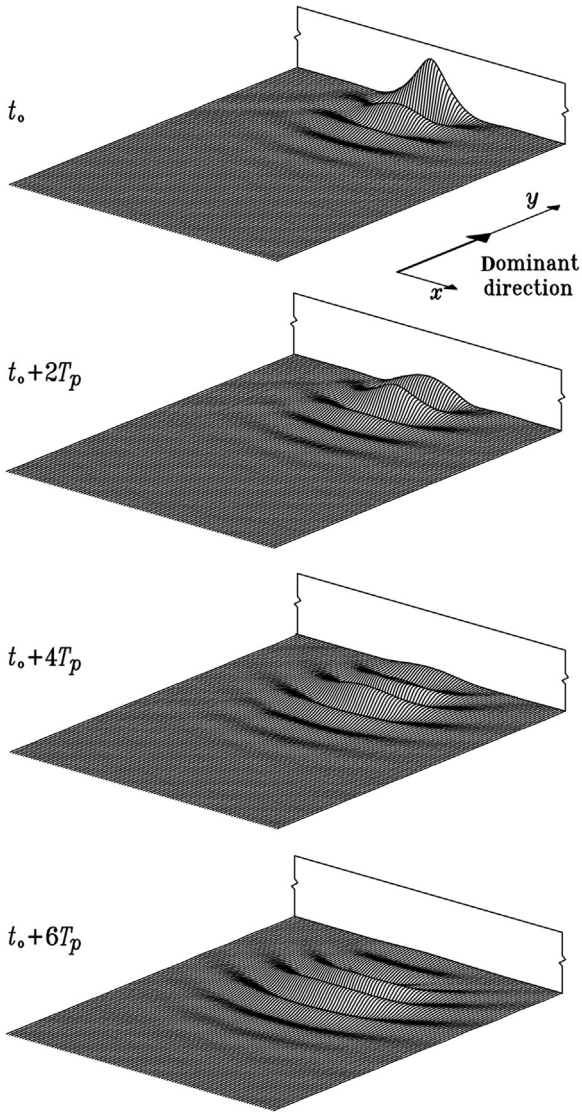

■ **FIGURE 11.1** Continued

11.1.3 Wave Loads on Structures

When an exceptionally large wave occurs at some point x_o,y_o of a breakwater, the segment of breakwater loaded by the wave crest will be particularly short, as we may see in Figs 11.1 and 11.3. The QD theory shows that the wave crest of an exceptionally large wave *must* be particularly short,

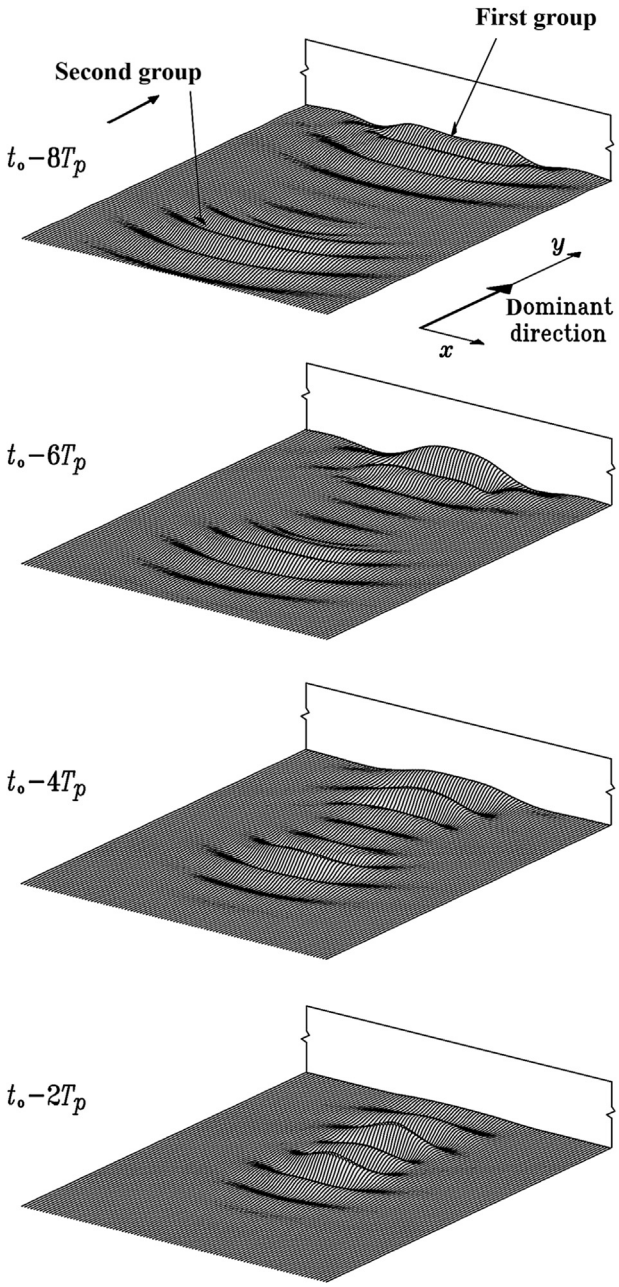

■ **FIGURE 11.2** If x_o, y_o is at a certain distance before an upright breakwater, deterministic wave function Eqn (8.83) represents two wave groups that strike each other at this point, the first one going back seawards after having been reflected, and the second one approaching the breakwater.

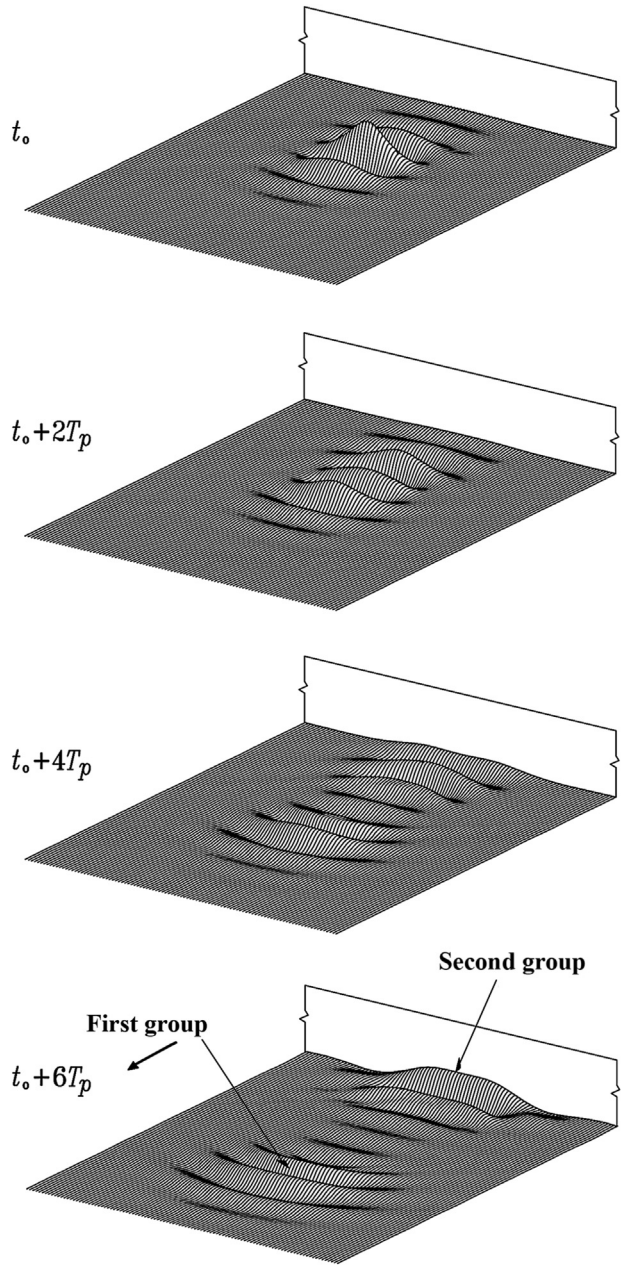

■ **FIGURE 11.2** Continued

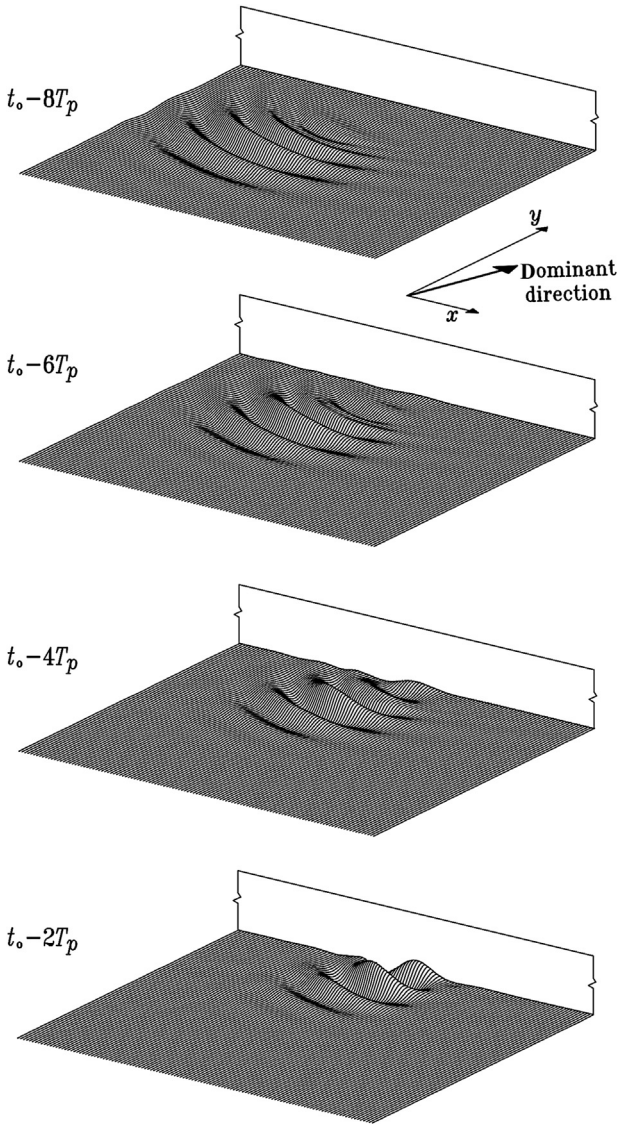

■ **FIGURE 11.3** If x_o, y_o is at an upright breakwater, and the dominant direction of the spectrum of the incident waves is inclined with respect to the wall-orthogonal; deterministic wave function Eqn (8.83) represents a wave group that strikes this point, and is subject to specular reflection.

given that an exceptionally large wave is yielded by a progressive focusing of the three-dimensional envelope, as it is evident in the two aforementioned figures. As a consequence, the effect of an exceptionally large wave on a breakwater is somewhat like the effect of a weapon fired from offshore.

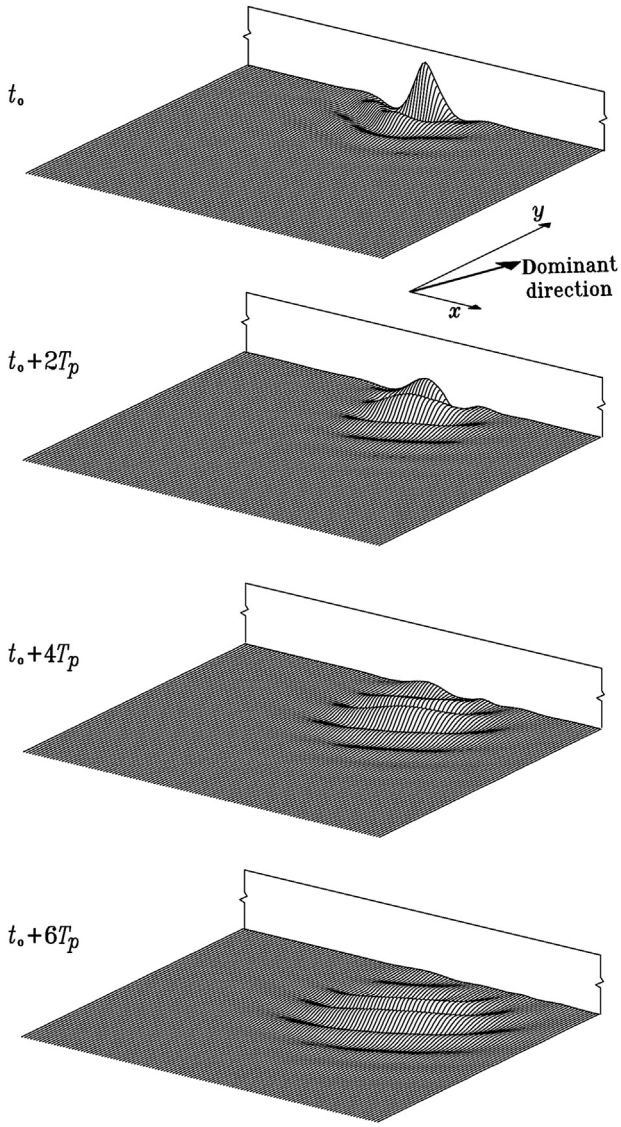

■ **FIGURE 11.3** Continued

Equations (11.5)—(11.8) may be applied for estimating extreme wave loads on various kinds of structures that may be in the sea area before a breakwater (e.g., mooring points, conduits). As an example, let us consider the loads on a vertical pile off a vertical breakwater. An exceptionally large wave at this pile most probably is due to the collision of two wave groups, as we have seen in Fig. 11.2. This exceptionally large wave is a standing wave being

yielded by the overlap of the central wave of the first group traveling seawards and the central wave of the second group traveling landwards. Point x_o,y_o is an isolated offshore antinode. Since the horizontal particle velocity and acceleration is zero at an antinode, if x_o,y_o is at the location of the pile, the pile is not loaded. Then we let vary x_o,y_o in a neighborhood of the location of the pile. If the dominant direction of the incident waves is orthogonal to the breakwater, the x_o,y_o for which we shall find the heaviest load on the pile is

$$x_o, y_o = x'_o, y'_o - L_p/4 \tag{11.9}$$

where x'_o, y'_o are the coordinates of the pile. In this case, the pile will be at the location of an isolated offshore node. The wave forces on the pile will be calculated with the Morison equation, with the particle velocities and accelerations being given by Eqns (11.5)–(11.8). Of course, H in these equations will be the maximum expected wave height in the design sea state at point x_o,y_o, which is dealt with in Section 7.4.

11.2 IN THE LEE OF A BREAKWATER

11.2.1 Equations of Deterministic Waves in the Lee of a Breakwater

With a semi-infinite breakwater the deterministic surface elevation, provided that a very large wave of given height H occurs at some given point x_o,y_o, is given by Eqn (8.83) with Eqn (7.41) of Ψ:

$$\begin{aligned}
&\overline{\eta}(R,\beta,T;r_o,\beta_o)\\
&= \frac{H}{2}\int_0^{\infty}\int_0^{2\pi} S(\omega,\theta)\{[F(r_o,\beta_o;\omega,\theta)F(R,\beta;\omega,\theta)\\
&\quad + G(r_o,\beta_o;\omega,\theta)G(R,\beta;\omega,\theta)][\cos(\omega T) - \cos(\omega T - \omega T^*)] + [F(r_o,\beta_o;\omega,\theta)\\
&\quad \cdot G(R,\beta;\omega,\theta) - G(r_o,\beta_o;\omega,\theta)F(R,\beta;\omega,\theta)]\\
&\quad \times[\sin(\omega T) - \sin(\omega T - \omega T^*)]\}\mathrm{d}\theta\mathrm{d}\omega /\\
&\int_0^{\infty}\int_0^{2\pi} S(\omega,\theta)\left[F^2(r_o,\beta_o;\omega,\theta) + G^2(r_o,\beta_o;\omega,\theta)\right]\left[1 - \cos\left(\omega T^*\right)\right]\mathrm{d}\theta\mathrm{d}\omega
\end{aligned} \tag{11.10}$$

As to T^*, it is the lag of the minimum of

$$\begin{aligned}
&\Psi(r_o,\beta_o,T;r_o,\beta_o)\\
&\quad = \int_0^{\infty}\int_0^{2\pi} S(\omega,\theta)\left[F^2(r_o,\beta_o;\omega,\theta) + G^2(r_o,\beta_o;\omega,\theta)\right]\cdot\cos(\omega T)\mathrm{d}\theta\mathrm{d}\omega
\end{aligned} \tag{11.11}$$

11.2.2 Occurrence of Exceptionally Large Waves in the Lee of a Breakwater

The C_d (and consequently the maximum expected wave height) is surprisingly high in the dark area of Fig. 7.2. On the other hand, the C_d in the more sheltered area is practically the same as the C_d of the periodic waves. What is the reason for this? To answer this question, let us see what we may expect to happen when the maximum expected wave height in a design sea state occurs at a point x_o,y_o of the more sheltered area; and what we may expect to happen when the maximum expected wave height occurs at a point x_o,y_o of the "dark area."

As to the point of the more sheltered area, we fix

$$x_o = 1.5L_p, \quad y_o = 0_+,$$

where 0_+ means "in contact with the lee wall." Figure 11.4 shows what happens when the maximum expected wave height occurs at this point: a wave group strikes the breakwater's tip in full; thus, one half of the wave crest hits the wall and one half enters the sheltered area and produces the exceptionally large wave height at the fixed point. As to the point of the "dark area," we fix

$$x_o = L_p, \quad y_o = 4L_p.$$

Figure 11.5 shows what happens when the maximum expected wave height occurs at this point. Here, we see a novelty: for the first time, the QD theory shows a wave group that does not travel in the dominant direction of the spectrum: the dominant direction is wall-orthogonal, whereas the group attacks from the left side. This wave group only grazes the tip of the breakwater with its right wing. The conclusion is evident: some wave groups with a direction slightly different from the dominant direction of the spectrum can nearly strike home the dark area. This is the reason why the maximum expected wave height in the dark area of the geometric shadow proves to be unexpectedly large. This possibility does not exist with the periodic waves, which are strictly unidirectional.

11.3 EXPERIMENTAL VERIFICATION

All that has been said in Section 9.4 re field verification of the QD theory holds for every configuration of the solid boundary. In 2011, an SSFE was performed with an array of 24 gauges along the y-axis orthogonal to a vertical breakwater—see Fig. 11.6. Figure 11.7 compares the random waves to the deterministic waves, in a case of $H/\sigma = 9.90$. It was the largest value of this ratio in the whole experiment. As we may see, the overall agreement

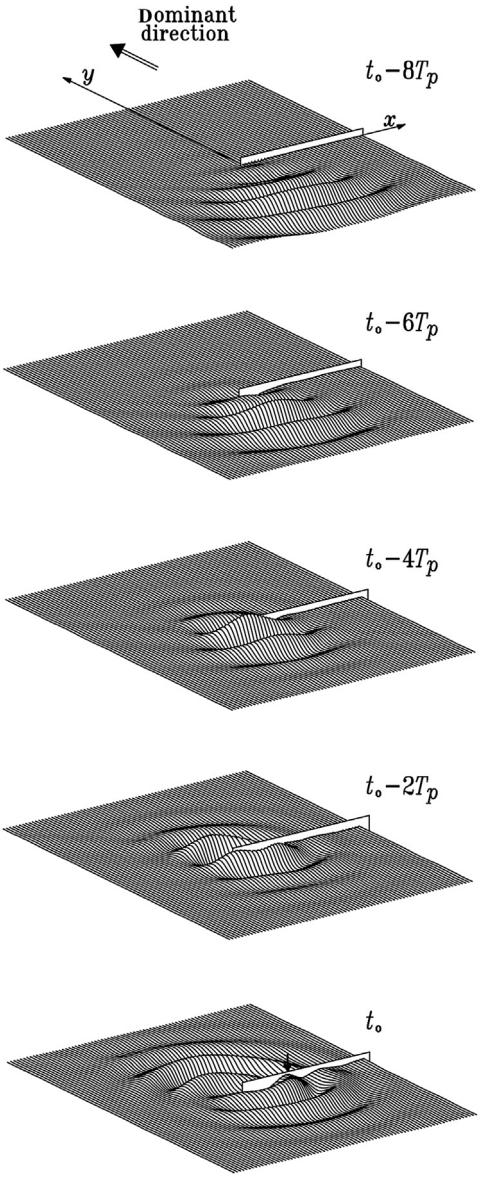

■ **FIGURE 11.4** If x_o, y_o is at the lee wall of a breakwater, deterministic wave function Eqn (8.83) represents a wave group that strikes the tip of the breakwater; and then one half of the wave crest penetrates the geometric shadow, by diffraction.

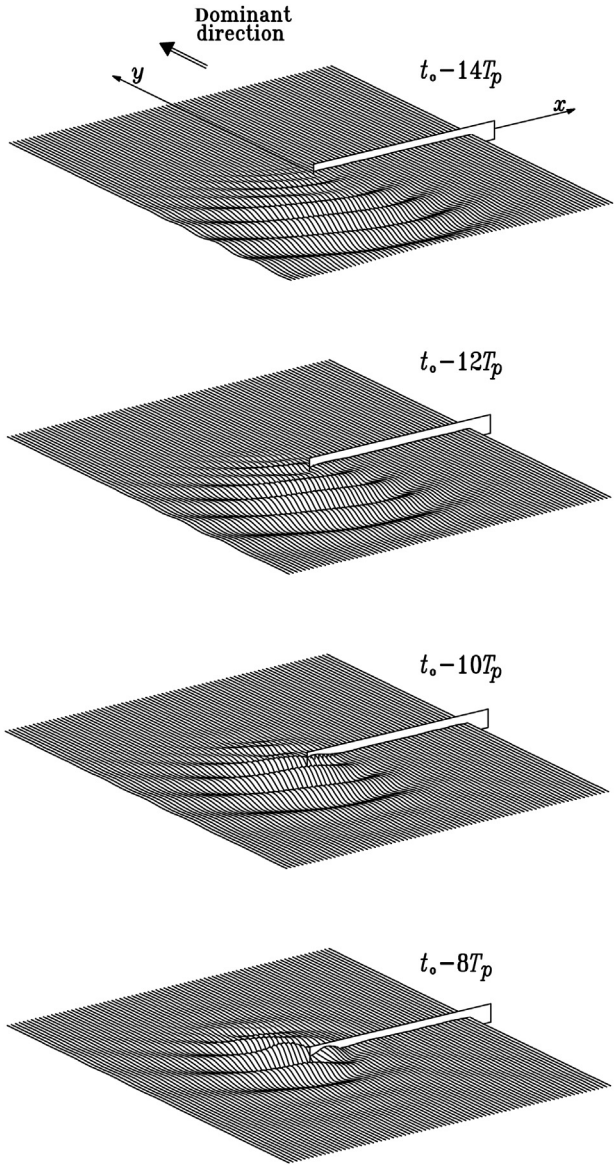

■ **FIGURE 11.5** If x_o, y_o is in the dark area of the geometric shadow of a breakwater (see Fig. 7.2), deterministic wave function Eqn (8.83) represents a wave group that can nearly strike this point, thanks to a small deviation from the dominant direction (the dominant direction of the spectrum of the incident waves is wall-orthogonal, whereas the direction of the wave group is slightly inclined).

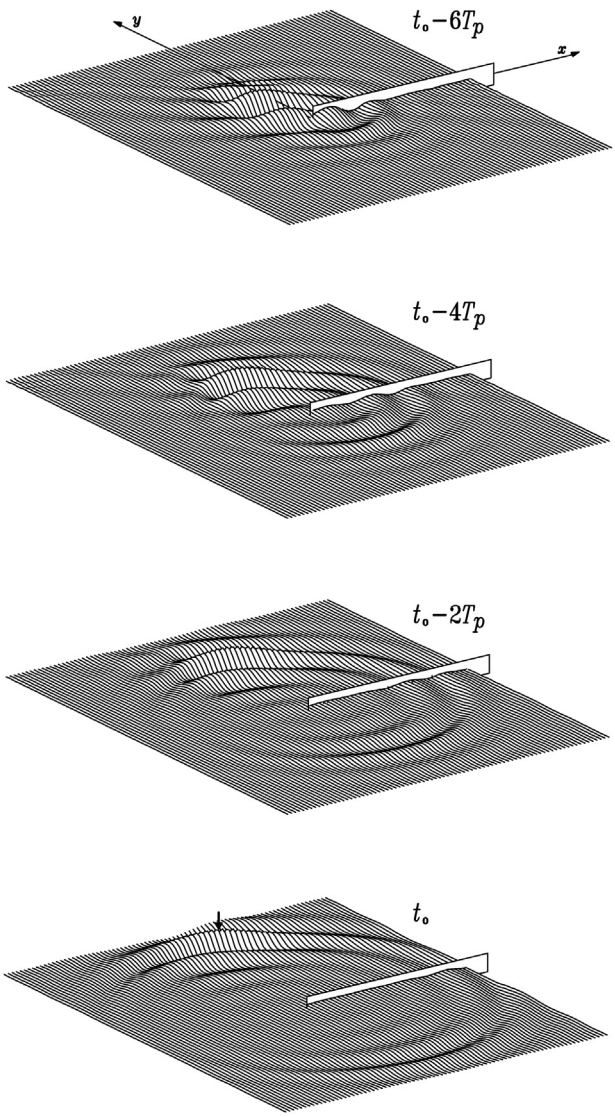

■ **FIGURE 11.5** Continued

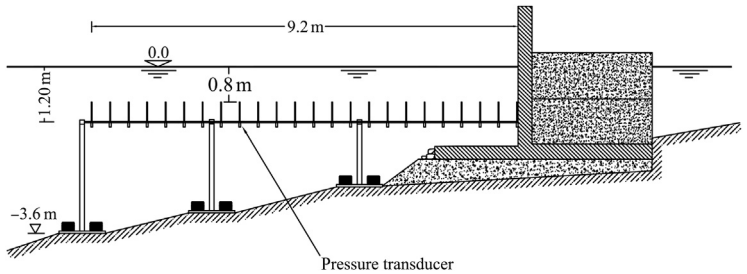

■ **FIGURE 11.6 The gauges of a recent small-scale field experiment (2011) aimed to verify the QD theory.** There was an array of 24 pressure transducers, each of which is being connected with a small vertical tube with a bending section (like a small periscope). Pressure head waves were measured 0.80 m beneath the MWL.

between the deterministic waves and the random waves is strong even if we are dealing with a case of a nonhomogeneous wave field, which is more complex than a wave field in an open sea. Figure 11.7 proves that the interaction of wave group and breakwater described by the QD theory occurs in the field. Specifically, the figure shows the occurrence of an exceptionally large wave height at the second antinode (at one-half wave length from the breakwater). According to the QD theory, this is due to a wave group that strikes the breakwater, when at the center of the envelope, there are two waves of nearly the same height: the first one that has just left the center of the group and the next one that is going to replace the first one at the center of the group. The wave of exceptionally large height at one-half wave length from the wall has its crest at instant t_o and the trough at instant $t_o + 1.5$ s. The two consecutive waves of nearly the same large height at the breakwater are: that with crest at $t_o - 1.4$ s and trough at $t_o + 0.1$ s, and that with crest at $t_o + 1.6$ s and trough at $t_o + 3.1$ 1s.

11.4 CONCLUSION

This part of the QD theory was disclosed by the author (1988). A first SSFE to verify the part of the QD theory concerning interactions between wind seas and vertical breakwaters was performed in 1991, and was described by the author (1997). It provided a confirmation that an exceptionally large wave off a vertical breakwater is yielded by the collision of two wave groups. However, that early experiment enabled only to test the predictions of the theory in the time domain at a discrete number of points. The SSFE of 2011, with its test of the theory in the space domain, was described by the author (2013). Some nonlinearity effects on the QD theory for what concerns interactions with vertical breakwaters have been dealt with by Romolo and Arena (2008, 2013).

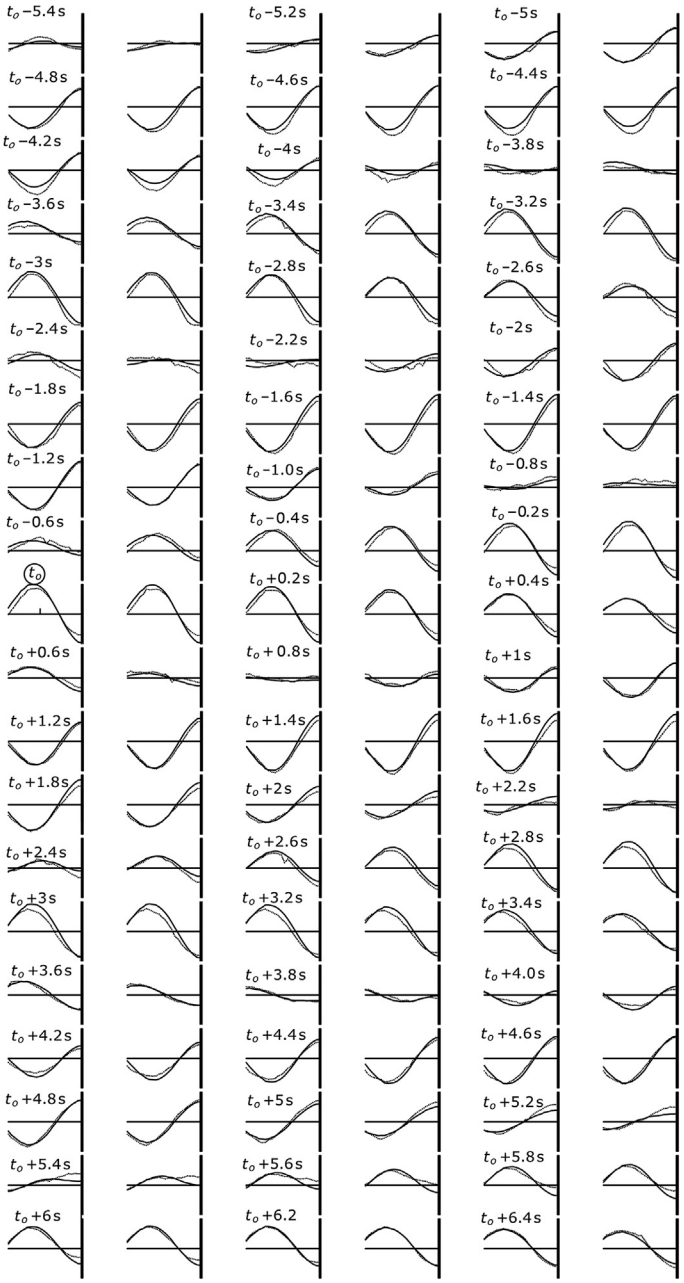

■ **FIGURE 11.7 Small-scale field experiment of 2011.** What happened when a zero up-crossing wave of $H/\sigma = 9.90$ was recorded by gauge no. 16 (the location of this gauge is shown by a small vertical segment in the picture relevant to time instant t_o). Dashed line: actual (random) wave. Continuous line: deterministic wave.

REFERENCES

Boccotti, P., 1988. Refraction, reflection and diffraction of irregular gravity waves. Excerpta Ital. Contrib. Field Hydraul. Eng. 3, 47–89.

Boccotti, P., 1997. A general theory of three-dimensional wave groups. Part II: interaction with a breakwater. Ocean Eng. 24 (3), 281–300.

Boccotti, P., 2013. Field verification of quasi-determinism theory for wind waves interacting with vertical breakwater. J. Waterway Port Coast. Ocean Eng. 139, 358–364.

Romolo, A., Arena, F., 2008. Mechanics of nonlinear random wave groups interacting with a vertical wall. Phys. Fluids 20, 1–16, 036604.

Romolo, A., Arena, F., 2013. Three-dimensional non-linear standing wave groups: formal derivation and experimental verification. Int. J. Non-linear Mech. 57, 220–239.

Chapter 12

Calculation of Wave Forces on Three-Dimensional Space Frames

CHAPTER OUTLINE

12.1 MORISON EQUATION AND DRAG AND INERTIA COEFFICIENTS

The sectional in-line force for the cylindrical members of a jacket platform is usually calculated by means of the Morison equation (Morison et al., 1950). With circular cylinders, this equation may be written in the form

$$\mathbf{f}(t) = C_{in}\rho\pi R^2\mathbf{a}_{\text{sect}} + C_{dg}\rho R v_{\text{sect}}\mathbf{v}_{\text{sect}} \tag{12.1}$$

where $\mathbf{v}_{\text{sect}}$ is the component of the local velocity vector, of the water, normal to the axis of the member; and $\mathbf{a}_{\text{sect}}$ is the component of the local acceleration vector, of the water, normal to the axis of the member. Here, we are interested only in the mechanics of the forces exerted by the largest waves on a whole frame structure. For a view of the conventional way to apply the Morison equation (for example: how is it considered the effect of a current; or what are the prescribed values of C_{in} and C_{dg}) or for a view of the various loads in the design of fixed space frame structures, reference is made to the

Wave Mechanics and Wave Loads on Marine Structures. http://dx.doi.org/10.1016/B978-0-12-800343-5.00012-3

handbook edited by Chakrabarti (2005) (see, in particular, contribution by Karsan (2005).

The inertia coefficient C_{in} and the drag coefficient C_{dg} depend on the Keulegan−Carpenter number (K_E) and the Reynolds number (R_E):

$$K_E \equiv \frac{v_{\max} T}{D} \tag{12.2}$$

$$R_E \equiv \frac{v_{\max} D}{\upsilon} \tag{12.3}$$

The relationship between C_{in}, C_{dg} and K_E, R_E is well-known thanks to the widespread plots of the book of Sarpkaya and Isaacson (1981), which are based on the work of Sarpkaya (1975, 1977, 1979). C_{in} increases with the increasing of R_E in a different manner according to K_E. C_{dg} decreases with the increasing of R_E in a different manner according to K_E, reaches a minimum, and then tends to an asymptotic value. Both C_{in} and C_{dg} are close to their asymptotes, for

$$R_E > 10^4 K_E, \quad \text{that is for} \tag{12.4a}$$

$$\frac{D^2}{\upsilon T} > 10^4 \tag{12.4b}$$

Given that the wave period of wind-generated waves typically is smaller than 20 s, a sufficient condition for C_{in} and C_{dg} being close to their asymptotic values is that

$$D > 0.45 \text{ m} \tag{12.5}$$

Sarpkaya's asymptotic values are 1.85 and 0.62, respectively, for C_{in} and C_{dg}. These values of C_{in} and C_{dg} are valid for smooth pipes. For roughened pipes (with rigid and/or soft excrescencies), the asymptotic value of C_{dg} grows (even markedly), and the asymptotic value of C_{in} decreases. Sumer and Fredsoe (1997), basing themselves on data of Justesen (1989), suggested a partially different picture for the smooth pipes. Specifically, on the range $6 \leq K_E \leq 20$ the asymptotic value of C_{in} is smaller than 1.85 and that of C_{dg} is greater than 0.62. The largest deviations occur at K_E of $10 \div 15$, where the asymptote of C_{in} falls at about 1.45 and the asymptote of C_{dg} rises up to nearly 1.0.

Besides the in-line force, there is a transverse (lift) force that is related to vortex shedding. For a vertical cylinder, the ratio between the frequency of the transverse force and the wave frequency generally grows with K_E (e.g., Williamson, 1985). In most cases of practical interest, the amplitude of the transverse force is markedly smaller than the amplitude of the drag component of the in-line force, as may be inferred from the above cited plots

in the book of Sarpkaya and Isaacson. For most range of K_E, the transverse force is irregular even if the wave is periodic (Hayashi and Takenouchi, 1985).

12.2 FIELD TESTS OF MORISON EQUATION

12.2.1 A Recent Method for Obtaining C_{in} and C_{dg}

The Morison equation gives any component of the sectional force on a cylinder that is either f_x, f_y, or f_z in the form

$$f_c(t) = C_{in}\hat{f}_{in}(t) + C_{dg}\hat{f}_{dg}(t) \tag{12.6}$$

Here, as said, f_c stands for either f_x, f_y, or f_z; $\hat{f}_{in}$ depends on particle acceleration; and $\hat{f}_{dg}$ depends on particle velocity. In a sea state, $\hat{f}_{in}(t)$ and $\hat{f}_{dg}(t)$ are stationary random functions. The problem is: provided that one knows $\hat{f}_{in}(t)$ and $\hat{f}_{dg}(t)$, find a pair C_{in}, C_{dg} such that the random function $f_c(t)$ (where the subscript c stands for "calculated") has the same basic statistical properties as the random function $f_m(t)$, which represents the x, y, or z component of the measured sectional force (being known). If the equality

$$\langle f_c^n(t)\rangle = \langle f_m^n(t)\rangle \tag{12.7}$$

was satisfied for every integer n, $f_c(t)$ would be equal to $f_m(t)$. Of course, we can find values of C_{in} and C_{dg} that satisfy only two of the infinite Eqn (12.7), and sometimes the solution does not exist (in particular, C_{in} and C_{dg} that satisfy Eqn (12.7) with $n = 2$ and $n = 4$ may not exist).

An effective method is obtaining C_{in} and C_{dg} so that the two following equations are satisfied:

$$\langle f_c^2(t)\rangle = \langle f_m^2(t)\rangle \tag{12.8}$$

$$\frac{\langle f_c(t)\hat{f}_{dg}(t)\rangle}{\langle f_c(t)\hat{f}_{in}(t)\rangle} = \frac{\langle f_m(t)\hat{f}_{dg}(t)\rangle}{\langle f_m(t)\hat{f}_{in}(t)\rangle} \tag{12.9}$$

The first equation is necessary because f_c must have the same variance as f_m. The second equation, conceptually, is like Eqn (12.7): it says that the result of a given operation must be the same either done with the f_c (LHS) or with the f_m (RHS). The two equations are of the type

$$\alpha_1 C_{dg}^2 + \alpha_2 C_{in}^2 = \alpha_3 \tag{12.10}$$

$$C_{dg} = \alpha_4 C_{in} \tag{12.11}$$

where the α_1, α_2, α_3, and α_4, are all known, and α_1, α_2, α_3 are greater than 0. (To check the step from Eqns (12.9)–(12.11), note that $\langle \hat{f}_{dg}(t)\hat{f}_{in}(t)\rangle = 0$).

The C_{in} and C_{dg} plotted in Fig. 12.1 have been obtained with these equations for submerged horizontal cylinders. K_E, the abscissa, represents the Keulegan–Carpenter number of the sea state as a whole (later, we shall see the technique of calculation of this K_E). The plot of Fig. 12.1(a) shows that $C_{dg}(K_E)$ clearly intersects the horizontal coordinate axis close to $K_E = 5$: for $K_E < 5$, C_{dg} is negative. This phenomenon is confirmed essentially in the same way by an experiment with a truncated vertical cylinder. The domain where C_{dg} is negative is a domain where the drag force plays

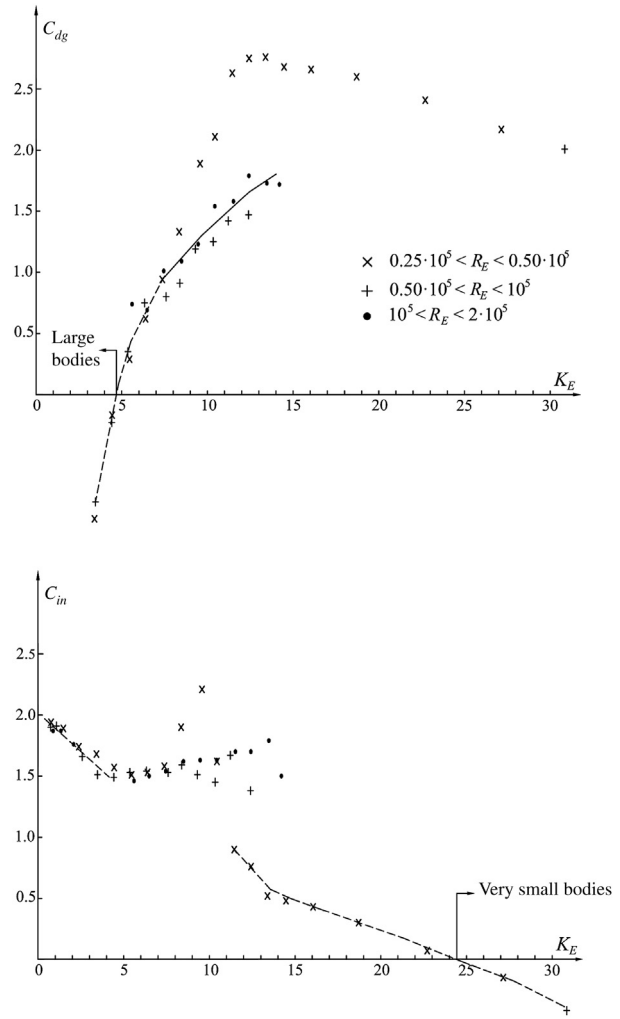

■ **FIGURE 12.1 Drag and inertia coefficient for a submerged horizontal cylinder as functions of K_E for several values of R_E.** *Obtained from an SSFE of 2009—2011.*

a negligible role. Hence, nature itself shows a clear-cut boundary for the domain of *large bodies* where the drag force gets negligible. A nearly specular situation proves to occur with K_E greater than about 25, where the inertia force plays a negligible role, and C_{in} takes on negative values. This could be called the domain of *very small bodies*.

The existence of ranges wherein C_{dg} and C_{in} take on opposite values has been found thanks to the linear form of Eqn (12.11). However, there are two more useful consequences of Eqn (12.11). The first is that Eqn (12.11), together with the commonly used Eqn (12.10), yields C_{in} and C_{dg} for every sea state. The second is that the C_{in} and C_{dg} obtained with Eqns (12.10) and (12.11) give a random process $f_c(t)$ that has the same basic statistical properties as the random process $f_m(t)$, as we are going to see, and this is all that counts from an engineering point of view.

12.2.2 Distribution of the Peaks of the Measured Wave Force and of the Force Calculated with the Morison Equation

Two small-scale field experiments (SSFEs), one on truncated vertical cylinders, and one on horizontal cylinders, were performed in 2009–2011. Cylinders of various diameters were used for each of the two experiments.

The f_m was obtained with an array of eight pressure transducers (see Fig. 12.2). The $\hat{f}_{in}$ and $\hat{f}_{dg}$ for the f_y on a horizontal cylinder are given by

$$\hat{f}_{in} = \rho\pi R^2 a_y \tag{12.12}$$

$$\hat{f}_{dg} = \rho R\sqrt{v_y^2 + v_z^2}\, v_y \tag{12.13}$$

where

$$v_y = g\sum_{i=1}^{N} a_i A_{1_i}(z_c)\omega_i^{-1} k_i \cos(\theta_i)\cos(-\omega_i t + \varepsilon_i) \tag{12.14}$$

$$v_z = g\sum_{i=1}^{N} a_i A_{2_i}(z_c)\omega_i^{-1} k_i \sin(-\omega_i t + \varepsilon_i) \tag{12.15}$$

$$a_y = g\sum_{i=1}^{N} a_i A_{1_i}(z_c) k_i \cos(\theta_i)\sin(-\omega_i t + \varepsilon_i) \tag{12.16}$$

and z_c is the depth of the cylinder center and $A_{1_i}(z)$ and $A_{2_i}(z)$ give the attenuation with depth:

$$A_{1_i}(z) = \frac{\cosh[k_i(d+z)]}{\cosh(k_i d)}, \quad A_{2_i}(z) = \frac{\sinh[k_i(d+z)]}{\cosh(k_i d)} \tag{12.17}$$

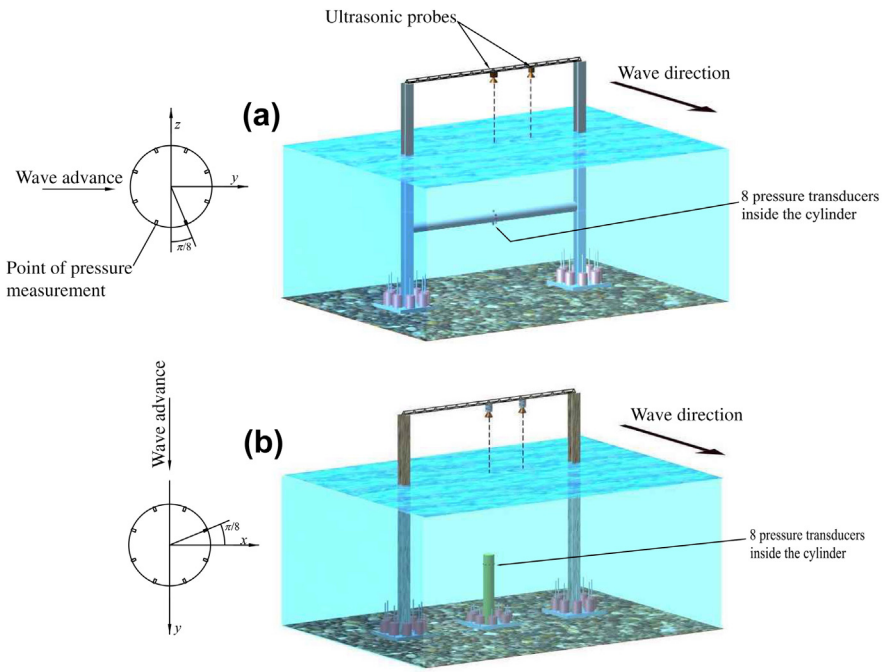

■ **FIGURE 12.2 The equipment of a small-scale field experiment of 2009–2011 on the effectiveness of the Morison equation.**
(a) The experiment on a horizontal cylinder. (b) The experiment on a truncated vertical cylinder. (The diameters of the cylinders were changed in the course of the experiment.)

The a_i, ω_i, and ε_i were obtained from the Fourier series of the random surface elevation measured by the ultrasonic probe above the instrumented section of the cylinder. The angles θ_i were obtained from the surface elevations measured by the pair of ultrasonic probes above the cylinder (see Fig. 12.2 for the locations of the ultrasonic probes). The method followed for obtaining angles θ_i is that described in Section 6.5.

In Fig. 12.3, the probability of exceedance of the peaks of the normalized random process

$$f_c^*(t) = \frac{f_c(t)}{\sigma_f} \tag{12.18}$$

is compared with the probability of exceedance of the peaks of the normalized random process

$$f_m^*(t) = \frac{f_m(t)}{\sigma_f} \tag{12.19}$$

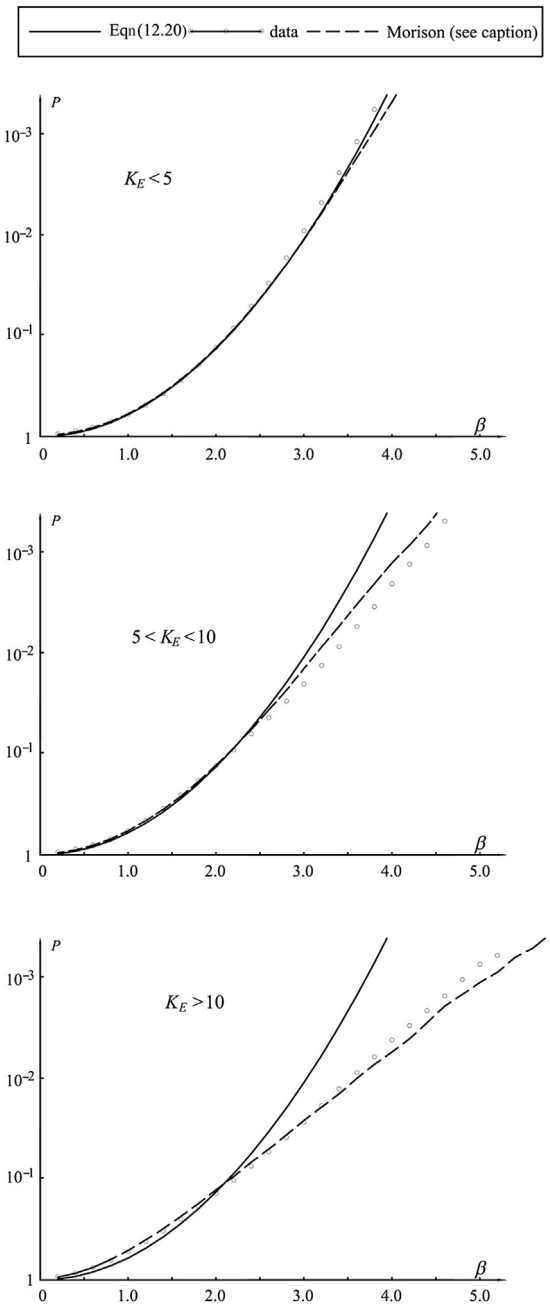

■ **FIGURE 12.3 Comparison between the distribution of the peaks of a random force process calculated with the Morison equation, and the distribution of the peaks of the actual random force process.** The v_y, v_z, a_y needed by the Morison equation were obtained by means of the theory of sea states (Eqns (12.14)—(12.16)) with the a_i, ω_i, ε_i, and θ_i being obtained from the time series data of the surface elevation recorded by a pair of ultrasonic probes (see Fig. 12.2(a)), with the method of Section 6.5. c_{in} and c_{dg} were obtained by means of the Eqns (12.8) and (12.9).

Figure 12.3 deals with the horizontal force on the horizontal cylinders. The three panels of the figure correspond to three distinct ranges of K_E of the sea state. The continuous line represents the Rayleigh distribution, that is,

$$P(peak > \beta) = \exp\left(-\frac{\beta^2}{2}\right) \tag{12.20}$$

where β is an arbitrary threshold value. The probability of exceedance of the peaks of the normalized force process grows as the K_E of the sea state grows. This trend is evident both with the f_c process and with the f_m process. The closeness between the probability of exceedance of the peaks of the normalized f_c process and the probability of exceedance of the peaks of the normalized f_m process is evident in each of the three panels of the figure. The same degree of agreement is found also with the horizontal wave force on the vertical cylinder, and with the vertical force on the horizontal cylinder. All of this proves that the Morison equation is effective with random wind-generated waves.

12.2.3 The K_E of a Sea State as a Whole

The $\hat{f}_{in}(t)$ and $\hat{f}_{dg}(t)$ for the y-component of the force on a vertical cylinder are

$$\hat{f}_{in}(t) = -\rho\pi R^2 v_{\max}\omega \sin(\omega t)\cos\theta \tag{12.21}$$

$$\hat{f}_{dg}(t) = \rho R v_{\max}^2 \left|\cos(\omega t)\right| \cos(\omega t)\cos\theta \tag{12.22}$$

where θ is the angle that the direction of wave advance makes with the y-axis. It follows that

$$\frac{\left\langle \hat{f}_{dg}^2(t)\right\rangle}{\left\langle \hat{f}_{in}^2(t)\right\rangle} = \frac{3}{4}\,\frac{v_{\max}^2 T^2}{\pi^4 4R^2} \tag{12.23}$$

where 3/4 on the RHS is the quotient between 3/8, which is the average of $\cos^4$, and 1/2, which is the average of $\cos^2$. On inverting the RHS with the LHS and using the definition Eqn (12.2), we obtain

$$K_E = \pi^2\sqrt{4/3}\sqrt{\frac{\left\langle \hat{f}_{dg}^2(t)\right\rangle}{\left\langle \hat{f}_{in}^2(t)\right\rangle}} \tag{12.24}$$

With a periodic wave, this equation gives the same value of K_E, which is given by Eqn (12.2). The advantage with respect to the definition Eqn (12.2) is that the RHS of Eqn (12.24) can be univocally evaluated

also for a random sea state, where $\hat{f}_{dg}$ and $\hat{f}_{in}$ may be obtained by means of Eqns (12.12)–(12.17), on replacing v_z by

$$v_x = g \sum_{i=1}^{N} a_i A_{1_i}(z_c)\, \omega_i^{-1} k_i \sin(\theta_i) \cos(-\omega_i t + \varepsilon_i) \tag{12.25}$$

12.3 WORKED EXAMPLE

12.3.1 Object and Input Data

Calculation of the resultant in-line force on a part of an ideal frame structure (Fig. 12.4).

Design sea state: $H_s = 15$ m; duration = 5 h; spectrum: mean JONSWAP with $A = 0.01$; dominant direction: parallel to the y-axis ($\theta_d = 0$); directional distribution: Mitsuyasu et al. with $n_p = 20$. For the aim of a preliminary estimate, we resort to the design sea state pattern (see Section 5.6.1), according to which we have

$$H = 27.8 \text{ m}, \quad H_s = 15.0 \text{ m}$$

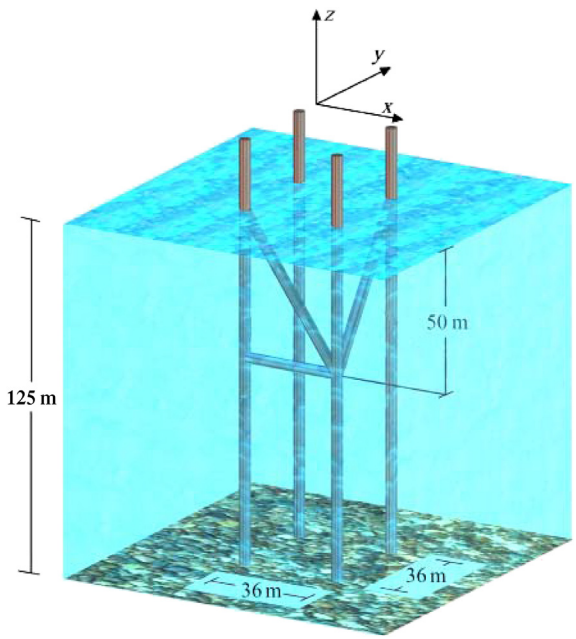

■ **FIGURE 12.4 Worked example of Chapter 12.** Scheme of a part of an ideal frame structure.

12.3.2 Zero Up-Crossing or Zero Down-Crossing Wave?

Let us consider the group of a zero up-crossing wave of a given, very large height H (group that we shall call z.u.) and the group of a zero down-crossing wave of the same height H (group that we shall call z.d.). These wave groups are represented, respectively, in Fig. 12.5(a) and (b).

Now let us consider the in-line force on a vertical pile being located at point x_o, y_o, and piercing the surface elevation. The time axis has been subdivided into eight intervals, and for each of these intervals, the sign has been marked of v_y (for the drag force) and a_y (for the inertia force) for both z.u. and z.d. From the figure, it may be recognized that the largest

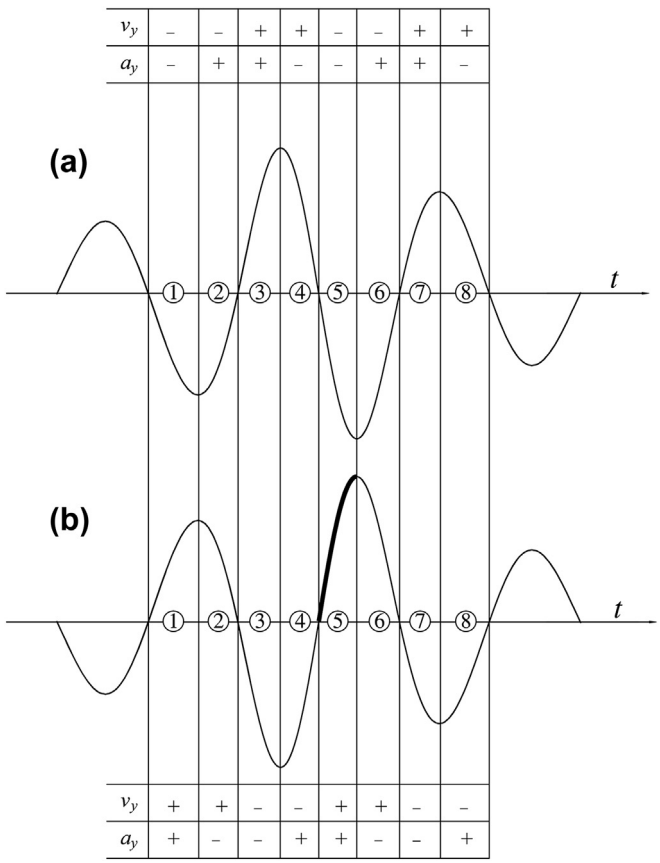

■ **FIGURE 12.5** (a) A zero up-crossing wave group (z.u.) and (b) a zero down-crossing wave group (z.d.). The largest force on a vertical cylinder piercing the sea surface is exerted by z.d. in time interval 5.

in-line force will occur on interval no. 5 of the z.d. To reach this conclusion, one should bear in mind that

1. the sectional drag force is larger, the larger the height of the wave crest (or the depth of the wave trough);
2. the sectional inertia force is larger, the larger the difference of level is between the trough and the crest (or the crest and the trough);

and value

1. whether or not the drag force has the same sign as the inertia force;
2. how much is the length of the pile that is loaded (this length being greater in a wave crest than in a wave trough).

If the wave force on a structure were inertial (no drag), the load exerted by z.d. would be equal and opposite to the load exerted by z.u. Because of the drag force, the largest wave load exerted by z.d. typically exceeds the largest wave load exerted by z.u., as we have just seen for the case of the vertical pile piercing the surface elevation. This is why in the worked example we shall consider the case of the maximum expected zero down-crossing wave in the design sea state (of course, the maximum expected zero down-crossing wave and the maximum expected zero up-crossing wave have the same height in a given sea state, that is, 27.8 m in the present worked example).

12.3.3 Calculation of Wave Force

FORTRAN program FRAME for a preliminary calculation of the resultant in-line force is listed here below. This program reads file BEAM, which, at the first line, gives the water depth d, and in the following lines gives the diameter and the coordinates of the end-points of each member of the frame structure:

```
File BEAM
  125.0

    2.4   −18.0   −18.0   −125.0   −18.0   −18.0    50.0
    2.4    18.0   −18.0   −125.0    18.0   −18.0    50.0
    2.4   −18.0    18.0   −125.0   −18.0    18.0    50.0
    2.4    18.0    18.0   −125.0    18.0    18.0    50.0
    1.2    18.0   −18.0    −50.0   −18.0   −18.0     0.0
    1.2    18.0   −18.0    −50.0    18.0    18.0     0.0
    1.2   −18.0   −18.0    −50.0    18.0   −18.0   −50.0
```

Loop 100 lets T range in $(-1.25T_p, 1.25T_p)$; loop 400 goes from member no. 1 to member no. 7; loop 500 subdivides each member into 100 segments, and computes the wave force on each of these segments; and the quasi-determinism (QD) subroutine listed in Section 9.3 is called inside loop 500 with input time T, and the coordinates X, Y, Z of the center of each segment. The program calculates the force on a member whether fully or partially beneath the water surface. As a conclusion, the program writes $\tau = T/T_p$, and the three components of the in-line wave force on the whole structure, being given in kN.

```
      PROGRAM FRAME
      CHARACTER*64 NOMEC
      DIMENSION X1V(200),Y1V(200),Z1V(200),DV(200)
      DIMENSION X2V(200),Y2V(200),Z2V(200)
      COMMON D,HS,H,TP,TST,ALPHA,TETAD,RNP
      COMMON IMAX,JMAX,OMV(300),TETV(150),RKV(300)
      COMMON SOT(300,150)
      PG=3.141592
      DPG=2.*PG
      WRITE(6,*)'number of members'
      READ(5,*)NB
      NOMEC='BEAM'
      OPEN(UNIT=50,STATUS='OLD',FILE=NOMEC)
      NOMEC='FORCE1'
      OPEN(UNIT=60,FILE=NOMEC)
      READ(50,*)D
      DO N=1,NB
      READ(50,*)DV(N),X1V(N),Y1V(N),Z1V(N),
      X2V(N),Y2V(N),Z2V(N)
      ENDDO
      WRITE(6,*)'Hs,H'
      READ(5,*)HS,H
      WRITE(6,*)'alpha, thetad(degree),np'
      READ(5,*)ALPHA,TETAD,RNP
      WRITE(6,*)'zero up-crossing wave -> 1, down-crossing -> -1'
      READ(5,*)UD
      TETAD=TETAD*PG/180

      RO=1.03E3
      CIN=1.85
      CDG=0.62
      DTAU=0.02
      NCALL=0
      CALL QD(NCALL,UD,X,Y,Z,T,VX,VY,VZ,AX,AY,AZ,ETA)
c this call of QD, with NCALL=0, serves to store the directional spectrum
      NCALL=1

      DO 100 J=1,126
c Loop 100: dimensionless time instants
```

```
      .TAU=-1.25+FLOAT(J-1)*DTAU
       T=TAU*TP
c FXT= x component in-line force on the whole structure
c FYT= y component in-line force on the whole structure
c FZT= z component in-line force on the whole structure
       FXT=0
       FYT=0
       FZT=0
       DO 400 N=1,NB
c Loop 400: all the members
       R=DV(N)/2.
       X1=X1V(N)
       Y1=Y1V(N)
       Z1=Z1V(N)
       X2=X2V(N)
       Y2=Y2V(N)
       Z2=Z2V(N)
       DEX=X2-X1
       DEY=Y2-Y1
       DEZ=Z2-Z1
       RL=SQRT(DEX*DEX+DEY*DEY+DEZ*DEZ)
       SX=DEX/RL
       SY=DEY/RL
       SZ=DEZ/RL
c SX,SY,SZ are the components of a unit vector parallel
c to the member axis
       DX=DEX/100.
       DY=DEY/100.
       DZ=DEZ/100.
       DS=RL/100.
       X=X1-DX/2.
       Y=Y1-DY/2.
       Z=Z1-DZ/2.
c FXB= x component in-line force on the Nth member
c FYB= y component in-line force on the Nth member
c FZB= z component in-line force on the Nth member
       FXB=0
       FYB=0
       FZB=0
       DO 500 I=1100
c Loop 500: each member is subdivided into 100 segments; loop 500 covers
c these segments
      X=X+DX
      Y=Y+DY
      Z=Z+DZ
c X,Y,Z are the coordinates of the center of one of the 100 segments
```

```
     .CALL QD(NCALL,UD,X,Y,Z,T,VX,VY,VZ,AX,AY,AZ,ETA)
      IF(Z.GT.ETA)GO TO 500
      VS=VX*SX+VY*SY+VZ*SZ
      VSECTX=VX-VS*SX
      VSECTY=VY-VS*SY
      VSECTZ=VZ-VS*SZ
c VSECTX, VSECTY, VSECTZ are the components of vector vsect
      VSECT=SQRT(VSECTX**2+VSECTY**2+VSECTZ**2)
      AS=AX*SX+AY*SY+AZ*SZ
      ASECTX=AX-AS*SX
      ASECTY=AY-AS*SY
      ASECTZ=AZ-AS*SZ
c ASECTX, ASECTY, ASECTZ are the components of vector asect
      FINX=RO*PG*R*R*ASECTX
      FDGX=RO*R*VSECT*VSECTX
      FINY=RO*PG*R*R*ASECTY
      FDGY=RO*R*VSECT*VSECTY
      FINZ=RO*PG*R*R*ASECTZ
      FDGZ=RO*R*VSECT*VSECTZ
      FXB=FXB+(CIN*FINX+CDG*FDGX)*DS
      FYB=FYB+(CIN*FINY+CDG*FDGY)*DS
      FZB=FZB+(CIN*FINZ+CDG*FDGZ)*DS
500   CONTINUE
      FXT=FXT+FXB
      FYT=FYT+FYB
      FZT=FZT+FZB
400   CONTINUE
c Conversion from N to kN
      FXT=1.E-3*FXT
      FYT=1.E-3*FYT
      FZT=1.E-3*FZT
      WRITE(60,1000)TAU,FXT,FYT,FZT
      WRITE(6,1000)TAU,FXT,FYT,FZT
1000  FORMAT(2X,F7.2,3(2X,E12.4))
100   CONTINUE
      WRITE(6,*)
      WRITE(6,*)'read results on file FORCE1'
      END
```

Figure 12.6 shows that F_y. F_x is negligible given that the dominant direction of the sea state is parallel to the y-axis, and hence, the wave group moves along the y-axis. F_z is due only to the diagonals and the horizontal member, and has a negative maximum of about -370 kN and a positive maximum of 290 kN.

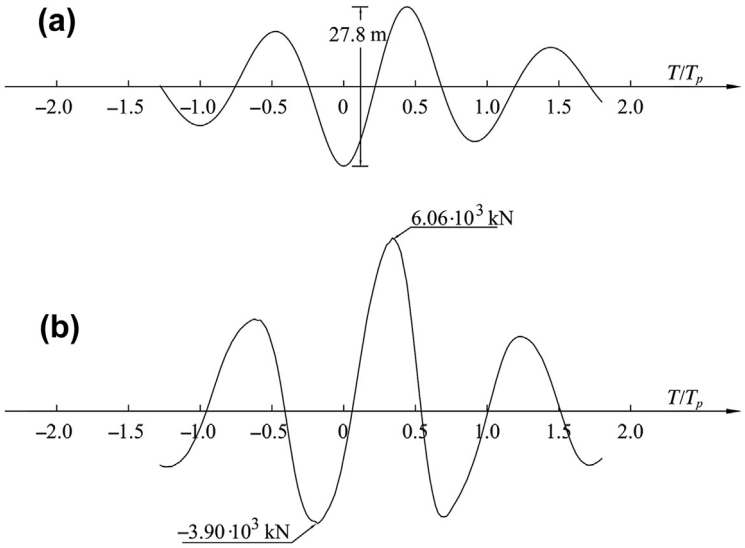

■ **FIGURE 12.6 Worked example of Chapter 12.** (a) Wave group of the maximum expected zero down-crossing wave height, in the design sea state; (b) horizontal in-line force exerted on the frame structure.

12.4 CONCLUSION

The SSFEs of 2009−2011 aiming to test the effectiveness of the Morison equation were described by Boccotti et al. (2011) and (2013). For the first time, the particle velocities were obtained from the database a_i, ω_i, θ_i of the directional spectrum (obtained with the technique of Section 6.5 and relevant software). This is preferable to proceed from time series data of particle velocity for two reasons: First, the new approach is consistent with engineering practice, wherein one typically starts from a given directional spectrum. Second, there are some difficulties with time series data of particle velocity when working in the field. This is because Morison equation calls for the particle velocity that would be at the center of the solid cylinder if this cylinder was not there, and, in the field, the time series of particle velocities are not repeatable, and the wave motion is three-dimensional (these ideas are explained most clearly by Wolfram and Naghipour, 1999). Also, the method to obtain C_{in} and C_{dg} with Eqns (12.8) and (12.9) was used for the first time in the two above cited SSFEs. Until now, a method that has often been used is the method of moments (Pierson and Holmes, 1965), which is based on the two equations that proceed from Eqn (12.7) with n being equal, respectively,

to 2 and 4. Another classic method is that of Borgman (1965), who suggested obtaining C_{in} and C_{dg} so that the spectrum E_{fc} of $f_c(t)$ is the best least square fit of the spectrum E_{fm} of $f_m(t)$.

Those commonly used to compute wave forces on frame structures are statistical methods. A relatively simple method can be applied with long-crested waves if the drag force is negligible with respect to the inertia force (although with diffraction effects being still negligible). In that case, one can obtain the response spectrum of $f_c(t)$ through a transfer function, from the wave spectrum $E(\omega)$ (see Naess and Moan, 2005 for the general procedure). In this special case, the random process $f_c(t)$ will be stationary Gaussian, and hence, it will have the set of statistical properties peculiar to these random processes (see Chapter 4). If one keeps the assumption that the waves are long-crested, removes the restriction about the weight of the drag component, and introduces the new restriction that the cylinder must be vertical, then the solution for the pdf of the wave force $f_c(t)$ exists, is due to Borgman (1972), and is reproposed in an alternative way by Hudspeth (2006). Of course, this time the pdf is generally not Gaussian. The statistical approach can overcome the aforementioned restrictions as to the nature of waves and/or geometry of the cylinder. For this aim, one must resort to Montecarlo simulations, specifically to numerical simulations of the random surface elevation (Eqn (6.8)) and particle velocities and accelerations that proceed from random velocity potential (Eqn (6.9)), for a given directional spectrum. With the worked example of Section 12.3, one will have to perform many numerical simulations of the design sea state, looking at the $F_y(t)$ in the largest wave of each simulation. The QD theory let us pass from this Montecarlo approach to the hard core of mechanics. It says: "when the largest wave in the lifetime will strike the structure, it will be (more or less) as if the center of the structure coincides with the center of the framed area of Fig. 9.1, and the largest wave is wave B of said figure."

REFERENCES

Boccotti, P., Arena, F., Fiamma, V., Barbaro, G., 2011. Field experiment on random wave forces acting on vertical cylinders. Probab. Eng. Mech. 28, 39–51.

Boccotti, P., Arena, F., Fiamma, V., Romolo, A., 2013. Two small-scale field experiments on the effectiveness of Morison's equation. Ocean Eng. 57, 141–149.

Borgman, L.E., 1965. Wave forces on piling for narrow-band spectra. J. Waterw. Harbours Div. ASCE 91, 65–90.

Borgman, L.E., 1972. Statistical Models for Ocean Waves and Wave Forces. In: Advances in Hydroscience, vol. 8. Academic Press, New York.

Chakrabarti, S., 2005. Handbook of Offshore Engineering, vol. 1. Elsevier, Amsterdam, pp. 1–661.

Hayashi, K., Takenouchi, T., 1985. Characteristics of flow around a vertical cylinder in a wave. Coastal Eng. Jpn. 28, 207–222.

Hudspeth, R.T., 2006. Waves and Wave Forces on Coastal and Ocean Structures. World Scientific, New Jersey, p. 932.

Justesen, P., 1989. Hydrodynamic forces on large cylinders in oscillatory flow. J. Waterw. Port Coastal Ocean Eng. 115, 497–514.

Karsan, D., 2005. Fixed offshore platform design. In: Handbook of Offshore Engineering, vol. I. Elsevier, Amsterdam, pp. 279–418.

Morison, J.R., O'Brien, M.P., Johnson, J.W., Schaaf, S.A., 1950. The force exerted by surface waves on piles. Petroleum Trans. Am. Inst. Min. Metal Eng. 189, 149–157.

Naess, A., Moan, T., 2005. Probabilistic Design of Offshore Structures. In: Handbook of Offshore Engineering, vol. I. Elsevier, Amsterdam, pp. 197–278.

Pierson, W.J., Holmes, P., 1965. Irregular wave forces on a pile. J. Waterw. Harbours Div. ASCE 91 (WW4), 1–10.

Sarpkaya, T., 1975. Forces on cylinders and spheres in a sinusoidally oscillating fluid. J. Appl. Mech. 42, 32–37.

Sarpkaya, T., 1977. In-line and transverse forces on cylinders in oscillatory flow at high Reynolds number. J. Ship Res. 21 (4), 200–216.

Sarpkaya, T., 1979. Vortex induced oscillations. J. Appl. Mech. 46, 241–258.

Sarpkaya, T., Isaacson, M., 1981. Mechanics of Wave Forces on Offshore Structures. Van Nostran Reinhold Co., p. 651.

Sumer, B.M., Fredsoe, J., 1997. Hydrodynamics around Cylindrical Structures. World Scientific Co., p. 650.

Williamson, C.H.K., 1985. Sinusoidal flow relative to circular cylinders. J. Fluid Mech. 155, 141–174.

Wolfram, J., Naghipour, M., 1999. On the estimation of Morison force coefficients and their predictive accuracy for very rough circular cylinders. Appl. Ocean Res. 21, 311–328.

Chapter 13

Calculation of Wave Forces on Gravity Platforms and Submerged Tunnels

CHAPTER OUTLINE

13.1 WAVE FORCES ON A GRAVITY OFFSHORE PLATFORM

What follows is a worked example of an estimate of the wave force on the offshore gravity platform of Fig. 13.1. The data of the design sea state and the estimate of the largest wave height in the lifetime are the same as in the worked example of Chapter 12.

13.1.1 Calculation of the Diffraction Coefficient

For calculating C_{d_o} of the base, we refer to the circular cylinder of the same area as the base. This has a radius of $R = 45$ m. Taking $\mathscr{F}_{\mathscr{R}} = 1.75$ for the platform base and $\mathscr{F}_{\mathscr{R}} = 2.00$ for the columns that have an average radius of 8.5 m, with the program of Section 10.7 (with $T_p = 16.5$ s), we obtain

$$\text{platform base} : C_{d_o} = 1.54$$
$$\text{columns} : C_{d_o} \cong 2.00$$

Wave Mechanics and Wave Loads on Marine Structures. http://dx.doi.org/10.1016/B978-0-12-800343-5.00013-5

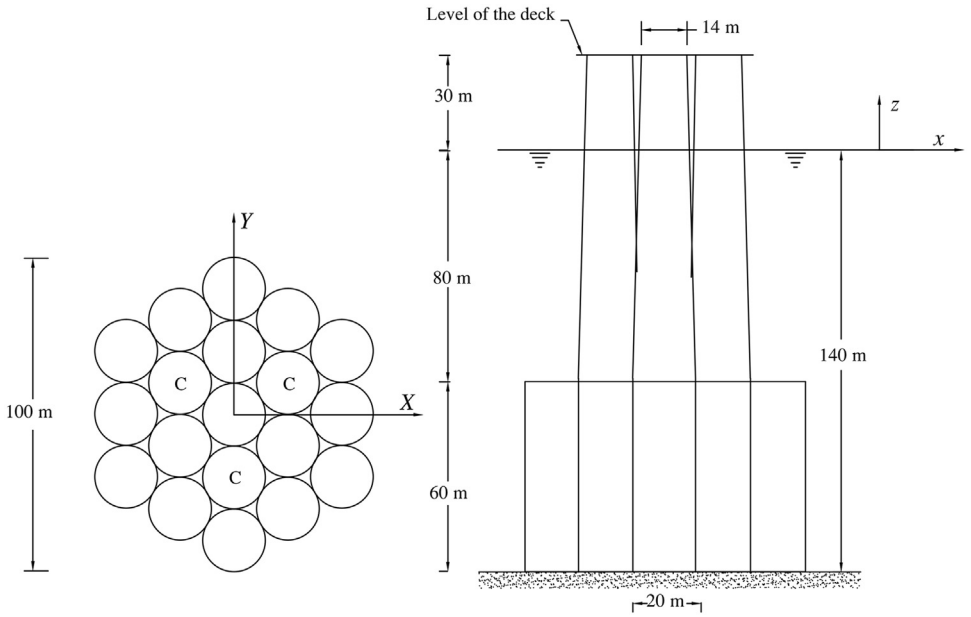

■ **FIGURE 13.1** First worked example, Chapter 13: plan and front view (essential scheme) of a hypothesis of support structure of a gravity offshore platform (for details on this kind of structure, see Dawson, 1983).

13.1.2 **Calculation of the Wave Force**

The FORTRAN program PLAT for a preliminary calculation of the wave force on a gravity offshore platform is listed here below. Point x_o,y_o is taken at the center of the platform. The data of the geometry of the structure are read from the following file:

```
File PLATGEO
140.0 d
60.0 HTANK (height vertical cylinders)
110.0 HCOL (height columns)
20.0 DCYL (diameter vertical cylinders)
20.0 DCOL1 (greater diameter column)
14.0 DCOL2 (smaller diameter column)
19 number of vertical cylinders
coordinates centers cylinders:

  0.0          −40.0
 17.3          −30.0
 34.6          −20.0
 34.6            0.0
 34.6           20.0
```

```
        17.3            30.0
        0.0             40.0
        −17.3           30.0
        −34.6           20.0
        −34.6            0.0
        −34.6          −20.0
        −17.3          −30.0
        0.0            −20.0
        17.3           −10.0
        17.3            10.0
        0.0             20.0
        −17.3           10.0
        0.0            −10.0
        0.0              0.0
c 3 number of columns
c coordinates centers columns:

        0.0            −20.0
        17.3            10.0
        −17.3           10.0
```

Loop 100 lets T range in $(-1.25T_p, 1.25T_p)$; loop 400 and loop 410 inside loop 100 compute, respectively, the force on the base and the columns, at the given T. Loop 500 inside loop 400 subdivides each of the 19 cylinders of the base into five segments of 12 m in height and computes the wave force on these segments. Loop 510 inside loop 410 subdivides the wet piece (i.e., from $z = -80$ m to $z = \eta$) of a column into 20 segments and computes the wave force on each of these segments. Subroutine QD is called both in the loop 500 and in the loop 510, and provides the $\overline{a_x}$, $\overline{a_y}$, which serve for computing the Froude−Krylov force.

A simple way to consider the effect of the 24 interstices among the 19 cylinders of the base is multiplying the force on the 19 cylinders by the ratio (=1.065) between the volume of the base and the volume of the 19 cylinders. The program writes T/T_p, and F_x, F_y in kN.

```
      PROGRAM PLAT
      CHARACTER*64 NOMEC
      DIMENSION XCI(20),YCI(20)
      DIMENSION XCO(10),YCO(10)
      COMMON D,HS,H,TP,TST,ALPHA,TETAD,RNP
      COMMON IMAX,JMAX,OMV(300),TETV(150),RKV(300)
      COMMON SOT(300,150)
      NOMEC='PLATGEO'
```

```
     .OPEN(UNIT=50,STATUS='OLD',FILE=NOMEC)
      READ(50,*)D
      READ(50,*)HTANK
      READ(50,*)HCOL
      READ(50,*)DCYL
      READ(50,*)DCOL1
      READ(50,*)DCOL2
      READ(50,*)NCYL
      READ(50,*)
      DO N=1,NCYL
      READ(50,*)XCI(N),YCI(N)
      ENDDO
      READ(50,*)NCOL
      READ(50,*)
      DO N=1,NCOL
      READ(50,*)XCO(N),YCO(N)
      ENDDO

      NOMEC='FORCE2'
      OPEN(UNIT=60,FILE=NOMEC)
      PG=3.141592
      DPG=2.*PG
      WRITE(6,*)'Hs,H'
      READ(5,*)HS,H
      WRITE(6,*)'alpha,thetad(degree),np'
      READ(5,*)ALPHA,TETAD,RNP
      WRITE(6,*)'zero up-crossing wave -> 1, down-crossing -> -1'
      READ(5,*)UD
      TETAD=TETAD*PG/180.
      WRITE(6,*)'diffraction coefficients base and columns'
      READ(5,*)CDBA,CDCO
      RO=1.03E3
      DTAU=0.02
      NCALL=0
      CALL QD(NCALL,UD,X,Y,Z,T,VX,VY,VZ,AX,AY,AZ,ETA)
c this call of QD, with NCALL=0, serves to store the directional spectrum.
      NCALL=1

      DO 100 J=1,126
c Loop 100: time
      TAU=-1.25+FLOAT(J-1)*DTAU
      T=TAU*TP
c FX x-component Froude-Krylov force on the base of the platform
c FY y-component Froude-Krylov force on the base of the platform
      FX=0
      FY=0
      DO 400 N=1,NCYL
```

```
c Loop 400: vertical cylinders of the base
         R=DCYL/2
         X=XCI(N)
         Y=YCI(N)
         DS=HTANK/10
         DO 500 I=1,10
c each vertical cylinder is subdivided into 10 pieces;
c loop 500 covers these 10 pieces.
         Z=-D+FLOAT(I-1)*DS+DS/2
         CALL QD(NCALL,UD,X,Y,Z,T,VX,VY,VZ,AX,AY,AZ,ETA)
         COFI=RO*PG*R*R*DS
         FX=FX+COFI*AX
         FY=FY+COFI*AY
500      CONTINUE
400      CONTINUE
c effect of the interstices among the vertical cylinders
         FBX=FX*1.065
         FBY=FY*1.065
c step from Froude-Krylov force to force on the solid body (base)
         FBX=FBX*CDBA
         FBY=FBY*CDBA
c conversion from N to kN
         FBX=FBX*1.E-3
         FBY=FBY*1.E-3

c Here the calculation of the wave force on the base has been completed.
c Now the calculation of the wave force on the columns starts

c FX x-component Froude-Krylov force on the columns
c FY y-component Froude-Krylov force on the columns
         FX=0
         FY=0
         DO 410 N=1,NCOL
c Loop 410 columns
         X=XCO(N)
         Y=YCO(N)
         CALL QD(NCALL,UD,X,Y,Z,T,VX,VY,VZ,AX,AY,AZ,ETA)
         HCOLW=d-HTANK
         DS=(HCOLW+ETA)/20
         DO 510 I=1,20
c the wet portion of a column is subdivided into 20 pieces;
c loop 510 covers these 20 pieces
         ZI=FLOAT(I-1)*DS+DS/2.
         Z=-HCOLW+ZI
         CALL QD(NCALL,UD,X,Y,Z,T,VX,VY,VZ,AX,AY,AZ,ETA)
         DIAM=DCOL1+(DCOL2-DCOL1)*ZI/HCOL
         R=DIAM/2
```

```
     .COFI=RO*PG*R*R*DS
      FX=FX+COFI*AX
      FY=FY+COFI*AY
510   CONTINUE
410   CONTINUE
c step from Froude-Krylov force to force on the solid body (columns)
      FCX=FX*CDCO
      FCY=FY*CDCO
c conversion from N to kN
      FCX=FCX*1.E-3
      FCY=FCY*1.E-3
c Here the calculation of the wave force on the columns has been completed
c FTX is the x-component of the wave force on the whole structure
c FTY is the y-component of the wave force on the whole structure
      FTX=FBX+FCX
      FTY=FBY+FCY
      WRITE(60,1000)TAU,FTX,FTY
      WRITE(6,1000)TAU,FTX,FTY
1000  FORMAT(2X,F7.2,2X,E12.4,2X,E12.4)
100   CONTINUE
      WRITE(6,*)
      WRITE(6,*)'read results on file FORCE2'
      END
```

Figure 13.2 shows the horizontal force F_y on the whole structure. Since the angle θ_d between the dominant direction and the y-axis is zero, the wave group moves along the y-axis, so that the horizontal force proves to be parallel to the y-axis (x-component negligible).

13.2 WAVE FORCES ON A SUBMERGED TUNNEL

What follows is a worked example of an estimate of the wave force on the submerged tunnel of Fig. 13.3, which has a length of 1000 m and is supported by five piers.

13.2.1 Wave Height and Diffraction Coefficients

Design sea state: $H_s = 8$ m; duration = 7 h; spectrum: mean JONSWAP, with $A = 0.01$; dominant direction: $\theta_d = 0$ (orthogonal to the tunnel axis); directional distribution: Mitsuyasu et al. with $n_p = 20$. For the aim of a preliminary estimate, we resort to the DSSP (see Section 5.6.1). The maximum bending moment in the tunnel occurs if the center of a wave group (like that of Fig. 9.1) strikes a pier. Hence, we must calculate the maximum expected wave height at the five locations of the piers, in the design sea state. Following Section 6.2, this maximum expected wave height at five points (roughly aligned with the wave crests, and with a distance from each other, greater than $L_{p0}/2$) may be estimated as the maximum expected wave height at one point in a duration of time five times greater than the actual duration of the sea state. The conclusion turns out to be

$$H = 16.8 \text{ m}, \quad H_s = 8.0 \text{ m}$$

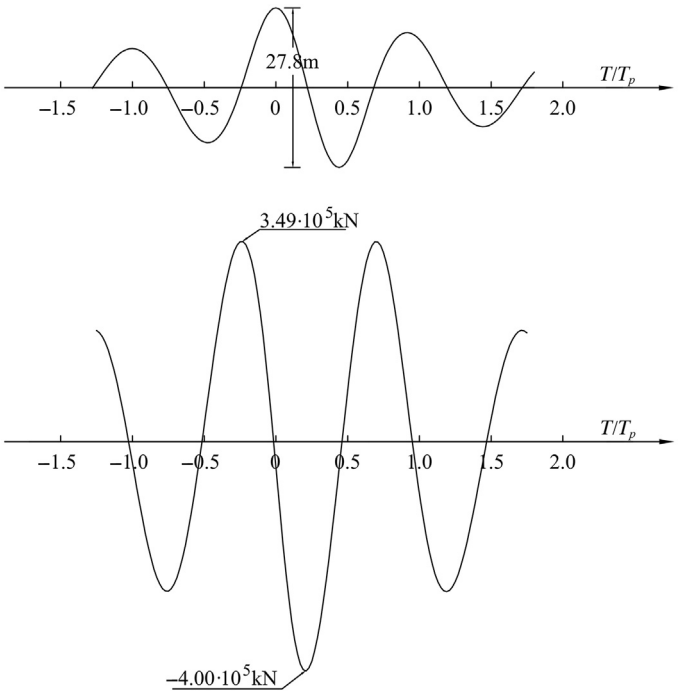

■ **FIGURE 13.2** First worked example, Chapter 13: (a) wave group of the maximum expected wave height in the design sea state, (b) horizontal force exerted on the structure (base + columns).

The suggested value of $\mathscr{F}_{\mathscr{R}}$ for a submerged tunnel is 2.0, and with this value of $\mathscr{F}_{\mathscr{R}}$ and T_p of 12.1s, the FORTRAN program of Section 10.7 gives

$$C_{d_o} = 1.91$$

Conservatively, C_{d_v} will be assumed equal to C_{d_o}.

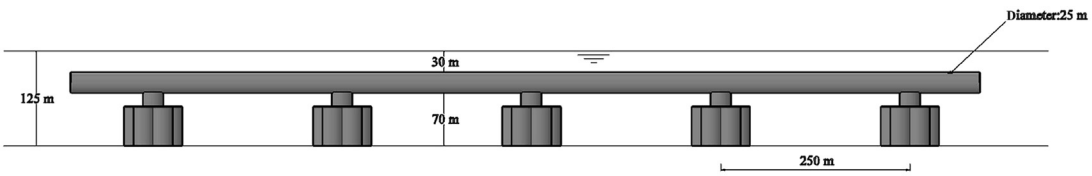

■ **FIGURE 13.3** Second worked example, Chapter 13: a hypothesis of submerged tunnel.

13.2.2 Calculation of Wave Force

FORTRAN program TUNN for a preliminary calculation of the wave load on the tunnel is listed below. Loop 100 lets T range in $(-1.3T_p, 1.8T_p)$; loop 400 computes the sectional wave force on a length of tunnel of 600 m that is, more or less, the length of the crest of a wave group at the apex of its development stage, in the design sea state.

Subroutine QD is called in the loop 400, and provides the $\overline{a_y}$, $\overline{a_z}$, which serve for computing the Froude–Krylov force. The sectional force f_y and the sectional force f_z are stored, respectively, on FPVY(J,N) and FPVZ(J,N), where J is associated with T, and N is associated with X. Loop 600 writes $f_y(X)$ or $f_z(X)$ in kN/m at the time instants $\tau = T/T_p$ in which these forces get a local maximum.

```
      PROGRAM TUNN
      CHARACTER*64 NOMEC
      DIMENSION FYV(300),FZV(300),TAUV(300)
      DIMENSION FPYV(300,200),FPZV(300,200)
      COMMON D,HS,H,TP,TST,ALPHA,TETAD,RNP
      COMMON IMAX, JMAX,OMV(300),TETV(150),RKV(300)
      COMMON SOT(300,150)
      NOMEC='LOAD1'
      OPEN(UNIT=60,FILE=NOMEC)
      PG=3.141592
      DPG=2.*PG
      WRITE(6,*)'Hs,H'
      READ(5,*)HS,H
      WRITE(6,*)'alpha,thetad(degree),np'
      READ(5,*)ALPHA,TETAD,RNP
      WRITE(6,*)'zero up-crossing wave -> 1, down-crossing -> -1'
      READ(5,*)UD
      TETAD=TETAD*PG/180
      WRITE(6,*)'horizontal and vertical diffraction
     coefficients'
      READ(5,*)CDO,CDV
      RO=1.03E3
      D=125.
c DIAM diameter tunnel
c ZCE z tunnel center
c RLT length of tunnel being considered
      DIAM=25
      R=DIAM/2.
      ZCE=-42.5
      RLT=600.
      DX=RLT/60.
      DTAU=0.02
```

```
     .NCALL=0
      CALL QD(NCALL,UD,X,Y,Z,T,VX,VY,VZ,AX,AY,AZ,ETA)
c this call of QD, with NCALL=0, serves to store the directional spectrum
      NCALL=1

      DO 100 J=1,156
c Loop 100:time
      TAU=-1.30+FLOAT(J-1)*DTAU
      WRITE(6,5010)TAU
5010  FORMAT(2X,F7.2)
      TAUV(J)=TAU
      T=TAU*TP
c FYV(J) resultant wave force (y-component) on the piece
c of tunnel being considered
c FZV(J) resultant wave force (z-component) on the piece
c of tunnel being considered
      FYV(J)=0
      FZV(J)=0
      DO 400 N=1,61
c Loop 400:X (axis tunnel)
      X=-RLT/2.+FLOAT(N-1)*DX
      Y=0
      Z=ZCE
      CALL QD(NCALL,UD,X,Y,Z,T,VX,VY,VZ,AX,AY,AZ,ETA)
      COFI=RO*PG*R*R
c FPYV(J,N) wave force per unit length (y-component)
c FPZV(J,N) wave force per unit length (z-component)
      FPYV(J,N)=CDO*RO*PG*R*R*AY
      FPZV(J,N)=CDV*RO*PG*R*R*AZ
c conversion from N to kN
      FPYV(J,N)=1.E-3*FPYV(J,N)
      FPZV(J,N)=1.E-3*FPZV(J,N)
      FYV(J)=FYV(J)+FPYV(J,N)*DX
      FZV(J)=FZV(J)+FPZV(J,N)*DX
400   CONTINUE
100   CONTINUE

      DO 600 J=2,154
c Loop 600: time
c tau=TAUV(J)
c |Fy(tau-dtau)|=AFY1
c |Fy(tau)|=AFY2
c |Fy(tau+dtau)|=AFY3
      AFY1=ABS(FYV(J-1))
      AFY2=ABS(FYV(J))
      AFY3=ABS(FYV(J+1))
      IF(AFY2.GT.AFY1.AND.AFY2.GT.AFY3)THEN
```

```
c a local maximum (or minimum) of Fy has been found
      WRITE(60,1000)TAUV(J)
1000  FORMAT(//,6X,'TAU = ',F7.2,4X,'(fy)',/)
      DO 490 N=1,61
c Loop 490:X (axis tunnel)
      X=-RLT/2.+FLOAT(N-1)*DX
      WRITE(60,1001)X,FPYV(J,N)
1001  FORMAT(2X,F6.0,2X,F6.1)
490   CONTINUE
      ENDIF
c |Fz(tau-dtau)|=AFZ1
c |Fz(tau)|=AFZ2
c |Fz(tau+dtau)|=AFZ3
      AFZ1=ABS(FZV(J-1))
      AFZ2=ABS(FZV(J))
      AFZ3=ABS(FZV(J+1))
      IF(AFZ2.GT.AFZ1.AND.AFZ2.GT.AFZ3)THEN
c a local maximum (or minimum) of Fz has been found
      WRITE(60,1002)TAUV(J)
1002  FORMAT(//,6X,'TAU = ',F7.2,4X,'(fz)',/)
      DO 491 N=1,61
c Loop 491:X (axis tunnel)
      X=-RLT/2.+FLOAT(N-1)*DX
      WRITE(60,1001)X,FPZV(J,N)
491   CONTINUE
      ENDIF
600   CONTINUE
      WRITE(6,*)
      WRITE(6,*)'read results on file LOAD1'
      END
```

Figure 13.4 shows the local maxima of f_y and f_z. A local maximum of f_y takes place when a zero of the wave group transits over the axis of the tunnel. A local maximum of f_z takes place when a crest or a trough of the wave group transits over the axis of the tunnel.

The SSFE of 1993 at the NOEL on submerged tunnels (Boccotti, 1996) showed a slight asymmetry between positive and negative peaks of the vertical wave force. This is a nonlinearity effect being due to the kinetic term of the wave pressure. This term reduces both the wave pressure on the upper half cylinder and on the lower half. However, the reduction on the upper half is greater than the reduction on the lower half that somewhat enhances the upward (positive) wave force and reduces the downward (negative) force. The kinetic term of the wave pressure can be evaluated from the v_x, v_y, and v_z obtained from the subroutine QD, on the cylinder surface. However, for the sake of simplicity in this example program, this term has been neglected.

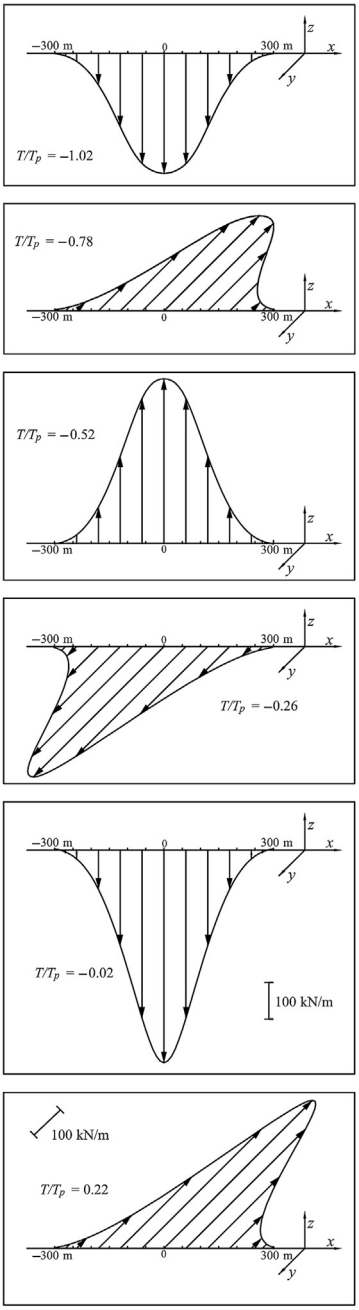

■ **FIGURE 13.4** Second worked example, Chapter 13: peaks of the wave load on the tunnel, under the wave group of the maximum expected wave height in the design sea state.

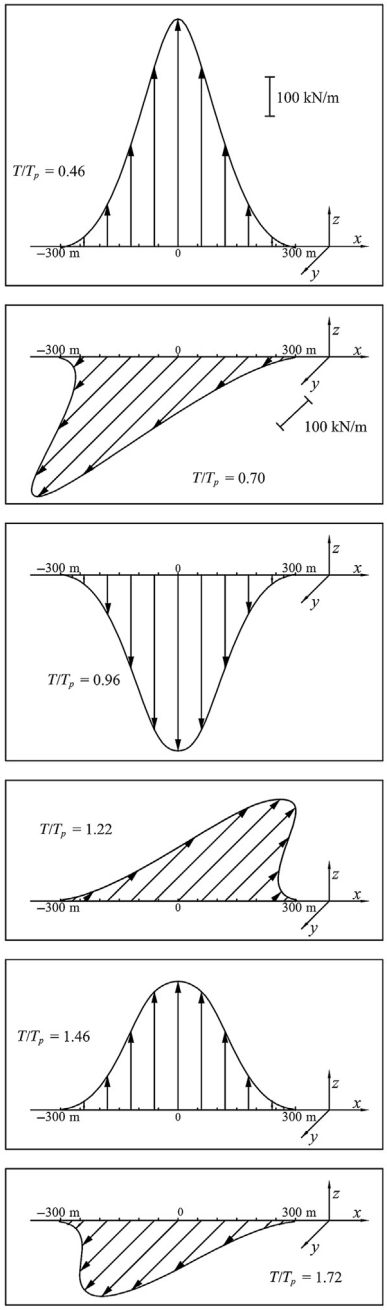

■ **FIGURE 13.4** Continued

13.3 CONCLUSION

Wave forces on large bodies under regime of wave diffraction are calculated with the use of Green's functions (John, 1949, 1950; Mei, 1989). The geometry of the structures is described with a large number of panels, which makes the program slower and requires a large PC memory (Chakrabarti, 2005). This is for a single periodic wave. If we would pass to a random sea state, that is, to a summation of harmonic wave components with different frequencies, with the need to cover some large time interval (for getting a satisfactory statistical confidence), the computational problems would become really very great. Chapter 10 eliminates these computational problems, so that the calculation of the wave force on large bodies is reduced to something simple as programs PLAT and TUNN of the present chapter. The gist of Chapter 10 is that there is a simple relationship between the deterministic force exerted by a wave group on a large body and the deterministic force that this wave group exerts on a water mass equivalent to the solid body. In the author's opinion, the progress of the models for calculation of wave load has the following sequence:

step 1 periodic, unidirectional wave,

step 2 long-crested random waves,

step 3 short-crested random waves,

step 4 deterministic mechanics of wave groups.

With "small bodies" (Chapter 12), the QD theory has enabled us to advance from step 3 to step 4; with "large bodies" (present chapter), the QD theory has enabled us to jump from step 1 to step 4.

REFERENCES

Boccotti, P., 1996. Inertial wave loads on horizontal cylinders: a field experiment. Ocean Eng. 23, 629–648.

Chakrabarti, S.K., 2005. Loads and responses. In: Chakrabarti, S. (Ed.), Hanbdbook of Offshore Engineering. Elsevier, Amsterdam, pp. 133–196.

Dawson, T.H., 1983. Offshore Structural Engineering. Prentice-Hall, p. 346.

John, F., 1949. On the motion of floating bodies, I. Commun. Pure Appl. Math. 2, 13–57.

John, F., 1950. On the motion of floating bodies, II. Commun. Pure Appl. Math. 3, 45–101.

Mei, C.C., 1989. The Applied Dynamics of Ocean Surface Waves. World Scientific, Singapore, p. 740.

Chapter 14

Loads of Sea Storms on Vertical Breakwaters

CHAPTER OUTLINE

14.1 OVERALL STABILITY OF AN UPRIGHT SECTION

14.1.1 The Equilibrium Problem

The wave pressures on an upright section (caisson + concrete crown), under a wave crest and a wave trough, are shown in Fig. 14.1.

Figure 14.2 shows the forces on the upright section: weight P^* in still water, wave forces F and S_w, and horizontal and vertical reactions R_o and R_v of the rubble mound. For the equilibrium, we have

$$|R_o| = |F| \tag{14.1}$$

$$R_v = P^* - S_w \tag{14.2}$$

where the uplift force S_w is positive under the wave crest and negative under the wave trough. The position of R_v is such that the free body is in equilibrium:

$$M + R_v e_R = P^* e_P \tag{14.3}$$

Wave Mechanics and Wave Loads on Marine Structures. http://dx.doi.org/10.1016/B978-0-12-800343-5.00014-7

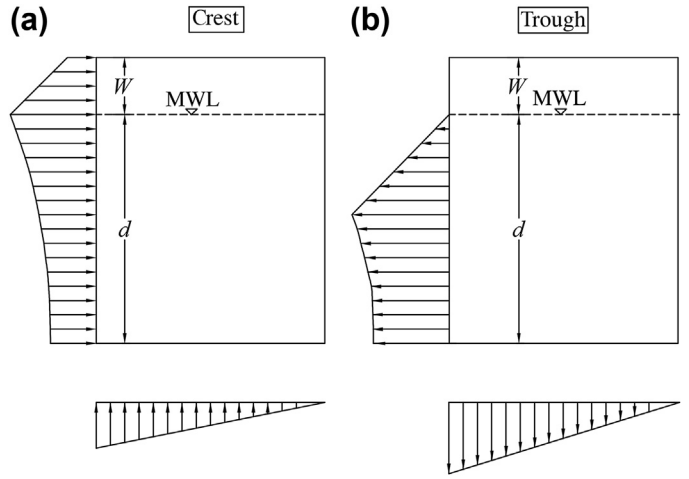

■ **FIGURE 14.1 Wave pressure on the wall and on the base of an upright breakwater.**

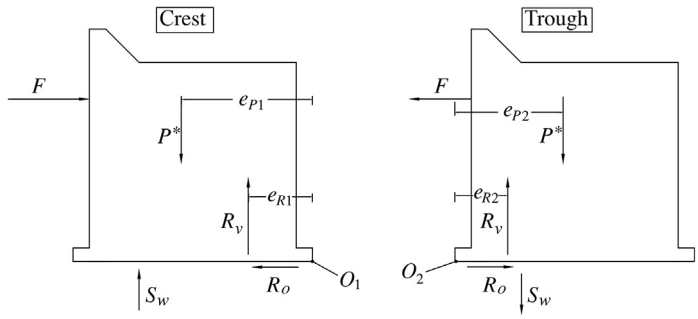

■ **FIGURE 14.2 Reference scheme for the stability analysis.**

with M being the overturning moment due to wave forces F and S_w (under a wave trough, S_w gives a negative contribution to M). Under a wave crest, the topple axis is O_1 so that $e_P = e_{P1}$ and $e_R = e_{R1}$; and under a wave trough, the topple axis is O_2 so that $e_P = e_{P2}$ and $e_R = e_{R2}$.

A static analysis of the upright section with the extreme wave load is usually done, at least for preliminary design purposes. The stability of the upright section is examined for three modes of failure.

Against sliding. We must verify that the safety factor

$$C_1 \equiv \frac{\mu R_v}{|R_o|} = \frac{\mu(P^* - S_w)}{|F|} \tag{14.4}$$

is greater than some dictated value $C_{1\ \min} > 1$. μR_v (friction coefficient × vertical reaction) is the limit shear force that can be developed at the base of the caisson. Thus, we check that the limit horizontal reaction (that the rubble mound can exert) is suitably greater than the actual horizontal reaction the rubble mound is expected to exert.

Against overturning. We must verify that the safety factor

$$C_2 \equiv \frac{P^* e_P}{M} \tag{14.5}$$

is greater than some dictated value $C_{2\ \min} > 1$. Indeed, were $P^* e_P$ equal to M, then e_R would be zero (cf. Eqn (14.3)), and hence the overturning would occur. Then, $C_{2\ \min}$ should be greater than $C_{1\ \min}$, given that C_1 can approach 1 without breakwater sliding, while a failure will occur certainly before than C_2 approaches 1. This will be the collapse of foundation, given that as C_2 approaches 1, e_R approaches zero, and hence the bearing pressure at O_1 tends to infinity.

Against collapse of foundation. A common procedure is to check that the largest toe pressure is within $4 \cdot 10^5 \div 5 \cdot 10^5$ N/m^2. An alternative way may be verifying that the safety factor

$$C_3 \equiv \frac{B_C}{R_v / 2e_R} \tag{14.6}$$

is greater than some dictated value $C_{3\ \min} > 1$. The denominator on the RHS of this formula gives the bearing pressure, and the numerator (B_C) represents the bearing capacity, which depends on the characteristics of the soil, on the ratio R_o/R_v, and on e_R.

The verifications of the stability against overturning and against collapse of foundation really aim to check the stability against one mode of failure: under the wave force, e_R is reduced so that the bearing pressure at the heel of upright section becomes too large, the soil collapses and the structure tilts and sinks into the ground.

14.2 WAVE PRESSURES

14.2.1 Goda's Model

Following Goda (2000), the H_s and H for the design of a breakwater are

$$H_s = C_s H_{s_0} \quad \text{if} \quad d_n/L_0 > 0.2 \tag{14.7}$$

$$H_s = \text{Min}\left(\beta_0 H_{s_o} + \beta_1 d_n, \beta_{\max} H_{s_o}, C_s H_{s_o}\right) \quad \text{if} \quad d_n/L_0 < 0.2 \tag{14.8}$$

$$H = 1.8C_sH_{s_0} \quad \text{if} \quad d_n/L_0 > 0.2 \tag{14.9}$$

$$H = \text{Min}\left(\widehat{\beta}_0 H_{s_0} + \widehat{\beta}_1 d_n, \widehat{\beta}_{\max} H_{s_0}, 1.8C_sH_{s_0}\right) \quad \text{if} \quad d_n/L_0 < 0.2 \tag{14.10}$$

where C_s is the shoaling coefficient: the terms β are due to dissipation of wave energy, with β_0, β_1, $\beta_{\max}$, and $\widehat{\beta}_0, \widehat{\beta}_1, \widehat{\beta}_{\max}$, depending on sea bottom slope λ, and β_0, β_{max}, $\widehat{\beta}_0, \widehat{\beta}_{\max}$, also depending on the wave steepness H_{s0}/L_0. If there is refraction and/or diffraction from deep water to water depth d_n, H_{s_0} must be intended as the actual deep water significant wave height multiplied by the diffraction coefficient (C_d) and the refraction coefficient (C_r). C_d is estimated by means of Eqn (7.50), and C_r by means of a similar equation based on the deep water directional spectrum.

The distribution of wave pressure on the wall and on the base is given by the following equations, wherein reference is made to Fig. 14.3:

$$\eta_{\max} = \frac{3}{4}(1 + \cos\theta)H \tag{14.11}$$

$$p_{w_1} = \frac{1}{2}(1 + \cos\theta)\left(\alpha' + \alpha''\cos^2\theta\right)\gamma H \tag{14.12}$$

$$p_w = \alpha''' p_{w_1} \tag{14.13}$$

$$p_{w_2} = \frac{1}{2}(1 + \cos\theta)\alpha'\alpha'''\gamma H \tag{14.14}$$

where

$$\alpha' = 0.6 + \frac{1}{2}\left[\frac{2kd_n}{\sinh(2kd_n)}\right]^2 \tag{14.15}$$

$$\alpha'' = \text{Min}\left[\left(\frac{d_n' - d}{3d_n'}\right)\left(\frac{H}{d}\right)^2, 2\frac{d}{H}\right] \tag{14.16}$$

$$\alpha''' = 1 - \frac{d'}{d_n}\left[1 - \frac{1}{\cosh(kd_n)}\right] \tag{14.17}$$

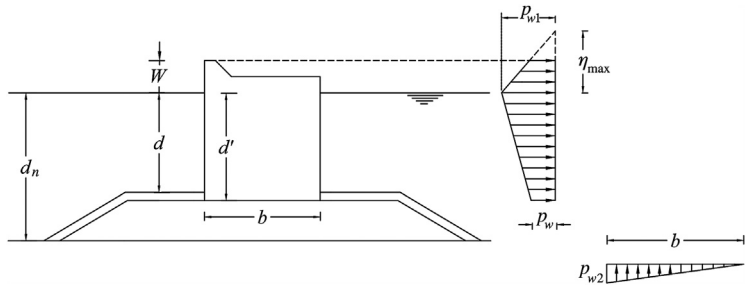

■ **FIGURE 14.3 Reference scheme for Goda's model (GM).**

where d'_n denotes the water depth at a distance of $5H_s$ seawards of the breakwater. Cautiously, it is suggested that the wave direction is rotated by an amount of up to 15° toward the line normal to the breakwater from the principal wave direction.

As to the wave period, Goda uses $T_{1/3}$, that is, the average period of the largest 1/3 waves of the sea state. This period proves to be very close to T_h—the wave period of very large waves, which proceeds from the autocovariance (see Section 4.5.1). In an SSFE on 750 sea states consisting of wind seas, the average $T_{1/3}/T_h$ was equal to 0.994 (cf. Boccotti et al., 2012). As for the negative wave pressures, under wave troughs, Goda (2000) supplies a diagram (see his Fig. 4.9) that enables one to estimate the resultant force for given wave height and period and water depth.

14.2.2 The Virtual-Height Model

Nonlinearity effects yield some characteristic deformation of wave pressure at a breakwater (without changing the overall configuration of wave groups). Roughly, it is as if the positive pressures were those of a linear wave, and the negative pressures were those of a linear wave with a larger height. This is what emerged from the SSFE described in Chapter 13 of a previous book. As a consequence, the following model was suggested for the largest positive pressures and the largest negative pressures, respectively, of a given sea state

$$\textit{wave crest} \quad \Delta p = \begin{cases} \gamma H^+ \dfrac{\cosh\left[k(d+z)\right]}{\cosh\left(kd\right)} & \text{if } z \le 0 \\ \gamma\left(H^+ - z\right) & \text{if } z > 0 \end{cases} \tag{14.18}$$

$$\textit{wave trough} \quad \Delta p = \begin{cases} -\gamma H^- \dfrac{\cosh\left[k(d+z)\right]}{\cosh\left(kd\right)} & \text{if } \Delta p > -p_{id} \\ -p_{id} & \text{otherwise} \end{cases} \tag{14.19}$$

Equation (14.18) gives the average pressure distribution of a given share of the largest positive peaks of the horizontal force on the breakwater. Equation (14.19) gives the average pressure distribution of a given share of the largest negative peaks of the horizontal force on the breakwater. In these equations, H^+ and H^- are virtual wave heights that depend on whether the given share is, for example, 1/1000 or 1/100. In particular,

$$H^+ = 1.40H_s, \quad H^- = 2.31H_s \tag{14.20}$$

with the 1/1000 largest waves of a sea state.

14.3 EVIDENCES FROM SSFEs

The SSFE of Boccotti (2000) covered only the range $0.15 < d/L_{p0} < 0.20$. An SSFE covering a wider range of d/L_{p0} was performed in 2009—see Fig. 14.4. For the aims of the following synthesis:

F^+ will be the average of the 1/1000 share of the largest positive force peaks measured in a sea state;
F^+_{GM}, the largest positive wave force in a sea state, calculated according to the GM;

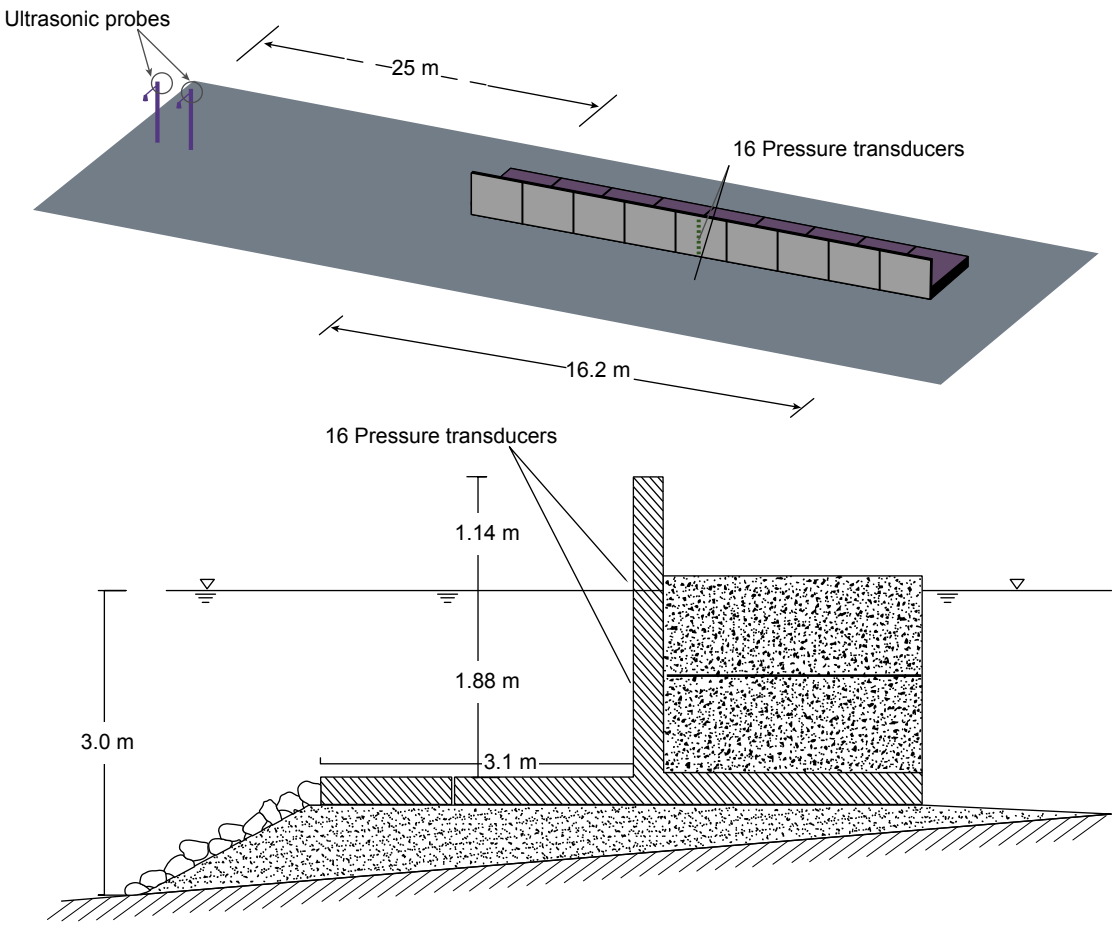

■ **FIGURE 14.4 The vertical breakwater used for the SSFE of 2009 on a wide range of d/L_{p0}.** Water depth d was equal to 1.88 m + tide level. The tide amplitude was within 0.16 m.

F^+_{VHM}, the average of the 1/1000 share of the largest positive force peaks in a sea state calculated according to the virtual-height model (VHM);
F^-, F^-_{GM}, and F^-_{VHM}, will have the same meaning as F^+, F^+_{GM}, and F^+_{VHM}, with the only difference to represent the absolute values of the force exerted by a wave trough instead of the force exerted by a wave crest. F^-_{GM} is based on the abacus of Fig. 4.9 of the book of Goda (2000), with H given by Eqn (14.10).
$F^+_{GM}, F^+_{VHM}, F^-_{GM}$, and F^-_{VHM} were obtained from the H_s, T_h or $T_{1/3}$ of the measured incident waves.

The following emerges from the SSFE of 2009:

F^+_{GM} is a 3% smaller than F^+ on the range $(0.10 < d/L_{p0} < 0.15)$,
F^+_{GM} is greater than F^+, of 7−9%, on the range $(0.15 < d/L_{p0} < 0.25)$,
F^+_{VHM} with the virtual wave height H^+ of 1.4 H_s underestimates F^+ from the 5% to the 10%,
F^- is smaller than F^+ for $d/L_{p0} < 0.15$,
F^- is equivalent to F^+ for $0.15 < d/L_{p0} < 0.20$,
F^- is greater than F^+ for $d/L_{p0} > 0.20$

which implies that the verification of the stability under wave trough usually becomes important only for $d/L_{p0} > 0.20$. Hence, we focus negative wave forces only on this range, where the picture is the following:

F^-_{GM} is about the 20% smaller than F^-, on $0.20 < d/L_{p0} < 0.30$,

whereas F^-_{VHM} with

$$H^- = 3.0H_s \text{ on the range } 0.20 < d/L_{p0} < 0.30 \tag{14.21}$$

gives a nearly perfect agreement with the measured pressure distributions.

The wide (though not exhaustive) test of the 2009 SSFE suggests that the GM is being widely used and yielding forces that are close to, or somewhat greater than, $F_{1/1000}$, and continue to be used for estimating positive pressure on vertical breakwaters. On the other hand, the VHM, with some appropriate values of the virtual wave height H^-, is effective for estimating negative pressures.

14.4 THE RISK OF IMPULSIVE BREAKING WAVE PRESSURES

If the breaking point of a progressive wave (in the absence of a structure) is located only slightly in front of the breakwater, or the combined sloping section and top berm of the rubble mound is rather broad, there may be danger of impulsive breaking wave pressure. Following Goda (2000), if

the rubble mound is sufficiently small enough to be considered negligible, then there is little danger of impulsive breaking wave pressure if at least one of the following conditions occur:

1. the sea bottom slope being smaller than 0.02,
2. $H_{s_0} C_r C_d / L_0$ being greater than 0.03 (L_0 being the deep water wave length corresponding to T_h),
3. the crest elevation of the wall allowing much overtopping.

A recent (May 2013) SSFE performed in the NOEL under my direction (results still unpublished) has evidenced that impulsive breaking wave pressures may occur even if both conditions (2) and (3) are fulfilled. However, the experiment has also shown that caisson breakwaters may resist unexpectedly well to these impulsive forces, whereas breakwaters consisting of solid concrete blocks collapse in line with the expectation. The high resistance of caissons should be due to the effect of mound foundation and ground, which are elastically deformed under the application of an impulsive wave breaking pressure (see Goda, 1992). This research is in due course: the configuration of the lee side of the rubble mound could prove to be important.

14.5 WORKED EXAMPLES

14.5.1 First Worked Example

Vertical breakwater with $d = 14$ m, $W = 7$ m, $d' = 15.5$ m, $d_n = 18$ m, $\lambda = 0.02$, straight contour lines; design sea state: $H_{s_0} = 8.0$ m, spectrum: mean JONSWAP with $A = 0.01$; directional distribution: Mitsuyasu et al. with $n_p = 20$ and $\theta_d = 0$.

Results of calculations (GM applied): $T_p = 12.1$ s, $T_h = 11.1$ s, $H_s = 7.18$ m, $H = 12.9$ m, $\eta_{\max} = 19.3$ m, $p_{w_1} = 114$ kN/m^2, $p_w = 87$ kN/m^2, $F^+ = 2210$ kN/m.

This is a case in which impulsive pressure could occur, and their intensity should be sensitive to the berm width (for a deeper insight into this item, see the questionnaire, Table 4.1 of Goda, 2000; prepared by referring to Tanimoto's examination).

The ratio d/L_{p0} (=0.06) is smaller than 0.20, hence the negative wave force is expected to be smaller than the positive wave force.

14.5.2 Second Worked Example

Vertical breakwater with $d = 50$ m, $W = 7$ m, $d' = 51$ m, $d_n = 54$ m, $\lambda = 0.02$, straight contour lines; design sea state: same deep water characteristics as for the first worked example.

Results of calculations (GM applied): $T_p = 12.1$ s, $T_h = 11.1$ s, $H_s = 7.36$ m, $H = 13.2$ m, $\eta_{max} = 19.8$ m, $p_{w_1} = 82$ kN/m^2, $p_w = 28.4$ kN/m^2, $F^+ = 3300$ kN/m.

In this case, because of the large water depth ($d/L_{p0} = 0.22$), it is also necessary to evaluate the effect of the wave trough. Result of calculations (VHM applied): $H^- = 22.1$ m, Δp is represented in Fig. 14.5, $F^- = 4570$ kN/m, which is definitely greater than F^+ (=3300 kN/m).

Notwithstanding the uplift force plays against stability under a wave crest, and pros stability under a wave trough, probably, the overall stability of this breakwater on 50-m water depth will prove to be more critical under the wave trough than under the wave crest.

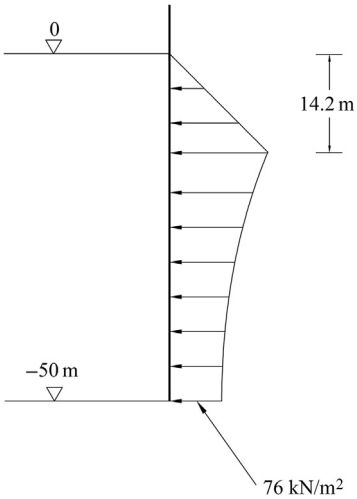

■ **FIGURE 14.5 Second worked example, Chapter 14: negative wave pressure on a 50-m-deep breakwater.** The resultant force on $(-d = -50 \text{ m} < z < 0)$ is about 4500 kN/m. Then there is an additional small force on $(-d' = -51 \text{ m} < z < -d)$, which is estimated to be 76 kN/m.

14.6 CONCLUSION

Wave loads on vertical breakwaters are estimated with empirical formulae based essentially on waveflume data, and in part on examination of full-scale failures or nonfailures (Goda, 1974; Oumeraci, 1994). This approach is effective, and especially the great experience accumulated by the Japanese School must be exploited. A fresh contribution may come from SSFEs. The results of the SSFEs of 1994 and 2009 were disclosed, respectively, in Chapter 13 of my book (2000) and in the paper by Boccotti et al. (2012).

REFERENCES

Boccotti, P., 2000. Wave Mechanics for Ocean Engineering. Elsevier, Amsterdam, p. 495.

Boccotti, P., Arena, F., Fiamma, V., Romolo, A., Barbaro, G., 2012. A small-scale field experiment on wave forces on upright breakwaters. J. Waterw. Port Coast. Ocean Eng.-ASCE 138 (2), 97−114.

Goda, Y., 1974. A new method of wave pressure calculation for the design of composite breakwaters. In: Proc. 14th Conf. Coastal Engineering. ASCE, New York, pp. 1702−1720.

Goda, Y., 1992. Dynamic response of upright breakwaters to impulsive breaking wave forces. Coast. Eng. 22, 135−158.

Goda, Y., 2000. Random Seas and Design of Maritime Structures. World Scientific, Singapore, 443 pp.

Oumeraci, H., 1994. Review and analysis of vertical breakwater failures − lesson learned. Coast. Eng. 22, 3−29.

Chapter 15

Conversion of Wave Energy

CHAPTER OUTLINE

15.1 AN OVERVIEW OF WORK DONE TO EXPLOIT WAVE ENERGY SOURCE

Many immersed oscillating systems have been disclosed for the aim of wave energy conversion. One of the first was a navigation buoy due to the pioneering research of Commander Yoshio Masuda in Japan. It consisted of a battery-charging generator driven by an oscillating water column (OWC) contained in a vertical pipe through a floating buoy. Masuda's developmental work of this device was in the mid-1960s (see ECOR, 2003; Falcao, 2010, for more details). The research of the 1970s concentrated mainly on resonant point absorbers (McCormick, 1974; Mei, 1976; Budal and Falnes, 1975, 1977). Two well-known devices of those years were the "Salter duck" (Salter, 1974) and the "Bristol cylinder" (Evans, 1976). According to the classification of Hagerman (1995), these belong, respectively, to the class of "pitching floats with mutual force reaction" and "submerged buoyant absorbers with sea-floor reaction point." Starting from the 1980s, most international attention was focused on fixed OWCs, whose prototypes were built in Australia, China, India, Japan, Norway, Portugal, and the United Kingdom. A conventional fixed OWC is essentially a box with a large opening on the wave-beaten wall. This opening usually goes from the seabed to nearly the mean water level (see the scheme of

Wave Mechanics and Wave Loads on Marine Structures. http://dx.doi.org/10.1016/B978-0-12-800343-5.00015-9

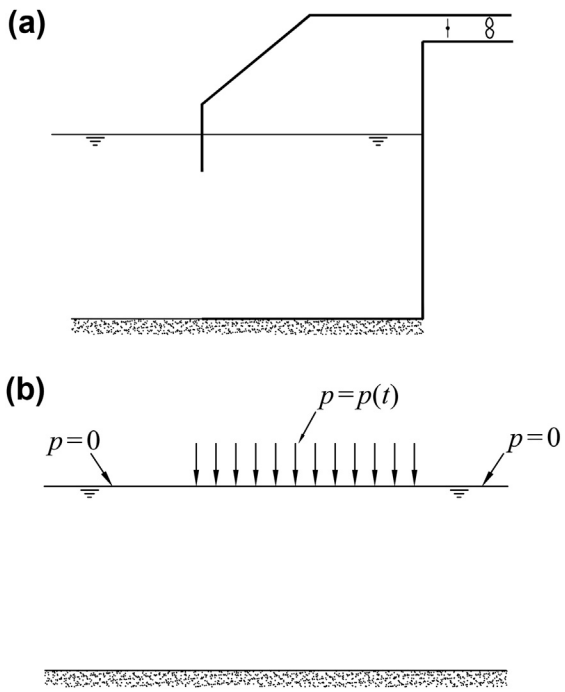

■ **FIGURE 15.1** (a) Cross-section of an oscillating water column. (b) Scheme of Stoker's type problem.

Fig. 15.1(a)). An air pocket remains between the roof and sea surface and is connected to the atmosphere by an exhaust tube with a turbine. Typically, this is a Wells turbine that rotates in the same direction even if the direction of the air flow is reversed (Raghunathan, 1995). Calculation of the performances of these kind of plants (Evans, 1982; Sarmento and Falcao, 1985) is founded on one pillar, that is, Stoker's solution (1957) for the waves generated by an oscillating pressure applied uniformly over a segment of the water surface (Fig. 15.1(b)). A first criticality of conventional OWCs is that their eigenperiod is smaller than the wave period. To overcome this problem, some devices were developed to create a sort of artificial resonance. This is known as "latching control" (Korde, 1991, 2002; Falcao and Justino, 1999). However, artificial resonance cannot compare with natural resonance. A second criticality of conventional OWCs deals with the stability of the structure. The geometry of conventional OWCs is different from the geometry of well-established structural types, such as, for example, offshore gravity platforms or caisson breakwaters. Hence, in designing a conventional OWC, we cannot exploit a consolidated experience, and this enhances the risk of failure; indeed, some failures must be registered among

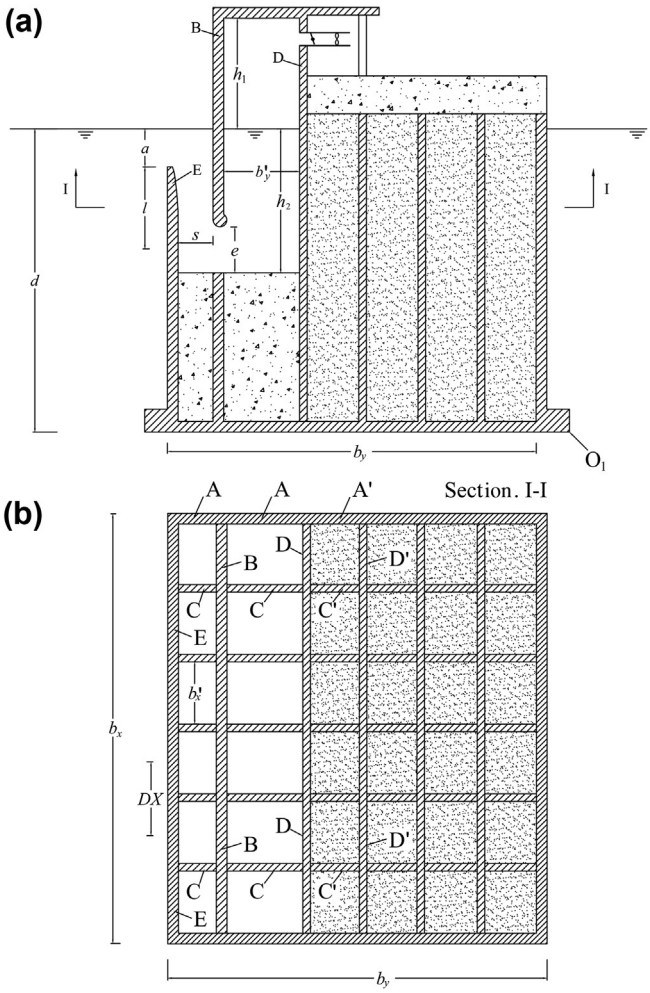

■ **FIGURE 15.2** (a) Cross-section and (b) horizontal section of an U-oscillating water column.

the prototypes (see ECOR, 2003). To overcome these criticalities, the author (2007a) introduced the U-OWC (see Fig. 15.2). Not only eigenperiods of U-OWCs are greater than eigenperiods of conventional OWCs, but the designer may tune the eigenperiod at his choice, on playing on the ratios s/b'_y and s/l. As to the overall stability, the design of U-OWCs can exploit the great experience accumulated with the design of caisson breakwaters (see Chapter 14). These are two evident pros for passing from conventional OWCs to U-OWCs. The cons should reduce themselves to the fact that Stoker's solution can no longer be exploited. Indeed, here there are not

two adjacent segments, one with a pulsating pressure and one with the atmospheric pressure, like in Fig. 15.1(a) and (b). This is because of the presence of the vertical duct connecting the sea with the chamber. This implies the need of leaving the territory explored initially by Lamb (1905), disclosed by Stoker (1957), further enlightened by Wehausen and Laitone (1960), and entering an unknown territory. Finding a solution for the interaction between wave and U-OWC took the author 2 years of work. The results were published in the paper (2007b) and are reproposed here below in a revised form.

15.2 THE PROPAGATION SPEED OF WAVE ENERGY

This section expands the reasoning of Section 1.10 so as to allow the solution for conversion of wave energy dealt with in the next section. The connection between the following analysis and wavemaker theories is discussed in the Conclusion to the chapter.

15.2.1 Re-analysis of the Problem of a Wavemaker

The wavemaker of Fig. 15.3 moves, alternately, rightwards and leftwards at section $y = 0$ of a waveflume, and yields a given oscillating water discharge

$$Q(t) = Q_{\max} \cos(\omega t + \varepsilon) \tag{15.1}$$

In Section 1.10, we assumed, as a matter of fact, that a wavemaker generates a progressive wave field. A more correct approach would have been assuming that the wavemaker generates a periodic waveform with the most general expression, given that a priori we do not know which is the waveform yielded by the wavemaker. The periodic wave function with the most general form is

$$\begin{aligned}\eta(y,t) = (&\alpha_1 \cos ky \cos \omega t + \alpha_2 \sin ky \cos \omega t + \alpha_3 \cos ky \sin \omega t \\ &+ \alpha_4 \sin ky \sin \omega t)H\end{aligned} \tag{15.2}$$

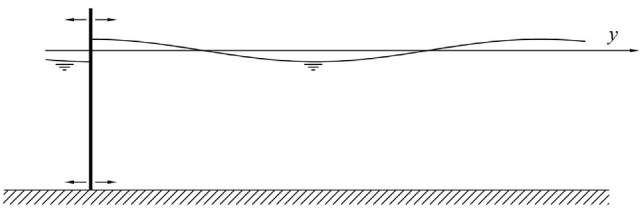

■ FIGURE 15.3 A wavemaker.

where parameters α_1, α_2, α_3, α_4, and height H are to be determined. The distribution of velocity potential associated with this wave function proves to be

$$\phi(y,z,t) = \frac{g}{\omega}(-\alpha_1 \cos ky \sin \omega t - \alpha_2 \sin ky \sin \omega t + \alpha_3 \cos ky \cos \omega t + \alpha_4 \sin ky \cos \omega t)H \frac{\cosh[k(d+z)]}{\cosh(kd)} \tag{15.3}$$

which implies that the water discharge at $y = 0$, the mean energy flux per unit length, and the mean energy per unit surface are

$$Q(t) = (-\alpha_2 \sin \omega t + \alpha_4 \cos \omega t)\frac{\omega}{k}H \tag{15.4}$$

$$\Phi = 0.50(\alpha_1\alpha_4 - \alpha_2\alpha_3)\rho g H^2 c_G \tag{15.5}$$

$$\mathscr{E} = 0.25\left(\alpha_1^2 + \alpha_2^2 + \alpha_3^2 + \alpha_4^2\right)\rho g H^2 \tag{15.6}$$

where c_G is the group velocity defined by Eqn (1.102). Equating the RHS of Eqn (15.4) to the RHS of Eqn (15.1), we get

$$H = \frac{Q_{\max} k}{\omega K} \tag{15.7}$$

$$\alpha_2 = K \sin(\varepsilon), \quad \alpha_4 = K \cos(\varepsilon) \tag{15.8}$$

where K is an arbitrary constant. Now let us assume that nature chooses the waveform that yields the largest value of the ratio

$$C = \frac{\Phi}{\mathscr{E} c_G} \tag{15.9}$$

(later, we shall discuss the base of this assumption). The expression of C proceeds from Eqns (15.5) and (15.6):

$$C = \frac{2(\alpha_1\alpha_4 - \alpha_2\alpha_3)}{\alpha_1^2 + \alpha_2^2 + \alpha_3^2 + \alpha_4^2} \tag{15.10}$$

C proves to vary between 0 and 1, and the maximum ($C = 1$) occurs for

$$\alpha_1 = \alpha_4, \quad \alpha_3 = -\alpha_2 \tag{15.11}$$

With Eqn (15.7) of H and Eqns (15.8) and (15.11) of the α_1, α_2, α_3, and α_4, Eqn (15.2) of $\eta(y, t)$ becomes

$$\eta(y,t) = Q_{\max}\frac{k}{\omega}(\cos \varepsilon \cos ky \cos \omega t + \sin \varepsilon \sin ky \cos \omega t - \sin \varepsilon \cos ky \sin \omega t + \cos \varepsilon \sin ky \sin \omega t) \tag{15.12}$$

where the unknown constant K cancels. Equation (15.12) can be reduced to

$$\eta(y,t) = Q_{\max}\frac{k}{\omega}\cos(ky-\omega t-\varepsilon) \tag{15.13}$$

which represents a progressive wave.

Let us summarize: we have two conclusions.

First conclusion: A wavemaker could generate an infinity of alternative waveforms. We knew that the wavemaker generates a progressive wave. Now we have realized that the progressive wave is the waveform giving the largest value of the dimensionless number C. Maximizing C is as if nature likes reaching the largest energy flux with the lowest storage of energy along the path of this energy flux, and indeed, we may call C the "energy-flux/energy factor."

Second conclusion: In the problem of the wavemaker that we have re-dealt with, C represents also the ratio between the speed with which the wave motion expands on the waveflume and c_G. Hence, in the infinite set of alternative waveforms that may be generated by the wavemaker, the aforementioned ratio ranges in (0, 1). In other words, the speed with which the wave motion expands on the waveflume can be smaller than or equal to c_G.

We shall assume that both the first conclusion and the second conclusion are valid in general, and in particular that they hold before a U-OWC. Note that, in the case of the U-OWC, the first conclusion will deal with the ratio between the mean energy flux reaching the plant, and the mean energy per unit surface before the plant. Whereas the second conclusion will concern the speed with which the reflected wave energy advances toward the open sea.

15.2.2 The Propagation Speed of Wave Energy

Now let us imagine to place an upright breakwater in the waveflume of Fig. 1.12. The new configuration is shown in Fig. 15.4. After the wave train strikes the breakwater, the wave field before the breakwater is changed

$$\text{from } 0.5\,H\cos(ky-\omega t) \text{ to } H\cos(ky)\cos(\omega t)$$

that is, from the progressive waves to the standing waves. The standing wave field gradually expands seawards with a propagation speed c_R. With the energy equation applied to the control volume of Fig. 15.4, we have

$$\Phi_{in} = (\mathscr{E} - \mathscr{E}_{in})c_R \tag{15.14}$$

where $\mathscr{E}_{in}$ and Φ_{in} are, respectively, the mean wave energy per unit surface and the mean energy flux per unit length of the incident waves, and $\mathscr{E}$ is the

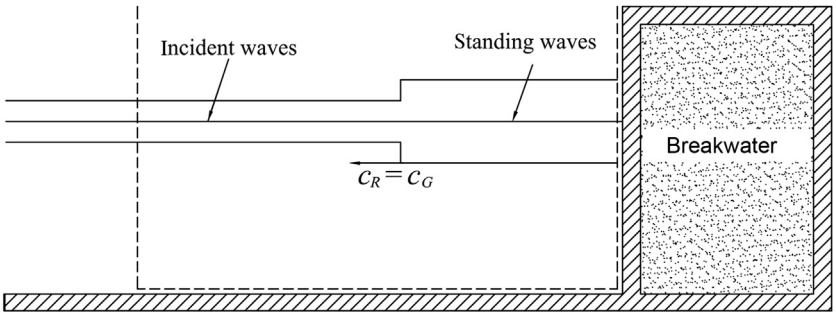

■ **FIGURE 15.4 After a wave train strikes a wall, a standing wave field expands toward the origin of the channel, with a propagation speed equal to group velocity c_G.**

mean wave energy per unit surface of the standing wave field. The LHS of Eqn (15.14) represents the average energy entering the control volume per unit time. The RHS represents the average increment of wave energy inside the control volume per unit time. Given that

$$\mathscr{E}_{in} = \frac{1}{8}\rho g H^2 \tag{15.15}$$

$$\Phi_{in} = \mathscr{E}_{in} c_G \tag{15.16}$$

$$\mathscr{E} = 2\mathscr{E}_{in} \tag{15.17}$$

it follows that

$$c_R = c_G \tag{15.18}$$

Finally, let the conventional breakwater be substituted by a breakwater embodying an energy converter (Fig. 15.5). We shall see in the next section that, after the wave train strikes the breakwater, the wave field before

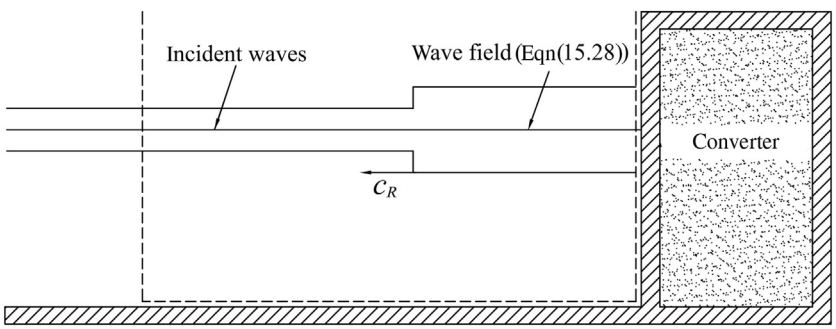

■ **FIGURE 15.5 After a wave train strikes a converter, a wave field given by Eqn (15.28) expands toward the origin of the channel, with a propagation speed c_R.** The ratio $\chi = c_R/c_G$ plays the central role in the wave-converter problem.

the breakwater is changed from $0.5H\cos(ky-\omega t)$ to a form given by Eqn (15.28), that is, from the progressive waves to a complex wave field, which in general will be different both from the progressive waves and from the standing waves. The complex wave field gradually expands seaward with a propagation speed c_R. With the energy equation applied to the control volume of Fig. 15.5, we have

$$(\Phi_{in}-\Phi) = (\mathscr{E}-\mathscr{E}_{in})c_R \tag{15.19}$$

where $\mathscr{E}$ and Φ are, respectively, the mean energy per unit surface and the mean energy flux per unit length of the complex wave field before the breakwater-converter.

Here, we have three inequalities:

$$\Phi_{in}-\Phi > 0 \tag{15.20}$$
$$\mathscr{E}-\mathscr{E}_{in} > 0 \tag{15.21}$$
$$c_R \le c_G \tag{15.22}$$

The third inequality is based on the assumption made at the end of Section 15.2.1. Indeed, c_R is the propagation speed with which the complex wave motion expands seawards. Inequalities (Eqns (15.20)–(15.22)) are equivalent to

$$0 < \chi \le 1 \tag{15.23}$$
$$A < 1 \tag{15.24}$$

where χ is the ratio between c_R and c_G, and A is the absorption coefficient:

$$\chi = \frac{c_R}{c_G} \tag{15.25}$$
$$A = \frac{\Phi}{\Phi_{in}} \tag{15.26}$$

15.3 INTERACTION BETWEEN WAVE AND U-OWC

15.3.1 The Logic Followed: Three Levels of Solution

The problem of the interaction between a wave of given height and period and a U-OWC aims to predict how much of the incident wave energy is absorbed by the plant, and which is the share of the absorbed energy that may be converted into electric power. There are three levels to deal with this problem: First level: it is assumed that the wave field before a breakwater embodying a U-OWC is the same as there would be before a vertical breakwater. Second level: the assumption that the wave field is equal to the wave field before a vertical breakwater is removed; however, the assumption remains that the wave field is periodic in space. Third level: the residual

assumption that the wave field be periodic in space is removed. With the second level, the wave height at the breakwater will no longer be $2H$, and the wave field will be that of the standing wave we saw in Section 1.7. This is because of the interaction with the U-OWC. Of course, it is possible that the third level will be approached; however, the author believes that the second level is valuable (for the aim of estimating the mean absorbed power) in that the solution obtained is exact under the assumption made. To say it better: were the waves periodic in space, that obtained here below would be the exact linear solution. Specifically, Section 15.3.2 gives the exact linear solution, if c_R (the propagation speed of the reflected wave energy) is equal to the group velocity c_G. Section 15.3.3 gives the exact linear solution, if nature maximizes the energy-flux/energy factor C, as it was suggested in Section 15.2.1.

15.3.2 Second Level: Basic Solution

Let us assume that the wave field before the breakwater-converter is periodic in time and space. Like in Section 15.1, we express this unknown wave field in the more general form for a periodic wave in time and space. This is given by Eqn (15.2), which may be rewritten in the form

$$\eta(y,t) = (\beta \cos ky \cos(\omega t + \varepsilon') + \alpha \sin ky \cos(\omega t + \varepsilon''))H \tag{15.27}$$

where β, α, ε', and ε'' are related to parameters α_1, α_2, α_3, α_4 of Eqn (15.2), and H here will be the height of the incident waves. Since the choice of the time origin is arbitrary, this origin may be shifted so as to rewrite Eqn (15.27) in the form

$$\eta(y,t) = (\beta \cos ky \cos(\omega t) + \alpha \sin ky \cos(\omega t + \varepsilon))H \tag{15.28}$$

where ε is equal to the difference $\varepsilon'' - \varepsilon'$. Associated to surface elevation Eqn (15.28) is a distribution of velocity potential in the water that is given by

$$\phi(y,z,t) = -g\beta H\omega^{-1} f(z)\cos(ky)\sin(\omega t) - g\alpha H\omega^{-1} f(z)\sin(ky)\sin(\omega t + \varepsilon) \tag{15.29}$$

where

$$f(z) = \frac{\cosh[k(d+z)]}{\cosh(kd)} \tag{15.30}$$

From the velocity potential, we obtain particle velocities v_y, v_z, and wave pressure Δp in the water. The wave pressure at ($y = 0$, $z = -a$) coincides with the $\Delta p(t)$ on the outer opening of the plant (see Fig. 15.2). From $v_y(z, t)$ at $y = 0$, we obtain the water discharge $Q(t)$ of the wave at the converter. From $v_y(y, z, t)$ and $\Delta p(y, z, t)$, we obtain the average wave energy flux

Φ. From $\eta(y, t)$, $v_y(y, z, t)$, and $v_z(y, z, t)$, we obtain the average wave energy $\mathscr{E}$ (average with respect to time and space) before the converter. The result is

$$\Delta p(t) = \rho g \beta H \cos(\omega t) \frac{\cosh[k(d-a)]}{\cosh(kd)} \tag{15.31}$$

$$Q(t) = -g\alpha H \omega^{-1} \tanh(kd) \sin(\omega t + \varepsilon) \tag{15.32}$$

$$\Phi = -4\alpha\beta \sin(\varepsilon) \Phi_{in} \tag{15.33}$$

$$\mathscr{E} = 2\left(\alpha^2 + \beta^2\right) \mathscr{E}_{in} \tag{15.34}$$

For a given plant and given incident waves, let us fix a tentative value of β, and let us take $\Delta p(t)$ as input for the calculation of the flow inside the plant, with the sequence described in Section 16.1 (next chapter). The knowledge of the flow inside the plant enables us to obtain $Q_p(t)$ and Φ_p, which are, respectively, the water discharge entering the plant, and the mean energy flux absorbed by the plant (per unit length). As a particular consequence of the knowledge of $Q_p(t)$, we can obtain the time shift T° between $\Delta p(t)$ and $Q_p(t)$ (see Fig. 15.6). At this point, we can get the three basic equations. The first one says that the phase angle between $\Delta p(t)$ and $Q_p(t)$ must be equal to the phase angle between $\Delta p(t)$ and $Q(t)$. The second one says that Φ must be equal to Φ_p. The third one gives the ratio χ between the propagation speed c_R of the reflected wave energy and c_G. These equations are

$$\varepsilon = -\omega T^\circ - \frac{\pi}{2} \tag{15.35}$$

$$\alpha = -\frac{\Phi_p}{4\beta \sin(\varepsilon) \Phi_{in}} \tag{15.36}$$

$$\chi = \frac{1 + 4\alpha\beta \sin(\varepsilon)}{2\left(\alpha^2 + \beta^2\right) - 1} \tag{15.37}$$

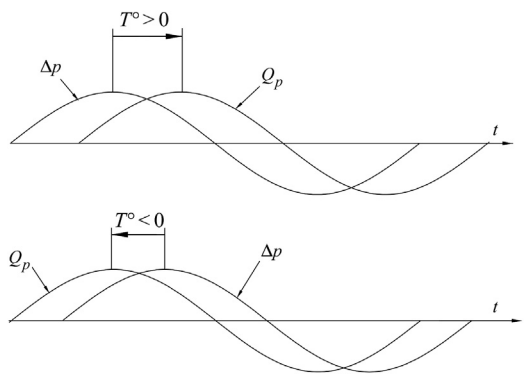

■ **FIGURE 15.6** T° **is the time shift between the water discharge entering the plant and the pressure fluctuation at the outer opening of the vertical duct.**

As to Eqn (15.35), the phase angle between $\Delta p(t)$ and $Q(t)$ is equal to $-\varepsilon - \pi/2$, and the phase angle between $\Delta p(t)$ and $Q_p(t)$ is the known value ωT°. Equation (15.35) proceeds on equating these phase angles to each other. As to Eqn (15.36), it proceeds straightforwardly from Eqn (15.33). As to Eqn (15.37) of χ, it proceeds from Eqn (15.19) of c_R, with Eqns (15.33) and (15.34) of Φ and $\mathscr{E}$.

Let us summarize: For a given β, Eqn (15.31) gives $\Delta p(t)$. Once $\Delta p(t)$ is known, it is possible to integrate the equations of water–air flow inside the plant (see the next chapter, Section 16.1) and to obtain, in particular, Φ_p and T°. Then, Eqn (15.35) yields ε. With ε being known, Eqn (15.36) yields α. With ε and α being known, Eqn (15.37) yields χ. Hence, one can obtain the functions $\varepsilon(\beta)$, $\alpha(\beta)$, and $\chi(\beta)$. If we assume that c_R must be equal to c_G (like with an upright breakwater), this assumption closes the problem: the solution will be represented by the β for which χ is equal to 1 (which generally proves to exist and to be unique), and this is the basic solution. Otherwise, if we follow assumption Eqn (15.23) that χ may be between 0 and 1, we may reason as in the next section, which gives the advanced solution.

15.3.3 Second Level: Advanced Solution

With Eqns (15.33) and (15.34) of Φ and $\mathscr{E}$, factor C defined by Eqn (15.9) takes on the form

$$C = -\frac{2\alpha\beta \sin(\varepsilon)}{(\alpha^2 + \beta^2)} \tag{15.38}$$

Besides C, there is a pair of numbers useful for an analysis of the wave field before a breakwater-converter. Of course, one is the absorption coefficient defined either as Φ/Φ_{in} or Φ_p/Φ_{in} (given that Φ and Φ_p are equal to each other). Hence, from Eqn (15.36), we have

$$A = -4\alpha\beta \sin(\varepsilon) \tag{15.39}$$

Then there is the resonance coefficient

$$R = 4\frac{T^\circ}{T} \tag{15.40}$$

where the time shift T° between $Q_p(t)$ and $\Delta p(t)$ may range in $(-T/4, T/4)$ (with T° in this range, the plant works as an absorber, else it would be a wavemaker). As a consequence, R ranges in $(-1, 1)$: R negative means that the wave period is greater than the eigenperiod; R positive means that the wave period is smaller than the eigenperiod.

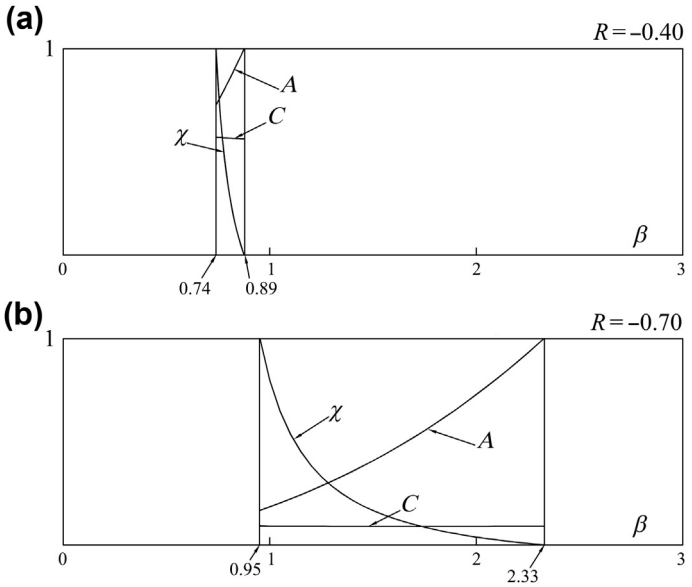

■ **FIGURE 15.7** Functions $\chi(\beta)$, $A(\beta)$, $C(\beta)$ for: (a) a case in which $|R|$ takes on a relatively small value, and (b) a case of a relatively large $|R|$.

If R approaches zero (resonance), inequality Eqn (15.23) is satisfied only on a small neighborhood $\Delta\beta$ of some special value β smaller than 1. On this small range of β, $\chi(\beta)$ decreases from 1 to 0, and A approaches 1; C approaches 1.

The range of β wherein inequality Eqn (15.23) is satisfied widens as $|R|$ grows, as we may see by comparing Fig. 15.7(a) and (b) to each other. Fig. 15.7(a) shows a case in which $R = -0.40$ and the inequality Eqn (15.23) prove to be satisfied on the range $(0.74 < \beta < 0.89)$. Figure 15.7(b) shows a case in which $R = -0.70$ and the range wherein the inequality Eqn (15.23) is satisfied becomes $(0.95 < \beta < 2.33)$. Over this range: χ decreases from 1 to 0, and A grows from 0.19 to 1. As to C, it remains essentially constant over the whole range. Therefore, from the reasoning of Section 15.1, nature should choose the solution at random, given that there is not a solution with a value of C greater than that of the other solutions. In this case, there should be the same probability to have any value of β between 0.95 and 2.33. Hence, in a case like that of Fig. 15.7(b), we should expect to find, most probably, a β definitely greater than 1. This expectancy has obtained many confirmations from a small-scale field experiment (SSFE) of 2005. An example is shown in Fig. 15.8 comparing the spectrum of waves at the breakwater-converter to the

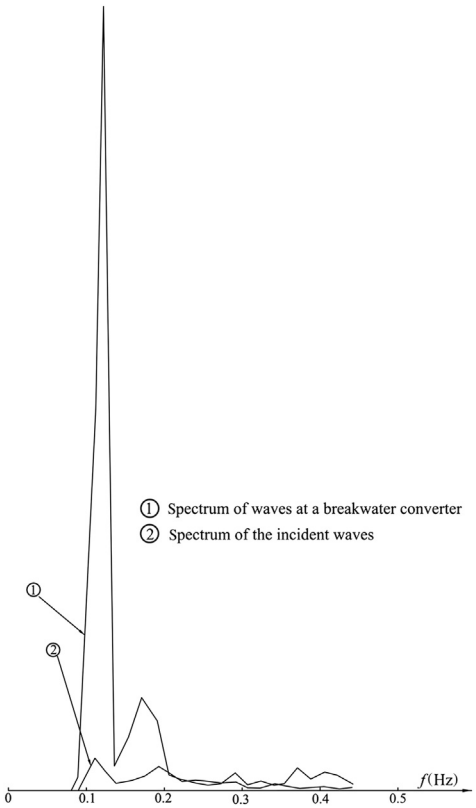

■ **FIGURE 15.8 A small-scale field experiment of 2005 on a U-oscillating water column:** the peak of the first mode, which has an estimated R of about -0.95, is amplified 23 times!

spectrum of the incident waves. The peak on the first mode, which has an estimated R of about -0.95, is amplified 23 times (!) on passing from the spectrum of the incident waves to the spectrum of the waves at the wall. This superamplification corresponds to a β of about 2.4. (β is equal to the ratio between the RMS surface elevation at the breakwater-converter and the RMS surface elevation that there would be at a conventional upright breakwater.)

The linear theory foresees superamplifications (possibility of very large β) both with large negative R and with large positive R. However, superamplifications require that waves have a very low steepness, otherwise there would be energy losses or wave breaking, and this, practically, limits superamplifications to some long swell with large negative R. In the next chapter we shall see how to address this face of the problem, on a technical-engineering ground.

Here we conclude with the following overall picture: If $\chi = 1$, β is smaller than 1. If β is greater than 1, χ is smaller than 1. If β takes on the total largest value (e.g., $\beta = 2.33$ in Fig. 15.7(b)) χ is equal to 0. This means that at the breakwater-converter there is a large wave amplification, which remains locked to the breakwater and cannot expand seawards. The fact that there is no energy advancing seaward implies that the whole incident wave energy is absorbed by the plant, and indeed, we see that the absorption coefficient gets equal to 1.

15.4 CONCLUSION

The wavemaker boundary value problem for planar wavemakers was given a complete solution thanks, in particular, to Havelock (1929), Hyun (1976), Hudspeth and Chen (1981). This problem aims to obtain the velocity potential yielded by a wavemaker with a given configuration. The area of wave-flume close to the wavemaker is focused, wherein waves are not periodic in space because of the presence of evanescent eigenmodes. It is assumed that, far from the wavemaker, the wave is a progressive one. We (Section 15.2.1) wonder whether this last sentence "far from the wavemaker, the wave is a progressive one" must be accepted as a matter of fact or may be explained as a consequence of a general principle (that nature tends to maximize the ratio between Φ and $\mathscr{E}$). Of course, in this context, there is no interest in the evanescent eigenmodes, nor in the configuration of the wavemaker. (Formally, one may shift the origin $y = 0$ far from the wavemaker; or, at his choice, may think of the configuration of the wavemaker as a curve in such a way that the wave motion can be periodic in space even close to the wavemaker.) Please don't believe that the question at the base of Section 15.2.1 is abstract philosophy. If nature tends to maximize the ratio $\Phi/\mathscr{E}$ (which is a velocity), this explains the huge amplification of Fig. 15.8, and let us look with greater optimism at the possibility of industrial exploitation of wave energy. A series of amplifications like that of Fig. 15.8 were found in the SSFE of 2005, illustrated by Boccotti et al. (2007).

REFERENCES

Boccotti, P., 2007a. Comparison between a U-OWC and a conventional OWC. Ocean Eng. 34, 799–805.

Boccotti, P., 2007b. Caisson breakwater embodying an OWC with a small opening. Part I: theory. Ocean Eng. 34, 806–819.

Boccotti, P., Filianoti, P., Fiamma, V., Arena, F., 2007. Caisson breakwater embodying an OWC with a small opening. Part II: a small-scale field experiment. Ocean Eng. 34, 820–841.

Budal, K., Falnes, J., 1975. A resonant point absorber of ocean-wave power. Nature 256, 478–479.

Budal, K., Falnes, J., 1977. Optimum operation of improved wave-power converter. Mar. Sci. Commun. 3, 133–150.
Engineering Committee on Oceanic Resources (ECOR), 2003. Wave Energy Conversion. Elsevier, Amsterdam, p. 187.
Evans, D.V., 1976. A theory for wave power absorption by oscillating bodies. J. Fluid Mech. 77, 1–25.
Evans, D.V., 1982. Wave power absorption by system of oscillating surface pressure distributions. J. Fluid Mech. 114, 481–499.
Falcao, A.F. de O., 2010. Wave energy utilization: a review of the technologies. Renewable Sustainable Energy Rev. 14, 899–918.
Falcao, A.F. de O., Justino, P.A.P., 1999. OWC wave energy devices with air flow control. Ocean Eng. 26, 1275–1295.
Hagerman, G., 1995. Wave power. In: Encyclopedia of Energy Technology and the Environment. John Wiley & Sons Inc., pp. 2859–2907.
Havelock, T.H., 1929. Forced surface-wave on water. Philos. Mag. F8, 569–576.
Hudspeth, R.T., Chen, M.-C., 1981. Design curves for hinged wavemakers: theory. J. Hydraul. Div. 107 (HY5), 533–552.
Hyun, J.M., 1976. Theory for hinged wavemakers of finite draft in water of constant depth. J. Hydronautics 10 (1), 2–7.
Korde, U.A., 1991. On the control of wave energy devices in multi-frequency waves. Appl. Ocean Res. 13, 132.
Korde, U.A., 2002. Active control in wave energy conversion. Sea Technol. 43 (7), 47–52.
Lamb, H., 1905. On deep water waves. Proc. Lond. Math. Soc. 2 (2), 371–400.
McCormick, M.E., 1974. Analysis of a wave energy conversion buoy. J. Hydronautics 8 (3), 77–82.
Mei, C.C., 1976. Power extraction from water waves. J. Ship Res. 21 (4), 248–253.
Raghunathan, S., 1995. The Wells air turbine for wave energy conversion. Prog. Aerosp. Sci. 31, 335.
Salter, S.H., 1974. Wave power. Nature 249, 720–724.
Sarmento, A.J., Falcao, A.F.de O., 1985. Wave generation by an oscillating surface-pressure and its application in wave energy extraction. J. Fluid Mech. 150, 467.
Stoker, J.J., 1957. Water Waves. Interscience.
Wehausen, J.W., Laitone, E.V., 1960. Surface waves. In: Handbuch der Physik, 9. Springer, pp. 446–778.

Chapter 16

Design of a Wave Energy Converter

CHAPTER OUTLINE

This chapter aims to suggest some ideas that could be useful for a preliminary design of a U-oscillating water column (OWC), in the present pioneering stage. Rationally approaching the design of wave energy converters, in general, is also a scope.

16.1 THE WATER AND AIR FLOW INSIDE A U-OWC

With reference to the scheme of Fig. 16.1, the equation of the water flow inside one cell may be expressed in the form

$$\frac{l'}{g}\,\frac{b'_y}{s}\,\frac{\mathrm{d}^2\xi}{\mathrm{d}t^2}+\frac{(l''-\xi)}{g}\,\frac{\mathrm{d}^2\xi}{\mathrm{d}t^2}=h'-h''-\Delta h_w \tag{16.1}$$

where

$$\Delta h_w = K_w\frac{u^2}{2g}\,\frac{u}{|u|} \tag{16.2}$$

Wave Mechanics and Wave Loads on Marine Structures. http://dx.doi.org/10.1016/B978-0-12-800343-5.00016-0

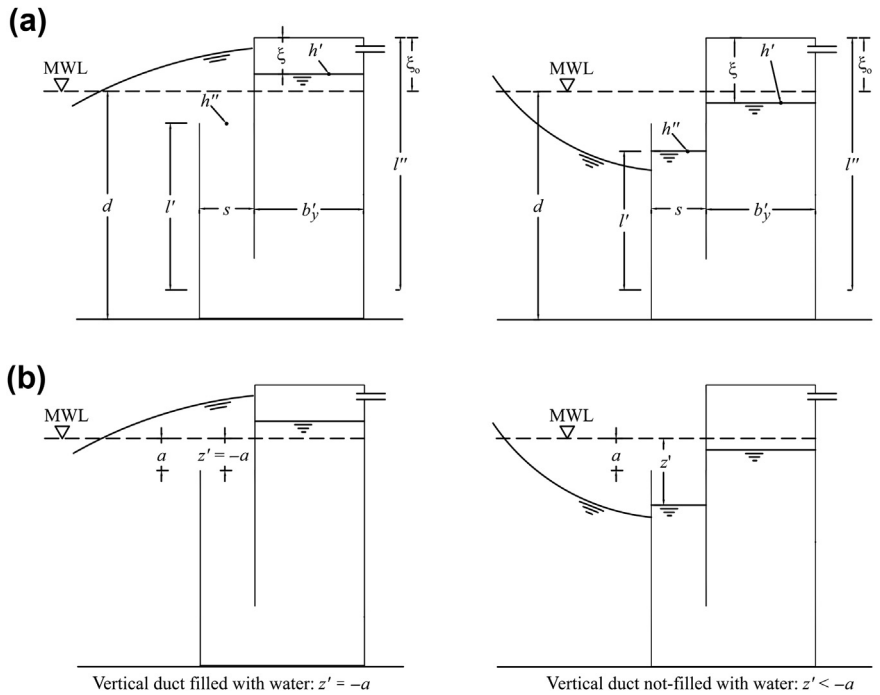

■ **FIGURE 16.1** (a) Reference scheme for Eqn (16.1). (b) Reference scheme for Eqn (16.7).

$$u = \frac{b'_y}{s}\,\frac{\mathrm{d}\xi}{\mathrm{d}t} \tag{16.3}$$

with K_w being the head loss factor in the vertical duct. The energy per unit weight at the water level in the chamber is

$$h' = (\xi_0 - \xi) + \frac{1}{2g}\left(\frac{\mathrm{d}\xi}{\mathrm{d}t}\right)^2 + \frac{(p_a - p_{\mathrm{atm}})}{\rho g} \tag{16.4}$$

The energy per unit weight at the outer opening of the vertical duct is estimated by means of

$$h'' = \frac{\Delta p}{\rho g} \quad \text{if} \quad \eta > -a \tag{16.5}$$

$$h'' = z' + \frac{u^2}{2g} \quad \text{if} \quad \eta < -a \tag{16.6}$$

where Δp is the wave pressure on the outer opening of the vertical duct, and z' is the level of the water in the vertical duct:

$$z' = -a \quad \text{if} \quad \eta \geq -a, \quad \text{otherwise} : \frac{\mathrm{d}z'}{\mathrm{d}t} = 0 \quad \text{if} \quad u > 0 \quad \text{and}$$

$$z' = -a, \quad \text{otherwise} \quad \frac{\mathrm{d}z'}{\mathrm{d}t} = u \tag{16.7}$$

Equation (16.5) holds with the linear wave theory. In order to smooth the step of $h''(t)$ at the time instant when $\eta = -a$, the RHS of Eqn (16.5) may be replaced by

$$\mathrm{Max}\left(\frac{\Delta p}{\rho g}, -a + \frac{u^2}{2g}\right)$$

The density in the air pocket is

$$\rho_a = \frac{M_a}{b'_y b'_x \xi} \tag{16.8}$$

and as such, it varies with time because of variations of air mass M_a and height ξ. The pressure in the air pocket is related to the air density by the gas law

$$\frac{p_a}{\rho_a^k} = \frac{p_{\mathrm{atm}}}{\rho_{\mathrm{atm}}^k} \tag{16.9}$$

The air velocity u_a through the turbine (we are thinking of a Wells turbine) is related to pressure p_a of the air pocket by

$$(K_{tube} + K_{turbine})\frac{u_a^2}{2}\frac{u_a}{|u_a|} = \frac{p_{\mathrm{atm}}}{\rho_{\mathrm{atm}}}\frac{k}{k-1}\left[\left(\frac{p_a}{p_{\mathrm{atm}}}\right)^{(1-1/k)} - 1\right] \tag{16.10}$$

where K_{tube} depends on the so-called minor losses in the air tube, and $K_{turbine}$ is a head loss factor in the turbine, which depends on parameter

$$u^* = \frac{|u_a|}{\omega D_e/2} \tag{16.11}$$

where ω and D_e are, respectively, the angular speed and diameter of the tip of the turbine.

The rate of change of the air mass in the air pocket may be approximately estimated by means of

$$\frac{\mathrm{d}M_a}{\mathrm{d}t} = -\frac{1}{2}(\rho_a + \rho_{\mathrm{atm}})\frac{\pi\left(D_e^2 - D_i^2\right)}{4}u_a \tag{16.12}$$

where D_i is the diameter of the bulk of the turbine.

Equations (16.1), (16.7), and (16.12) are integrated numerically, from the knowledge of $\Delta p(t)$ and of conditions at time $t = 0$, which are

$$\frac{\mathrm{d}\xi}{\mathrm{d}t} = 0, \quad \xi = \xi_0, \quad M_a = \rho_{\mathrm{atm}} b'_y b'_x \xi_0 \tag{16.13}$$

The flow chart is shown in Fig. 16.2. The average electrical power produced may be related to the head loss in the turbine by

$$\mathscr{P} = \left\langle eff\ K_{turbine}\frac{1}{2}\left|\frac{\mathrm{d}M_a}{\mathrm{d}t}\right|u_a^2 \right\rangle \tag{16.14}$$

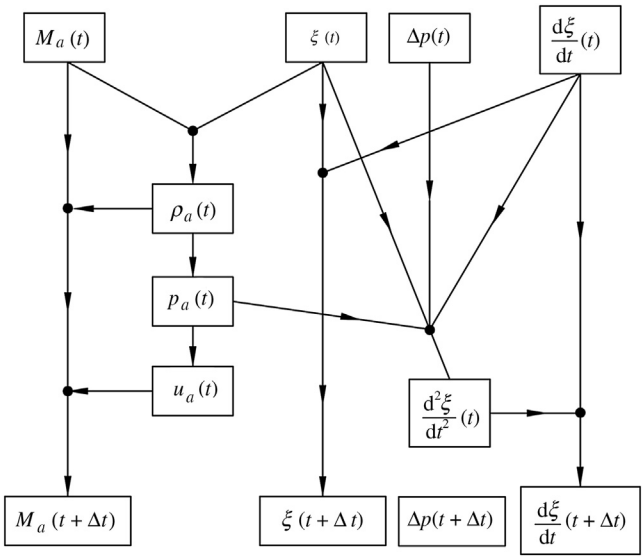

■ **FIGURE 16.2 Flow chart for integration of Eqns (16.1) and (16.12).**

where *eff* depends on u^* and on the characteristics of the generator. For an in-depth analysis of this subject, see Gato and Falcao (1990, 1991), Curran and Gato (1997).

16.2 PRODUCTION OF ELECTRICAL ENERGY FROM A GIVEN SEA STATE

We may apply Eqns (15.35−15.37) to a sea state of a given narrow-band spectrum. The surface elevation and the mean energy flux of the incident waves are given by

$$\eta(y,t) = \sum_{i=1}^{N} a_i \cos(k_i y - \omega_i t + \delta_i) \tag{16.15}$$

$$\Phi_{in} = \sum_{i=1}^{N} \rho g \frac{a_i^2}{2} c_{G_i} \tag{16.16}$$

where a_i and ω_i are such as to form a given spectrum, and phase angles δ_i are distributed uniformly on $(0, 2\pi)$ and are stochastically independent of one another, and number N is very large, and c_{G_i} is the group velocity relevant to angular frequency ω_i. The Δp on the outer opening of the plant is numerically simulated by means of

$$\Delta p(t) = \beta \rho g \sum_{i=1}^{N} a_i \frac{\cosh[k_i(d-a)]}{\cosh(k_i d)} \cos(\omega_i t + \delta_i) \tag{16.17}$$

with a tentative value of β. The calculation of the flow inside the plant is executed from this $\Delta p(t)$ with the sequence of Section 16.1, and yields $Q_p(t)$ and Φ_p. For estimating the time lag T° between $Q_p(t)$ and $\Delta p(t)$ (which now are random functions) we may resort to the cross-covariance

$$\psi_p(\tau) = \langle \Delta p(t) Q_p(t+\tau) \rangle \tag{16.18}$$

Figure 16.3 shows how to obtain T° and T from $\psi_p(\tau)$. After that, ε is obtained by means of Eqn (15.35), α proceeds straightforwardly from Eqn (15.36) since β, ε, Φ_p, Φ_{in} are known. The range ($\beta_{\min}$, $\beta_{\max}$) wherein inequality Eqn (15.23) is satisfied is found. The ratio χ decreases from 1 to 0 on this range.

If the incident waves are long swell with a H_s/L_{p0} smaller than 10^{-2}, which typically have some large negative R, we may take the value of β corresponding to $\chi = 0.25$. Otherwise, we may take the value of β corresponding to $\chi = 1$. These suggestions are based on the results of an SSFE of 2005 (Boccotti et al., 2007). Passing from $\chi = 1$ to $\chi = 0.25$, the estimate of wave energy absorption with long swells may grow of the very 50%. Resorting always to the solution $\chi = 1$ would be conservative in the oceans wherein the weight of long swells is great; it would be slightly conservative in the Mediterranean Sea where the share of wave energy carried by long swells is smaller than in the oceans.

The following is the flow chart of a numerical program aimed to calculate the wave energy conversion for a given sea state and configuration of the plant:

1. fix a frequency spectrum;
2. obtain N pairs a_i, ω_i so as to fit this frequency spectrum;

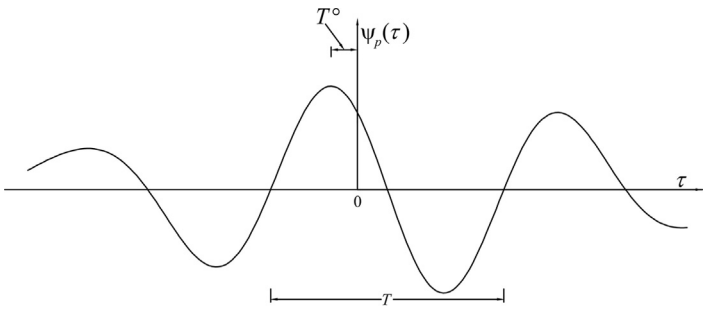

■ **FIGURE 16.3 Cross-covariance of pressure fluctuation at the outer opening and discharge in the plant.**

3. by means of Eqn (16.16) compute the mean energy flux Φ_{in} of the incident waves;
4. obtain N phase angles δ_i uniformly distributed in 0, 2π and stochastically independent from one another;
5. let β increase from a given β_{inf} to a given β_{sup} with a given step $\Delta\beta$ (suggested values: $\beta_{\text{inf}} = 0.5$, $\beta_{\text{sup}} = 3$, $\Delta\beta = 0.02$);
6. simulate numerically $\Delta p(t)$ by means of Eqn (16.17) for an interval $(0, \mathscr{T})$;
7. from $\Delta p(t)$ calculate the water flow and the air flow inside the plant through numerical integration of the differential flow equations given in Section 16.1;
8. as particular outputs of item 7, obtain $Q_p(t)$ (the water discharge in the plant), Φ_p the mean energy flux absorbed by the plant, EP the mean electrical power produced by the plant;
9. from $\Delta p(t)$ and $Q_p(t)$ obtain the cross-covariance $\psi_p(\tau)$ (def. Eqn (16.18));
10. from $\psi_p(\tau)$ obtain T° and T as it is shown in Fig. 16.3;
11. calculate ε by means of Eqn (15.35);
12. calculate α by means of Eqn (15.36);
13. calculate χ by means of Eqn (15.37);
14. calculate R by means of Eqn (15.40);
15. calculate

$$A = \frac{\Phi_p}{\Phi_{in}} \tag{16.19}$$

16. calculate

$$A_p = \frac{EP}{\Phi_{in}} \tag{16.20}$$

17. store $\chi(\beta)$, $R(\beta)$, $A(\beta)$, $A_p(\beta)$;
18. GO TO 5.

This program gives χ, A, A_p, R as functions of β for given sea state and plant. If H_s/L_{p0} is greater than 10^{-2}, we shall take the values corresponding to $\chi = 1$; otherwise, we shall take the values corresponding to $\chi = 0.25$. These values are exhaustive in that: β represents the ratio between the RMS surface elevation at the breakwater-converter and the RMS surface elevation that there would be at a conventional upright breakwater; A represents the ratio between the mean energy flux absorbed by the plant and the mean energy flux of the incident waves; A_p represents the ratio between the mean electrical power generated by the plant and the mean energy flux of the incident waves; R quantifies the difference between the wave period and the eigenperiod of the plant.

16.3 HYDRAULIC VERIFICATIONS

16.3.1 Method and Objectives

The factor β of the design sea state typically proves to be close to 1, which implies that the design sea state is close to that before a conventional upright breakwater. For the aim of estimating the conditions inside the vertical duct and the chamber in the extreme waves, we may integrate the equations of Section 16.1, taking as input the deterministic surface elevation $\overline{\eta}$ (Eqn (11.1)) at the breakwater, and the deterministic pressure fluctuation $\overline{\Delta p}$ (Eqn (11.4)) at the depth $z = -a$ of the outer opening of the vertical duct. The same $\overline{\eta}$ and $\overline{\Delta p}$ serve also for estimating the wave load on the outer face of wall B, above the elevation of the outer opening. The wave height H in Eqns 11.1 and 11.4 will be the maximum expected wave height in the design sea state either at the breakwater ($y_o = 0$) or at some point off the breakwater ($y_o < 0$).

The calculation aims to obtain

1. the safety margin between water level and roof of the chamber;
2. the largest positive and the largest negative pressure in the air pocket;
3. the largest loads on the walls of the chamber and of the vertical duct;
4. the vertical force ΔR_v due to the water flow inside the breakwater (so as to allow the verification of the overall stability);
5. the lowest level reached by the water surface in the vertical duct;
6. the lowest level reached by the water surface in the chamber.

In general, there should be no problems with the last two items in the sense that the lowest levels in both the chamber and the duct generally should remain well above the opening connecting the vertical duct with the chamber. Here below we consider in some details the items from (1) to (4).

16.3.2 Safety Margin between Water Level and Roof of the Chamber and Pressure in Air Pocket

Figure 16.4 shows the surface elevation, the water level in the chamber, and the pressure in the air pocket for a cell struck home by a wave group like that of Fig. 11.1 or 11.3. The water level in the chamber grows with the surface elevation. At time instant t_o the surface elevation starts decreasing; whereas the water level in the chamber greatly reduces its rate of growth. The pressure in the air pocket grows up to a maximum at time instant t_o and then is reduced reaching zero (atmospheric pressure) at a time instant t_1. Starting on t_1 the pressure in the air pocket falls below the atmospheric pressure, so that

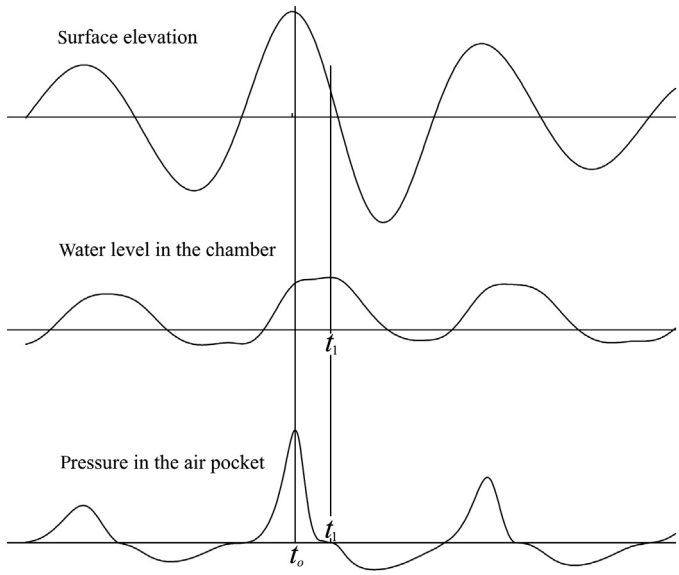

■ **FIGURE 16.4 Effect of the largest expected wave in the design sea state. First example: no shock pressure.**

the plant starts sucking air from the atmosphere, and this occurs jointly with a decreasing of the water level in the chamber.

It may occur that the water level in the chamber exceeds the elevation of the exhaust tube (Fig. 16.5), so that the air between the water surface and roof can no longer flow toward the atmosphere. In this case, the air pressure in the chamber grows rapidly (the growth is quasi-impulsive) up to a maximum at instant t_2 when the water level in the chamber reaches its maximum elevation. After t_2, the water level in the chamber decreases; the air pocket is stretched with the consequence of decreasing the air pressure. If the water level exceeds the elevation of the exhaust tube, two peaks of pressure occur in the air pocket: the pressure peak at time instant t_o of the wave crest, which will be called "primary pressure peak," and the pressure peak at time instant t_2, which will be called "shock pressure peak" because of its very short duration. The shock pressure peak may be very high. Therefore, it is advisable to take at least the following precautions in calculations. First, assume that the turbine has stopped: a stoppage of the turbine implies smaller head losses in the exhaust tube, so the rise of water in the chamber is greater. Second, assume that the maximum expected wave height occurs with the high tide. Third, repeat the calculation twice: first assume that the flow is isothermal, then a second time assuming that the flow is adiabatic. Take the larger value

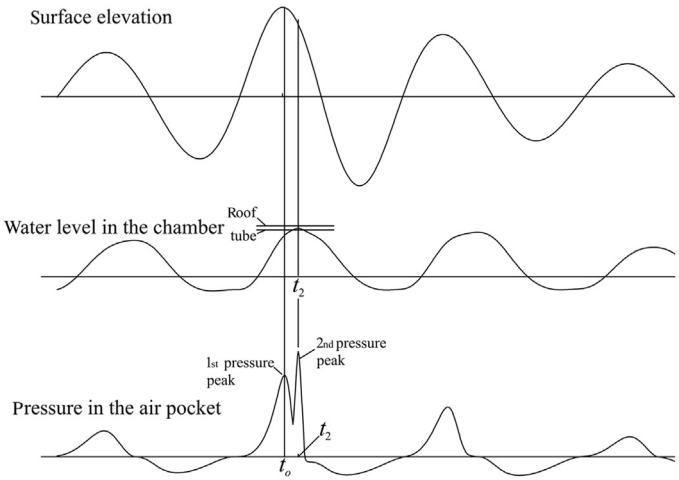

■ **FIGURE 16.5 Effect of the largest expected wave in the design sea state. Second example: primary pressure peak + shock pressure peak.**

of the two calculations for the rise of water in the chamber (there is usually only a small difference between the results of these two calculations).

16.3.3 Extreme Loads on Walls A, B, D

With the method of Section 16.3.1, the largest loads on walls A, B, and D (see Fig. 15.2) under the action of the maximum expected wave prove to be those with the air pocket under pressure. These loads act from the inside toward the outside of the chamber. If the shock pressure peak does not occur, wall B proves to be less loaded than walls A and D. Indeed, at instant t_o when inside the chamber there is the primary pressure peak, outside there is the wave crest, which means that the load on the external face partially counterbalances the load on the internal face of wall B.

The largest load acts on the roof and on the upper part of wall D. The pressure of the air pocket acts on the internal face, and the atmospheric pressure acts on the external face. We may assume that the load on wall A varies linearly from the load on wall B to the load on wall D.

The largest inward loads may occur either at the top of walls A, B, and D or beneath the mean water level. On the top of walls A, B, and D, the largest inward load coincides with the lowest (negative) pressure of the air pocket. The inward load on wall D at a given elevation beneath the mean water level is equal to the difference between the pressure of the fillet (sand) of the cells behind the chamber and the pressure of the chamber at the given elevation.

16.3.4 Extreme Loads on Wall C

If waves were long-crested, the wave attack was orthogonal to the breakwater, and the configuration of the hydraulic plant was the same for all cells, wall C would not be loaded; in other words, it would have the same pressure on the left and right faces. The shorter the wave crest, the greater the angle between the wave crest and breakwater; the greater the difference in the configuration of the hydraulic plant from one cell to the next, the larger the load on wall C. The length of the wave crest of a wave group decreases as the directional spread of the sea state grows. For the angle between the wave crest and breakwater, the quasi-determinism (QD) theory shows that the direction of a wave group advance has a high probability of coinciding with the dominant direction of the directional spectrum. Hence, it is advisable, cautiously, assuming some increment of the angle between the dominant direction and the orthogonal to the breakwater. For the configuration of the hydraulic plant, we may assume that the turbine in a cell is running at maximum speed while the turbine in the neighboring cell has stopped. We denote the cells before and after wall C under examination as cells 1 and 2, respectively. We must cover the following situations:

```
do i=1,2
the turbine of cell i is stopped
do j=1,2
the center of the wave crest strikes the center of cell j
enddo
enddo
```

As an example, let us deal with the case of $i = 1, j = 2$: the turbine of cell 1 is stopped, and the center of the wave crest strikes the center of cell 2. This implies that point x_o, y_o coincides with the center of cell 2, and the local coordinates of the center of cell 1 are

$$X = -DX, \quad Y = 0 \tag{16.21}$$

where DX is the length of a cell. The wave pressure $\overline{\Delta p}(t_o + T; \text{cell } 1)$ on the outer opening of cell 1 is obtained by means of Eqn (11.4) with $X = -DX$. The wave pressure $\overline{\Delta p}(t_o + T; \text{cell } 2)$ on the outer opening of cell 2 is obtained by means of Eqn (11.4) with $X = 0$. The water flow inside cell 1 is calculated from $\overline{\Delta p}(t_o + T; \text{cell } 1)$ by means of the flow equations of Section 16.1 with the turbine stopped. The water flow inside cell 2 is calculated from $\overline{\Delta p}(t_o + T; \text{cell } 2)$ by means of the flow equations of Section 16.1 with the turbine running at maximum speed. The pressures at various elevations in cells 1 and 2 at many time instants during the impact of the wave group are calculated, and the largest load on wall C (difference between the pressures on the two faces of said wall) are estimated.

16.3.5 **Overall Stability**

The vertical force ΔR_v due to the water flow inside the breakwater depends on: the variation of the weight of the water mass in the chamber; the inertia of the water mass in the chamber and vertical duct; the flux of momentum through the upper opening of the vertical duct; and on the wave pressure on the upper opening of the vertical duct and on the top of wall E. The force ΔR_v proves to be positive (that is, downwards oriented) at the time instant t_o of the crest of the maximum expected wave at the wall, when the maximum horizontal wave load and the maximum overturning moment is expected. As such ΔR_v plays a role favorable for stability. It is a non-negligible role: ΔR_v may reach the 10% of the weight P^* in still water. For the rest, the verification of the overall stability under the wave crest may be done as it is shown in Section 14.1. The connection between the conventional caisson breakwater and the chamber represents a novelty. Here, a critical situation might arise under the largest wave trough, given that under a wave trough, the chamber and duct is subject to a seaward force, and resistance to this force could be given only by the part in reinforced concrete of Section A-A of Fig. 16.6, if the concrete crown is simply in contact with wall D of the

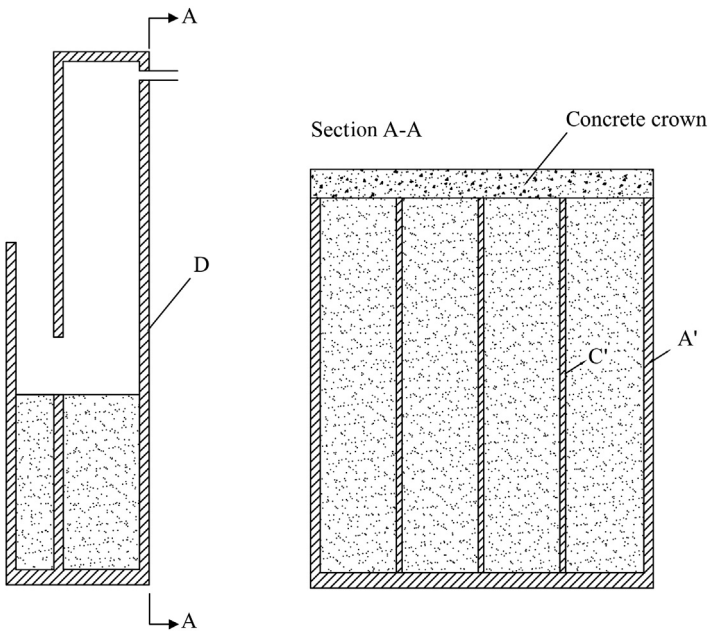

■ **FIGURE 16.6 In some plants the verification of Section A-A to the action of the wave trough could be not negligible.**

chamber. The chamber exerts a tensile force, shear force, and bending moment. The largest horizontal force F and uplift force S_w under a wave trough in the design sea state may be estimated as for a conventional caisson breakwater (see Chapter 14). The pressure exerted by the soil is obtained by applying the equilibrium equations to the whole caisson breakwater. Once all the forces acting on the chamber and duct are known (including the force exerted on wall D by the ballast in the cells behind this wall), the equilibrium equations applied to the chamber and duct yield the forces and bending moment acting on the vertical section. The vertical force due to the water flow inside the caisson at the time instant of the largest wave trough usually plays a role smaller than at the time instant of the largest wave crest.

16.4 FORTRAN PROGRAMS

16.4.1 QD Software for Hydraulic Verifications

Program UOWC1 computes $\overline{\eta}$ and $\overline{\Delta p}$ by means of QD Eqns (11.1) and (11.4). This program calls subroutine QD2, which has the four following differences with respect to subroutine QD introduced in Chapter 9:

1. it calculates wave pressure (not particle velocities and accelerations);
2. it is relevant to the wind-generated wave field before a long breakwater (not in the open sea);
3. it applies the directional distribution on finite water depth (not on deep water);
4. it applies the TMA spectrum (not the JONSWAP spectrum).

As to item (3) QD2 calls subroutine TRASDIR that requires as input the values of the parameters $n(\omega)$ and θ_d of the directional distribution (Eqn (6.17)) on deep water, and returns as output the values of $n(\omega)$ and $\theta_d(\omega)$ of the directional distribution on the given water depth d, under the assumption of straight contour lines. This is essentially the same as Goda (2000) calls the refraction effect on the spreading parameter. Program UOWC1 provides the time series of $\overline{\eta}$ and $\overline{\Delta p}$, which serve as input for the numerical integration of Eqns (16.1), (16.7), and (16.12). This integration requires a small step: typically $\Delta\tau = 2 \cdot 10^{-4}$ (τ being the ratio T/T_p). In order to reduce the computation time, UOWC1 writes the time series of $\overline{\eta}$ and $\overline{\Delta p}/\gamma$ with step $\Delta\tau = 0.05$. Then a new program will read these time series and compute $\overline{\eta}$ and $\overline{\Delta p}/\gamma$ with the $\Delta\tau$ of $2 \cdot 10^{-4}$, by means of a Fourier series. Lastly, a glance to the values of the space variables X and Y. X will be 0 for the estimate of the extreme air pressure in a cell; that is, it will be assumed that the largest wave group strikes this cell. X may be different from 0 (specifically $X = -DX$) for the estimate of the maximum load on walls C, as it has been shown in Section 16.3.4. As to Y, given that we

are interested in pressure and surface elevation at the wall, that is, at $y = 0$, we shall have

$$Y = y - y_o = -y_o \tag{16.22}$$

Note: in the following program UOWC1, the geometry ($d = 20$ m, $a = 2$ m) and the $T^*/T_p = 0.38$ of the local spectrum have been specified for the case of the worked example of the next section. The value of T^*/T_p has been obtained by running program SUMM1 (see Section 4.8.2).

```
      PROGRAM UOWC1
      CHARACTER*64 NOMEC
      COMMON D,HS,H,Tp,TST,ALPHA, TETAD0,RNP
      COMMON IMAX, JMAX,OMV(300),TETV(150),RKV(300)
      COMMON SOT(300,150)
      NOMEC='OUTP'
      OPEN(UNIT=60,FILE=NOMEC)
      PG=3.141592
      DPG=2.*PG
c geometry (to be changed): d and a - see Fig. 15.2 -
      D=20.
      A=2.

      Z=-A
      WRITE(6,*)'deep water: Hs,alpha,thetad(degree),np'
      READ(5,*)HS,ALPHA,TETAD0,RNP
      WRITE(6,*)'yo and Hmax at yo'
      READ(5,*)YO,H
      WRITE(6,*)'zero up-crossing wave -> 1, down-crossing -> -1'
      READ(5,*)UD
      TETAD0=TETAD0*PG/180.
      WRITE(6,*)'X'
      READ(5,*)X
      Y=-YO
      NCALL=0
      CALL QD2(NCALL,UD,X,Y,Z,T,YO,ETA,DP)
c this call of QD2, with NCALL=0, serves to store the directional spectrum
      NCALL=1
      TAUIN=-3.
      NMAX=121
      N=0
      DTAU=0.05
      TAU=TAUIN-DTAU
90    TAU=TAU+DTAU
      N=N+1
      IF(N.GT.NMAX)GO TO 91
      T=TAU*TP
      CALL QD2(NCALL,UD,X,Y,Z,T,YO,ETA,DP)
      WRITE(60,1000)TAU,ETA,DP
      WRITE(6,1000)TAU,ETA,DP
```

```
1000  FORMAT(2X,F7.2,2X,f7.3,2X,f7.3)
      GO TO 90
91    CONTINUE
      WRITE(6,*)
      WRITE(6,*)'read results on file OUTP'
      END

      SUBROUTINE QD2(NCALL,UD,X,Y,Z,T,YO,ETA,DP)
      COMMON D,HS,H,Tp,TST,ALPHA,TETADO,RNP
      COMMON IMAX,JMAX,OMV(300),TETV(150),RKV(300)
      COMMON SOT(300,150)
      DIMENSION EO(300),DTE(150)
      G=9.8
      G2=G*G
      PG=3.141592
      DPG=2.*PG
      IF(NCALL.EQ.1)GO TO 500
c*****************************************
c parameters deep water spectrum
      CO=1.345
      CHI1=3.3
      CHI2=0.08
c*****************************************
c T*/Tp local spectrum
      CST=0.38
c*****************************************
      COST=CO/ALPHA**0.25
      TP=COST*PG*SQRT(HS/G)
      TST=CST*TP
      ALCHI1=ALOG(CHI1)
      CHI2Q=CHI2*CHI2
      OP=DPG/TP
      DOMEGA=OP/50
      O1=0.5*OP
      O2=3.*OP
      OPQ=OP*OP
      DTETA=PG/100.
      TE1=-PG/2.
      TE2=PG/2.
      OM=O1-DOMEGA/2.
      I=0
c Loop 90: the grid of values of the directional spectrum, being necessary
c for the execution of the double integrals, is loaded on memory
90     OM=OM+DOMEGA
      IF(OM.GT.O2)GO TO 91
      I=I+1
      OMV(I)=OM
```

```
c values of omega stored on OMV(I) (I=1,IMAX)
      PE=DPG/OM
      RLO=(G/DPG)*PE*PE
      DLO=D/RLO
      IF(DLO.GT.0.5)THEN
      RKV(I)=DPG/RLO
      ELSE
      RLP=RLO
300   RL=RLO*TANH(DPG*D/RLP)
      TES=ABS(RL-RLP)/RL
      RLP=RL
      IF(TES.GT.1.E-4)GO TO 300
      RKV(I)=DPG/RL
      ENDIF
c k(omega) stored on RKV(I)
      OMM5=1./OM**5
      ARG=(OM-OP)**2/(2.*CHI2Q*OPQ)
      E3=EXP(-ARG)
      ARG=ALCHI1*E3
      E2=EXP(ARG)
      ARG=1.25*(OP/OM)**4
      E1=EXP(-ARG)
      EJON=ALPHA*G2*OMM5*E1*E2
c transformation function : from JONSWAP to TMA
      ARG=RKV(I)*D
      TA=TANH(ARG)
      DARG=2.*ARG
      SI2=SINH(DARG)
      TFUN=SI2*TA*TA/(SI2+DARG)
      EO(I)=EJON*TFUN
c EO(I)=E(omega)
c*****************************************
      W=OM/OP
      IF(W.LE.1)THEN
      RN=RNP*W**5
      ELSE
      RN=RNP/W**2.5
      ENDIF
c*****************************************
      CALL TRASDIR(D,OP,TETADO,W,RN,TETAD)
      DN=2.*RN
      TE=TE1-DTETA/2
      J=0
80    TE=TE+DTETA
      IF(TE.GT.TE2)GO TO 81
      J=J+1
      TETV(J)=TE+TETAD
```

```
c values of theta stored on TETV(J) (J=1,JMAX)
      ACO=ABS(COS(TE/2))
      DTE(J)=ACO**DN
      GO TO 80
81    CONTINUE
      JMAX=J
      J=0
      SOMT=0
      DO J=1,JMAX
      SOMT=SOMT+DTE(J)*DTETA
      ENDDO
      RKN=1./SOMT
c RKN=K(n) (Eqn (6.18))
      DO J=1,JMAX
      DTE(J)=RKN*DTE(J)
c DTE(J)=D(teta;omega)
      ENDDO
      DO J=1,JMAX
      SOT(I,J)=EO(I)*DTE(J)
c directional spectrum stored on SOT(I,J)
      ENDDO
      GO TO 90
91    CONTINUE
      IMAX=I
      IF(NCALL.EQ.0)GO TO 501
500   CONTINUE

c ETAINT = double integral numerator RHS of Eqn (11.1)
c DPINT = double integral numerator RHS of Eqn (11.4)
c DENOINT = double integral denominator RHS of Eqns (11.1) or (11.4)
      ETAINT=0
      DPINT=0
      DENOINT=0
      DO I=1,IMAX
      DO J=1,JMAX
      OM=OMV(I)
      OM1=1./OM
      RK=RKV(I)
      IF(RK*D.GT.20)THEN
      A1=EXP(RK*Z)
      ELSE
      A1=COSH(RK*(D+Z))/COSH(RK*D)
      ENDIF
      TE=TETV(J)
      S=SOT(I,J)
      ST=SIN(TE)
      CT=COS(TE)
      ARG1=RK*X*ST-OM*T
```

```
     .ARG2=RK*X*ST-OM*(T-TST)
      ARG3=RK*YO*CT
      ARG4=RK*(YO+Y)*CT
      CO1=COS(ARG1)
      CO2=COS(ARG2)
      CO3=COS(ARG3)
      CO4=COS(ARG4)
      ETAINT=ETAINT+S*CO3*CO4*(CO1-CO2)
      DPINT=DPINT+S*A1*CO3*CO4*(CO1-CO2)
      DENOINT=DENOINT+S*CO3*CO3*(1.-COS(OM*TST))
      ENDDO
      ENDDO
      ETA=UD*0.5*H*ETAINT/DENOINT
      DP=UD*0.5*H*DPINT/DENOINT
501   CONTINUE
      RETURN
      END

      SUBROUTINE TRASDIR(D,OP,TETADO,W,RN,TETAD)
c for the angular frequency omega=w omegap (W*OP)
c input: n(RN) of D(theta;omega) on deep water
c output: n(RN) of D(theta;omega) on water depth d
c input: thetad(TETADO) for every frequency on deep water
c output: thetad(TETADO) for the given frequency omega on water depth d
      DIMENSION DV(1000),TEV(1000),TEOV(1000)
      PG=3.141592
      DPG=2.*PG
      DN=2.*RN
      OM=W*OP
      T=DPG/OM
      RLO=1.56*T*T
      RLP=RLO
60    RL=RLO*TANH(DPG*D/RLP)
      TEST=ABS(RL-RLP)/RL
      RLP=RL
      IF(TEST.GT.1.E-4)GO TO 60
c RL wavelength on water depth d
      RKD=DPG*D/RL
      SINTE=SIN(TETADO)*TANH(RKD)
      TETAD=ASIN(SINTE)
c TETADO: dominant wave direction on deep water
c TETAD: dominant wave direction on water depth d
      DTEO=PG/200.
      TEO=-PG/2.-DTEO
      I=0
      SOMT=0
80    TEO=TEO+DTEO
      IF(TEO.GT.PG/2.)GO TO 81
```

```
     .I=I+1
      TEOV(I)=TEO
      COSA=COS(0.5*TEO)
      ACOSA=ABS(COSA)
      COSADN=ACOSA**DN
      DV(I)=COSADN
      SOMT=SOMT+DV(I)*DTEO
      GO TO 80
81    CONTINUE
      IMAX=I
      RKN=1./SOMT
      DO 90 I=1,IMAX
      SINTE=SIN(TEOV(I))*TANH(RKD)
      TEV(I)=ASIN(SINTE)
      DV(I)=RKN*DV(I)
c TEOV(I) ith value into which the theta domain on deep water is partitioned
c TEV(I) corresponding ith value of theta domain on water depth d
c DV(I) directional distribution
90    CONTINUE

      VARD=0
      I=0
      DO 100 I=1,IMAX-1
c Loop 100 calculates the variance (VARD) of the directional distribution
c on water depth d
      AA=0.5*(DV(I)+DV(I+1))*DTEO
      CC=0.5*(TEV(I)+TEV(I+1))
      VARD=VARD+AA*CC*CC
100   CONTINUE

c Now the subroutine looks for the directional distribution cos**2n
c with the n such that the variance is equal to the known value VARD
c For this scope the function 'variance vs n' (VART vs RNT) is calculated
c for increasing values of n (RNT), with step DRN.
      DRN=1
      RNT=RN-DRN
200   RNT=RNT+DRN
      DNT=2.*RNT
      DTE=PG/200.
      TE=-PG/2.-DTE
      I=0
      SOMT=0
c Loop 88 calculates the directional distribution DV(I) for a given n (RNT)
88    TE=TE+DTE
      IF(TE.GT.PG/2.)GO TO 89
      I=I+1
      COSA=COS(0.5*TE)
```

```
     .ACOSA=ABS(COSA)
      COSADN=ACOSA**DNT
      DV(I)=COSADN
      SOMT=SOMT+DV(I)*DTE
      GO TO 88
89    CONTINUE
      IMAX=I
      RKN=1./SOMT
      DO I=1,IMAX
      DV(I)=RKN*DV(I)
      ENDDO
      TE=-PG/2.-DTE
      VART=0
      DO 95 I=1,IMAX
c Loop 95 calculates the variance (VART) of the given directional
c distribution DV(I)
      TE=TE+DTE
      VART=VART+TE*TE*DV(I)*DTE
95    CONTINUE
      IF(VART.GT.VARD)GO TO 200
      RNT=RNT-DRN
      DRN=DRN/10.
      IF(DRN.GT.0.05)GO TO 200
      RN=RNT
      RETURN
      END
```

16.5 WORKED EXAMPLE

For the aim of a preliminary prototype design, estimate water level and air pressure in the chamber of the U-OWC of Fig. 15.2 with the following size: depth of the seabed: $d = 20$ m (in Chapter 14 this is denoted by d_n); depth of the outer opening: $a = 2$ m; vertical duct: $s = 1.6$ m; inner opening: $e = 2.0$ m; chamber: $b'_x = 3.8$ m, $b'_y = 4.0$ m; $h_1 = 7.0$ m; $h_2 = 8.0$ m; interaxis: $DX = 4.25$ m. The details of the exhaust tube and turbine are given in Fig. 16.7(c). Sea bottom slope = 3%, straight contour lines.

Design sea state (deep water): $H_{s0} = 8$ m, mean JONSWAP spectrum with $A = 0.01$, directional distribution of Mitsuyasu et al. with $n_p = 20$, $\theta_d = 0$ (dominant direction orthogonal to the contour lines), duration: 6 h.

The T_p proves to be 12.06 s, so that $d/L_{p0} = 0.088$. With Goda's model (Eqn (14.8)) we obtain $H_s = 7.20$ m on the local depth of 20 m.

With program SUMM1 and the use of the transformation function TFU (see Section 4.8.2) we obtain

$$T^*/T_p = 0.38,\ \ T_m/T_p = 0.67,\ \ K_1 = 1.31,\ \ K_2 = 6.40$$

for the TMA spectrum shape on the given water depth. From the T_m and the duration of the design sea state, it follows that the number of waves is

$$N = 2673.$$

With this number of waves, and the value of H_s (7.20 m) and the values of K_1 (=1.31) and K_2 (=6.40) program HMAX of Section 4.8.3 gives

$$\overline{H_{\max}} = 13.45 \text{ m}$$

This is the maximum expected height of the incident waves at any fixed point. At a point of the breakwater the maximum expected wave height will be twice as great, that is, 26.9 m (bear in mind Eqn (7.49), and the fact that $C_d = 2$ at a long breakwater). Letting program UOWC1 run with input $y_o = 0$ and $H = 26.9$ m we obtain the time series of $\overline{\eta}$ and $\overline{\Delta p}$, which serve for the numerical integration of Eqns (16.1), (16.7), and (16.12). The result (T/T_p, $\overline{\eta}$, $\overline{\Delta p}/\gamma$) is given in file OUTP. The time series of $\overline{\eta}$ represents a wave group whose kernel consists of the following sequence of wave heights (in meters):

$$6.4,\ 11.5,\ 26.9,\ 11.5,\ 6.4.$$

With the butterfly valve fully open, and turbine running at the maximum speed $\xi_{\min}$ (the safety margin between water level and roof of the chamber), and $p_{ra_{\min}}$ and $p_{ra_{\max}}$ (the minimum and maximum relative air pressure) are estimated to be

$$\xi_{\min} = 1.02 \text{ m}, \quad p_{ra_{\min}} = -36 \text{ kN/m}^2, \quad p_{ra_{\max}} = 134 \text{ kN/m}^2$$

Complements of the worked example: estimate of some performances of the plant. These estimates are done with the flow chart given in Section 16.2:

wind sea: $H_s = 2.0$ m, $T_p = 6.0$ s $\rightarrow A = 81\%$, EP = 3.2 kW/m
wind sea: $H_s = 2.5$ m, $T_p = 6.7$ s $\rightarrow A = 71\%$, EP = 4.7 kW/m (°)
swell: $H_s = 1.25$ m, $T_p = 10$ s $\rightarrow A = 67\%$, EP = 2.0 kW/m (°°)
(°) bounded by the power of the turbine-generator system (20 kW)
(°°) the turbine does not rotate at the maximum speed, in order to get the maximum efficiency.

16.6 OVERALL DESIGN

Two main faces of the design of a converter concern loads from extreme waves and (of course) production. I stated a holistic overview of these

two faces in the paper (2012). This has been reproposed in this chapter in an expanded form. A summary of this holistic overview may be the following (the reader should bear in mind that U-OWCs are in a pioneering stage).

The plant may be built either in place of a caisson breakwater with a scope of port defense (alternative (a)), or only for production of electrical power (alternative (b)). With alternative (a) the plant might even be turbineless, and the scope of the vertical duct and the chamber should be that of absorbing wave energy so as to reduce overtoppings. With alternative (b) it is convenient to build the plant on the smallest water depth that is possible. This should be a depth of about 10 m. Here note that

1. typically the average flux of the most valuable energy for conversion (that of swell) on 10 m water depth is not significantly smaller than on deep water;
2. the strongest wind seas are subject to great dissipation before reaching 10 m water depth; however, the production of electrical power by these seas is bounded by the power of the turbine-generator system, so that, typically there is no significant reduction due to wave energy dissipation.

The conclusion is that on 10 m water depth we should produce almost the same electrical energy as on some greater water depth. On the contrary, the largest wave height in the lifetime on 10 m water depth, especially off ocean coasts, may be much smaller than on deep water, with some much smaller extreme wave loads. On these small depths the waves of the design sea state will be breaking, and this will imply a rougher computation of the wave pressure on the outer opening (to a first approximation, the hypotheses of plants of Figs 16.7 and 16.8 were calculated, essentially, as in the worked example of Section 16.5 with the H_{max} of the incident waves being limited by the water depth induced wave breaking, with the breaker index of Battjes and Stive, 1985). Moreover, on these small depths, the risks and the effects of impulsive breaking wave pressures (see Section 14.4) must be considered.

The overall design of the system duct + chamber + exhaust tube calls for a complex synthesis between performances and safety. To enhance the performances of the plant, the resonance coefficient R of the sea states conveying the largest share of wave energy in a year must be close to zero. For tuning R the designer may play on the ratio b'_y/s between the width of the chamber and the width of the duct. Letting b'_y/s grow, R grows. Sometimes with alternative (a) (plant built in place of an upright breakwater) the designer may

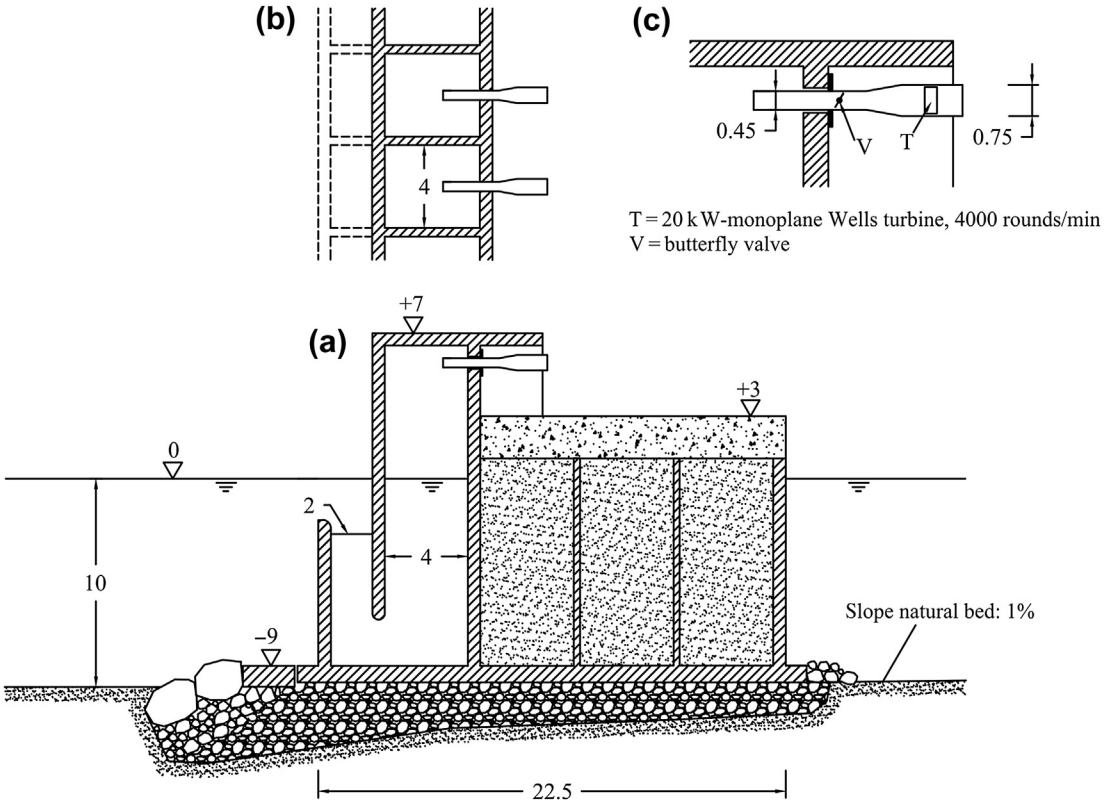

■ **FIGURE 16.7** A hypothesis of U-oscillating water column for the Mediterranean Sea. (a) Cross-section. (b) Horizontal section chambers and exhaust tubes. (c) Details of the cross-section.

exploit the ratio l/s to tune R. This occurs whenever the water depth prescribed for the breakwater is large enough (see Fig. 15.2). Letting l/s grow, R grows. Under the same R the absorption of wave energy increases with the width s of the intake.

There are three ways to increase safety margin ($\xi_{\min}$), and hence to lower the risk of a shock pressure peak inside the chamber, or attenuate the entity of this peak. These ways are the following:

First way: reducing the diameter of the exhaust tube and/or increasing the head losses in the butterfly valve.
Second way: increasing the height of the chamber.
Third way: increasing the width b'_y of the chamber and reducing the width s of the duct.

The second and the third of these three ways lead also to a reduction of the primary peak of pressure in the air pocket. On the contrary, the first way leads to an increase of the primary peak of pressure. Given that s and b'_y are the main parameters concerning performances there is not a great degree of freedom to be exploited with the third way. The second way (increasing the height of the chamber) is the more straight forward, and to some extent it must be run. However, this way has cost and environmental impact greater than the first way. It's true that the first way increases the primary pressure peak, but with an increase of the order of 10% of the primary pressure peak, the designer may increase the safety margin $\xi_{\min}$ of the order of 100%. One may decide to partially close the butterfly valve whenever the H_s exceeds some risk threshold. Doing so one increases safety against the shock pressure peak, without loss of production of electrical power. This is because the production of electrical power in strong seas is already bounded by the power of the turbine-generator system. A simpler solution may be to keep the valve

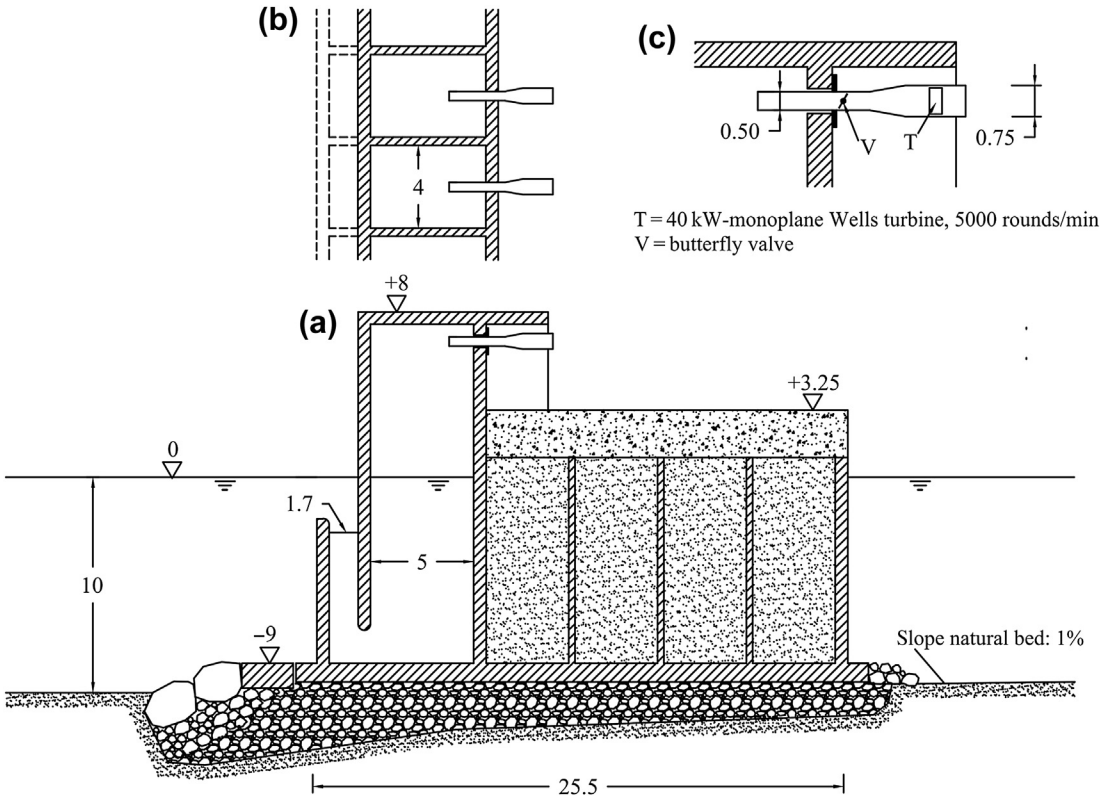

■ **FIGURE 16.8** An hypothesis of U-oscillating water column for oceans. (a) Cross-section. (b) Horizontal section chambers and exhaust tubes. (c) Details of the cross-section.

always partially closed. Doing so, safety does not depend on control software but on a certain physical phenomenon, and the reduction in the annual estimate production of electrical energy usually proves to be smaller than the 10%. An improved solution of this kind should be that shown in Figs 16.7 and 16.8: an exhaust tube consisting of two pieces—one with the diameter of the turbine and one with a smaller diameter—with a gradual expansion between the two pieces. Here the head losses take place in the piece with the smaller diameter rather than in the valve, and the re-entrant opening allows to reduce the length of the tube out of the chamber.

As to the quantity of electrical energy, a hypothesis of breakwater conceived for the Mediterranean Sea like that of Fig. 16.7 is expected to give about 4.5 kW/m with wind seas of 2.5 m H_s and T_p of about 7 s. A hypothesis of breakwater conceived for oceanic coasts like that of Fig. 16.8 is expected to give about 9 kW/m with wind seas of 4.0 m H_s and 8.5 s T_p, or 6.5−7.0 kW/m with swells of 2.5 m H_s and 12 s T_p. Should these figures be confirmed by a full-scale test, a realistic target should be exceeding the threshold of 50,000 MWh/km/year off some oceanic coast. This means that a 100 km breakwater would yield 500 million MWh in a lifetime of 100 years.

16.7 CONCLUSION

A new breakwater of the Civitavecchia port near Rome of about 500 m length is being built with U-OWC caissons. The breakwater is turbineless, that is, the U-OWC, has been preferred to a conventional caisson breakwater only for its capacity of absorbing wave energy. Of course, the plant may be transformed into a converter simply by insertion of turbines and generators. With a potential array of 136 Wells turbines, that of Civitavecchia could be the first big plant for industrial exploitation of wave energy.

REFERENCES

Battjes, J.A., Stive, M.J.F., 1985. Calibration and verification of a dissipation model for random breaking waves. J. Geophys. Res. 90 (C5), 9159−9167.

Boccotti, P., 2012. Design of breakwater for conversion of wave energy into electrical energy. Ocean Eng. 51, 106−118.

Boccotti, P., Filianoti, P., Fiamma, V., Arena, F., 2007. Caisson breakwater embodying an OWC with a small opening. Part II: a small-scale field experiment. Ocean Eng. 34, 820−841.

Curran, R., Gato, L.M.C., 1997. The energy conversion performance of several types of wells turbine designs. Proc. Inst. Mech. Eng. 211, 133−145.

Gato, L.M.C., Falcao, A.F. de O., 1990. Performances of wells turbines with double row of guide vanes. JSME Int. J. Ser. II 33 (2), 265–271.

Gato, L.M.C., Falcao, A.F. de O., 1991. Performances of wells turbines with variable pitch rotor blades. Trans. ASME J. Energy Resour. Technol. 113 (33, 2), 265,271.

Goda, Y., 2000. Random Seas and Design of Maritime Structures. Word Scientific, Singapore, 443 pp.

Index

Note: Page numbers followed by "f" indicate figures.

D

E

M

N

O

P

Q

R

S

T

U

V

W

Z